RĪGAS TEHNISKĀ UNIVERSITĀTE
Materiālzinātnes un lietišķās ķīmijas fakultāte
Organiskās ķīmijas tehnoloģijas institūts

RIGA TECHNICAL UNIVERSITY
Faculty of Materials Science and Applied Chemistry
Institute of Technology of Organic Chemistry

Armands Sebris
Doktora studiju programmas "Ķīmija" doktorants
Student of the Doctoral Programme "Chemistry"

PURĪNA ATVASINĀJUMU SINTĒZE JAUNU OPTISKO MATERIĀLU IEGŪŠANAI

Promocijas darbs

SYNTHESIS OF PURINE DERIVATIVES EN ROUTE TO NOVEL OPTICAL MATERIALS

Doctoral Thesis

Zinātniskie vadītāji / Supervisors
profesors *Dr. chem.* / Professor Dr. chem. MĀRIS TURKS
asociētā profesore *Dr. chem.* / Associate professor Dr. chem. IRINA NOVOSJOLOVA

RTU Izdevniecība
Rīga 2023
RTU Press
Riga 2023

Sebris, A. Purīna atvasinājumu sintēze jaunu optisku materiālu iegūšanai. Promocijas darbs. Rīga: RTU Izdevniecība, 2023. 132 lpp.

Sebris, A. Synthesis of Purine Derivatives en Route to Novel Optical Materials. Doctoral Thesis. Riga: RTU Press, 2023. 132 p.

Iespiests saskaņā ar RTU promocijas padomes "P-01" 2023. gada 11. aprīļa lēmumu, protokols Nr. 04030-9.1/43.

Published in accordance with the decision of the Promotion Council "P-01" of April 11, 2023, Minutes No. 04030-9.1/43.

PATEICĪBAS

Paldies par finansiālo atbalstu!

- ERAF projektam Nr. 1.1.1.1/16/A/131 "Gaismu emitējošu un ar šķīdumu metodēm apstrādājamu organisku molekulāro stiklu dizains un pētījumi" no 2017. līdz 2020. gadam.
- Latvijas Zinātnes padomei granta Nr. LZP-2018/2-0037 "Azidopurīnu un 1,2,3-triazolilpurīnu izmantošana jaunu sintēzes metožu attīstībā ar pielietojumu bioorganiskajā un materiālu ķīmijā" ietvaros no 2019. līdz 2021. gadam.
- Latvijas Zinātnes padomei granta Nr. LZP-2020/1-0348 "Azidogrupa kā reģioselektivitātes un reakcijas spējas slēdzis annelētos pirimidīnos: medicīnas un materiālu ķīmijā pielietojamu priviliģēto struktūru sintēzes metodoloģiju jaunrade" ietvaros no 2021. gada.

ACKNOWLEDGEMENTS

The research was carried out with the financial support from:

- ERDF project No. 1.1.1.1/16/A/131 "Design and Investigation of Light Emitting and Solution Processable Organic Molecular Glasses" from 2017 to 2020.
- Latvian Council of Science grant No. LZP-2018/2-0037 "Novel Synthetic Tools for Bioorganic and Materials Chemistry Based on Azidopurines and 1,2,3-Triazolylpurines" from 2019 to 2021.
- Latvian Council of Science grant No. LZP-2020/1-0348 "Azido group as regioselectivity and reactivity switch for fused pyrimidines: a redesign of synthetic methodologies towards privileged structures in medicinal and materials chemistry" from 2021 and ongoing.

PROMOCIJAS DARBS IZVIRZĪTS ZINĀTNES DOKTORA GRĀDA IEGŪŠANAI RĪGAS TEHNISKAJĀ UNIVERSITĀTĒ

Promocijas darbs zinātnes doktora (*Ph. D.*) grāda iegūšanai ķīmijas nozares organiskās ķīmijas apakšnozarē tiek publiski aizstāvēts 2023. gada 29. maijā Rīgas Tehniskās universitātes Materiālzinātnes un lietišķās ķīmijas fakultātē, Rīgā, Paula Valdena ielā 3, 272. auditorijā ar attālinātās pieslēgšanās iespēju saitē *zoom: https://rtucloud1.zoom.us/j/9352086644*.

OFICIĀLIE RECENZENTI

Dr. chem. Edgars Sūna,
Latvijas Universitāte, Latvija

Dr. chem. Pāvels Arsenjans,
Latvijas Organiskās sintēzes institūts, Latvija

Dr. Jørn H. Hansen,
Norvēģijas Arktiskā universitāte, Norvēģija

APSTIPRINĀJUMS

Apstiprinu, ka esmu izstrādājis šo promocijas darbu, kas iesniegts izskatīšanai Rīgas Tehniskajā universitātē zinātnes doktora (*Ph. D.*) grāda iegūšanai. Promocijas darbs zinātniskā grāda iegūšanai nav iesniegts nevienā citā universitātē.

Armands Sebris ……..….
(*paraksts*)

Datums …...……...….

Promocijas darbs sagatavots kā tematiski vienotu zinātnisko publikāciju kopa ar kopsavilkumu latviešu un angļu valodā. Tas ietver četrus zinātniskos oriģinālrakstus un vienu mikroapskatrakstu. Publikācijas zinātniskajos žurnālos uzrakstītas angļu valodā, to kopējais apjoms, ieskaitot pielikumus, ir 149 lpp.

SATURS

PROMOCIJAS DARBA VISPĀRĒJS RAKSTUROJUMS

Tēmas aktualitāte

Purīna struktūru modificēšana ir plaši pētīta, jo šie savienojumi pārstāv priviliģēto struktūru klasi medicīnas ķīmijā.[1] Lielākai daļai modificētu purīnu piemīt ne tikai bioloģiskā aktivitāte, bet daudziem bieži tiek novērota arī fluorescence, ko plaši lieto šūnu vizualizēšanai bioloģiskos pētījumos.[2] Attiecīgajiem atvasinājumiem ir jābūt ūdenī šķīstošiem un ar zemu citotoksicitāti. To var panākt ar atbilstošām funkcionālām grupām, piemēram, aminogrupu, hidroksilgrupu vai ribozilfragmentu pie purīna cikla. No otras puses, purīna atvasinājumu izmantošana optoelektronikā ir pētīta daudz mazāk. Optisko materiālu izstrādē ir svarīgi sasniegt augstu emisijas efektivitāti, izmantoto savienojumu stabilitāti un zemas izmaksas. Ievadot purīna ciklā tādas optoelektronikā bieži izmantotas grupas kā karbazolu, tiofēnu vai cianogrupu, var iegūt savienojumus ar piemērotām īpašībām izmantošanai organiskās gaismu emitējošās diodēs (*OLED*).

Kopš pirmā piedāvātā *OLED* dizaina 1987. gadā,[3] ir veikti plaši pētījumi augstas efektivitātes baltas vai sarkanas, zaļas un zilas krāsas diožu izstrādē displeju veidošanai. Salīdzinot ar šobrīd plaši izplatītajiem šķidro kristālu ekrāniem (*LCD*), *OLED* piemīt vairākas priekšrocības: tiem ir augstāka energoefektivitāte, lielāki krāsu atveidošanas un spektra līdzības indeksi, augsts kontrasts, kā arī plāna un viegla uzbūve, kas ļauj radīt lokanus displejus. *OLED* ir raksturīga arī dabiska krāsu gamma, kas sniedz pozitīvu efektu gan estētiskā, gan veselības ziņā.[4] *OLED* galvenie trūkumi ir augstākas izmaksas, īsāks dzīves laiks, it īpaši zilas krāsas gadījumā, kā arī degradēšanās, nonākot saskarsmē ar skābekli. Viens no veidiem izmaksu samazināšanai ir tādu materiālu izmantošana, no kuriem iespējams izgatavot *OLED* ar šķīdumu metodi, kas ir lētāka par uznešanu vakuumā.[5] Tieši amorfizējošu grupu ievadīšana purīna struktūrā pavērs iespēju plānu kārtiņu izveidei ar šķīduma metodi.

Līdz šim optoelektronikā ir zināmi daži piemēri purīna atvasinājumu lietošanai par sensoriem[6] vai fluorescentiem,[7] fosforescentiem[8] vai termiski aktivētas aizkavētās fluorescences (*TADF*)[9] emiteriem. Minētajos pētījumos[6–9] iegūtās iekārtas ir ar vājākām īpašībām nekā attiecīgie komerciālie produkti. Pamatojoties uz mazo pētījumu apjomu, ir jāpaplašina zināšanas šajā jomā, jādizainē jaunas struktūras ar elektrondonoriem un akceptoriem aizvietotājiem, jāattīsta jaunas metodes vai jāpielāgo zināmas pieejas savienojumu iegūšanai, par pamatu izmantojot dabā plaši sastopamo purīna heterociklu.

Literatūrā ir zināmas metodes aizvietotāju ievadīšanai pie purīna cikla atomiem *C*(2), *C*(6) un *C*(8) pozīcijās, izmantojot nukleofīlās aromātiskās aizvietošanas (S_NAr)[11–21] un pārejas metālu katalizētas šķērssametināšanas reakcijas.[22–26] Tomēr daudzu interesējošu elektrondonoru un elektronakceptoru aizvietotāju ievadīšana nav aprakstīta, kas prasa pielāgot zināmās metodes vai izstrādāt jaunas. Ja vajadzīgo aizvietotāju nav iespējams ievadīt tiešā veidā, dažos gadījumos to ir iespējams konstruēt, izmantojot funkcionālo grupu pārvērtības, piemēram, 1,2,3-triazolu saslēdzot vara katalizētā azīda-alkīna dipolārās ciklopievienošanās (CuAAC) reakcijā.[21]

Purīna cikla atomi *C*(2), *C*(6) un *C*(8) pozīcijās nav savstarpēji simetriski, katrs no tiem ir ar raksturīgu augstāku vai zemāku reaģētspēju. Izmaiņas aizvietotāju izvietojumā ietekmē savienojumu absorbciju, emisijas viļņa garumu un efektivitāti, tāpēc nepieciešams iegūt dažādi aizvietotus purīna atvasinājumus, lai atrastu savienojumus ar labākajām īpašībām. Ja meklētās struktūras nav iespējams iegūt, izmantojot purīnu ierasto reģioselektivitāti, ir jāizstrādā metodes selektivitātes apgriešanai. Viens no veidiem ir izmantot azīda-tetrazola līdzsvaru, kas ļauj veikt aizvietošanu pie atoma *C*(2) pozīcijā.[27]

Literatūrā ir zināmas metodes purīna slāpekļa *N*(9) un *N*(7) atomu funkcionalizēšanai ar alifātiskiem un aromātiskiem aizvietotājiem, un parasti slāpekļa atoms *N*(9) pozīcijā ir reaģētspējīgāks. Alifātiskus aizvietotājus var ievadīt, izmantojot alkilhalogenīdus vai Micunobu reakciju,[28] savukārt aromātiskus aizvietotājus var ievadīt vara katalizētā šķērssametināšanas reakcijā ar diariljodāniem[29] vai Čana-Lama šķērssametināšanā.[30] Lai ievadītu purīna heterociklā interesējošos aizvietotājus – karbazolu saturošas, elektroniem bagātas sistēmas, kā arī trifenilmetilgrupu, kas veicinātu savienojumu amorfas īpašības, ir jāpielāgo minētās metodes.[31]

Ne visas vēlamās pārvērtības ir iespējams realizēt ar saslēgtu purīna gredzenu. Gadījumā, ja cita purīna pozīcija ir ar augstāku reaģētspēju vai pārvērtību nav iespējams realizēt stērisku traucējumu dēļ, to var mēģināt paveikt ar *de novo* sintēzi. Vispirms var ievadīt vajadzīgos aizvietotājus pirimidīna vai imidazola ciklos, tad – saslēgt purīna gredzenu. *De novo* sintēze un imidazola cikla saslēgšana iepriekš modificētam pirimidīnam paver iespēju sintēzes izstrādei aromātisku aizvietotāju ievadīšanai pie mazāk reaģētspējīgā slāpekļa atoma *N*(7) pozīcijā (1. shēma).

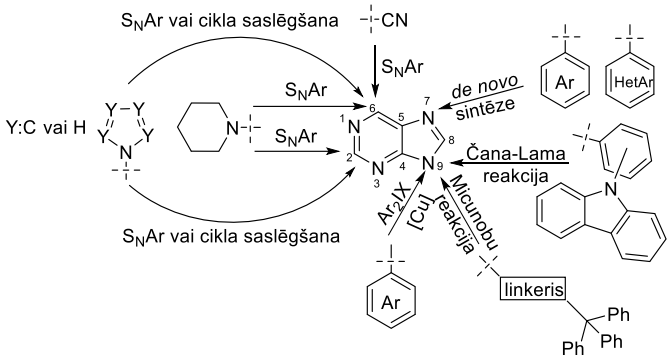

1. shēma. Purīna cikla numerācija un vēlamās reakcijas.

Promocijas darba gaitā ir iegūti ar dažādiem aizvietotājiem mērķtiecīgi funkcionalizēti luminescenti purīna atvasinājumi ar amorfizējošām grupām, kam ir noteikts potenciāls lietojums ar šķīdumu metodi iegūstamās *OLED* iekārtās. Darbā apskatītas purīna-karbazola konjugātu *TADF* īpašības un potenciālais lietojums *OLED* iekārtās. Ir izstrādāti jauni sintēzes ceļi specifiski funkcionalizētu *N*(9)-arilpurīnu, *N*(9)-alkilpurīnu un azolilpurīnu iegūšanai. Izmantojot *de novo* sintēzi, ir radīts jauns sintēzes ceļš *N*(7)-arilpurīnu iegūšanai.

Pētījuma mērķis un uzdevumi

Par promocijas darba mērķi tika izvirzīta jaunu purīna atvasinājumu sintēze, lai iegūtu savienojumus ar amorfām īpašībām, augstu emisijas efektivitāti un atbilstošām fizikālām īpašībām potenciālam lietojumam *OLED* izveidē.

Darba mērķa sasniegšanai definēti vairāki uzdevumi.

1. Izstrādāt metodes reakciju veikšanai, kas ļautu ievadīt elektrondonoras un elektronakceptoras grupas pie purīna cikla atomiem:
    - meklēt jaunus sintēzes ceļus purīna funkcionalizēšanai, izmantojot 2,6-diazidopurīna azīda-tetrazola tautomēro formu līdzsvaru;
    - atrast reakcijas apstākļus aizvietotu un neaizvietotu azolu ievadīšanai purīna *C*(2) un *C*(6) pozīcijās;
    - uzlabot un atrast jaunus reakcijas apstākļus dažādu arilaizvietotāju ievadīšanai purīna *N*(9) un *N*(7) pozīcijās.
2. Iegūt purīna atvasinājumus ar lietojumu optoelektronikā *OLED* izveidē:
    - iegūt amorfus, fluorescentus purīna atvasinājumus un noteikt to fotofizikālās īpašības;
    - sintezēt purīna atvasinājumus, kam raksturīga termiski aktivēta aizkavētā fluorescence.

Zinātniskā novitāte un galvenie rezultāti

Promocijas darba gaitā izstrādātas jaunas organiskās sintēzes metodes azolu aizvietotāju ievadīšanai purīna gredzenā, kā arī *N*(7) arilpurīnu iegūšanai *de novo* sintēzē no aizvietotiem pirimidīniem. Ietekmējot azīda-tetrazola tautomēro formu līdzsvaru 2,6-diazidopurīnam, izstrādātas sintēzes metodes ar reģioselektivitātes maiņu purīna *C*(2) un *C*(6) pozīcijās. Radīts jauns struktūru dizains iekšmolekulārās lādiņu pārneses ("*push-pull*") tipa fluorescentiem purīna atvasinājumiem un stēriski traucētiem purīna-karbazola konjugātiem, izstrādātas sintēzes metodes attiecīgo savienojumu iegūšanai. "*Push-pull*" tipa purīna atvasinājumiem raksturīga fluorescence, šos savienojumus var potenciāli lietot kā organiskos lauka efekta tranzistorus. Purīna-karbazola konjugāti, kā arī purīna un karbazola atvasinājumu maisījums cietā fāzē veido eksipleksus, kam ir raksturīga termiski aktivēta aizkavētā fluorescence. Šos savienojumus var potenciāli lietot kā aktīvās matricas materiālus *OLED*.

Darba struktūra un apjoms

Promocijas darbs ietver tematiski vienotu zinātnisko publikāciju kopu, kas veltīta pētījumiem par purīna atvasinājumiem ar lietojumu materiālzinātnē optoelektronikas problēmu risināšanai. Tajā apkopotas četras oriģinālpublikācijas *SCI* žurnālos un viens apskatraksts.

Darba aprobācija un publikācijas

Promocijas darba galvenie rezultāti publicēti četros zinātniskajos oriģinālrakstos. Promocijas darba izstrādes laikā sagatavots viens apskatraksts. Pētījumu rezultāti prezentēti 13 konferencēs.

Zinātniskās publikācijas

1. **Sebris, A.**; Novosjolova, I.; Turks, M. Synthesis of 7-Arylpurines from Substituted Pyrimidines. *Synthesis* **2022**, *54*, 5529. doi: 10.1055/a-1898-9675.
2. **Sebris, A.**; Novosjolova, I.; Traskovskis, K.; Kokars, V.; Tetervenoka, N.; Vembris, A.; Turks, M. Photophysical and Electrical Properties of Highly Luminescent 2/6-Triazolyl-Substituted Push–Pull Purines. *ACS Omega* **2022**, *7*, 5242. doi: 10.1021/acsomega.1c06359.
3. Traskovskis, K.; **Sebris, A.**; Novosjolova, I.; Turks, M. Guzauskas, M.; Volyniuk, D.; Bezvikonnyi, O.; Grazulevicius, J.; Mishnev, A.; Grzibovskis, R.; Vembris, A. All-organic Fast Intersystem Crossing Assisted Exciplexes Exhibiting Sub-Microsecond Thermally Activated Delayed Fluorescence. *J. Mater. Chem. C* **2021**, *9*, 4532. doi: 10.1039/D0TC05099G.
4. **Sebris, A.**; Traskovskis, K.; Novosjolova, I.; Turks, M. Synthesis and Photophysical Properties of 2-Azolyl-6-piperidinylpurines. *Chem. Heterocycl. Compd.* **2021**, *57*, 560. doi: 10.1007/s10593-021-02943-1.
5. **Sebris, A.**; Turks. M. Recent Investigations and Applications of Azidoazomethine-Tetrazole Tautomeric Equilibrium. *Chem. Heterocycl. Compd.* **2019**, *55*, 1041. doi: 10.1007/s10593-019-02574-7.

Pētījumu rezultātu prezentācijas konferencēs

1. **Sebris, A.** Novosjolova, I., Turks, M. New Synthetic Pathway to 7-Arylpurines. In: *Balticum Organicum Syntheticum 2022 Program and Abstract Book*, Lithuania, Vilnius, 3-6 July, 2022. Vilnius: UAB Kalanis, 2022, p. 152.
2. **Sebris, A.**, Kapilinskis, Z., Kriķis, K., Traskovskis, K., Novosjolova, I., Turks, M. Functionalized Purines for Materials Science Applications. In: *Balticum Organicum Syntheticum 2022 Program and Abstract Book*, Lithuania, Vilnius, 3–6 July, 2022. Vilnius: UAB Kalanis, 2022, p. 162.
3. **Sebris, A.** Synthesis and Photophysical Properties of Fluorescent Purine-Carbazole Conjugates. In: *12th Paul Walden Symposium on Organic Chemistry: Program and Abstract Book*, Latvia, Riga, 28–29 October, **2021**. Riga: RTU Press, 2021, p. 37.
4. **Sebris, A.**; Traskovskis, K.; Novosjolova, I.; Turks, M. Synthesis and Photophysical Properties of Purine-Carbazole Donor Acceptor Systems. In: *The 27th Croatian Meeting of Chemists and Chemical Engineers: 27HSKIKI Abstracts*, Croatia, Veli Lošinj, 5–8 October, **2021**. Croatia: 2021, p. 105.

5. **Sebris, A.;** Burcevs, A.; Traskovskis, K.; Novosjolova, I.; Vembris, A.; Turks, M. Synthesis and Photophysical Properties of Fluorescent Purine Derivatives. In: *IS3NA-IRT Virtual Symposium 2021: Book of Abstracts*, Virtual, 26–27 August, **2021**. Online: 2021, p. p67.
6. **Sebris, A.**; Novosjolova, I.; Turks, M. Synthesis and Photophysical Properties of Sterically Hindered Purine Derivatives. In: *Thesis book of University of Latvia 79th International Scientific Conference, Section: Organic Chemistry*, Latvia, Riga, February 5, **2021**. Riga: 2021, p. 61.
7. **Sebris, A.**; Novosjolova, I.; Turks, M. Synthesis and Photopysical Properties of Substituted Purine-Carbazole Conjugates. In: *Thesis book of University of Latvia 78th International Scientific Conference, Section: Organic Chemistry*, Latvia, Riga, March 6, **2020**. Riga: 2020, p. 54.
8. **Sebris, A.**; Traskovskis, K.; Novosjolova, I.; Turks, M. Purine-Azole Conjugates as Fluorescent Materials. In: *Materials Science and Applied Chemistry 2019: 60th International Scientific Conference: Programme and Abstract Book*, Latvia, Riga, October 24, **2019**. Riga: 2019, p. 25.
9. **Sebris, A.**; Novosjolova, I.; Turks, M. Synthesis and Photophysical Properties of Functionalized Purine Derivatives. In: *11th Paul Walden Symposium on Organic Chemistry: Program and Abstract Book*, Latvia, Riga, 19–20 September, **2019**. Riga: 2019, p. 41.
10. **Sebris, A.**; Traskovskis, K.; Novosjolova, I.; Turks, M. Triazolyl Purine Derivatives as Amorphous Fluorescent Materials. In: *International Symposium on Synthesis and Catalysis: Book of Abstracts*, Portugal, Evora, 3–6 September, **2019**. Evora: 2019, p. 294.
11. Novosjolova, I.; Kapilinskis, Z.; **Sebris, A.**; Burcevs, A.; Zaķis, J.; Turks, M. Synthesis and Photophysical Properties of *N*(9)-Alkylated 2,6- Substituted Purine Derivatives. In: *International Symposium on Synthesis and Catalysis: Book of Abstracts*, Portugal, Evora, 3–6 September, **2019**. Evora: 2019, p. 286.
12. **Sebris, A.**; Traskovskis, K.; Novosjolova, I.; Turks, M. Synthesis and Photophysical Analysis of Fluorescent Purine-Azole Conjugates. In: *International Symposium on Synthesis and Catalysis: Book of Abstracts*, Portugal, Evora, 3–6 September, **2019**. Evora: 2019, p. 295.
13. **Sebris, A.**; Novosjolova, I.; Traskovskis, K.; Turks, M. Amorphous Purine-Azole Conjugates and Their Photophysical Properties. In: *21st European Symposium on Organic Chemistry Poster Abstracts*, Austria, Vienna, 14–18 July, **2019**. Vienna: 2019, p. 290.
14. Novosjolova, I.; Ozols, K.; **Sebris, A.**; Zaķis, J.; Cīrule, D.; Kapilinskis, Z.; Jeminejs, A.; Kriķis, K.; Bizdēna, Ē.; Turks, M. Azidopurines and 1,2,3-Triazolylpurines as Useful Building Blocks for Bioorganic and Materials Chemistry. In: *Proceedings of GRC2019: Nucleosides, Nucleotides and Oligonucleotides*, United States of America, Newport, 23–28 June, **2019**. Newport: 2019, p. 1.
15. **Sebris, A.**; Kapilinskis, Z.; Novosjolova, I.; Turks, M. Synthesis and Photopysical Properties of Functionalized Purine-Heterocycle Conjugates. In: *Thesis book of University*

of Latvia 77th International Scientific Conference, Section: Organic Chemistry, Latvia, Riga, February 19, **2019**. Riga: LU, 2019, p. 51.

16. Bizdēna, Ē.; Goliškina, S.; **Sebris, A.**; Mishnev, A.; Turks, M. 2,4-Diazidoquinazoline as Useful Starting Material in Heterocyclic Chemistry. In: *XXII International Conference on Organic Synthesis: Scientific Program & Abstract Book*, Italy, Florence, 16–21 September, **2018**. Florence: 2018, p. P271.
17. Turks, M.; Ozols, K.; Novosjolova, I.; **Sebris, A.**; Cīrule, D.; Kapilinskis, Z.; Hopmann, K.; Zaķis, J.; Šišuļins, A.; Bizdēna, Ē. Azidopurines and 1,2,3-Triazolylpurines as Novel Synthetic Tools for Bioorganic and Materials Chemistry. In: *22nd International Conference on Organic Synthesis: Scientific Program and Abstract Book*, Italy, Florence, 16–21 September, **2018**. Florence: 2018, p. P19.
18. Novosjolova, I.; **Sebris, A.**; Kapilinskis, Z.; Traskovskis, K.; Kokars, V.; Turks, M. Purine Hybrids Containing Five-Membered Heterocycles: Synthesis and Photophysical Properties. In: *XXII International Conference on Organic Synthesis: Scientific Program and Abstract Book*, Italy, Florence, 16–21 September, **2018**. Florence: 2018, p. P361.
19. **Sebris, A.**; Kapilinskis, Z.; Novosjolova, I.; Traskovskis, K.; Vembris, A.; Turks, M. Synthesis and Photophysical Properties of *N*(9)-Alkylated Purines with Amorphousing Groups. In: *XXII International Conference on Organic synthesis: Scientific Program and Abstract Book*, Italy, Florence, 16–21 September, **2018**. Florence: 2018, p. P214.

PROMOCIJAS DARBA GALVENIE REZULTĀTI

Purīns ir dabā viens no izplatītākajiem slāpekļa heterocikliem, tā biežāk zināmie piemēri ir adenīns un guanīns – divas no DNS un RNS slāpekļa bāzēm. Traubes sintēze ir visplašāk zināmā purīnu atvasinājumu ķīmiskā iegūšanas metode, taču, ņemot vērā šādu savienojumu plašo sastopamību dabā, daudzi atvasinājumi tiek iegūti pārtikas pārstrādes procesā vai no citiem bioloģiskiem avotiem. Piemēri šo savienojumu lietojumam ārpus laboratorijas ir purīna nukleotīdu, piemēram, guanozīna monofosfāta kā garšas pastiprinātāja un kofeīna kā stimulanta izmantošana.[10]

Promocijas darbā izstrādātas metodes jaunu purīna atvasinājumu iegūšanai, izmērītas šādu savienojumu fotofizikālās īpašības un noteikts lietojums materiālzinātnē optoelektronikas jomā. Sākotnēji tika veikta purīna cikla atomu funkcionalizēšana ar elektrondonorām un elektronakceptorām grupām, lai iegūtu fluorescentas "*push-pull*" sistēmas. Tālāk purīna slāpekļa atoms *N*(9) pozīcijā tika modificēts ar elektroniem bagātiem heterocikliem, kā saistošo grupu izmantojot neitrālu aromātisku sistēmu. Iegūtajiem atvasinājumiem ir potenciāls lietojums kā organiskiem lauka efekta tranzistoriem vai aktīvām matricām *OLED*.

1. Aizvietotāju ievadīšana purīna gredzenā

Pateicoties augstai interesei par purīna modificēšanu medicīnas ķīmijā, ir izstrādātas dažādas metodes aizvietotāju ievadīšanai. Visplašāk izmantotās metodes ir S_NAr un šķērssametināšanas reakcijas aizvietotāju ievadīšanai pie purīna cikla atomiem *C*(2), *C*(6) un *C*(8) pozīcijās. Ir zināmas gan selektīvas, gan neselektīvas metodes purīna slāpekļa *N*(9) un *N*(7) atomu funkcionalizēšanai ar alifātiskiem un aromātiskiem aizvietotājiem. Kā citu pieeju izmanto *de novo* sintēzi, kurā lieto iepriekš attiecīgi funkcionalizētu pirimidīnu vai imidazolu, savukārt otru ciklu, lai iegūtu purīnu, saslēdz, kad tas ir izdevīgāk sintēzes realizēšanai.

Purīna *C*(6) pozīcijas atoms ir reaģētspējīgākais, to var funkcionalizēt ar azīdiem,[11] alkilamīniem,[12] arilamīniem,[13] azoliem,[14] alkiltioliem,[15] ariltioliem,[15] sulfinātiem,[15] alkoksīdiem,[16] fenolātiem[17] un 1,3-dikarbonilatvasinājumiem,[18] izmantojot S_NAr reakciju (2. shēma). Alifātiskos amīnus pie purīna cikla atoma *C*(6) pozīcijā var ievadīt zemā temperatūrā Cu(II) veicinātā S_NAr reakcijā.[19] Visbiežāk šajā pārvērtībā aizejošā grupa ir halogēns, bet literatūrā ir aprakstītas arī metodes, kurās izmanto azīdu,[20] sulfonilgrupu,[15] 1,2,4-triazolu vai 1,2,3-triazolu.[21] Ar C-N saiti saistītus azolus var ievadīt arī modificētos Appela apstākļos, izmantojot hipoksantīnu.[14] Dažādus aromātiskus un alifātiskus aizvietotājus var ievadīt, izmantojot pārejas metālu katalizētas šķērssametināšanas reakcijas (3. shēma). Izmantojot Suzuki–Mijauras,[22] Negiši[22a, 23, 24] vai Stilles[22a, 25] reakciju apstākļus, purīna gredzenā iespējams ievadīt aromātiskus aizvietotājus. Izmantojot Negiši[22a, 23, 24] vai Kumadas reakcijas[22a, 26] apstākļus vai trialkilalumīnija reaģentus,[22a, 26] purīna gredzenā iespējams ievadīt alifātiskus aizvietotājus. Izmantojot Sonogaširas reakcijas[22a] apstākļus, purīna gredzenā iespējams ievadīt alkinilaizvietotājus. Lietojot stehiometrisku reaģentu attiecību, alkilgrupas pie atoma *C*(6) pozīcijā var ievadīt, izmantojot organokuprātus.[22a] Jodpurīnu gadījumā, izmantojot Cu(I)[32] vai palādija[33] katalīzi, ir iespējams iegūt purīna dimērus. Dimerizēšanās

reakcija ir raksturīga purīna atvasinājumiem, kuru atomiem *C*(2) vai *C*(6), vai *C*(8) pozīcijā ir jodaizvietotājs.

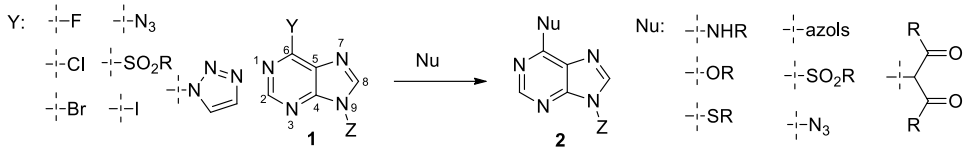

2. shēma. Purīna cikla numerācija un iespējamās S_NAr reakcijas.[11–21]

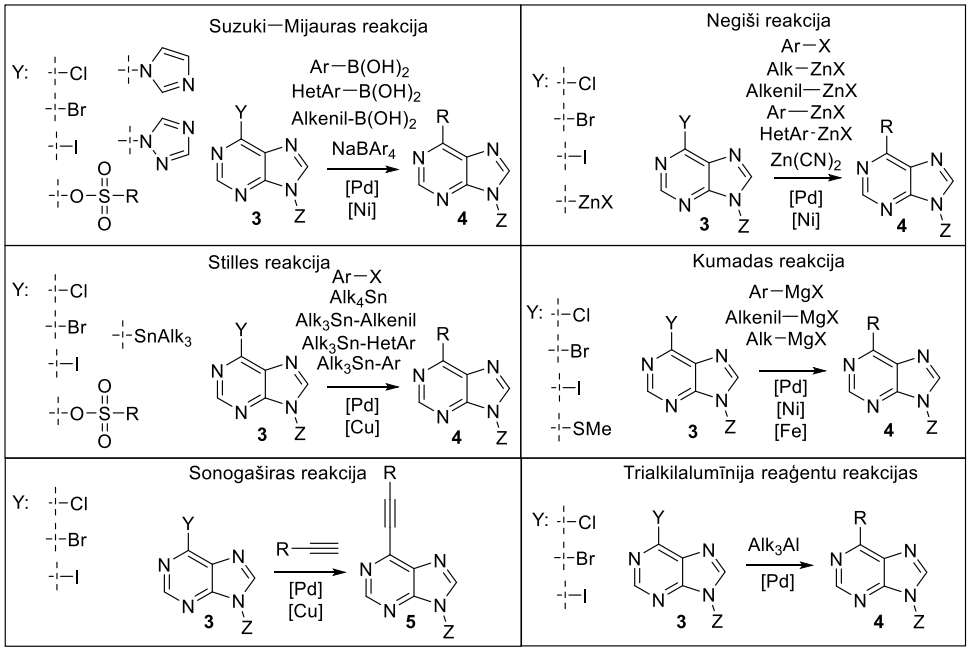

3. shēma. Šķērssametināšanas iespējas *C*(6) pozīcijas funkcionalizēšanai.[22–26]

Atoms purīna *C*(2) pozīcijā ir mazāk reaģētspējīgs par atomu *C*(6) pozīcijā. S_NAr reakcijā atomu *C*(2) pozīcijā var funkcionalizēt, ja reakcija nav iespējama pie atoma *C*(6) pozīcijā. S_NAr reakciju var realizēt ar azīdiem,[11] alkilamīniem,[34] arilamīniem,[12] azoliem,[14, 35] alkiltioliem,[36] ariltioliem,[37] alkoksīdiem[38] un fenolātiem.[38] Aizvietošanas reakcijas pie atoma *C*(2) pozīcijā notiek skarbākos apstākļos nekā *C*(6), tāpēc ir iespējams realizēt secīgas reakcijas ar dažādiem reaģentiem vai vienlaikus veikt aizvietošanu abās pozīcijās. Šķērssametināšanu gadījumā var veikt aizvietošanu pie atoma *C*(2) pozīcijā, izmantojot Suzuki–Mijauras,[22b] Negiši,[23] Kumadas,[39] Sonogaširas[40] vai Stilles[41] reakciju apstākļus, kā arī trialkilalumīnija reaģentus,[26] ja *C*(6) pozīcija nav pieejama, vai arī vienlaikus ievadīt grupas gan pie *C*(6), gan *C*(2) atomiem. Šo selektivitāti var apgriezt, ja aizvietotāji purīna ciklā pie *C*(6) atoma ir hlors, bet pie *C*(2) atoma ir jods. Šādā gadījumā Suzuki–Mijauras,[42] Negiši,[43] Sonogaširas[44] un Stilles[45] reakcijas notiek selektīvi *C*(2) pozīcijā. Joda izmantošana ļauj apgriezt selektivitāti arī starp atomiem

C(6) un *C*(8) pozīcijās, bet gadījumos, ja pie atomiem gan *C*(2), gan *C*(8) pozīcijās ir jodaizvietotājs, reakcija notiek pie atoma *C*(2) pozīcijā.[44]

Atoms purīna *C*(8) pozīcijā arī ir mazāk reaģētspējīgs par atomu *C*(6) pozīcijā. *C*(8) pozīcija iesaistās S_NAr[46] un šķērssametināšanas[47] reakcijās, līdzīgi kā *C*(2) pozīcija, taču atoms *C*(8) pozīcijā ir ar skābāku protonu, ko var selektīvi deprotonēt vai litijēt,[48] kā arī iesaistīt C-H aktivācijas reakcijās. Dažādus aromātiskos un alifātiskos aizvietotājus var ievadīt purīna gredzenā, izmantojot pārejas metālu katalizētas C-H aktivācijas reakcijas (4. shēma). Iekšmolekulārās reakcijās ar *C*(8) pozīcijas C-H aktivāciju ir iespējams iegūt arī annelētus purīnu atvasinājumus.[30, 49]

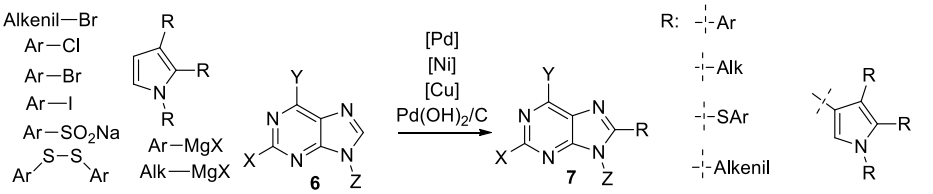

4. shēma. *C*(8) pozīcijas C-H aktivācijas reakcijas.[30]

Salīdzinot purīna slāpekļa atomus *N*(7) un *N*(9) pozīcijās, atoms *N*(9) pozīcijā ir daudz reaģētspējīgāks un kā nukleofīlā komponente dos galveno produktu. Visbiežāk izmantotās metodes, lai iegūtu *N*(9) aizvietotus alkilpurīnus, ir alkilēšana ar alkilhalogenīdiem un Micunobu reakcija.[28] Specifiskus aizvietotājus var iegūt palādija katalizētā alilacetāta un purīna šķērssametināšanas reakcijā,[28, 50] skandija katalizētā reakcijā ar diazoatvasinājumiem,[51] kā arī atverot epoksīda ciklu.[52] Slāpekļa atoma *N*(9) pozīcijā alkilēšanas reakcijās parasti rodas arī neliels daudzums *N*(7) pozīcijas alkilēšanas produkta. Visbiežāk izmantotā purīna cikla *N*(9) slāpekļa atoma arilēšanas metode ir Čana–Lama reakcija, kurā notiek purīna atvasinājuma šķērssametināšana ar arilborskābēm.[30] Citas vara katalizētas metodes izmanto arilhalogenīdus[53] vai jodānus, ko var izmantot arī alkenilaizvietotāju ievadīšanai.[29] Ja ievadāmajai aromātiskajai grupai ir pietiekami spēcīgi elektronus atvelkoši aizvietotāji, ir iespējams veikt arilēšanu saskaņā ar S_NAr reakcijas mehānismu.[54] Arilēšanas reakcijas atkarībā no aizvietotāja pie *C*(6) atoma bieži ir pilnīgi selektīvas *N*(9) pozīcijā.

Slāpekļa atoms purīna *N*(7) pozīcijā ir mazāk reaģētspējīgs. Izmantojot Griņjāra reaģentus kā bāzi reakcijā ar alkilhalogenīdiem, iegūst lielākoties *N*(7) pozīcijas alkilēšanas produktu.[55] Selektīvi *N*(7) aizvietotus alkilpurīnus var iegūt, alkilējot reducētus purīnus **10**, kas ir aizsargāti *N*(9) pozīcijā (5. shēma).[56] Purīna slāpekļa atoma *N*(7) pozīcijā arilēšanas produkta veidošanos pārākumā atkarībā no aizvietotāja pie *C*(6) var panākt optimizētos Čana–Lama reakcijas apstākļos.[57]

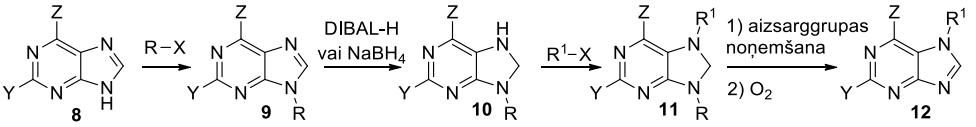

5. shēma. 7,8-Dihidropurīnu **10**,**11** izmantošana 7-alkilpurīnu iegūšanai.[56a]

Gadījumos, kad aizvietotāju ievadīšana purīna gredzenā ir sarežģīta, to var panākt, izmantojot *de novo* purīna sintēzi, kurā saslēdz pirimidīna vai imidazola gredzenus (6. shēma). Saslēdzot pirimidīna ciklu, purīna atvasinājumu ar vēlamajām funkcionālajām grupām *N*(9), *N*(7) un *C*(8) pozīcijās iespējams sintezēt, izvēloties attiecīgu imidazola izejvielu **13**, **14**, **17**, **18**. Aizvietotāju Y var ievadīt *C*(2) pozīcijā ar atbilstošu reaģentu pirimidīna cikla saslēgšanai, savukārt aizvietotājs Z var būt tikai –OH vai $–NH_2$ atkarībā no izmantotās imidazola izejvielas.[58] Saslēdzot imidazola gredzenu, purīna atvasinājumu ar vēlamajām funkcionālajām grupām *N*(9), *N*(7), *C*(2) un *C*(6) pozīcijās var iegūt, izvēloties attiecīgu pirimidīna izejvielu **15**, **19**. Aizvietotāju Q var ievadīt *C*(8) pozīcijā ar atbilstošu reaģentu imidazola cikla saslēgšanai.[59] 7-Arilpurīnu *de novo* sintēze, saslēdzot imidazola ciklu uz pirimidīna prekursora, nav plaši pētīta. Tas rosināja attīstīt šādu metodi promocijas darba izstrādes gaitā.

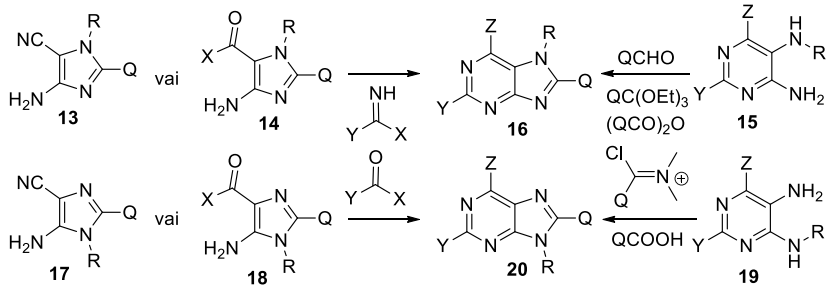

6. shēma. Purīna *de novo* cikla saslēgšana no pirimidīna vai imidazola atvasinājumiem.[58, 59]

1.1. Purīna reakciju selektivitātes kontrole ar azīda-tetrazola līdzsvaru

Azīda-tetrazola līdzsvars ir iespējams azolos, kuros azidogrupa atrodas blakus slāpekļa atomam (7. shēma). Šādu savienojumu tautomērām formām var pastāvēt līdzsvars, taču atkarībā no savienojuma struktūras un citiem faktoriem (1. tab.) var tikt novērota tikai azīda vai tikai tetrazola forma. Azīda-tetrazola tautomēro formu klātbūtne var ietekmēt savienojumu reaģētspēju un reakciju selektivitāti, tāpēc ir svarīgi izprast līdzsvara ietekmi uz reakcijām un faktorus, kas to ietekmē. Azīda grupa var iesaistīties S_NAr reakcijās[20] vai dipolārā ciklopievienošanā,[21] kā arī citās reakcijās, kurās tetrazols neiesaistās. Annelēta tetrazola cikla izveidošanās, kas var aktivēt vai dezaktivēt savienojumu reakcijām kādā citā reakcijas centrā, izmaina savienojuma elektroniskās īpašības.

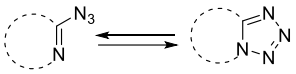

7. shēma. Azīda-tetrazola tautomēro formu līdzsvars.

1. tabula

Azīda vai tetrazola tautomērās formas veicinošie faktori

Faktors	Azīda tautomērās formas īpatsvara palielināšana	Tetrazola tautomērās formas īpatsvara palielināšana
Heterocikls, aizvietotāju efekti	Ar elektroniem nabadzīgs	Ar elektroniem bagāts
Šķīdinātāja polaritāte	Nepolārs	Polārs
Temperatūra	Paaugstināta	Pazemināta
Stēriski traucējumi tetrazola cikla tuvumā	Ir	Nav

Lai gan diazidopurīnu gadījumā var eksistēt piecas tautomērā līdzsvara formas (8. shēma), visbiežāk tiek novērota diazīda tautomērā forma **AA**, jo purīns ir elektroniem nabadzīgs cikls. Kristāliskā formā šie savienojumi pastāv diazīda tautomērajā formā, taču polāros šķīdinātājos var novērot arī vienu no tetrazola tautomērajām formām **AT1**, kuras klātbūtne ir jau iepriekš mūsu zinātniskajā grupā izmantota purīna parastās reaģētspējas apgriešanai.[27, 60]

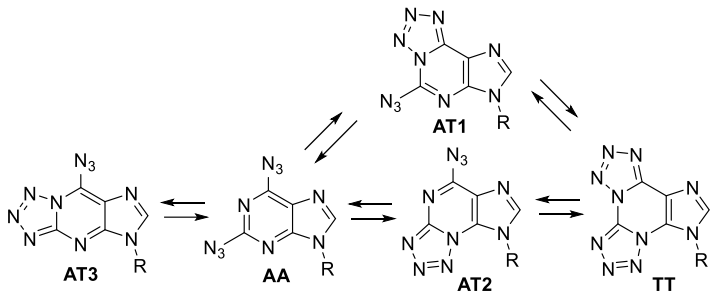

8. shēma. Diazidopurīna teorētiskie azīda-tetrazola tautomēro formu līdzsvari.

Jaunākā informācija par azīdu-tetrazolu līdzsvaru dažādos heterociklos apkopota apskatrakstā 1. pielikumā.

Ņemot vērā iepriekšminēto informāciju, tika piedāvāta pārvērtību virkne, ar kuru varētu iegūt "*push-pull*" tipa fluorescentus purīna atvasinājumus. Šādiem savienojumiem ir potenciāls lietojums optoelektronikā kā ar šķīdumu uzklājamiem materiāliem. Šim nolūkam savienojumam ir jāpiemīt amorfām īpašībām, kuras var veicināt, ievadot molekulā trifenilmetilaizvietotājus.[61]

Alkilaizvietotājs pie slāpekļa atoma *N*(9) pozīcijā tika ievadīts Micunobu reakcijā, kurā veidojās arī neliels daudzums blakusprodukta, jo reakcija notiek arī ar slāpekļa atomu *N*(7) pozīcijā. Iegūtā savienojuma **22** S_NAr reakcijā ar NaN_3 produkts **23** veidojas ar gandrīz kvantitatīvu iznākumu. Izmantojot starpprodukta **23** iepriekšminētās **AT1** tautomērās formas reaģētspēju, savienojums **24** tika iegūts S_NAr reakcijā ar piperidīnu ar *C*(2)-selektivitāti. Reakcijas veikšana DMF 20 °C temperatūrā palielināja tetrazola tautomērās formas īpatsvaru starpproduktā **23**. Šādos apstākļos reakcija notiek lielākoties *C*(2) pozīcijā, taču pilnībā novērst aizvietošanos pie purīna *C*(6) atoma neizdevās.

Lai nonāktu līdz pretēji aizvietotajam reģioizomēram **27**, ar sākotnējo izejvielu **21** vispirms tika veikta S_NAr reakcija ar NaN_3, kas šajā gadījumā deva savienojumu **25** ar zemāku iznākumu nekā *N*(9) aizvietota purīna gadījumā, jo veidojās arī monoazidoaizvietots purīna atvasinājums. Nākamajā stadijā tika veikta S_NAr reakcija ar piperidīnu, kas šajā gadījumā notiek pie atoma *C*(6) pozīcijā. Reakcijas selektivitātes apgriešana varēja notikt, jo ar izmaiņām savienojuma struktūrā (*N*(9) pozīcijā neatrodas elektrondonora alkilgrupa) un reakcijas apstākļiem (paaugstinātu temperatūru) tika veicināta azīda forma. Reakcijas gaitā notika azīda degradēšanās, kas pazemināja iznākumu, bet *C*(2) aizvietošanās netika novērota. Alternatīvi, savienojumu **26** varētu mēģināt iegūt, vispirms veicot savienojuma **21** S_NAr reakciju ar piperidīnu un tad tam sekojošu azidēšanu *C*(2) pozīcijā. Taču šis ceļš netika izvēlēts, jo elektrondonoru grupu ievadīšana dezaktivē purīnu S_NAr reakcijām, kas nozīmē, ka azidēšana ir jāveic skarbos apstākļos. Iegūtajam savienojumam **26** pie atoma *N*(9) pozīcijā Micunobu reakcijā tika ievadīta trifenilpentilgrupa (9. shēma). Substrātam **26** ir iespējama arī Štaudingera reakcija, kuras produkts tika novērots ar Micunobu apstākļos lietoto fosfīnu. Šo blakusreakciju izdevās novērst, veicot Micunobu reakciju lielākā atšķaidījumā.

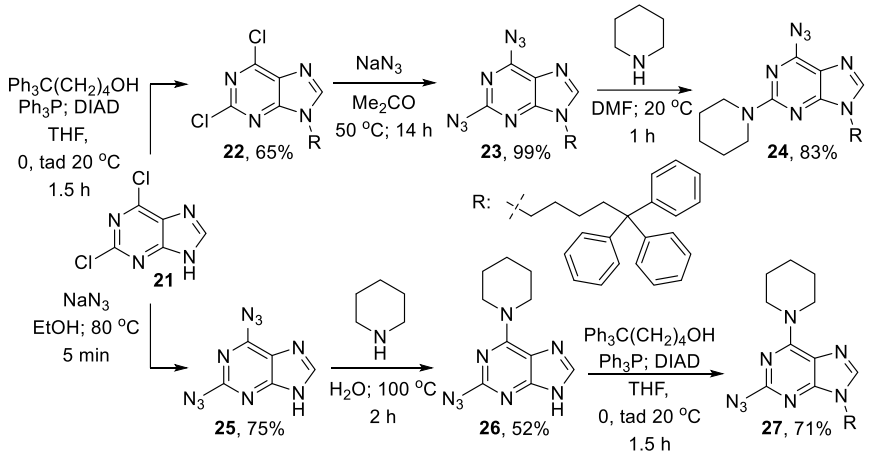

9. shēma. Diazidopurīna funkcionalizēšana ar piperidīnu purīna cikla atomu *C*(2) vai *C*(6) pozīcijā.

Oriģinālpublikācija par šajā apakšnodaļā aprakstītajiem pētījumiem – 4. pielikumā.

1.2. Purīnu funkcionalizēšana ar azoliem *C*(2) vai *C*(6) pozīcijās

Azoli ir slāpekli saturoši heterocikli, kas ir elektroniem nabadzīgi un "*push-pull*" fluorescentās sistēmās var kalpot kā elektronu akceptori.[27] Azolu aizvietotājus purīna gredzenā var iegūt, saslēdzot heterociklu ar atbilstošu funkcionālo grupu vai ievadot ciklu aizvietošanas reakcijā. Šajā nodaļā tiks apskatīti purīna-azolu konjugāti, kas ir saistīti ar C-N saiti.

Dažādi aizvietotus 1,2,3-triazolilpurīnus var vienkārši iegūt, veicot Cu(I) katalizētu alkīna-azīda ciklopievienošanas reakciju ar azidopurīnu un aizvietotu alkīnu.[21] Šādā reakcijā ar labiem iznākumiem tika iegūti četri 2/6-(1,2,3-triazolil)purīna atvasinājumi ar aromātiskiem

aizvietotājiem. "*Push-pull*" sistēmu izpētei interesantas ir aromātiskas sistēmas ar elektrondorām un elektronakceptorām grupām, tāpēc tika iegūti atvasinājumi ar metoksigrupu **28b** un **29b**, dimetilaminogrupu **28c** un **29c**, cianogrupu **28d** un **29d** vai bez papildu grupām **28a** un **29a**. Ciklopievienošanas reakcijas 20 °C norit tīri, bez azīda reducēšanās, toties reakcijas ātrums ir lēns un samazinās, pieaugot konversijai. Reakcijas temperatūras paaugstināšana izraisa blakusproduktu veidošanos. Savienojums **24** un elektronakceptoras grupas saturoši alkīni izrādījās reaģētspējīgāki par savienojumu **27** un elektrondonoras grupas saturošiem alkīniem, kā rezultātā savienojuma **29c** reakcijas maisījums tika izturēts 11 dienas, lai sasniegtu vajadzīgo konversiju (10. shēma).

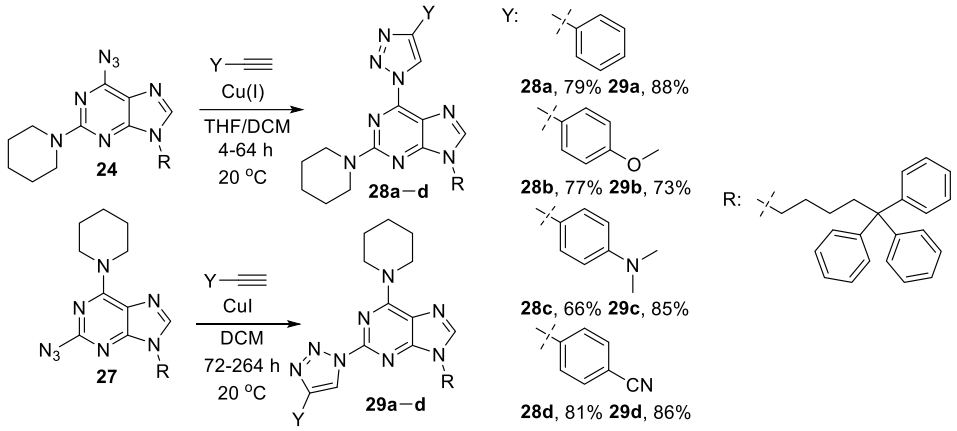

10. shēma. 1,2,3-Triazola ievadīšana purīna *C*(2) vai *C*(6) pozīcijās.

Lai gan S_NAr reakcijas ar azoliem pie atoma *C*(6) pozīcijā ir apskatītas plašāk, dažādus azolus var ievadīt purīna cikla atoma *C*(2) pozīcijā S_NAr reakcijā skarbos apstākļos, kā tas tika parādīts ar pirazolu un benzimidazolu citu autoru darbos.[14, 34] Purīna atvasinājumiem ar azolaizvietotājiem *C*(2) pozīcijā tika sagaidītas fluorescentas īpašības, tāpēc tika ieplānots tajos ieviest trifenilmetilgrupu amorfu īpašību veicināšanai. Šoreiz šim mērķim tika izvēlēts savienojums **35**, jo tas ir vienkāršāk iegūstams nekā 5,5,5-trifenilpentanols. Šī izmaiņa struktūrā neietekmē fluorescenci, jo abos gadījumos π konjugētās sistēmas, kurās notiek ierosināšana un emisija, ir identiskas. Lai iegūtu savienojumus **32** ar dažādām azolu grupām, slāpekļa atomu *N*(9) pozīcijā izejvielā **21** vispirms nācās aizsargāt ar THP aizsarggrupu. Tālāk ar piperidīnu tika veikta S_NAr reakcija, kas notiek selektīvi pie atoma *C*(6) pozīcijā. Savienojumam **31** var veikt S_NAr reakciju ar imidazolu vai 1,2,4-triazolu, vai 4-fenil-1,2,3-triazolu. Iepriekšminētā reakcija nenotiek ar tetrazolu, jo šis heterocikls ir pārāk vājš nukleofīls, ko var izskaidrot ar augsto NH skābumu. Attiecīgu reakciju veicot savienojuma **31** analogam, kas ir *N*(9) funkcionalizēts ar savienojumu **35** Micunobu reakcijā, aizvietošanās pie atoma *C*(2) pozīcijā notika, taču tika novērota arī estera grupas šķelšana. Izmēģinājumā ar *N*(9) neaizvietotu purīnu azola aizvietošanās pie atoma *C*(2) pozīcijā nenotika. 1,2,4-Triazola un 4-fenil-1,2,3-triazola gadījumā šajā reakcijā var veidoties reģioizomēru maisījums. 1,2,4-Triazola gadījumā tika novērota tikai **32b** veidošanās, savukārt reakcijā ar 4-fenil-1,2,3-triazolu veidojās reģioiziomēri

32c un **32d** līdzīgos daudzumos. Savienojumiem **32a**,**b** tika noņemtas THP aizsarggrupas, lai tos Micunobu apstākļos funkcionalizētu ar savienojumu **35** un iegūtu galaproduktus **36a**,**b** (11. shēma).

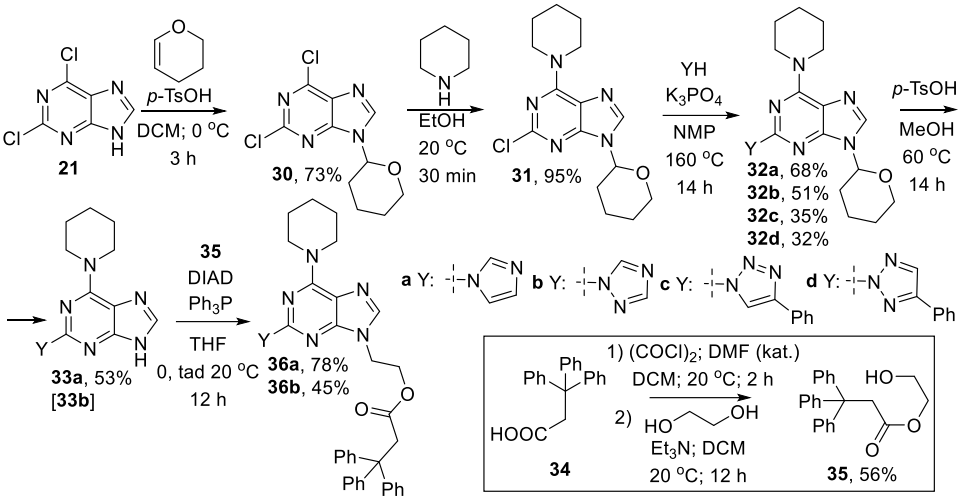

11. shēma. Azolu ievadīšana purīna *C*(2) pozīcijā S_NAr reakcijā.

Lai identificētu savienojumus **32c**,**d**, tika veikta savienojuma **32c** sintēze, ietekmējot azīda-tetrazola tautomēro formu līdzsvaru. Iepriekš iegūtais savienojums **30** tika funkcionalizēts par diazīdu **37**. Sekojošā S_NAr reakcija ar piperidīnu tika veikta toluolā paaugstinātā temperatūrā, lai veicinātu azīda tautomēro formu, kā rezultātā aizvietošana pārsvarā notiek pie atoma *C*(6) pozīcijā, taču tāpat veidojas salīdzinoši liels *C*(2) pozīcijas aizvietošanas produkta daudzums, un savienojums **38** tika iegūts ar 56% iznākumu. Dipolārās ciklopievienošanās reakcijā var veidoties tikai savienojums **32c** (12. shēma), un, salīdzinot to ar savienojuma **31** S_NAr reakcijā iegūtajiem produktiem, tika veikta **32c** reģioselektivitātes pierādīšana.

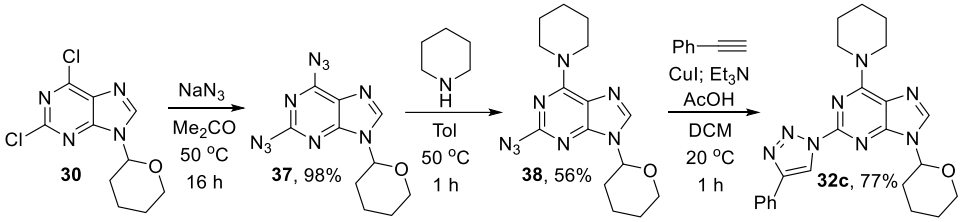

12. shēma. Savienojuma **32c** iegūšana ar citu sintēzes ceļu.

Tetrazola ievadīšana S_NAr reakcijā neizdevās, tāpēc tika apsvērta šī cikla saslēgšana uz aminogrupas savienojumā **39** pēc literatūrā zināmas metodes citu savienojumu klasēs.[62] Aminogrupu pie purīna atoma *C*(2) pozīcijā var vienkārši iegūt, katalītiski reducējot azidogrupu savienojumā **26**. Tetrazola konstruēšana *C*(2) pozīcijā notika ar labu iznākumu. Iegūtajam savienojumam **40** Micunobu reakcijā ar dažādām grupām tika funkcionalizēts slāpekļa atoms *N*(9) pozīcijā (13. shēma). Trifenilmetilgrupu saturošais fragments veicina savienojuma **41a** amorfās īpašības, hloretilgrupas ievadīšana paver iespējas tālākai funkcionalizēšanai, savukārt

3,5-dikarbazolilbenzola fragments purīna atvasinājumā **41c** varētu uzlabot savienojuma īpašības lietojumam elektronikā, jo šis fragments bieži tiek izmantots optoelektronikā.[63]

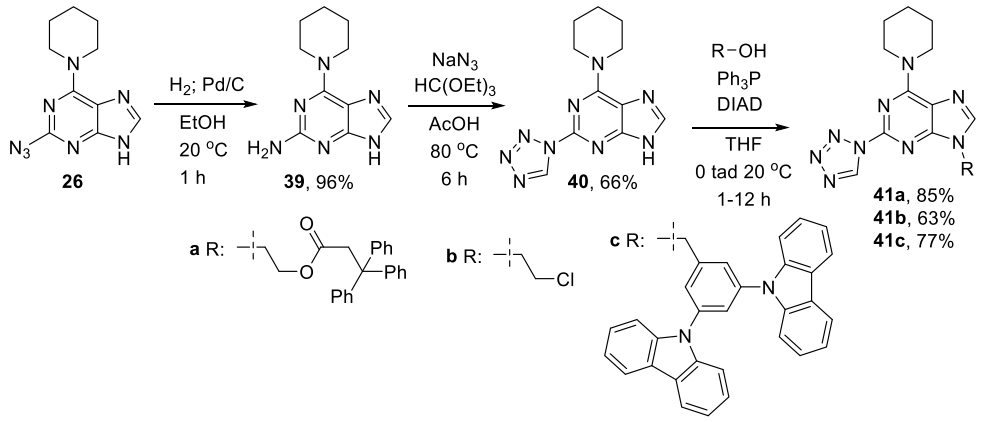

13. shēma. Tetrazola cikla konstruēšana pie purīna atoma *C*(2) pozīcijā.

Oriģinālpublikācijas par šajā apakšnodaļā aprakstītajiem pētījumiem – 2. un 4. pielikumā.

1.3. Arilaizvietotāju ievadīšana purīna *N*(9) vai *N*(7) pozīcijās

Aromātisku aizvietotāju ieviešana pie purīna slāpekļa atoma *N*(9) un *N*(7) pozīcijās ir potenciāli noderīgs pētījumu virziens gaismu emitējošu savienojumu izpētei, jo šādi atvasinājumi lielākoties sastāv no saistītiem aromātiskiem cikliem ar vai bez kompleksēta pārejas metāla.[64] Purīna slāpekļa atoma *N*(9) pozīcijā arilēšanai ir zināmas literatūras metodes,[29, 49a, 53, 54] taču slāpekļa atoma *N*(7) pozīcijā arilēšana ir apskatīta daudz mazāk.[57] Ja arilēšanas reakcijās nav iespējams ievadīt vajadzīgo arilaizvietotāju, to var panākt purīna *de novo* sintēzē no aizvietota imidazola[58] vai pirimidīna.[59]

Sākotnējais izpētes objekts bija savienojums **44a**,[65] kas tika iegūts, katalītiski arilējot savienojumu **42** ar difeniljodānu[29] ar tam sekojošu cianogrupas ievadīšanu pie atoma *C*(6) pozīcijā, izmantojot sulfināta aktivētu S_NAr reakciju ar KCN.[65] Diariljodānu izmantošanai slāpekļa atoma *N*(9) pozīcijā arilēšanā tika dota priekšroka, jo šī reakcija ir selektīva un ar augstu iznākumu. Tālākie izpētes objekti bija ar karbazoliem aizvietoti benzola gredzeni, ko ar diariljodāniem neizdevās ievadīt, jo karbazola gredzens ir pārāk spēcīgs elektronu donors. Mēģinot iegūt ar karbazolu aizvietotus nesimetriskus diariljodānus, tika novērota tūlītēja degradēšanās. Savienojumus **44b-d** izdevās iegūt Čana–Lama reakcijā ar attiecīgi aizvietotām arilborskābēm, pēc tam ievadot cianogrupu (14. shēma). Čana–Lama reakcija tika izvēlēta arilēšanai, jo tā bija vienīgā metode, kas deva vajadzīgos produktus, taču metodei ir arī nopietni trūkumi, piemēram, iznākumi 51–57% un ekvimolārs katalizatora daudzums.

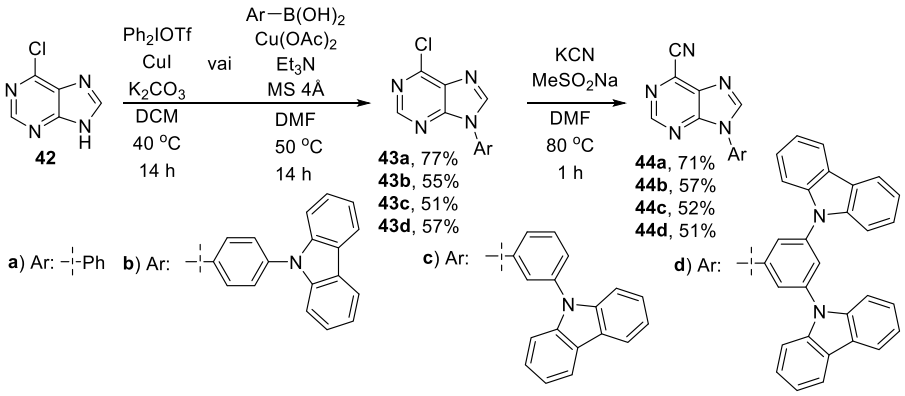

14. shēma. 6-Ciano-9-arilpurīnu **44a-d** iegūšana.

Purīna slāpekļa atoma *N*(7) pozīcijā arilēšana ir literatūrā maz pētīta. 7-Arilpurīnu iegūšana, izmantojot *de novo* sintēzi ar imidazola gredzena saslēgšanu, nav zināma, tāpēc tika nolemts izpētīt šo metodi. Optimālu reakcijas apstākļu meklēšana tika veikta, izmantojot izejvielas **45** un **47**, jo šo pirimidīnu simetrija ļāva izvairīties no blakusreakcijām. Atslēgas solis šajā pārvērtību sekvencē bija arilamīnu ievadīšana pie pirimidīna atoma *C*(5) pozīcijā, jo tā ir izteikti mazāk reaģētspējīga nekā *C*(4/6) pozīcijas. Sākotnējie mēģinājumi ar pirimidīna atvasinājumu **45** ļāva iegūt intermediātu **48**, taču, veicot optimizāciju, noskaidrojās pieejas trūkumi. S_NAr reakcija ar anilīnu notiek ar zemāku iznākumu, ja tiek izmantoti šķīdinātāji, bet veikt reaciju bez šķīdinātāja vajadzīgajā daudzumā (20 ekv.) ar citiem anilīna atvasinājumiem bija ekonomiski neizdevīgi. Savienojuma **46** dehidroksihlorēšanu ar $POCl_3$ neizdevās tālāk optimizēt – citi hlorējoši reaģenti un šķīdinātāji deva vai nu zemāku iznākumu, vai arī tikai degradēšanos. Savukārt izmēģinājumi ar diariljodāniem un Cu(I) katalīzi ļāva iegūt pirimidīna atvasinājumu **48** no izejvielas **47** vienā solī. Iedvesmojoties no Cu(0) katalīzes piemēra literatūrā,[66] izdevās panākt pilnīgu konversiju un iegūt pirimidīna atvasinājumu **48** ar 81% iznākumu. Tālākā S_NAr reakcija tika veikta, izmantojot piesātinātu amonjaka šķīdumu *i*-PrOH, lai novērstu hidrolīzi. Pēdējam solim ir zināmas daudzas imidazola saslēgšanas metodes,[59] savukārt ar substrātu **49** pilnīgu konversiju bez blakusproduktu veidošanās izdevās panākt skābes katalizētā reakcijā ar ortoesteri, iegūstot purīna atvasinājumu **50** kvantitatīvi (15. shēma).

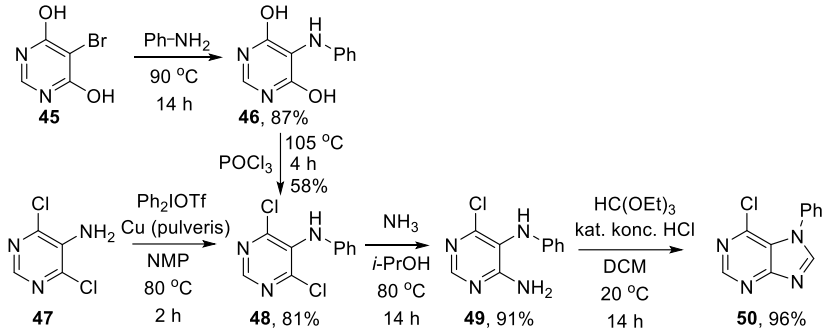

15. shēma. 7-Fenil-6-hlorpurīna (**50**) iegūšanas sekvence *de novo* sintēzē.

Pārbaudot arilēšanas apstākļus ar dažādiem diariljodāniem un aizvietotiem pirimidīna atvasinājumiem **47**, noskaidrojās, ka ar šo metodi iespējams ievadīt gan elektroniem bagātas, gan elektroniem nabadzīgas aromātiskas sistēmas, gan heterociklu, kā redzams savienojuma **48d** gadījumā (2. tab.). Izmaiņas pirimidīna aizvietotājos, kas nevar iesaistīties reakcijā, neizraisa negatīvas izmaiņas arilēšanā, kā redzams savienojumiem **48e**-**g**. Vienīgais pārbaudītais izņēmums ir 5-amino-4-hlorpirimidīns, kas degradējas reakcijas apstākļos. Reakcijā ar elektrondonoru grupu saturošiem ariljodāniem jodāna degradēšanās ir pastiprināta, un netika sasniegta pilnīga konversija. Reakcijā ar elektronatvelkošu grupu saturošiem ariljodāniem jodāna degradēšanās ir minimāla, taču reaģētspēja arī samazinās, un reakcijas laiks ir jāpalielina līdz 48 h.

Tālāk monoaizvietošanas S_NAr reakcijā ar amonjaku labākie rezultāti tika iegūti 80 °C temperatūrā. Ar elektroniem bagātiem substrātiem **48b**,**e** vajadzēja ilgāku reakcijas laiku pilnīgas konversijas sasniegšanai. Savienojumiem **48f**,**g** reakcija notika gan pirimidīna atomu *C*(2), gan *C*(4/6) pozīcijās, tāpēc **49f**,**g** tika iegūts ar nedaudz zemākiem iznākumiem. Aizvietošanās produkts *C*(2) pozīcijā veidojas nelielos daudzumos, jo *C*(4/6) pozīcija ir reaģētspējīgāka (2. tab.).

2. tabula

Aizvietotu pirimidīnu **49a-g** iegūšanas apstākļi

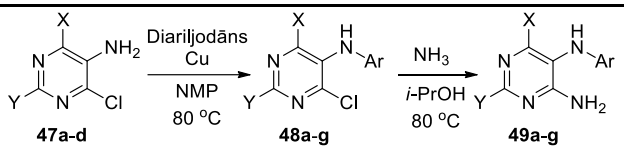

Nr.	X	Y	Reakcija **47→48**				Reakcija **48→49**	
			Diariljodāns	**Ar**	**t(h)**	**Iznākums (%)**	**t(h)**	**Iznākums (%)**
1.	Cl	H	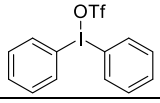		2	**48a**, 81	16	**49a**, 91
2.	Cl	H	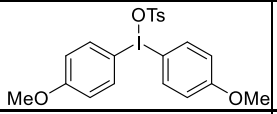	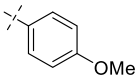	2	**48b**, 65	48	**49b**, 90
3.	Cl	H	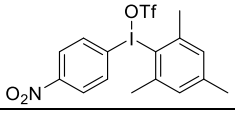	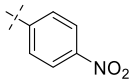	48	**48c**, 66	16	**49c**, 97
4.	Cl	H	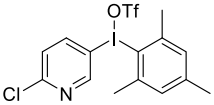	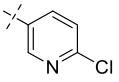	48	**48d**, 61	16	**49d**, 80
5.	Cl	Me	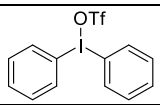		2	**48e**, 71	24	**49e**, 93
6.	H	Cl			2	**48f**, 78	16	**49f**, 73
7.	Cl	Cl			2	**48g**, 71	16	**49g**, 75

Imidazola saslēgšanas reakcijas, kurās R = H, vislabākie iznākumi tika sasniegti, izmantojot ortoesteri (3. tab., 1., 4.–9. rinda). Veicot šo pārvērtību ar skudrskābi, neizdevās novērst hidrolīzi pie atoma *C*(6) pozīcijā. Lai nenotiktu hidrolīze pie atoma *C*(6) pozīcijā reakcijās ar ortoesteri, elektroniem nabadzīgāku substrātu gadījumā tika izmantots bezūdens HCl dioksānā paaugstinātā temperatūra. Imidazola cikla saslēgšana, izmantojot ortoesteri, ja R ≠ H, notiek slikti vai nenotiek vispār. Pie atoma *C*(8) pozīcijā var ievadīt alifātiskus aizvietotājus, saslēdzot ciklu ar anhidrīdu. Trifluormetilgrupu var ievadīt pie atoma *C*(8) pozīcijā divu stadiju procesā ar $(CF_3CO)_2O$, kurā sākotnēji veidojas trifluoracetamīds, tad paaugstinātā temperatūrā tiek saslēgts cikls.[67] Cikla saslēgšanas gaitā notiek hidrolīze pie atoma *C*(6) pozīcijā. Lai iegūtu produktu **50c**, hloru pie atoma *C*(6) pozīcijā atjauno dehidroksihlorēšanas reakcijā ar $POCl_3$.

3. tabula

Aizvietotu 7-arilpurīnu **50a-i** iegūšanas apstākļi

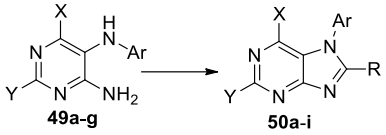

Nr.	X	Y	R	Ar	Reaģents	Šķīdinātājs	Piedeva	T (°C)	T (h)	Iznākums (%)
1.	Cl	H	H		$HC(OEt)_3$	DCM	aq. HCl	20	16	**50a**, 96
2.	Cl	H	Me		Ac_2O	–	–	120	1	**50b**, 78
3.	Cl	H	CF_3		$(CF_3CO)_2O$	1)DCM 2)THF	Py	1)20 2)95	1)16 2)24	**50c**, 70*
4.	Cl	H	H	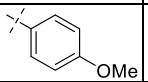	$HC(OEt)_3$	DCM	aq. HCl	40	16	**50d**, 98
5.	Cl	H	H	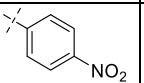	$HC(OEt)_3$	DCE	HCl dioksānā	80	3	**50e**, 91
6.	Cl	H	H	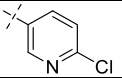	$HC(OEt)_3$	DCE	HCl dioksānā	80	3	**50f**, 82
7.	Cl	Me	H		$HC(OEt)_3$	DCM	aq. HCl	20	16	**50g**, 89
8.	H	Cl	H		$HC(OEt)_3$	DCM	aq. HCl	20	16	**50h**, 91
9.	Cl	Cl	H		$HC(OEt)_3$	DCE	HCl dioksānā	80	16	**50i**, 78

* Summārais iznākums 2 stadijās

Oriģinālpublikācijas par šajā apakšnodaļā aprakstītajiem pētījumiem – 3. un 5. pielikumā.

2. Purīna atvasinājumu fotofizikālās īpašības un lietojums

Veiktie pētījumi par purīnam un 6-metilpurīna īpašībām ierosinātā stāvoklī parāda, ka fotoierosināšanas rezultātā izveidotais singleta stāvoklis ātri iesaistās starpsistēmu pārejas procesā un izveidojas relatīvi stabils tripleta stāvoklis ar dzīves laiku 1,7 μs istabas temperatūrā, vai dzīves laiku pat 1 s 77 K temperatūrā.[68] Šo savienojumu tripletu kvantu iznākums ir 88%.[69] Citos pētījumos tika apskatīta purīna *C*(2) un *C*(6) pozīciju aizvietotāju ietekme uz ierosinātā stāvokļa relaksācijas ceļu un ātrumu, kā arī piedāvāts relaksācijas mehānisms 9-metilpurīnam no ierosināta singleta stāvokļa uz tripletu caur diviem starpstāvokļiem.[70]

Purīna atvasinājumi dažādu funkciju veikšanai ir iesaistīti *OLED* struktūrās, taču kopumā tamlīdzīgu piemēru ir maz. Viens no šādiem piemēriem ir fluorescentas purīna "*push-pull*" sistēmas izmantošana *OLED*. Ierīces ar purīna atvasinājumu **51** sasniedza 3,1% ārējo kvantu efektivitāti. Fluorescentu sistēmu maksimālā iespējamā efektivitāte ir 25%, jo ierosināto singleta un tripleta stāvokļu sadalījums ir 1 : 3.[7] Citā piemērā divi purīni ir savienoti ar aromātisku tiltu, un atkarībā no aromātiskā cikla īpašībām var iegūt donora-akceptora-donora, akceptora-donora-akceptora vai neitrālu fluorescentu sistēmu. Šādiem savienojumiem, piemēram, **52**, ir potenciāls lietojumam *OLED* vai sensoros.[6] Adenīns un guanīns tika pārbaudīti kā elektronus bloķējošie un caurumus transportējošie slāņi *OLED* struktūrā. No izmēģinātajiem purīna un pirimidīna atvasinājumiem ierīce ar adenīnu izrādīja labāko strāvas vadīšanu un emisijas efektivitāti.[69] Daži piemēri ar termiski aktivētu aizkavēto fluorescenci ir zināmi purīna atvasinājumiem, kas ir saistīti ar elektroniem bagātu fenoksazīnu, kur aromātiskās sistēmas ir izgrieztas ārpus plaknes. Ar purīna atvasinājumu **53** tika iegūts *OLED* ar 16% ārējo kvantu iznākumu.[9] Nesen publicēti ir arī pirmie fosforescentie irīdija kompleksi ar purīna atvasinājumu ligandiem, piemēram, savienojums **54** (1. att.). Neitrāli irīdija kompleksi emitē gaismu oranži-sarkanajā reģionā, savukārt katjonie kompleksi emitē gaismu dzelteni-zaļajā reģionā.[8]

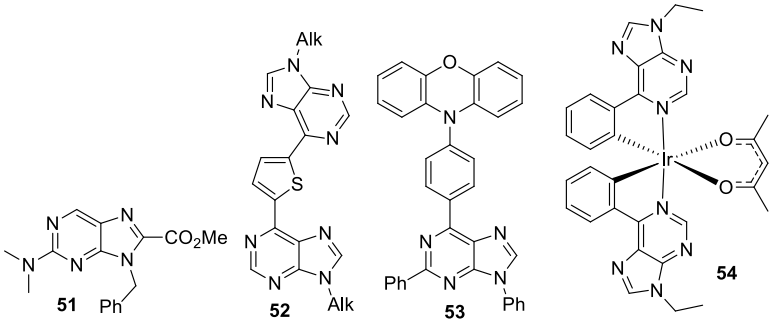

1. att. Literatūrā zināmi purīna atvasinājumi ar lietojumu *OLED*.[6–9]

OLED sastāv no diviem elektrodiem – katoda un anoda, starp kuriem atrodas vairāki organisku materiālu slāņi, kas nodrošina caurumu un elektronu pārvietošanos uz emisijas slāni (*EML*), kurā notiek lādiņu rekombinācija un emisija (2. att.). Vienam vai abiem elektrodiem ir jābūt caurspīdīgiem, lai izstarotā gaisma varētu izkļūt ārpus iekārtas. Kā piemērus bieži izmantotiem materiāliem var minēt LiF/Al katodu un indija alvas oksīda (ITO) anodu.[72] Dažādi

palīgslāņi nodrošina efektīvu caurumu un elektronu nokļūšanu līdz *EML* un rekombinēšanos tajā. Caurumu un elektronu ievadīšanu sistēmā regulē ar caurumu injekcijas slāni (*HIL*), kura enerģijas līmeņi ir pieskaņoti anodam, un elektronu injekcijas slāni (*EIL*), kura enerģijas līmeņi ir pieskaņoti katodam. Caurumu transporta slāni (*HTL*) un elektronu transporta slāni (*ETL*) izmanto, lai saskaņotu elektronu un caurumu mobilitāti, to enerģijas līmeņi ir pieskaņoti *EML*. Lai sekmētu rekombinācijas notikšanu *EML*, dažkārt izmanto elektronus bloķējošu slāni (*EBL*) vai caurumus bloķējošu slāni (*HBL*), kas kalpo kā enerģētiskas barjeras un kavē elektronu vai caurumu aizplūšanu uz pretējo elektrodu.[73] *EML* sastāv no aktīvā matricā iejauktas emitējošā savienojuma, retos gadījumos šo slāni veido tikai no emitera.[74]

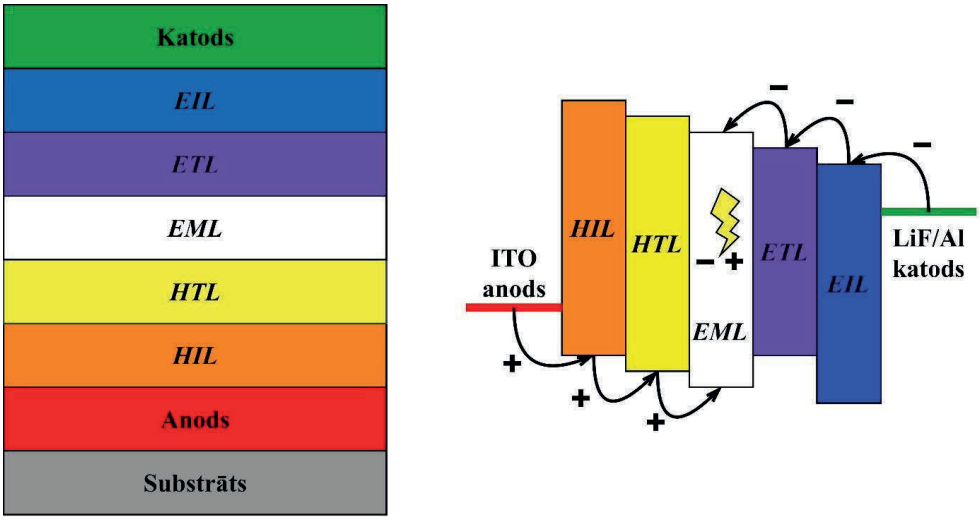

2. att. OLED struktūras un darbības mehānisma atspoguļojums.

Daudz plašāk fluorescenti purīna atvasinājumi ir izmantoti jonu sensoros[75] fluorescentai iezīmēšanai[76] un šūnu vizualizēšanai.[77,27] Izmantojot tamlīdzīgus sensorus, iespējams arī noteikt jonu koncentrāciju atkarībā no fluorescences pastiprināšanas vai dzēšanas. Vielām ar lietojumu šūnu vizualizēšanā svarīgākie parametri ir biosavietojamība, caurlaidība caur membrānām, citotoksicitāte un ietekme uz šūnu vairošanos. Šiem mērķiem var izmantot arī savienojumus ar zemāku emisijas kvantu iznākumu, ja tie ir nepieciešami kvalitatīvai analīzei (3. att.).

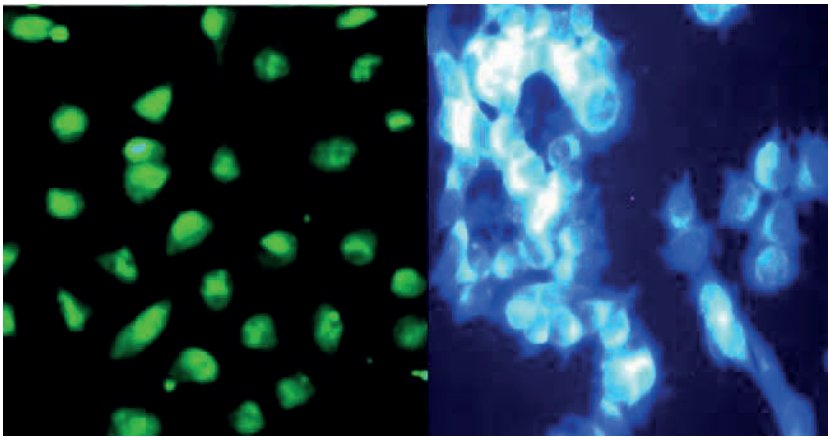

a) b)

3. att. Šūnu vizualizēšana ar purīna-zelta nanoklasteriem (a)[77b] vai "*push-pull*" purīna atvasinājumu (b).[27]

2.1. Fluorescentu purīnu atvasinājumu fotofizikālās īpašības

Organiskas "*push-pull*" fluorescentas sistēmas sastāv no elektronu donora un akceptora, kas ir savienoti ar π sistēmas konjugētu tiltu. Pievadot šādai molekulai enerģiju, piemēram, ar UV starojumu, tā tiek ierosināta. Ierosinātā stāvoklī elektrons no augstākās aizņemtās molekulārās orbitāles (*HOMO*), kas atrodas uz elektrona donora un tā tuvumā, ir pārvietojies uz zemāko neaizņemto molekulāro orbitāli (*LUMO*), kas atrodas uz elektrona akceptora un tā tuvumā. Ierosinātais elektrons ir ar pretēju spinu nekā otram šī pāra elektronam, tas ir, singleta stāvoklī. Lai atgrieztos pamatstāvoklī, ierosinātā sistēma atdod enerģiju videi fotona veidā – notiek fluorescence. Ja molekulu, kurai ir iespējama fluorescence, ierosina ar elektrību, veidojas gan singleta, gan tripleta ierosinātie stāvokļi. Šādā gadījumā emisija notiek tikai no singleta stāvokļiem, savukārt tripleta stāvokļi atdod videi enerģiju, visbiežāk siltuma veidā, un arī atgriežas pamatstāvoklī (4. att.).[78] Ierosināta stāvokļa ģeometrija var atšķirties no pamatstāvokļa. Ierosinātais stāvoklis var izgriezties no sākotnēji planāra stāvokļa un notikt fluorescence pēc izgriezta iekšmolekulāra lādiņa pārneses (*TICT*) mehānisma.[79] Pretējā gadījumā sākotnēji neplanāra struktūra ierosinātā stāvoklī var kļūt vairāk planāra un fluorescence notiek pēc planāra iekšmolekulāra lādiņa pārneses (*PICT*) mehānisma, kam ir raksturīga augsta Stoksa nobīde.[80] "*Push-pull*" sistēmas fluorescences kvantu iznākumu, fluorescences laiku, Stoksa nobīdi un citas fotofizikālās īpašības var izmainīt, modificējot elektronu donoru, akceptoru vai π sistēmas konjugēto tiltu.[78] Slāpekli saturoši heterocikli ir plaši apskatīti kā elektronu akceptori šādās "*push-pull*" sistēmās.[81]

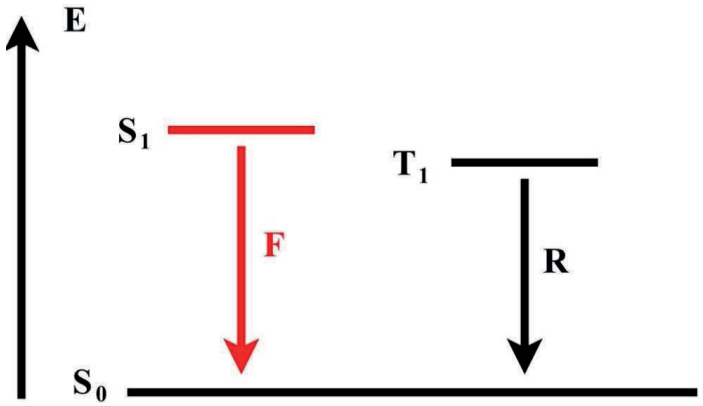

4. att. Ar elektrību ierosinātas fluorescences shematisks atspoguļojums – fluorescence (F) no singleta stāvokļa un bezstarojuma relaksācija (R) no tripleta stāvokļa.

1.2. apakšnodaļā sintezētajiem purīna atvasinājumiem tika izmērītas fotofizikālās īpašības un veikti izmēģinājumi lietojumam *OLED*. Tika apskatīta savienojumu absorbcija, emisija, kvantu iznākumi, enerģijas līmeņi un citi dati.

Iegūtie savienojumi **28a-d**, **29a-d**, **36a**,**b** un **41a** satur trifenilmetilgrupas, kas veicina amorfās īpašības,[61] lai tos varētu iekārtās uzklāt ar šķīdumu metodēm, kas ir vieglāk realizējamas nekā uznešana ar vakuumu. Izmēģinājumi ar minētajiem savienojumiem parādīja, ka šie savienojumi patiešām veido plānu amorfu slāni uz stikla, uzklājot no šķīduma. *DSC* mērījumi ar savienojumiem **28a**,**d** un **29a**,**b**,**d** parādīja, ka tie ir amorfi ar stiklošanās temperatūrām 82–102 °C. Cianogrupu saturošiem savienojumiem ir raksturīga augstāka stiklošanās temperatūra. Termogravimetriskā analīze savienojumiem **28d** un **29d** parāda, ka 2-amino-6-triazolilpurīni **28** ir termiski stabilāki par 6-amino-2-triazolilpurīniem **29**, jo sadalīšanās temperatūras ir attiecīgi 298 °C un 258 °C.

Iegūtie "*push-pull*" purīna atvasinājumi **28a-d**, **29a-d**, **36a**,**b** un **41a**,**c** ir fluorescenti, un atkarībā no azola un piperidīna izvietojuma purīna *C*(2) un *C*(6) pozīcijās izteikti mainās to absorbcijas un emisijas spektru maksimumu izvietojums. Savienojumiem **28a-d** zemākās enerģijas absorbcijas maksimums, kas atbilst iekšmolekulārai lādiņu pārnesei, atrodas ap 365 nm (5. att.), savienojumiem **29a-d** šis maksimums atrodas ap 305 nm (6. att.). Savienojumiem **28a**,**b**,**d** emisijas maksimums atrodas 440–450 nm, savienojumiem **29a**,**b**,**d** tas atrodas tuvajā UV reģionā 390–400 nm. Izņēmumi ir dimetilaminogrupu saturošie purīna atvasinājumi **28c** un **29c**, kuru emisijas maksimumi ir nobīdīti batohromi par aptuveni 60 nm, salīdzinot ar pārējiem atvasinājumiem. Tas tika skaidrots ar izteiktu solvatohromiju, kas ir raksturīga dimetilaminogrupu saturošiem savienojumiem.[82] Savienojumu **36a**,**b** un **41a**,**c** absorbcijas un emisijas spektri minimāli atšķiras no analoģisko savienojumu **29a**,**b**,**d** spektriem. Savienojuma **41c** gadījumā absorbcijas spektrā tika novērota arī karbazolam raksturīga absorbcija, kā arī daži maksimumi emisijas spektrā, kas attiecās uz karbazolu (4. tab.). Mērījumi savienojumiem **28a** un **29a** parādīja, ka abiem reģioizomēriem ir raksturīga pozitīva solvatohromija.

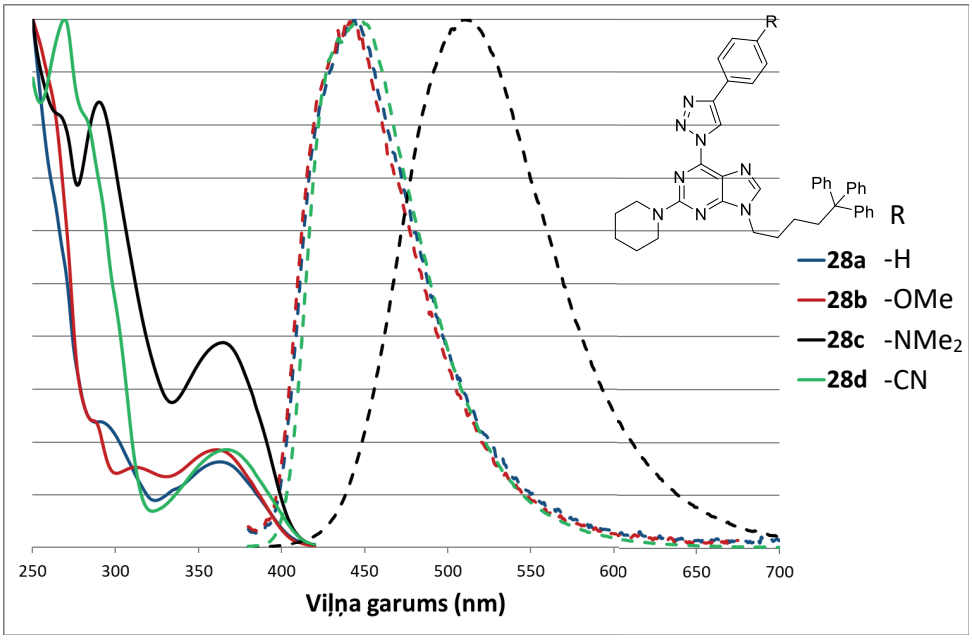

5. att. 2-Amino-6-triazolilpurīnu **28a-d** normalizēti absorbcijas(—) un emisijas(- -) spektri DCM šķīdumā.

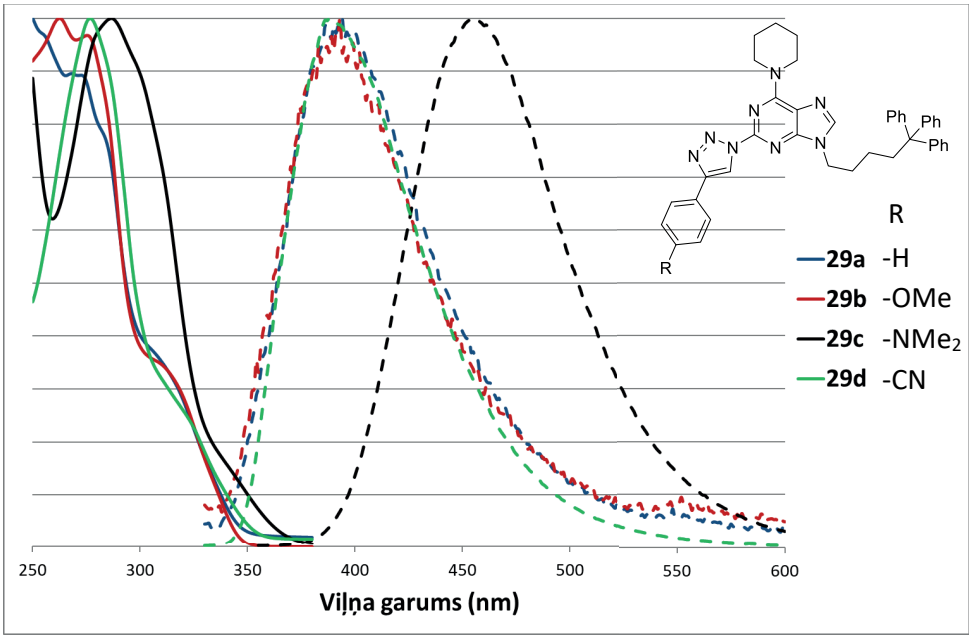

6. att. 6-Amino-2-triazolilpurīnu **29a-d** normalizēti absorbcijas(—) un emisijas(- -) spektri DCM šķīdumā.

4. tabula

Purīna atvasinājumu absorbcijas, emisijas un kvantu iznākumu eksperimentālie dati

Nr.	Savienojums	$\lambda_{abs\ max}$, (nm)*	$\lambda_{em\ max}$, (nm)*	Φ_{FL} (DCM)	Φ_{FL} (plānā kārtiņa)
1.	**28a**	364	446	0,91	0,32
2.	**28b**	360	439	0,78	0,28
3.	**28c**	365	511	0,74	0,03
4.	**28d**	367	448	0,90	0,40
5.	**29a**	320 (plecs)	394	0,31	0,22
6.	**29b**	320 (plecs)	399	0,17	0,15
7.	**29c**	330 (plecs)	455	0,30	0,03
8.	**29d**	330 (plecs)	388	0,44	0,20
9.	**36a**	305 (plecs)	356	0,01	0,12
10.	**36b**	300 (plecs)	373	0,07	0,45
11.	**41a**	310 (plecs)	398	0,66	0,42
12.	**41c**	292, 323, 338	362, 378, 397	0,51	0,20

*Mērīts $5 \cdot 10^{-5}$ M DCM šķīdumā.

Fluorescentajiem savienojumiem DCM šķīdumā un plānā kārtiņā tika noteikti kvantu iznākumi, ko varēja paveikt amorfo īpašību dēļ. Savienojumi **28a-d**, **29a-d** un **41a**,**c** deva sagaidāmus rezultātus – fluorescences kvantu iznākums šķīdumā sasniedza pat 91%, bet plānā kārtiņā bija ievērojami mazāks, jo šķīdumā molekulas ir savstarpēji izolētas un nenotiek fluorescences dzēšana. Savienojumiem **36a**,**b** tika novērots pretējs efekts – fluorescences kvantu iznākums izteikti pieaug plānā kārtiņā. To var izskaidrot ar aromātisko gredzenu rotāciju šķīdumā, kas dzēš fluorescenci, bet tiek novērsta cietā fāzē. 2-Amino-6-triazolilpurīniem **28a-d** šķīdumā tika novēroti vidēji augstāki kvantu iznākumi nekā 6-amino-2-triazolilpurīniem **29a-d**, taču šiem savienojumiem arī tika novērots lielāks kvantu iznākuma kritums, pārejot uz cieto fāzi plānā kārtiņā (4. tab.).

Savienojumiem **28a-d** un **29a-d** tika noteikta jonizācijas enerģija un fotovadītspējas slieksnis, no kā tika izrēķināta afinitātes enerģija (A. Vembris, CFI). Mērījumos noskaidrojās, ka jonizācijas enerģija gandrīz nemainās atkarībā no aizvietotāju izvietojuma *C*(2) un *C*(6) pozīcijās, bet mainās atkarībā no donora vai akceptora aizvietotāja pie feniltriazola. Fotovadītspējas slieksnis mainās gan atkarībā no aizvietotāju izvietojuma, gan donorā vai akceptorā aizvietotāja klātbūtnes. Šīs vērtības ir izteikti augstākas 6-amino-2-triazolilpurīniem **29a-d** (3.07–3.45 eV), salīdzinot ar apgrieztajiem reģioizomēriem **28a-d** (2,75–2,95 eV).

Šiem savienojumiem tika noteikti arī tripletu enerģijas līmeņi, kas ir svarīgi tādam potenciālam lietojumam kā OLED aktīvās matricas. Savienojumiem **28a-d** tripletu līmeņu vērtības ir 2,52–2,54 eV, savienojumiem **29a**,**b**,**d** – 2,87–2,95 eV, savienojumam **29c** – 2,75 eV. Savienojumu **29** īpašības ir atbilstošas teorētiskajam lietojumam aktīvo matricu materiālos zili fosforescējošiem emiteriem.

DFT aprēķini parādīja, ka neitrālu vai elektronakceptoru aizvietotāju gadījumā pie feniltriazola savienojumiem **28a**,**d** *HOMO* orbitāles ir centrētas uz purīna, *LUMO* ir centrētas uz feniltriazola, savukārt **29a**,**d** *HOMO* un *LUMO* orbitāles ir delokalizētas pa visu konjugēto

sistēmu. Šis izkārtojums liecina par izteiktāku "*push-pull*" raksturu savienojumiem **29a**,**d**, kā arī zemāku tieksmi ierosinātam stāvoklim relaksēties bez emisijas. Elektrondonoru aizvietotāju gadījumā pie triazola savienojumiem **28b**,**c** un **29b**,**c** *HOMO* orbitāles ir centrētas uz feniltriazola, *LUMO* orbitāles – uz purīna.

Purīna atvasinājumi **28a**,**d** un **29a**,**d** tika izmēģināti kā emiteri *OLED*, jo tie uzrādīja augstākos kvantu iznākumus. Savienojums **29b** tika izmēģināts kā aktīvo matricu materiāls *OLED* ar FIrpic emiteri, jo tam bija augstākā tripletu enerģija. Emiteru gadījumā netika novērota elektroluminescence, savukārt eksperimentā ar purīna atvasinājumu kā *OLED* aktīvās matricas materiālu, kāpinot spriegumu, ierīces efektivitāte strauji kritās, salīdzinot ar kontrolekspērimentu, kurā aktīvā matrica ir polivinilkarbazols (PVK). Šos rezultātus var izskaidrot ar augstu strāvas blīvumu *OLED*, izmantojot purīna atvasinājumus iekārtā. Augsto lādiņu vadītspēju var izskaidrot ar iegūto atvasinājumu planāro struktūru un dipolo dabu, iegūtos savienojumus iespējams nākotnē izmantot kā organiskos lauka efekta tranzistorus.

Organisko lauka efekta tranzistoru izpēte ir pētījumu virziens, kas mēģina aizstāt neorganisko amorfo silīciju pusvadītājos. Izmantojot mazmolekulārus savienojumus vai polimērus, var iegūt ar šķīduma metodēm veidojamu lokanu elektroniku. Šādiem materiāliem viens no svarīgākajiem parametriem ir lādiņu vadītspēja, kas nodrošina energoefektivitāti, darbību ierīcēs ar zemu enerģijas padevi un stabilu ierīces temperatūru. Šādas ierīces var konstruēt divos veidos – ar aizvara elektrodu virs pārējiem slāņiem vai zem tiem (7. att.). Ja aizvara elektrods atrodas virs pārējiem slāņiem, tad kā pamatne tiek izmantots polimēra substrāts, pretējā gadījumā kā pamatne var kalpot aizvara elektrods. Pārējie struktūrelementi ir izteces un noteces elektrodi, organisks pusvadītājs un izolators. [83]

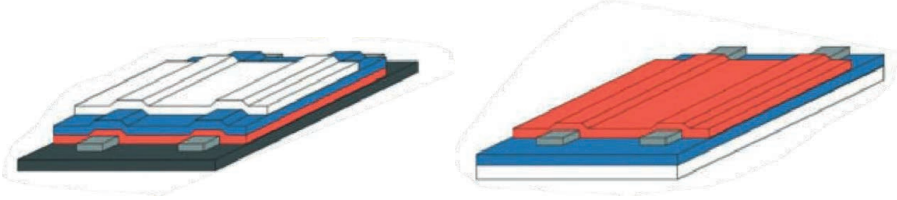

7. att. Organiskā lauka efekta tranzistoru shematisks atspoguļojums ar aizvara elektrodu virspusē (pa kreisi) un apakšā (pa labi). Polimēra substrāts (melns), izteces un noteces elektrodi (pelēki), organisks pusvadītājs (oranžs), izolators (zils), aizvara elektrods (balts).[83]

Oriģinālpublikācijas par šajā apakšnodaļā aprakstītajiem pētījumiem – 2. un 4. pielikumā.

2.2. Termiski aktivēta aizkavētā fluorescence purīnu atvasinājumos

Sākotnējie *OLED* ar fluorescentiem emiteriem spēj lietderīgi izmantot tikai 25% pievadītās enerģijas, jo, izmantojot elektrību, tikai ceturtdaļa ierosināto molekulu ir singleta stāvoklī, kas ir spējīgas emitēt gaismu, savukārt pārējās ir tripleta stāvoklī, un enerģija netiek lietderīgi izmantota. Šo situāciju uzlaboja fosforescenti metālu kompleksi, kas spēj izmantot visu pievadīto enerģiju, taču šajos kompleksos tiek izmantoti dārgi un izsīkstoši pārejas metāli – visbiežāk irīdijs, dažkārt platīns, kuru lietojumu cenšas mazināt. Termiski aktivēta aizkavētā fluorescence (*TADF*) ir pētījumu joma, kas ir attīstījusies pēdējā desmitgadē un var potenciāli

aizstāt fosforescentus pārejas metālu kompleksus. *TADF* apskata savienojumus, kas spēj realizēt visu pievadīto enerģiju, izmantojot apgrieztu starpsistēmu pāreju (*RISC*), kurā ierosināta molekula pāriet no tripleta stāvokļa uz singletu. Šādā gadījumā molekulas, kas ir sākotnēji ierosinātas singleta stāvoklī, rada fluorescenci (F), savukārt molekulas no sākotnēja tripleta stāvokļa caur *RISC* nonāk singleta stāvoklī un veido aizkavēto fluorescenci (*DF*) (8. att.).[84]

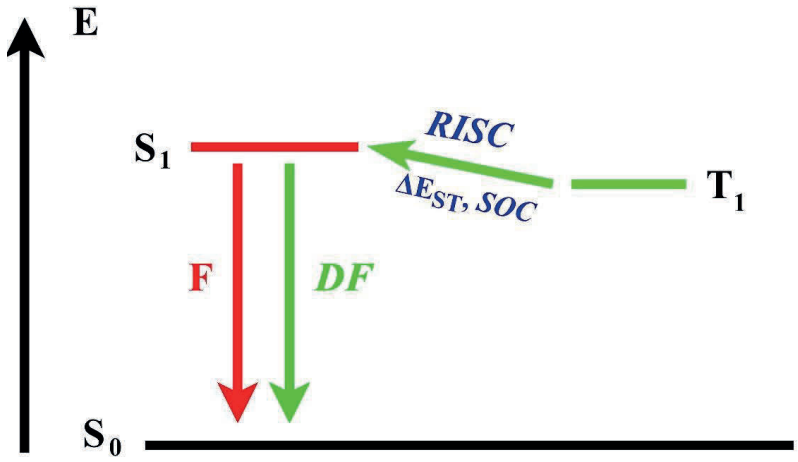

8. att. *TADF* emisijas shematisks atspoguļojums.

Lai *RISC* process varētu notikt, spina-orbītas sadarbības (*SOC*) vērtībai jābūt pēc iespējas augstākai, savukārt starpībai starp singleta un tripleta līmeņiem (ΔE_{ST}) ir jābūt pietiekami zemai. Augstāku *SOC* var sasniegt struktūrās, kas satur smagos atomus. Zemu ΔE_{ST} panāk, samazinot *HOMO* un *LUMO* orbitāļu pārklāšanos. Molekulās ar kovalenti saistītiem donoru-akceptoru pāriem to panāk ar stēriskiem traucējumiem, kas pārtrauc konjugāciju starp donoru un akceptoru. Cita alternatīva ir eksipleksu sistēmu izmantošana ar atsevišķām donora un akceptora komponentēm[84] (9. att.). Šādus savienojumus var modificēt, lai iegūtu vajadzīgās fizikālās īpašības, iekļaujot aktīvo komponenti polimēros vai dendrimēros, lai tos varētu izmantot *OLED* izgatavošanai ar šķīdumu metodi.[85] Purīna gredzenam ir raksturīgs ātrs starpsistēmu pārejas process[70] ar augstu tripletu kvantu iznākumu,[69] kas ir atbilstoši parametri *TADF* sistēmu izpētei. Karbazols ir plaši izmantots kā elektronu donors *TADF* emiteros un *OLED* aktīvās matricās, pateicoties tā augstajai stabilitātei, labai caurumu vadītspējai un tripleta enerģijas līmeņiem, kas ir augstāki nekā fluorēnam vai bifenilam.[86]

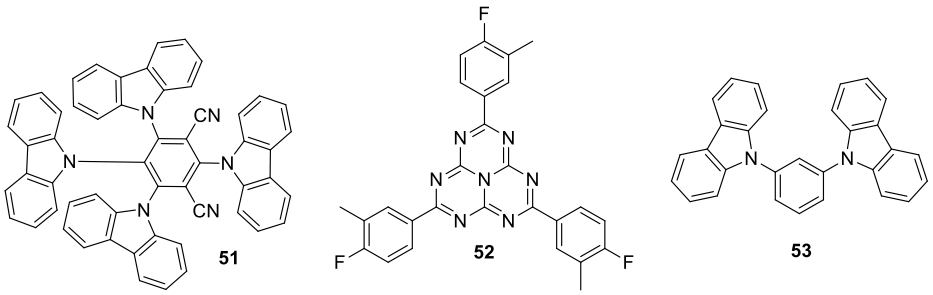

9. att. Stēriski traucētu savienojuma **51** un eksipleksu pāra **52** + **53** piemēri, kuriem ir iespējams *RISC*.[84a]

Pētījumi tika veikti ar 6-ciano-9-fenilpurīnu (**24a**), jo cianogrupa samazina purīna elektronu afinitāti, savukārt fenilgrupa novērš *N*(9)-*N*(7) tautomerizāciju. Mērījumi savienojumam parādīja vāju fluorescenci, toties izteiktu fosforescenci pie 77 K temperatūras, kas liecina par tripleta stāvoklī esošu molekulu klātbūtni pietiekamā daudzumā, kas atbilst enerģijas līmeņu teorētiskajos aprēķinos atrastajam.

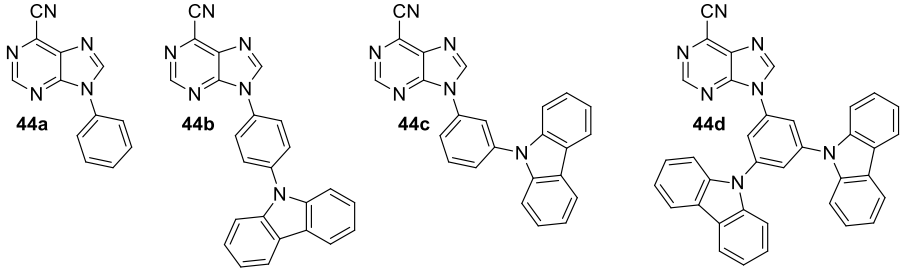

10. att. 6-Cianopurīna komponente **44a** un kovalenti saistītie konjugāti **44b-d**.

Savienojums **44a** tika izmēģināts eksipleksu sistēmā ar PVK un 9-fenilkarbazolu (9-PhCbz) šo donoru atbilstošo enerģijas līmeņu dēļ. Fiziskiem maisījumiem var rasties tehniskas problēmas ar molekulu sakārtojumu, kā rezultātā eksipleksu pāru veidošanās ir mazāk ticama. Alternatīva ir kovalenti saistīti eksipleksu pāri, kuros lādiņu pārneses process nevar notikt iekšmolekulāri. Tika iegūti savienojumi **44b-d** (10. att.), kuros cianopurīns un karbazols ir savienots caur benzola gredzenu, kas ir izgriezts ārpus plaknes. Stēriski traucēts aromātisks fragments traucē π-elektronu sistēmu konjugācijai, gan kopumā strādā kā donora-donora'-akceptora sistēma,[87] kas neļauj notikt iekšmolekulāram procesam. Iegūtā savienojuma **44b** rentgenstruktūra parāda, ka purīns un karbazols ir koplanāri, savukārt benzola gredzens ir par 50° izgriezts no plaknes (11. att.).

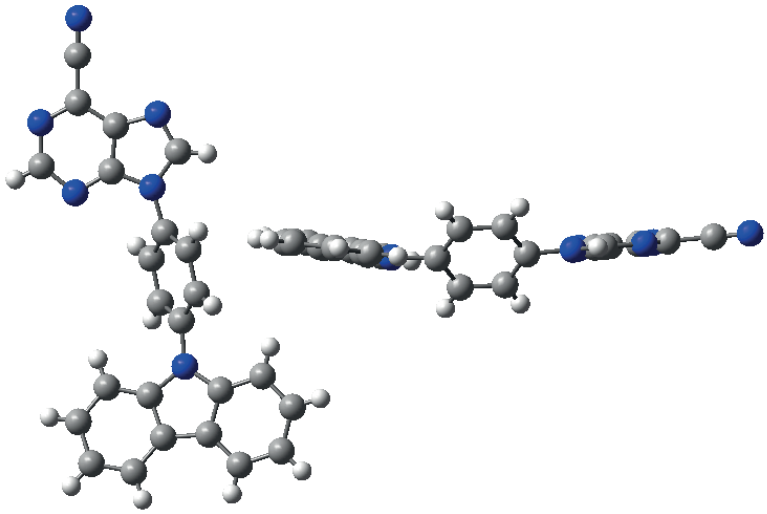

11. att. Savienojuma **44b** XRD struktūra divās projekcijās ar benzola gredzenu ārpus plaknes.

Nesaistītā purīna un karbazola maisījumam šķīdumā novēroja karbazola emisijas dzēšanu, kas liecina par ierosinātā stāvokļa pārnesi no karbazola uz purīnu. Kovalenti saistītajiem **44b-d** istabas temperatūrā tika novērota vāja fluorescence, bet 77 K temperatūrā savienojumiem **44c**,**d** fosforescence ir vairākas reizes intensīvāka par fluorescenci, kas liecina par starpmolekulāru procesu. Savukārt iekšmolekulāro procesu nomāc izjauktā konjugācija. Šādu novērojumu pamato arī absorbcijas spektri, kas kovalenti saistītajiem savienojumiem ir veidoti no savienojuma **44a** un karbazola komponenšu summas bez papildu absorbcijas joslas kopējai sistēmai. Savienojumam **44b** 77 K tika novērota salīdzināmas intensitātes fluorescence un fosforescence, kas liecina par paaugstinātu iekšmolekulārā procesa varbūtību.

Mērījumi plānā kārtiņā (5. tab.) parādīja, ka emisija notiek no eksipleksiem 473–528 nm reģionā ar kvantu iznākumu līdz pat 41% un skābekļa klātbūtnē tiek novērota emisijas dzēšana. Temperatūras pazemināšana diapazonā 300–77 K veicina kvantu iznākuma pieaugumu lielākajā diapazona daļā. Šis novērojums ir pretrunā ar sagaidāmo rezultātu *TADF*, taču tika izskaidrots ar tripleta stāvokļa paaugstinātu stabilitāti zemās temperatūrās, kas ir svarīgi ierosinātā stāvokļa relaksācijā. Šī sakarība nav lineāra, un *TADF* efekts tika novērots ar kvantu iznākuma lokālu maksimumu 100–180 K. Fotoluminescence sastāv no vairākām dažāda ilguma komponentēm, kas ir raksturīgi eksipleksu sistēmām. Ātrākā komponente paraugos ir 31–55 ns, kas ir lēnāk nekā tipiska fluorescence, tātad tika novērota aizkavēta emisija. Zemās temperatūrās ātrākā komponente tiek ietekmēta maz, savukārt nākamā komponente tiek paildzināta apmēram par 80 ns, kas ir raksturīgi *TADF*. Ātrākā un lēnākā komponente veidojas pēc dažādiem mehānismiem, kas ir sagaidāms eksipleksu sistēmās, jo attālums starp donoro un akceptoro komponenti ir mainīgs. Divkomponentu sistēmās attiecību starp lēnāko un ātrāko komponenti iespējams ietekmēt, izmainot donora-akceptora daudzuma attiecību. Eksperimenti ar **44c** polimetilmetakrilāta matricā dažādās koncentrācijas parādīja emisijas nobīdi uz zilo reģionu un kvantu iznākuma samazināšanos, pieaugot **44c** atšķaidījumam.

5. tabula

Eksipleksu sistēmu fotofizikālās īpašības plānā kārtiņā

Nr.	Sistēma	λ_{FL}, (nm)[a]	Φ_{FL}	t, (ns)	t, (%)[b]	E_S, (eV)[c]	E_T, (eV)[d]	ΔE_{ST}, (eV)[e]
1.	**44a**/ 9-PhCbz (1:1)	473	0,25	49	21	2,98	2,95	0,03
				137	56			
				682	16			
2.	**44a**/ PVK (1:1)	528	0,08	31	12	2,81	2,95	–0,14
				140	56			
				692	32			
3.	**44b**	501	0,17	34	21	2,97	2,92	0,05
				149	79			
4.	**44c**	502	0,41	54	39	2,82	2,94	–0,12
				246	61			
5.	**44d**	497	0,13	55	27	2,85	2,94	–0,09
				183	73			

[a] Emisijas maksimums.

[b] Fotoluminescences komponenšu procentuāls sadalījums.

[c] Fluorescences aktivācijas enerģija istabas temperatūrā.

[d] Fosforescences aktivācijas enerģija 77 K.

[e] $\Delta E_{ST} = E_S - E_T$.

Kovalenti saistītām *TADF* molekulām var būt dažādi emisijas mehānismi atkarībā no cietās fāzes morfoloģijas.[88] Mērījumos ar savienojumu **44c** tika noskaidrots, ka amorfā fāzē notiek iepriekš apskatītā *TADF* emisija, savukārt kristāliskā fāzē notiek fluorescence ar emisijas maksimumu 471 nm, kvantu iznākumu 52%. Emisijas mehānisma izmaiņa kristāliskā fāzē tiek skaidrota ar stiprāku donora-akceptora konjugāciju, ko veicina konformācijas fiksēšana kristāliskajā režģī.

Iegūtie purīna atvasinājumi ir atbilstošāki *OLED* aktīvās matricas lomai, jo to fotoluminescence dzēšas, pieaugot temperatūrai. *OLED* izmēģinājumi tika veikti ar savienojumu **44d**, jo tas uzrādīja labāko lādiņu mobilitāti. Tika iegūts *OLED* ar zaļo *TADF* DAcIPN emiteri ar **44d** kā aktīvo matricu ar maksimālo ārējo kvantu iznākumu 11,6% un spožumu virs 50000 cd/m^2. Izmantojot zemu emitera koncentrāciju (5%), tika novērota nepilnīga enerģijas pārnese uz emiteri. *OLED* ar aktīvo matricu **44d** parādīja augstākus ārējos kvantu iznākumus nekā iepriekš publicētos rezultātos ar zināmām aktīvām matricām.[89]

Oriģinālpublikācija par šajā apakšnodaļā aprakstītajiem pētījumiem – 3. pielikumā.

SECINĀJUMI

1. Izmantojot azīda-tetrazola līdzsvaru, pie 2,6-diazidopurīna mazāk reaģētspējīgā atoma *C*(2) pozīcijā ir iespējams veikt S_NAr reakciju ar amīniem.

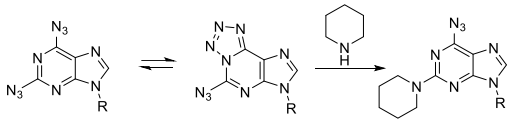

2. Trifenilmetilgrupas saturošu aizvietotāju izmantošana veicina amorfas īpašības savienojumiem un ļauj izveidot purīnu atvasinājumu paraugus amorfās plānās kārtiņās, izmantojot savienojuma šķīdumu.

3. Imidazolu, 1-1*H*-1,2,4-triazolu, 1-1*H*-1,2,3-triazolu un 2-2*H*-1,2,3-triazolu var ievadīt pie purīna atoma *C*(2) pozīcijā, izmantojot S_NAr reakciju 160 °C temperatūrā.

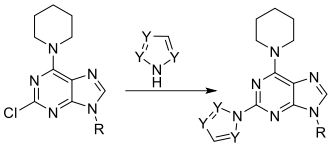

4. Aromātiskos aizvietotājus var ievadīt pie purīna slāpekļa atoma *N*(9) pozīcijā, izmantojot diariljodānus vai Čana–Lama reakcijas apstākļus.

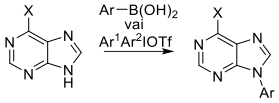

5. *N*(7) Arilpurīnus ar augstiem iznākumiem var iegūt no aizvietotiem 5-aminopirimidīniem *de novo* sintēzē.

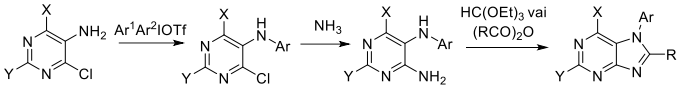

6. 2/6-Amino-2/6-azolilpurīni, atkarībā no aizvietotāju izvietojuma *C*(2) un *C*(6) pozīcijās, fluorescē ar emisijas maksimumu ap 390 nm vai 450 nm. Kvantu iznākumi sasniedz 91% šķīdumā un 45% plānā kārtiņā. Šādiem savienojumiem ir potenciāls lietojums kā organiskiem lauka efekta tranzistoriem.

7. Gan kovalenti saistītiem purīna-karbazola eksipleksiem, gan to analogu maisījumiem piemīt *TADF* īpašības. Šādi savienojumi un to maisījumi izrāda eksipleksiem raksturīgu dažāda ilguma emisiju ar maksimumu ap 500 nm. Emisijas efektivitāti dažādās temperatūrās nosaka tripleta stāvokļa stabilitāte un *TADF* efekts. Kvantu iznākumi galaproduktos sasniedz 41% plānā kārtiņā. Šādiem savienojumiem ir potenciāls lietojums kā aktīvām matricām *OLED*.

LITERATŪRAS SARAKSTS

1. Seley-Radtke, K. L.; Yates, M. K. *Antiviral Res.* **2018**, *154*, 66.
2. Saito, Y.; Hudson, R. H. E. *J. Photochem. PhotoBiol. C: Photochem. Rev.* **2018**, *36*, 48.
3. Tang, C. W.; VanSlyke, S. A. *Appl. Phys. Lett.* **1987**, *51*, 913.
4. Jou, J.-H.; Kumar, S.; Jou, Y. C. In *Disruptive characteristics and lifetime issues of OLEDs*, Buckley, A., Ed.; Woodhead Publishing, United Kingdom, 2013; pp. 410–442.
5. (a) Jou, J.-H.; Sahoo, S.; Dubey, D. K.; Yadav, R. A. K.; Swayamprabha, S. S.; Chavhan, S. D. *J. Mater. Chem. C* **2018**, *6*, 11492. (b) Chen, H.-W.; Lee, J.-H.; Lin, B.-Y.; Chen, S.; Wu, S. T. *Light Sci. Appl.* **2018**, *7*, 17168.
6. Collier, G. S.; Brown, L. A.; Boone, E. S.; Kaushal, M.; Ericson, M. N.; Walter, M. G.; Long, B. K.; Kilbey II, S. M. *J. Mater. Chem. C* **2017**, *5*, 6891.
7. (a) Butler, R. S.; Cohn, P.; Tenzel, P.; Abboud, K. A.; Castellano, R. K. *J. Am. Chem. Soc.* **2009**, *131*, 623. (b) Yang, Y.; Cohn, P.; Dyer, A. L.; Eom, S.-H.; Reynolds, J. R.; Castellano, R. K.; Xue, J. *Chem. Mater.* **2010**, *22*, 3580. (c) Yang, Y.; Cohn, P.; Eom, S.-H.; Abboud, K. A.; Castellano, R. K.; Xue, J. *J. Mater. Chem. C* **2013**, *1*, 2867.
8. Lorenzo-Aparicio, C.; Gallego, M. R.; de Arellano, C. R.; Sierra, M. A. *Dalton Trans*. **2022**, *51*, 5138.
9. (a) Wang, Z.; Yao, J.; Zhan, L.; Gong, S.; Ma, D.; Yang, C. *Dyes Pigm.* **2020**, *180*, 108437. (b) Wu, Y.; Zhang, Y.; Ran, C.; Lan, J.; Bin, Z.; You, J. *Org. Lett.* **2021**, *23*, 3839.
10. Rosemeyer, H. *Chem. Biodivers.* **2004**, *1*, 361.
11. Cīrule, D.; Ozols, K.; Platnieks, O.; Bizdēna, Ē.; Māliņa, I.; Turks, M. *Tetrahedron* **2016**, *72*, 4177.
12. Singh, B.; Diaz-Gonzalez, R.; Ceballos-Perez, G.; Rojas-Barros, D. I.; Gunaganti, N.; Gillingwater, K.; Martinez-Martinez, M. S.; Manzano, P.; Navarro, M.; Pollastri, M. P. *J. Med. Chem.* **2020**, *63*, 9912.
13. Malínková, V.; Řezníčková, E.; Jorda, R.; Gucký, T.; Kryštof, V. *Bioorg. Med. Chem.* **2017**, *25*, 6523.
14. Novosjolova, I.; Bizdēna, Ē.; Turks, M. *Eur. J. Org. Chem.* **2015**, *2015*, 3629.
15. Zaķis, J. M.; Ozols, K.; Novosjolova, I.; Vilšķērsts, R.; Mishnev, A.; Turks, M. *J. Org. Chem.* **2020**, *85*, 4753.
16. Kania, J.; Gundersen, L.-L. *Eur. J. Org. Chem.* **2013**, *2013*, 2008.
17. Guo, H.-M.; Xin, P.-Y.; Niu, H.-Y.; Wang, D.-C.; Jiang, Y.; Qu, G.-R. *Green Chem.* **2010**, *12*, 2131.
18. Qu, G.-R.; Mao, Z.-J.; Niu, H.-Y.; Wang, D.-C.; Xia, C.; Guo, H.-M. *Org. Lett.* **2009**, *11*, 1745.
19. Parmar, U.; Somvanshi, D.; Kori, S.; Desai, A. A.; Dandela, R.; Maity, D. K.; Kapdi, A. R. *J. Org. Chem.* **2021**, *86*, 8900.
20. Frieden, M.; Aviñó, A.; Eritja, R. *Nucleosides Nucleotides Nucleic Acids* **2003**, *22*, 193.
21. Cīrule, D.; Novosjolova, I.; Bizdēna, Ē.; Turks, M.; *Beilstein J. Org. Chem.* **2021**, *17*, 410.
22. (a) Hocek, M. *Eur. J. Org. Chem.* **2003**, *2003*, 245. (b) Čerňa, I.; Pohl, R.; Klepetářová, B.; Hocek, M. *J. Org. Chem.* **2008**, *73*, 9048. (c) Liu, J.; Robins, M. J. *Org. Lett.* **2004**, *6*, 3421.

23. Wang, D.-C.; Niu, H.-Y.; Qu, G.-R.; Liang, L.; Wei, X.-J.; Zhang, Y.; Guo, H. M. *Org. Biomol. Chem.* **2011**, *9*, 7663.
24. Bhanu Prasad, A. S.; Stevenson, T. M.; Citineni, J. R.; Nyzam, V.; Knochel, P. *Tetrahedron* **1997**, *53*, 7237.
25. Elzein, E.; Palle, V.; Wu, Y.; Maa, T.; Zeng, D.; Zablocki, J. *J. Med. Chem.* **2004**, *47*, 4766.
26. Hocek, M.; Pohl, R.; Císařová, I. *Eur. J. Org. Chem.* **2005**, *2005*, 3026.
27. Šišuļins, A.; Bucevičius, J.; Tseng, Y.-T.; Novosjolova, I.; Traskovskis, K.; Bizdēna, Ē.; Chang, H.-T.; Tumkevičius, S.; Turks, M. *Beilstein J. Org. Chem.* **2019**, *15*, 474.
28. Mahajan, T. R.; Ytre-Arne, M. E.; Strøm-Andersen, P.; Dalhus, B.; Gundersen, L.-L. *Molecules*, **2015**, *20*, 15944.
29. (a) Niu, H.-Y.; Xia, C.; Qu, G.-R.; Zhang, Q.; Jiang, Y.; Mao, R.-Z.; Li, D.-Y.; Guo, H.-M. *Org. Biomol. Chem.* **2011**, *9*, 5039. (b) Csenki, J. T.; Mészáros, Á.; Gonda, Z.; Novák, Z. *Chem. Eur. J.* **2021**, *27*, 15638.
30. Abdoli, M.; Mirjafary, Z.; Saeidian, H.; Kakanejadifard, A. *RSC Adv.* **2015**, *5*, 44371.
31. Traskovskis, K.; Mihailovs, I.; Tokmakovs, A.; Jurgis, A.; Kokars, V.; Rutkis, M. *J. Mater. Chem.* **2012**, *22*, 11268.
32. Tobrman, T.; Štěpnička, P.; Císařová, I.; Dvořák, D. *Eur. J. Org. Chem.* **2008**, *2008*, 2167.
33. Tobrman, T.; Dvořák, D. *Collect. Czech. Chem. Commun.* **2007**, *72*, 1365.
34. Isobe, Y.; Kurimoto, A.; Tobe, M.; Hashimoto, K.; Nakamura, T.; Norimura, K.; Ogita, H.; Takaku, H. *J. Med. Chem.* **2006**, *49*, 2088.
35. Carrera, D.; Angelaud, R.; Sheng, P.; Safina, B.; Li, J. *Org. Process Res. Dev.* **2013**, *17*, 138.
36. Kurimoto, A.; Ogino, T.; Ichii, S.; Isobe, Y.; Tobe, M.; Ogita, H.; Takaku, H.; Sajiki, H.; Hirota, K.; Kawakami, H. *Bioorg. Med. Chem.* **2004**, *12*, 1091.
37. Crestey, F.; Zimdars, S.; Knochel, P. *Synthesis* **2013**, *45*, 3029.
38. Stokes, S. S.; Huynh, H.; Gowravaram, M.; Albert, R.; Cavero-Tomas, M.; Chen, B.; Harang, J.; Loch III, J. T.; Lu, M.; Mullen, G. B.; Zhao, S.; Liu, C.-F.; Mills, S. D. *Bioorg. Med. Chem. Lett.* **2011**, *21*, 4556.
39. Pohl, R.; Hocek, M. *Synthesis* **2004**, *17*, 2869.
40. Hocek, M.; Votruba, I.; Dvořáková, H. *Tetrahedron* **2003**, *59*, 607.
41. Nicolaou, K. C.; Ellery, S. P.; Rivas, F.; Saye, K.; Rogers, E.; Workinger, T. J.; Schallenberger, M.; Tawatao, R.; Montero, A.; Hessell, A.; Romesberg, F.; Carson, D.; Burton, D. *Bioorg. Med. Chem.* **2011**, *19*, 5648.
42. Havelková, M.; Dvořák, D.; Hocek, M. *Synthesis*, **2001**, *11*, 1704.
43. Costanzi, S.; Tikhonova, I. G.; Ohno, M.; Roh, E. J.; Joshi, B. V.; Colson, A.-O.; Houston, D.; Maddileti, S.; Harden, T. K.; Jacobson, K. A. *J. Med. Chem.* **2007**, *50*, 3229.
44. Ibrahim, N.; Chevot, F.; Legraverend, M. *Tetrahedron Lett.* **2011**, *52*, 305.
45. Langli, G.; Gundersen, L.-L.; Rise, F. *Tetrahedron* **1996**, *52*, 5625.
46. Borrmann, T.; Abdelrahman, A.; Volpini, R.; Lambertucci, Alksnis, E.; Gorzalka, S.; Knospe, M.; Schiedel, A. C.; Cristalli, G.; Müller, C. E. *J. Med. Chem.* **2009**, *52*, 5974.

47. (a) Laufer, S. A.; Domeyer, D. M.; Scior, T. R. F.; Albrecht, W.; Hauser, D. R. J. *J. Med. Chem.* **2005**, *48*, 710. (b) Bilbao, N.; Vázquez-González, V.; Aranda, M. T.; González-Rodríguez, D. *Eur. J. Org. Chem.* **2015**, *2015*, 7160.
48. Mahajan, T. R.; Gundersen, L.-L. *Tetrahedron Lett.* **2015**, *56*, 5899.
49. Liang, Y.; Wnuk, S. F. *Molecules*, **2015**, *20*, 4874.
50. Amblard, F.; Nolan, S. P.; Gillaizeau, I.; Agrofoglio, L. A. *Tetrahedron Lett.* **2003**, *44*, 9177.
51. Zhou, P.; Xie, M.-S.; Qu, G.-R.; Li, R.-L.; Guo, H.-M. *Asian J. Org. Chem.* **2016**, *5*, 1100.
52. Horhota, A. T.; Szostak, J. W.; McLaughlin, L. W. *Org. Lett.* **2006**, *8*, 5345.
53. Larsen, A. F.; Ulven, T. *Chem. Commun.* **2014**, *50*, 4997.
54. Khalafi-Nezhad, A.; Zare, A.; Parhami, A.; Navid, M.; Rad, S.; Nejabat, G. R. *Can. J. Chem.* **2006**, *84*, 979.
55. Chen, S.; Graceffa, R. F.; Boezio, A. A. *Org. Lett.* **2016**, *18*, 16.
56. (a) Kotek, V.; Chudíková, N.; Tobrman, T.; Dvořák, D. *Org. Lett.* **2010**, *24*, 5724. (b) Kotek, V.; Tobrman, T.; Dvořák, D. *Synthesis*, **2012**, *44*, 610. (c) Aarhus, T. I.; Fritze, U. F.; Hennum, M.; Gundersen, L.-L. *Tetrahedron Lett.* **2014**, *55*, 5748.
57. Keder, R.; Dvořáková, H.; Dvořák, D. *Eur. J. Org. Chem.* **2009**, *2009*, 1522.
58. (a) Hirota, K.; Kazaoka, K.; Niimoto, I.; Sajiki, H. *Org. Biomol. Chem.* **2003**, *1*, 1354. (b) Biagi, G.; Giorgi, I.; Livi, O.; Pacchini, F.; Salerni, O. L.; Scartoni, V. *J. Heterocycl. Chem.* **2005**, *42*, 743. (c) Guchhait, S. K.; Chaudhary, V. *Org. Biomol. Chem.* **2014**, *12*, 6694. (d) Bollier, M.; Klupsch, F.; Six, P.; Dubuquoy, L.; Azaroual, N.; Millet, R.; Leleu-Chavain, N. *J. Org. Chem.* **2018**, *83*, 422. (e) Tber, Z.; Biteau, N. G.; Agrofoglio, L.; Cros, J.; Goffinont, S.; Castaing, B.; Nicolas, C.; Roy, V. *Eur. J. Org. Chem.* **2019**, *2019*, 5756.
59. (a) Liu, J.; Dang, Q.; Wei, Z.; Shi, F.; Bai, X. *J. Comb. Chem.* **2006**, *8*, 410. (b) Chorvat, R. J.; Bakthavatchalam, R.; Beck, J. P.; Gilligan, P. J.; Wilde, R. G.; Cocuzza, A. J.; Hobbs, F. W.; Cheeseman, R. S.; Curry, M.; Rescinito, J. P.; Krenitsky, P.; Chidester, D.; Yarem, J. A.; Klaczkiewicz, J. D.; Hodge, C. N.; Aldrich, P. E.; Wasserman, Z. R.; Fernandez, C. H.; Zaczek, R.; Fitzgerald, L. W.; Huang, S.-M.; Shen, H. L.; Wong, N.; Chien, B. M.; Quon, C. Y.; Arvanitis, A. *J. Med. Chem.* **1999**, *42*, 833. (c) Gordon, M. R.; Lindell, S. D.; Richards, D. *Synlett* **2018**, *29*, 473. (d) Zelli, R.; Zeinyeh, W.; Haudecouer, R.; Alliot, J.; Boucherle, B.; Callebaut, I.; Décout, J.-L. *Org. Lett.* **2017**, *19*, 6360.
60. (a) Novosjolova, I.; Bizdēna, Ē.; Turks, M. *Tetrahedron Lett.* **2013**, *54*, 6557. (b) Novosjolova, I.; Bizdēna, Ē.; Turks, M. *Phosphorus Sulfur Silicon Relat. Elem.* **2015**, *190*, 1236.
61. Traskovskis, K.; Rudušs, A.; Kokars, V.; Mihailovs, I.; Lesina, N.; Vembris, A. *New J. Chem.* **2019**, *43*, 37.
62. Satoh, Y.; Marcopulos, N. *Tetrahedron Lett.* **1995**, *36*, 1759.
63. Kim, S. H.; Jang, J.; Lee, J. Y. *Appl. Phys. Lett.* **2007**, *90*, 223505.
64. Hong, G.; Gan, X.; Leonhardt, C.; Zhang, Z.; Seibert, J.; Busch, J. M.; Bräse, S. *Adv. Mater.* **2021**, *33*, 2005630.
65. Miyashita, A.; Suzuki, Y.; Ohta, K.; Higashino, T. *Heterocycles* **1994**, *39*, 345.

66. Matsuzaki, K.; Okuyama, K.; Tokunaga, E.; Saito, N.; Shiro, M.; Shibata, N. *Org. Lett.* **2015**, *17*, 3038.
67. Šála, M.; Kögler, M.; Plačková, P.; Mejdrová, I.; Hřebabecký, H.; Procházková, E.; Strunin, D.; Lee, G.; Birkus, G.; Weber, J.; Mertlíková-Kaiserová, H.; Nencka, R. *Bioorg. Med. Chem. Lett.* **2016**, *26*, 2706.
68. Arce, R.; Quiñones, E. *J. Am. Chem. Soc.* **1989**, *111*, 8218.
69. Murgida, D. H.; Bilmes, G. M.; Erra-Balsells, R. *Photochem. Photobiol.* **1996**, *64*, 777.
70. Crespo-Hernández, C. E.; Martínez-Fernández, L.; Rauer, C.; Reichardt, C.; Mai, S.; Pollum, M.; Marquetand, P.; González, L.; Corral, I. *J. Am. Chem. Soc.* **2015**, *137*, 4368.
71. Gomez, E. F.; Venkatraman, V.; Grote, J. G.; Steckl, A. J. *Adv. Mater.* **2015**, *27*, 7552.
72. (a) Wei, Q.; Fei, N.; Islam, A.; Lei, T.; Hong, L.; Peng, R.; Fan, X.; Chen, L.; Gao, P.; Ge, Z. *Adv. Optical Mater.* **2018**, *6*, 1800512. (b) Geffroy, B.; le Roy, P.; Prat, C. *Polym. Int.* **2006**, *55*, 572.
73. Negi, S.; Mittal, P.; Kumar, B. *Microsyst. Technol.* **2018**, *24*, 4981.
74. Godumala, M.; Choi, S.; Cho, M. J.; Choi, D. H. *J. Mater. Chem. C* **2019**, *7*, 2172.
75. (a) Jovaisaite, J.; Cīrule, D.; Jeminejs, A.; Novosjolova, I.; Turks, M.; Baronas, P.; Komskis, R.; Tumkevicius, S.; Jonusauskas, G.; Jursenas, S. *Phys. Chem. Chem. Phys.* **2020**, *22*, 26502. (b) Xu, H.; Chen, W.; Ju, L.; Lu, H. *Spectrochim. Acta A* **2021**, *247*, 119074.
76. Wang, H.-Y.; Yu, K.-K.; Tan, C.-Y.; Li, K.; Liu, Y.-H.; Shi, L.; Lu, K.; Yu, X.-Y. *J. Mater. Chem. C* **2021**, *9*, 2864.
77. (a) Cocca, L. H. Z.; Abegao, L. M. G.; Sciuti, L. F.; Vabre, R.; Siqueira, J. P.; Kamada, K.; Mendonça, C. R.; Piguel, S.; De Boni, L. *J. Phys. Chem. C* **2020**, *124*, 12617. (b) Venkatesh, V.; Shukla, A.; Sivakumar, S.; Verma, S. *ACS Appl. Mater. Interfaces* **2014**, *6*, 2185.
78. Patrizi, B.; Cozza, C.; Pietropaolo, A.; Foggi, P.; de Cumis, M. S. *Molecules*, **2020**, *25*, 430.
79. Sasaki, S.; Drummen, G. P. C.; Konishi, G. *J. Mater. Chem. C* **2016**, *4*, 2731.
80. Patrizi, B.; Iagatti, A.; Abbondanza, L.; Bussotti, L.; Zanardi, S.; Salvalaggio, M.; Fusco, R.; Foggi, P. *J. Phys. Chem. C* **2019**, *123*, 5840.
81. Verbitskiy, E. V.; Rusinov, G. L.; Chupakhin, O. N.; Charushin, V. N. *Dyes Pigm.* **2020**, *180*, 108414.
82. Reichardt, C.; *Chem. Rev.* **1994**, *94*, 2319.
83. (a) Allard, S.; Forster, M.; Souharce, B.; Thiem, H.; Scherf, U. *Angew. Chem. Int. Ed.* **2008**, *47*, 4070. (b) Wang, C.; Zhang, X.; Dong, H.; Chen, X.; Hu, W. *Adv. Energy Mater.* **2020**, *10*, 2000955.
84. (a) Yang, Z.; Mao, Z.; Xie, Z.; Zhang, Y.; Liu, S.; Zhao, J.; Xu, J.; Chi, Z.; Aldred, M. P. *Chem. Soc. Rev.* **2017**, *46*, 915. (b) Chen, X.-K.; Kim, D.; Brédas, J.-L. *Acc. Chem. Res.* **2018**, *51*, 2215.
85. Huang, T.; Jiang, W.; Duan, L. *J. Mater. Chem. C* **2018**, *6*, 5577.
86. Wex, B.; Kaafarani, B. R. *J. Mater. Chem. C* **2017**, *5*, 8622.
87. Auffray, M.; Balijapalli, U.; Ribierre, J.-C.; Tsuchiya, Y.; Adachi, C. *Chem. Lett.* **2020**, *49*, 932.
88. Zhang, D.-D.; Suzuki, K.; Song, X.-Z.; Wada, Y.; Kubo, S.; Duan, L.; Kaji, H. *ACS Appl. Mater. Interfaces* **2019**, *11*, 7192.

89. Skuodis, E.; Bezvikonnyi, O.; Tomkeviciene, A.; Volyniuk, D.; Mimaite, V.; Lazauskas, A.; Bucinskas, A.; Keruckiene, R.; Sini, G.; Grazulevicius, J. V. *Org. Electron.* **2018**, *63*, 29.

DOCTORAL THESIS PROPOSED TO RIGA TECHNICAL UNIVERSITY FOR THE PROMOTION TO THE SCIENTIFIC DEGREE OF DOCTOR OF SCIENCE

To be granted the scientific degree of Doctor of Science (Ph. D.), the present Doctoral Thesis has been submitted for the defence at the open meeting of RTU Promotion Council on May 29, 2023 at the Faculty of Materials Science and Applied Chemistry of Riga Technical University, 3 Paula Valdena Street, Room 272 with online participation option at zoom link *https://rtucloud1.zoom.us/j/9352086644*.

OFFICIAL REVIEWERS

Dr. chem. Edgars Sūna,
University of Latvia, Latvia

Dr. chem. Pāvels Arsenjans,
Latvian Institute of Organic Synthesis, Latvia

Dr. Jørn H. Hansen,
The Arctic University of Norway, Norway

DECLARATION OF ACADEMIC INTEGRITY

I hereby declare that the Doctoral Thesis submitted for the review to Riga Technical University for the promotion to the scientific degree of Doctor of Science (Ph. D.) is my own. I confirm that this Doctoral Thesis had not been submitted to any other university for the promotion to a scientific degree.

Armands Sebris ……..….
(*signature*)

Date …...……...….

The Doctoral Thesis has been prepared as a collection of thematically related scientific publications complemented by summaries in both Latvian and English. The Doctoral Thesis unites four scientific publications and one review. The scientific publications have been written in English, with the total volume of 149 pages, including supplementary data.

CONTENTS

GENERAL OVERVIEW OF THE THESIS

Introduction

The modification of purine ring has been studied extensively, since these compounds are a class of privileged structures in medicinal chemistry.[1] Most purine derivatives exhibit not only biological activity, but in several cases also fluorescence, which is commonly used for cell visualization in biological studies.[2] Such derivatives have to be soluble in water and have low cytotoxicity. That may be achieved with respective functional groups such as amino or hydroxyl groups or ribosylfragment on the purine cycle. On the other hand, the use of purine derivatives in optoelectronics has been studied to a lesser extent. In the development of optical materials, the most important aspects are high emission efficiency, stability of the used compounds and low costs. By introducing functional groups, which are commonly used in optoelectronics, such as carbazole, thiophene or cyano group, in the purine cycle, compounds with adequate properties for applications in organic light-emitting diodes (OLED) could be obtained.

Since the first OLED design was proposed in 1987,[3] extensive research has been conducted to obtain highly efficient white or red, green and blue diodes for production of displays. Compared to currently widespread liquid crystal displays (LCD), OLED offers several advantages: higher energy efficiency, bigger color rendering and spectral similarity index values, higher contrast, and a thin and lightweight design, which enables creation of flexible displays. OLED also emits a more natural color range, which is an advantage both aesthetically and healthwise.[4] The main disadvantages of OLED are higher costs, shorter lifespans, especially for blue color, and degradation upon contact with oxygen. A way to reduce costs is the use of materials that enable OLED production via solution method, which is cheaper than using vacuum.[5] Introduction of amorphousing groups into the purine structure will open the possibility of creating thin layer films via the solution method.

Current research in optoelectronics contains examples regarding the use of purine derivatives as sensors,[6] fluorescent,[7] phosphorescent,[8] or thermally activated delayed fluorescence (TADF)[9] emitters. The devices obtained in the aforementioned studies[6–9] have inferior properties to those of the corresponding commercial products. Based on the sparsity of research, knowledge in this field should be expanded, new structures with electron donors and acceptors should be designed, new methods should be developed or known approaches for compound preparation should be adapted, using the widely occurring purine heterocycle as a basis.

There are methods described in literature for the introduction of substituents at the *C*(2), *C*(6) and *C*(8) positions of the purine ring atoms using nucleophilic aromatic substitution (S_NAr)[11–21] and transition metal catalyzed cross-coupling reactions.[22–26] Introduction of many electron donors and acceptors of our interest has not been described, requiring adaptation of known methods or development of new ones. If the required substituent cannot be introduced directly, in some cases it is possible to construct it using functional group transformations, such as the formation of 1,2,3-triazole in a copper catalyzed azide-alkyne dipolar cycloaddition (CuAAC) reaction.[21]

The atoms at *C*(2), *C*(6) and *C*(8) positions are not symmetrical in the purine cycle and each position has a characteristic higher or lower reactivity. Differences in the arrangement of substituents often have an effect on the absorption and emission wavelengths and efficiency, so it is necessary to obtain variously substituted purine derivatives to find compounds with the best properties. In order to prepare compounds that cannot be obtained using the usual purine regioselectivity, we need to develop methods for reversing the selectivity. One way to achieve this is via azide-tetrazole equilibrium, that enables substitution at the atom in *C*(2) position.[27]

Methods for functionalizing purine nitrogen atoms *N*(9) and *N*(7) with aliphatic and aromatic substituents are known in the literature, usually the nitrogen atom in the *N*(9) position is more reactive. Aliphatic substituents can be introduced using alkyl halides or the Mitsunobu reaction,[28] while aromatic substituents can be introduced by a copper catalyzed cross-coupling reaction with diaryliodanes[29] or Chan–Lam cross-coupling reaction.[30] We need to adapt these methods to introduce the substituents we are interested in – carbazole-containing, electron-rich systems and structures containing a triphenylmethyl group, which would contribute to the amorphous properties of the compounds.[31]

Not all desired transformations can be realized with a closed purine ring. If another purine position is far more reactive, or the transformation cannot be performed due to steric hindrance, it can be attempted by *de novo* synthesis. This approach enables introduction of the required substituents on the pyrimidine or imidazole followed by closing of the purine ring. Use of *de novo* synthesis and closing the imidazole ring on a previously modified pyrimidine opens a synthetic route for introduction of aromatic substituents at the less reactive nitrogen atom at the *N*(7) position (Scheme 1).

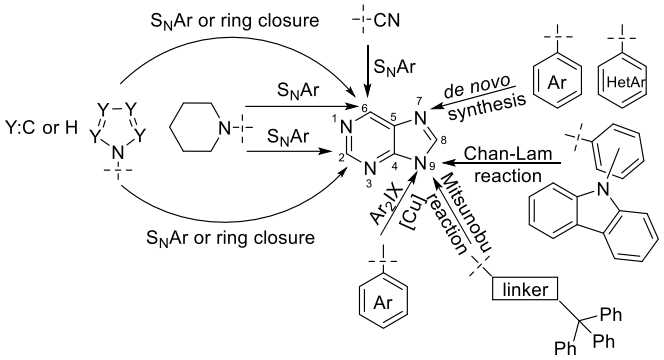

Scheme 1. Purine cycle numbering and the desired reactions.

During the preparation of Doctoral Thesis, purposefully functionalized luminescent purine derivatives with amorphousing groups were obtained, for which the potential applications in OLED devices were researched. TADF properties and potential application in OLED devices were tested for purine-carbazole conjugates. New synthetic routes for the preparation of specifically functionalized *N*(9)-arylpurines, *N*(9)-alkylpurines, and azolylpurines were developed. A new synthetic route to *N*(7)-arylpurines was developed, employing *de novo* synthesis.

Aims and objectives

The aim of the Thesis was the synthesis of new purine derivatives to obtain compounds with amorphous properties, high emission efficiency, and corresponding physical properties for potential application in the development of OLEDs.

The following tasks were defined:

1. To develop purine reactions that enable the introduction of electron donating and accepting functional groups at the appropriate purine ring atoms:
    - to search for new synthetic routes for purine functionalization using the equilibrium of 2,6-diazidopurine azide-tetrazole tautomeric forms;
    - to find reaction conditions for the introduction of substituted and unsubstituted azoles at the *C*(2) and *C*(6) positions of purine;
    - to develop reaction conditions for introduction of various aryl substituents at the *N*(9) and *N*(7) positions of purine.
2. To create purine derivatives with application in optoelectronics for the development of OLEDs:
    - to obtain amorphous, fluorescent purine derivatives and determine their photophysical properties;
    - to synthesize purine derivatives exhibiting thermally activated delayed fluorescence.

Scientific novelty and main results

During the course of Doctoral Thesis, new organic synthesis methods for the introduction of azole substituents into the purine ring as well as for the preparation of *N*(7) arylpurines by *de novo* synthesis from the substituted pyrimidines were developed. Synthesis methods with altered regioselectivity at purine *C*(2) and *C*(6) positions were developed by influencing the equilibrium of azide-tetrazole tautomeric forms of 2,6-diazidopurine. A new structural design was developed for intramolecular push-pull fluorescent purines and sterically hindered purine-carbazole conjugates. New synthetic methods were developed for the synthesis of such compounds. Push-pull type purine derivatives exhibit fluorescence and can potentially be used as organic field effect transistors. Purine-carbazole conjugates and a mixture of purine and carbazole derivatives in solid state forms exciplexes exhibiting thermally activated delayed fluorescence. These compounds can potentially be used as host materials in OLEDs.

Structure and volume of the Thesis

The Doctoral Thesis has been prepared as a set of thematically related scientific publications, dedicated to purine derivatives with applications in materials science to solve problems in optoelectronics. The Thesis unites four original research publications in the SCI journals and one review.

Publications and approbation of the Thesis

The results of the Thesis have been reported in four scientific publications. One review has been published. The main results have been presented at 13 conferences.

Scientific publications:

1. **Sebris, A.**; Novosjolova, I.; Turks, M. Synthesis of 7-Arylpurines from Substituted Pyrimidines. *Synthesis* **2022**, *54*, 5529. doi: 10.1055/a-1898-9675
2. **Sebris, A.**; Novosjolova, I.; Traskovskis, K.; Kokars, V.; Tetervenoka, N.; Vembris, A.; Turks, M. Photophysical and Electrical Properties of Highly Luminescent 2/6-Triazolyl-Substituted Push–Pull Purines. *ACS Omega* **2022**, *7*, 5242. doi: 10.1021/acsomega.1c06359
3. Traskovskis, K.; **Sebris, A.**; Novosjolova, I.; Turks, M. Guzauskas, M.; Volyniuk, D.; Bezvikonnyi, O.; Grazulevicius, J.; Mishnev, A.; Grzibovskis, R.; Vembris, A. All-organic Fast Intersystem Crossing Assisted Exciplexes Exhibiting Sub-Microsecond Thermally Activated Delayed Fluorescence. *J. Mater. Chem. C* **2021**, *9*, 4532. doi: 10.1039/D0TC05099G
4. **Sebris, A.**; Traskovskis, K.; Novosjolova, I.; Turks, M. Synthesis and Photophysical Properties of 2-Azolyl-6-piperidinylpurines. *Chem. Heterocycl. Compd.* **2021**, *57*, 560. doi: 10.1007/s10593-021-02943-1
5. **Sebris, A.**; Turks. M. Recent Investigations and Applications of Azidoazomethine-Tetrazole Tautomeric Equilibrium. *Chem. Heterocycl. Compd.* **2019**, *55*, 1041. doi: 10.1007/s10593-019-02574-7

Results of the Thesis were presented at the following conferences:

1. **Sebris, A.;** Novosjolova, I.; Turks, M. New Synthetic Pathway to 7-Arylpurines. In: *Balticum Organicum Syntheticum 2022: Program and Abstract Book*, Lithuania, Vilnius, 3–6 July 2022. Vilnius: UAB Kalanis, 2022, p. 152.
2. **Sebris, A.**; Kapilinskis, Z.; Kriķis, K.; Traskovskis, K.; Novosjolova, I.; Turks, M. Functionalized Purines for Materials Science Applications. In: *Balticum Organicum Syntheticum 2022: Program and Abstract Book*, Lithuania, Vilnius, 3–6 July 2022. Vilnius: UAB Kalanis, 2022, p. 162.
3. **Sebris, A.** Synthesis and Photophysical Properties of Fluorescent Purine-Carbazole Conjugates. In: *12th Paul Walden Symposium on Organic Chemistry: Program and Abstract Book*, Latvia, Riga, 28–29 October **2021**. Riga: RTU Press, 2021, p. 37.
4. **Sebris, A.**; Traskovskis, K.; Novosjolova, I.; Turks, M. Synthesis and Photophysical Properties of Purine-Carbazole Donor Acceptor Systems. In: *The 27th Croatian Meeting of Chemists and Chemical Engineers: 27HSKIKI Abstracts*, Croatia, Veli Lošinj, 5–8 October **2021**. Croatia: 2021, p. 105.
5. **Sebris, A.;** Burcevs, A.; Traskovskis, K.; Novosjolova, I.; Vembris, A.; Turks, M. Synthesis and Photophysical Properties of Fluorescent Purine Derivatives. In: *IS3NA-IRT Virtual Symposium 2021: Book of Abstracts*, Virtual, 26–27 August **2021**. Online: 2021, p. p67.

6. **Sebris, A.**; Novosjolova, I.; Turks, M. Synthesis and Photophysical Properties of Sterically Hindered Purine Derivatives. In: *Thesis book of University of Latvia 79th International Scientific Conference, Section: Organic Chemistry*, Latvia, Riga, February 5, **2021**. Riga: 2021, p. 61.
7. **Sebris, A.**; Novosjolova, I.; Turks, M. Synthesis and Photopysical Properties of Substituted Purine-Carbazole Conjugates. In: *Thesis book of University of Latvia 78th International Scientific Conference, Section: Organic Chemistry*, Latvia, Riga, March 6, **2020**. Riga: 2020, p. 54.
8. **Sebris, A.**; Traskovskis, K.; Novosjolova, I.; Turks, M. Purine-Azole Conjugates as Fluorescent Materials. In: *Materials Science and Applied Chemistry 2019: 60th International Scientific Conference: Programme and Abstract Book*, Latvia, Riga, October 24, **2019**. Riga: 2019, p. 25.
9. **Sebris, A.**; Novosjolova, I.; Turks, M. Synthesis and Photophysical Properties of Functionalized Purine Derivatives. In: *11th Paul Walden Symposium on Organic Chemistry: Program and Abstract Book*, Latvia, Riga, 19–20 September **2019**. Riga: 2019, p. 41.
10. **Sebris, A.**; Traskovskis, K.; Novosjolova, I.; Turks, M. Triazolyl Purine Derivatives as Amorphous Fluorescent Materials. In: *International Symposium on Synthesis and Catalysis: Book of Abstracts*, Portugal, Evora, 3–6 September **2019**. Evora: 2019, p. 294.
11. Novosjolova, I.; Kapilinskis, Z.; **Sebris, A.**; Burcevs, A.; Zaķis, J.; Turks, M. Synthesis and Photophysical Properties of *N*(9)-Alkylated 2,6- Substituted Purine Derivatives. In: *International Symposium on Synthesis and Catalysis: Book of Abstracts*, Portugal, Evora, 3–6 September **2019**. Evora: 2019, p. 286.
12. **Sebris, A.**; Traskovskis, K.; Novosjolova, I.; Turks, M. Synthesis and Photophysical Analysis of Fluorescent Purine-Azole Conjugates. In: *International Symposium on Synthesis and Catalysis: Book of Abstracts*, Portugal, Evora, 3–6 September **2019**. Evora: 2019, p. 295.
13. **Sebris, A.**; Novosjolova, I.; Traskovskis, K.; Turks, M. Amorphous Purine-Azole Conjugates and Their Photophysical Properties. In: *21st European Symposium on Organic Chemistry Poster Abstracts*, Austria, Vienna, 14–18 July **2019**. Vienna: 2019, p. 290.
14. Novosjolova, I.; Ozols, K.; **Sebris, A.**; Zaķis, J.; Cīrule, D.; Kapilinskis, Z.; Jeminejs, A.; Kriķis, K.; Bizdēna, Ē.; Turks, M. Azidopurines and 1,2,3-Triazolylpurines as Useful Building Blocks for Bioorganic and Materials Chemistry. In: *Proceedings of GRC2019: Nucleosides, Nucleotides and Oligonucleotides*, United States of America, Newport, 23–28 June **2019**. Newport: 2019, p. 1.
15. **Sebris, A.**; Kapilinskis, Z.; Novosjolova, I.; Turks, M. Synthesis and Photopysical Properties of Functionalized Purine-Heterocycle Conjugates. In: *Thesis book of University of Latvia 77th International Scientific Conference, Section: Organic Chemistry*, Latvia, Riga, February 19, **2019**. Riga: LU, 2019, p. 51.

16. Bizdēna, Ē.; Goliškina, S.; **Sebris, A.**; Mishnev, A.; Turks, M. 2,4-Diazidoquinazoline as Useful Starting Material in Heterocyclic Chemistry. In: *XXII International Conference on Organic Synthesis: Scientific Program & Abstract Book*, Italy, Florence, 16–21 September **2018**. Florence: 2018, p. P271.
17. Turks, M.; Ozols, K.; Novosjolova, I.; **Sebris, A.**; Cīrule, D.; Kapilinskis, Z.; Hopmann, K.; Zaķis, J.; Šišuļins, A.; Bizdēna, Ē. Azidopurines and 1,2,3-Triazolylpurines as Novel Synthetic Tools for Bioorganic and Materials Chemistry. In: *22nd International Conference on Organic Synthesis: Scientific Program and Abstract Book*, Italy, Florence, 16–21 September **2018**. Florence: 2018, p. P19.
18. Novosjolova, I.; **Sebris, A.**; Kapilinskis, Z.; Traskovskis, K.; Kokars, V.; Turks, M. Purine Hybrids Containing Five-Membered Heterocycles: Synthesis and Photophysical Properties. In: *XXII International Conference on Organic Synthesis: Scientific Program and Abstract Book*, Italy, Florence, 16–21 September **2018**. Florence: 2018, p. P361.
19. **Sebris, A.**; Kapilinskis, Z.; Novosjolova, I.; Traskovskis, K.; Vembris, A.; Turks, M. Synthesis and Photophysical Properties of *N*(9)-Alkylated Purines with Amorphousing Groups. In: *XXII International Conference on Organic synthesis: Scientific Program and Abstract Book*, Italy, Florence, 16–21 September **2018**. Florence: 2018, p. P214.

MAIN RESULTS OF THE THESIS

Purine is one of the most common nitrogen heterocycles in nature, the most known derivatives of which are adenine and guanine, two of the nitrogen bases of deoxyribonucleic and ribonucleic acids. Traube synthesis is the most widely known chemical method for the preparation of purine derivatives, but due to the widespread occurrence of such compounds in nature, many are obtained from food processing or other biological sources. Examples of non-laboratory applications include the use of purine nucleotides as flavor enhancers, such as guanosine monophosphate, and the use of caffeine as a stimulant.[10]

In the Thesis, methods for obtaining novel purine derivatives were developed, photophysical properties of such compounds were measured and their application in materials science field of optoelectronics was determined. Initially, purine cycle atoms were functionalized with electron donating and withdrawing groups to obtain fluorescent push-pull systems. The nitrogen atom at purine *N*(9) position was modified with electron-rich heterocycles, which were bridged by a neutral aromatic system. The prepared derivatives can potentially be used as organic field effect transistors or host materials in OLEDs.

1. Introduction of substituents in the purine ring

Due to the high interest towards modification of purine in medicinal chemistry, various methods for the introduction of substituents have been developed. The most widely used methods are nucleophilic aromatic substitution (S_NAr) and cross-coupling reactions for the introduction of substituents at the *C*(2), *C*(6) and *C*(8) positions. Both selective and non-selective methods for functionalization of purine nitrogen atoms at *N*(9) and *N*(7) with aliphatic and aromatic substituents have been reported. Another notable approach employs *de novo* synthesis with a prefunctionalized pyrimidine or imidazole, followed by purine ring closure at an opportune stage of the synthesis.

The atom at the *C*(6) position of purine is the most reactive one and can be functionalized with azides,[11] alkylamines,[12] arylamines,[13] azoles,[14] alkylthiols,[15] arylthiols,[15] sulfinates,[15] alkoxides,[16] phenolates[17] and 1,3-dicarbonyl derivatives,[18] using the S_NAr reaction (Scheme 2). Aliphatic amines at the *C*(6) position of purine can be introduced at low temperatures in a Cu(II)-associated S_NAr reaction.[19] The most common leaving groups for the S_NAr reactions are halogens, but such reactions with azide,[20] sulfonylgroup,[15] 1,2,4-triazole or 1,2,3-triazole[21] leaving groups have also been described in literature. C-N bonded azoles may also be introduced via modified Appel conditions for hypoxanthine.[14] Various aromatic and aliphatic substituents may be introduced using transition metal catalyzed cross-coupling reactions (Scheme 3). Aromatic substituents are most often introduced in the purine ring employing the Suzuki–Miyaura,[22] Negishi[22a, 23, 24] or Stille[22a, 25] reaction conditions, while alkyl substituents are introduced using the Negishi[22a, 23, 24] or Kumada reaction conditions,[22a, 26] or by using trialkylaluminum reagents.[22a, 26] Introduction of alkynyl substituents has been achieved via the Sonogashira reaction conditions.[22a] Using stoichiometric reagent amount, alkyl groups at the *C*(6) position may be introduced using organocuprates.[22a] For iodopurines, purine dimers may

be obtained in Cu(I)[32] or palladium[33] catalyzed reactions. The dimerization reaction is reported for purines with an iodine substituent at *C*(2), *C*(6) and *C*(8) positions.

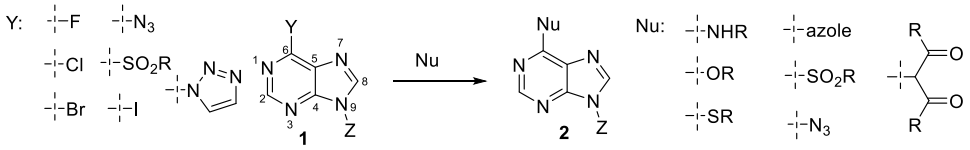

Scheme 2. Purine ring numbering and possible S_NAr reactions.[11–21]

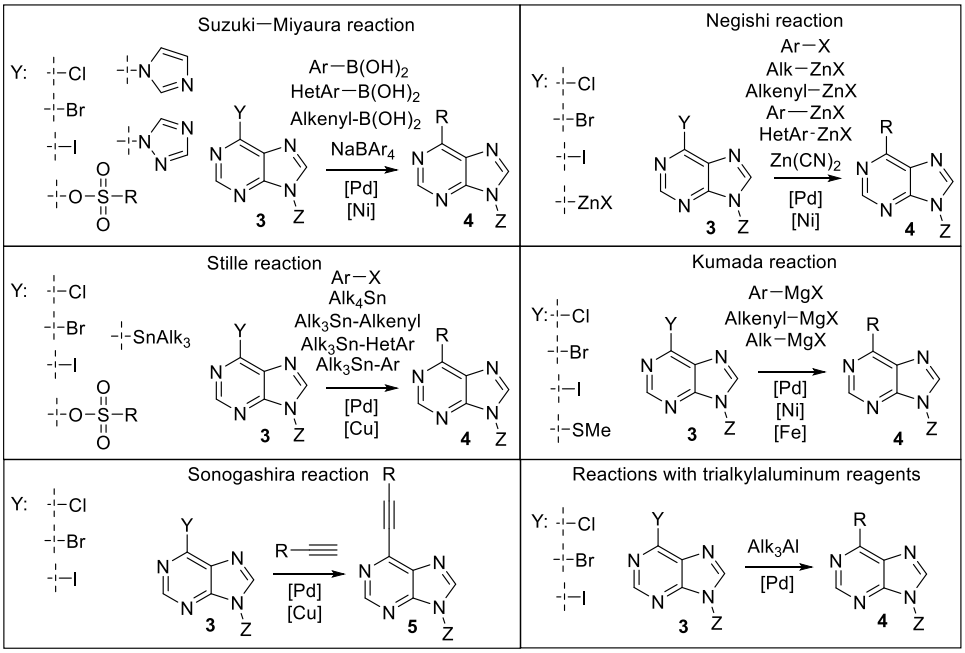

Scheme 3. Cross-coupling for functionalization of *C*(6) position.[22–26]

Atom at the *C*(2) position of purine is less reactive than the atom at the *C*(6) position. Atom at the *C*(2) position can be functionalized in the S_NAr reaction if such a reaction is not possible for the *C*(6) position. S_NAr reaction can be performed with azides,[11] alkylamines,[34] arylamines,[12] azoles,[14, 35] alkylthiols,[36] arylthiols,[37] alkoxides[38] and phenolates.[38] Substitutions at the *C*(2) position are achieved under harsher conditions than at *C*(6), so it is possible to perform successive reactions with different reagents, or to carry out simultaneous substitution at both positions. In the case of cross-coupling, reactions at the *C*(2) position can be done using the Suzuki–Miyaura,[22b] Negishi,[23] Kumada,[39] Sonogashira[40] or Stille[41] reaction conditions, as well as trialkylaluminum reagents,[26] if the *C*(6) position is not available, or by simultaneously introducing groups at *C*(6) and *C*(2) positions. This selectivity can be reversed if there is iodine at the atom in C(2) position and chlorine at the atom in C(6) position. In this case, the Suzuki–Miyaura,[42] Negishi,[43] Sonogashira[44] and Stille[45] reactions proceed selectively at the *C*(2) position. The use of iodine allows reversal of selectivity between *C*(6) and *C*(8) positions, but

if both *C*(2) and *C*(8) are substituted with iodine, the reaction takes place at the atom in *C*(2) position.[44]

The atom at the *C*(8) position of purine is also less reactive than the atom at the *C*(6) position. The *C*(8) position takes part in S_NAr[46] and cross-coupling[47] reactions, similarly to the C(2) position, but the atom at the *C*(8) position is unique with the more acidic proton that can be selectively deprotonated or lithiated,[48] or interacts in C-H activation reactions. A variety of aromatic and aliphatic substituents can be introduced via transition metal catalyzed C-H activation reactions (Scheme 4). In intramolecular reactions with C-H activation at *C*(8) position, it is also possible to obtain annelated purine derivatives.[30, 49]

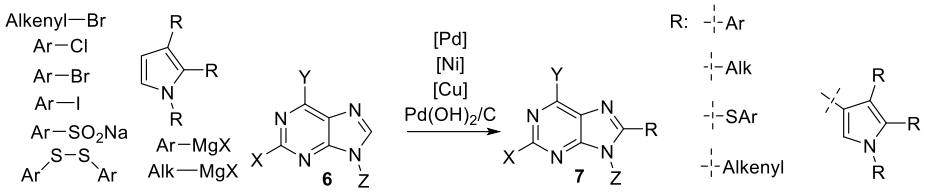

Scheme 4. C-H Activation reactions for *C*(8) position.[30]

Comparing the nitrogen atoms at *N*(7) and *N*(9) positions of purine, the atom at *N*(9) position is more reactive and in reactions as a nucleophilic component it will give the main product. The most often used methods to obtain *N*(9) alkylpurines are alkylation with alkyl halides and the Mitsunobu reaction.[28] Specific substituents can be introduced by palladium-catalyzed cross-coupling with allyl acetates,[28, 50] scandium-catalyzed reaction with diazo derivatives,[51] and via epoxide ring opening reactions.[52] Purine cycle *N*(9) nitrogen alkylation reactions usually also produce a small amount of substituted product at *N*(7) position. The most often used method of purine cycle *N*(9) nitrogen arylation is the Chan–Lam reaction, where purine derivatives are cross-coupled with aryl boronic acids.[30] Other copper-catalyzed methods use aryl halides[53] or iodanes, which can also be used to introduce alkenyl substituents.[29] It is possible to perform arylation via S_NAr reaction if the aromatic group contains sufficiently strong electron-withdrawing substituents.[54] Arylation reactions, depending on the substituent at *C*(6), are often completely *N*(9) selective.

The nitrogen atom at purine *N*(7) position of the purine is less reactive. In reaction with alkyl halides, mostly *N*(7) alkylation product is obtained if Grignard reagents are employed as bases.[55] Selectively *N*(7) alkylpurines can be obtained by alkylation of reduced purines **10** that are protected at the *N*(9) position (Scheme 5).[56] Arylation in which the *N*(7) substitution is the major product, depending on the substituent at *C*(6), can be achieved in optimized Chan–Lam reaction conditions.[57]

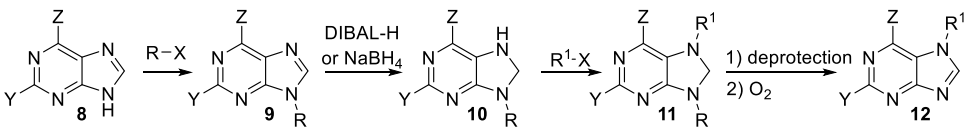

Scheme 5. Use of 7,8-dihydropurines **10**, **11** for the preparation of 7-alkylpurines.[56a]

If the introduction of the required substituents into the purine ring is difficult, it can be achieved by *de novo* ring synthesis by closing either pyrimidine or imidazole rings (Scheme 6). When closing the pyrimidine ring, the purine derivatives with the desired functional groups at *N*(9), *N*(7) and *C*(8) positions may be prepared by choosing the respective imidazole starting material **13**, **14**, **17**, **18**. Substituent Y can be introduced at the *C*(2) position with an appropriately substituted pyrimidine ring closing reagent. In pyrimidine closure, the substituent Z can only be –OH or –NH_2, depending on the imidazole starting material.[58] When closing the imidazole ring, the purine derivatives with the desired functional groups at *N*(9), *N*(7), *C*(2) and *C*(6) may be prepared by choosing the respective pyrimidine starting material **15**, **19**. Substituent Q can be introduced with an appropriately substituted imidazole ring closing reagent.[59] It should be noted that the *de novo* synthesis of 7-arylpurines by imidazole ring closure on a pyrimidine precursor has not been widely studied. This prompted the development of such a method during the development of the Doctoral Thesis.

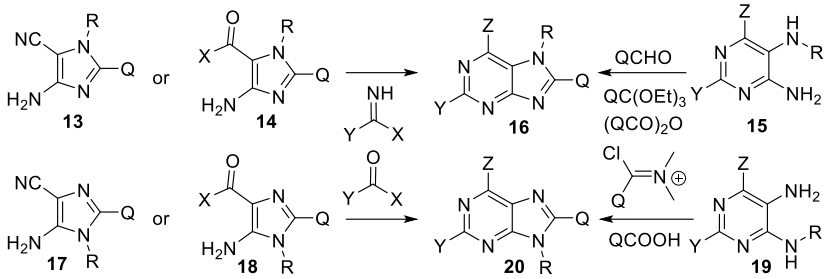

Scheme 6. *De novo* ring closures of purine from pyrimidine or imidazole derivative.[58, 59]

1.1. Selectivity control of purine reactions using azide-tetrazole equilibrium

Azide-tetrazole equilibrium is possible in azoles in which the azido group is next to a nitrogen atom (Scheme 7). Tautomeric forms of such compounds may exhibit the equilibrium, but depending on the structure of the compound and other factors (Table 1), only azide or only tetrazole form may be observed. The possibility of the azide-tetrazole tautomeric form equilibrium in a molecule can affect the reactivity of compounds and the selectivity of reactions, so it is important to understand its effect on reactions and the factors that shift this equilibrium. The azide group is able to participate in S_NAr reactions as a leaving group,[20] or in dipolar cycloaddition as a dipole[21] and also in other reactions in which tetrazole is not involved. The formation of an annulated tetrazole ring changes the electronic properties of a compound, which can activate or deactivate the compound for reactions at another reaction center.

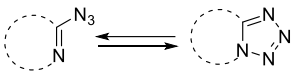

Scheme 7. Azide-tetrazole tautomeric form equilibrium.

Table 1

Favoring Factors for the Azide or Tetrazole Tautomeric Forms

Factor	Favoring azide tautomeric form	Favoring tetrazole tautomeric form
Heterocycle, substituent effects	Electron deficient	Electron rich
Solvent polarity	Nonpolar	Polar
Temperature	Increased	Decreased
Steric hinderance near tetrazole ring	Yes	No

Although five tautomeric equilibrium forms can exist in the case of 2,6-diazidopurines (Scheme 8), the diazide **AA** is the most abundant because purine is an electron-deficient ring. In crystalline form, these compounds exist in diazide tautomeric form, but one of the tetrazole tautomeric forms, **AT1**, can also be observed in polar solvents. The presence of the tetrazole tautomeric form **AT1** has previously been used in our research group to reverse the normal reactivity of purine.[27, 60]

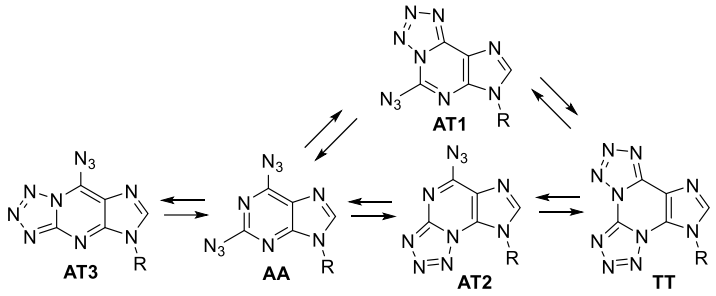

Scheme 8. Theoretically possible azide-tetrazole tautomeric form equilibria for diazidopurine.

The most recent information regarding azide-tetrazole equilibrium is summarized in the review found in Appendix I.

Based on this information, a series of transformations was proposed to obtain push-pull fluorescent purine derivatives with potential application in optoelectronics as solution-processed materials. For this purpose, the compound must have amorphous properties, which can be facilitated by introducing triphenylmethyl substituents into the molecule.[61]

The alkyl substituent at the nitrogen atom at the *N*(9) position was introduced in the Mitsunobu reaction, and a small amount of substitution at the nitrogen atom in the *N*(7) position also ocurred. The obtained compound **22** formed product **23** in a S_NAr reaction with NaN_3 in almost quantitative yield. Taking advantage of the reactivity of the **AT1** tautomeric form of intermediate **23**, compound **24** was obtained with *C*(2)-selectivity in the S_NAr reaction with piperidine. Carrying out the reaction in DMF at 20 °C increased the proportion of the tetrazole tautomeric form in intermediate **23** and allowed the highest ratio of *C*(2) to *C*(6) substitution, but failed to completely prevent substitution at *C*(6).

To obtain the inversely substituted regioisomer **27**, starting material **21** was first used in the S_NAr reaction with NaN_3, which gave compound **25** in a lower yield than for the *N*(9)

substituted purine, as monoazidopurine derivative was also formed. The next step was the S_NAr reaction with piperidine, which in this case took place at the *C*(6) position. The reversal of selectivity for this reaction can be explained by changes in the structure of the compound (no electron-donating alkyl group at the *N*(9) position) and reaction conditions (elevated temperature) favoring the azide form. Degradation of the azide occurred during the reaction, which lowered the yield, but no *C*(2) substitution was observed. Alternatively, compound **26** could be obtained by the S_NAr reaction of compound **21** with piperidine followed by azidation at the *C*(2) position. This route was not chosen, since the introduction of electron-donating groups deactivates the purine for the S_NAr reactions. This would require to do the azidation under harsh conditions. Triphenylpentyl group was introduced at the *N*(9) position of compound **26** by the Mitsunobu reaction (Scheme 9). Substrate **26** may also participate in the Staudinger reaction with phosphine under the Mitsunobu conditions. This side reaction was initially observed but later prevented by performing the Mitsunobu reaction at a higher dilution.

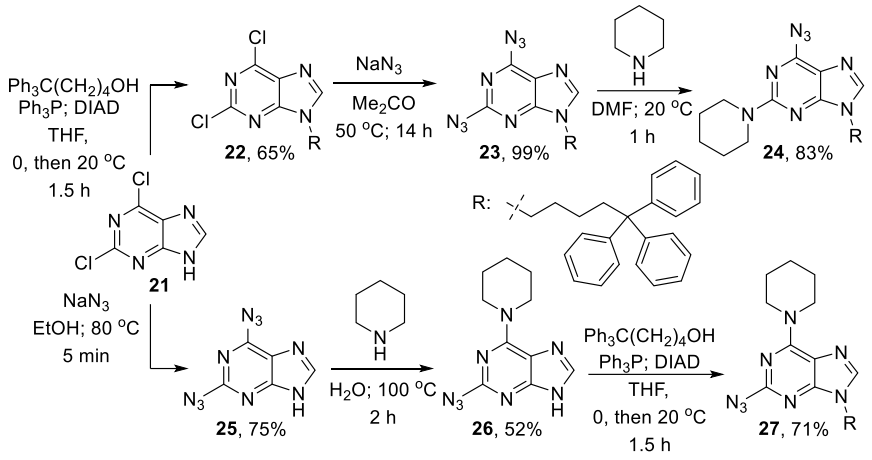

Scheme 9. Functionalization of diazidopurine with piperidine at *C*(2) or *C*(6) positions.

The scientific publication of the research described in this chapter can be found in Appendix IV.

1.2. Functionalization of purine with azoles at *C*(2) or *C*(6) positions

Azoles are nitrogen containing heterocycles that are electron-deficient and can serve as electron withdrawing groups in push-pull fluorescent systems.[27] Azole substituents on the purine ring can be achieved by forming the heterocycle on an appropriate functional group or by introducing it by a substitution reaction. This chapter will discuss purine-azole conjugates that are connected by a C-N bond.

Variously substituted 1,2,3-triazolylpurines can be readily obtained in the Cu(I)-catalyzed alkyne-azide cycloaddition reaction with azidopurine and a substituted alkyne.[21] In such a transformation, four 2/6-(1,2,3-triazolyl)purine derivatives with aromatic substituents were obtained in high yields. Aromatic systems with electron-donating and electron-withdrawing

groups are interesting for the study of push-pull systems, so derivatives with methoxy group **28b** and **29b**, dimethylamino group **28c** and **29c**, cyano group **28d** and **29d** or without additional groups **28a** and **29a** were obtained. The cycloaddition reactions at 20 °C proceed cleanly, without azide reduction, yet slowly and with a decreasing rate. Increasing the reaction temperature leads to formation of by-products. Compound **24** and alkynes containing electron withdrawing groups proved to be more reactive than compound **27** and alkynes containing electron donating groups. As a result, the reaction mixture to obtain compound **29c** was kept for 11 days to achieve the desired conversion (Scheme 10).

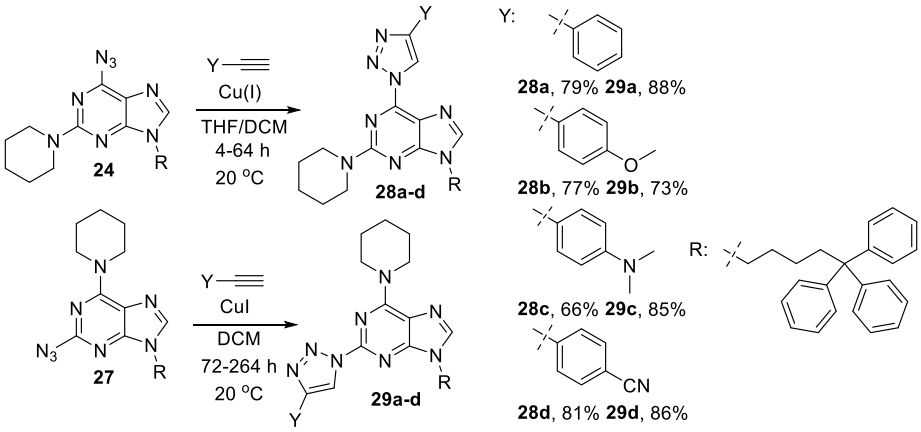

Scheme 10. Introduction of 1,2,3-triazole at purine C(2) or C(6) positions.

Although S_NAr reactions with azoles at the *C*(6) position have been studied more extensively, various azoles can be introduced at the *C*(2) position of the purine in the S_NAr reaction under harsh conditions, as shown with pyrazole and benzimidazole in studies of other authors.[14, 34] Fluorescent properties were expected for purine derivatives with azole substituents at *C*(2) position, so it was planned to introduce a triphenylmethyl group in these structures to promote amorphous properties. Thus, compound **35** was chosen for this purpose, as it is easier to obtain than 5,5,5-triphenylpentanol. This change has no impact on fluorescence, since in both cases the π systems, which are excited and subsequently emit light, are identical. In order to obtain compounds **32** with different azole groups, the starting material **21** had to be firstly protected with a THP protecting group at the nitrogen atom of the *N*(9) position and then used in the S_NAr reaction with piperidine, which proceeds selectively at the *C*(6) position. Compound **31** undergoes the S_NAr reaction with imidazole or 1,2,4-triazole, or 4-phenyl-1,2,3-triazole, but not with tetrazole, as this heterocycle is likely not sufficiently nucleophilic, which can be explained by high NH acidity. When a similar reaction was performed on the analog of **31**, containing *N*(9)-substituent derived from compound **35**, substitution at *C*(2) occurred, but a cleavage of the ester group was also observed. In an experiment with *N*(9)-unsubstituted purines, azole substitution at *C*(2) did not occur. When using 1,2,4-triazole and 4-phenyl-1,2,3-triazole, a mixture of regioisomers may be formed in this reaction. In the case of 1,2,4-triazole, only the formation of **32b** was observed, but the reaction with 4-phenyl-1,2,3-triazole produced

32c and **32d** in similar amounts. THP groups in compounds **32a**,**b** were removed for further functionalization with compound **35** under Mitsunobu conditions to give the final products **36a**,**b** (Scheme 11).

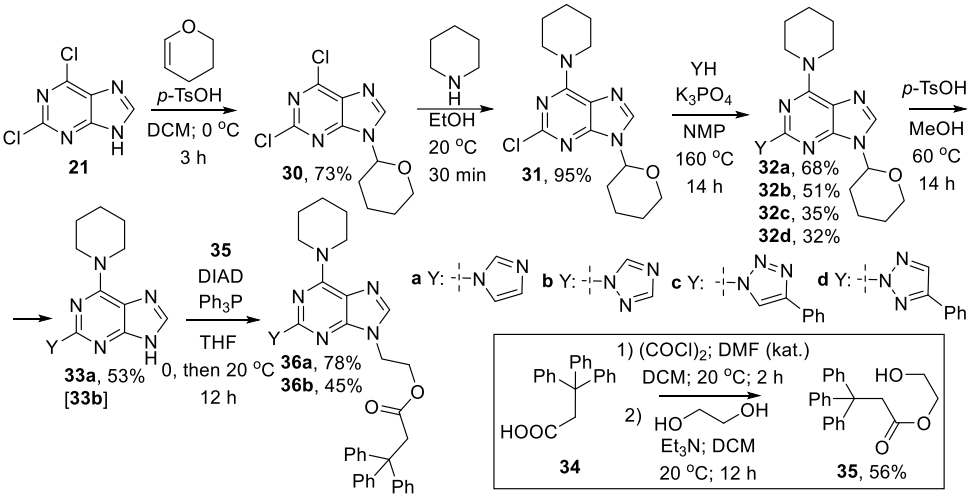

Scheme 11. Introduction of azoles at the purine *C*(2) position in a S_NAr reaction.

In order to identify compounds **32c**,**d**, the synthesis of compound **32c** was performed by influencing the equilibrium of azide-tetrazole tautomeric forms. The previously obtained compound **30** was functionalized into diazide **37**. The subsequent S_NAr reaction with piperidine was carried out in toluene at elevated temperature to promote the azide tautomeric form, resulting in substitution mostly at *C*(6), yet a rather large amount of the C(2) substitution product was still formed, and compound **38** was obtained in 56% yield. Only compound **32c** can be formed in the dipolar cycloaddition reaction (Scheme 12), so the regioselectivity of **32c** was proven by comparison with the products obtained in the reaction of compound **31**.

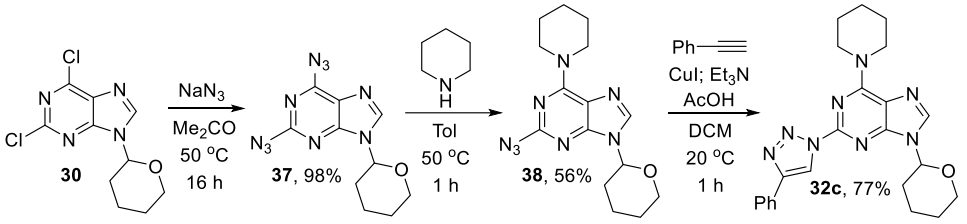

Scheme 12. Preparing compound **32c** with a different synthetic route.

Since the introduction of tetrazole via the S_NAr reaction failed, the ring formation of this cycle on amino group in compound **39** was considered according to a method known in the literature for other classes of compounds.[62] The amino group at the *C*(2) position of purine can be readily obtained by catalytic reduction of the azido group in previously obtained compound **26**. Ring formation of tetrazole at *C*(2) proceeded with a good yield. Compound **40** was functionalized in the Mitsunobu reaction at the nitrogen atom in *N*(9) position with different groups (Scheme 13). The fragment containing the triphenylmethyl group promotes amorphous

properties of compound **41a**, introduction of a chloroethyl group enables options for further functionalization, and the 3,5-dicarbazolylbenzene fragment of purine derivative **41c** is often used in optoelectronics and could improve the properties for electronics.[63]

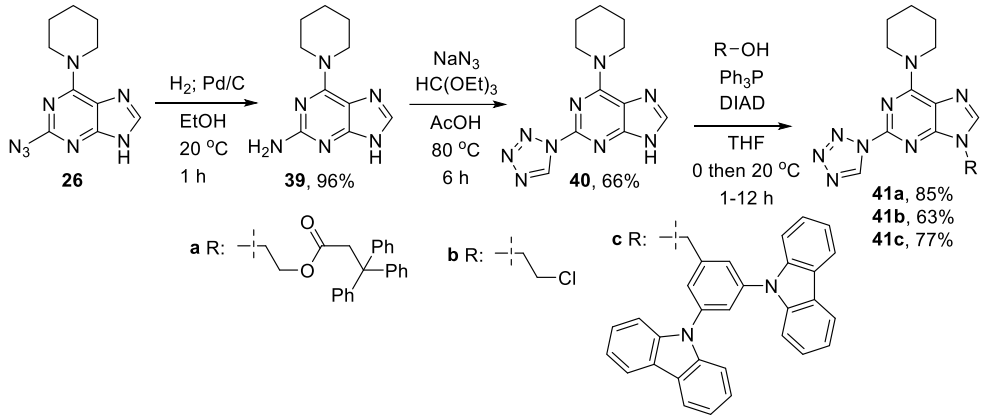

Scheme 13. Formation of tetrazole ring at purine *C*(2) position.

The scientific publications of the research described in this chapter can be found in Appendices II and IV.

1.3. Introduction of aromatic substituents at purine *N*(9) or *N*(7) positions

The introduction of aromatic substituents at the purine nitrogen atoms at *N*(9) and *N*(7) positions of purine is a potentially useful approach of research in the study of light-emitting compounds, since such derivatives mostly consist of connected aromatic rings with or without a complex-forming transition metal.[64] Several literature methods are known for the arylation of purine *N*(9) position,[29, 49a, 53, 54] but the arylation at *N*(7) position has been studied less frequently.[57] If it is not possible to introduce the required aryl substituent by arylation, it can be attempted using *de novo* synthesis of purine from a substituted imidazole[58] or pyrimidine.[59]

The initial object of research was compound **44a**,[65] which was obtained by a catalytic arylation of compound **42** with diphenyliodane[29] followed by introduction of the cyano group at the *C*(6) position using a sulfinate mediated S_NAr reaction with KCN.[65] Arylation of *N*(9) position using diaryliodanes was preferred, as this reaction is selective and high yielding. Further objects of research were benzene rings substituted with carbazoles, which could not be introduced using diaryliodanes, since the carbazole ring is a strong electron donor. During attempts to obtain carbazole-substituted unsymmetrical diaryliodanes, rapid degradation was observed. Compounds **44b-d** were obtained in the Chan–Lam reaction with substituted arylboronic acids and subsequent introduction of the cyano group (Scheme 14). The Chan–Lam reaction was chosen for the arylation because it was the only method that gave the desired products. This method also has drawbacks, such as yields of 51–57% and an equimolar catalyst amount.

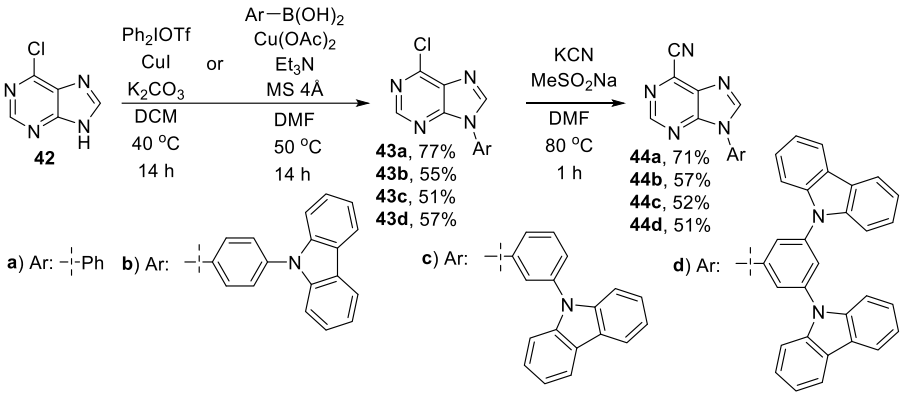

Scheme 14. Preparation of 6-cyano-9-arylpurines **44a-d**.

Research regarding the *N*(7) arylation of purines is scarce. Preparation of 7-arylpurines using *de novo* synthesis with imidazole ring closure is not known in literature, so we decided to research this method. The search for optimal reaction conditions was carried out using starting materials **45** and **47**, since the symmetry of these pyrimidines allowed avoiding side reactions at the beginning of the study. The key step in this sequence was the introduction of arylamines at the *C*(5) position of the pyrimidine, which is markedly less reactive than the *C*(4/6) positions. Initial attempts with pyrimidine **45** led to intermediate **48**, but the optimization revealed the shortcomings of this approach. The S_NAr reaction with aniline occured with a low yield when solvents were used, but performing the reaction neat at the required excess (20 equiv.) was economically unfeasible for other anilines. Dehydroxychlorination of pyrimidine **46** could not be improved over the initial $POCl_3$ reaction. Other chlorinating agents produced either lower yields or only degradation. On the other hand, experiments with diaryliodanes and Cu(I) catalysis produced pyrimidine **48** from starting material **47** in one step. Inspired by an example of Cu(0) catalysis[66] known for the *N*-arylation, we could achieve complete conversion and obtain pyrimidine **48** in 81% yield. The further S_NAr reaction was performed using a saturated ammonia solution in *i*-PrOH to prevent hydrolysis. For the last step, several imidazole coupling methods are known,[59] but complete conversion of substrate **49** without the formation of side products was achieved in an acid-catalyzed reaction with an orthoester, producing purine **50** almost quantitatively (Scheme 15).

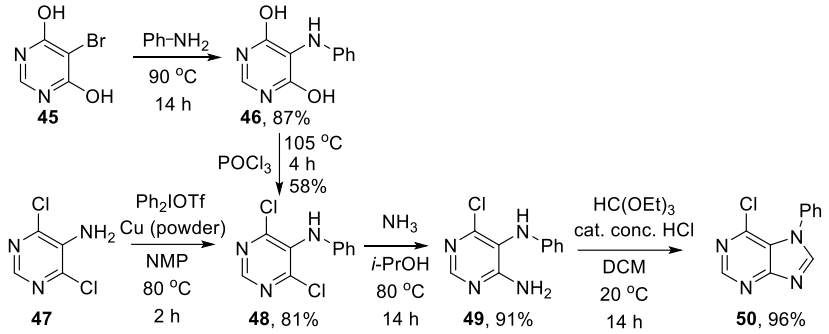

Scheme 15. Preparation sequence 6-chloro-7-phenylpurine (**50**) in a *de novo* synthesis.

Testing the arylation conditions with various diaryliodanes and substituted pyrimidine derivatives **47** revealed that this method can introduce both electron-rich and electron-deficient aromatic systems, as well as heterocycles in the case of compound **48d** (Table 2). Changes in the pyrimidine substituents, which cannot participate in the reaction, do not negatively impact arylation, as shown in compounds **48e**-**g**. The only exception in our hands was 5-amino-4-chloropyrimidine, which degraded under the reaction conditions. In the reaction with aryliodanes containing an electron-donating group, the degradation of iodane was intensified and complete conversion was not achieved. In the reaction with electron-deficient aryliodanes, the degradation of iodane is minimal, however the reactivity also decreases, and the reaction time must be increased to 48 h.

Further, in the monosubstitution S_NAr reaction with ammonia, the best results were obtained at 80 ºC. Electron-rich substrates **48b**,**e** required a longer reaction time to achieve complete conversion. For compounds **48f**,**g**, formation of both pyrimidine *C*(2) and *C*(4/6) adducts occurred, so **49f**,**g** were obtained in slightly lower yields. The *C*(2) position substitution product is formed in small amounts because the *C*(4/6) position is more reactive (Table 2).

Table 2

Reaction Conditions for Obtaining Substituted Pyrimidines **49a-g**

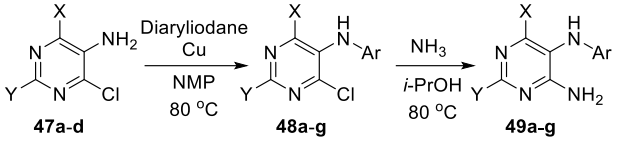

47a-d **48a-g** **49a-g**

No.	X	Y	Reaction **47→48**				Reaction **48→49**	
			Diaryliodane	**Ar**	**t(h)**	**Yield (%)**	**t(h)**	**Yield (%)**
1	Cl	H	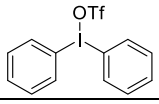		2	**48a**, 81	16	**49a**, 91
2	Cl	H	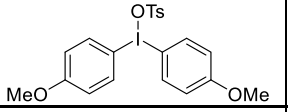	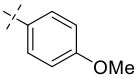	2	**48b**, 65	48	**49b**, 90
3	Cl	H	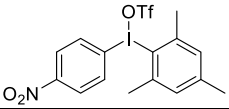	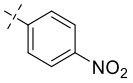	48	**48c**, 66	16	**49c**, 97
4	Cl	H	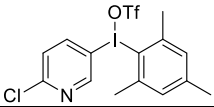	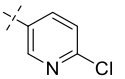	48	**48d**, 61	16	**49d**, 80
5	Cl	Me	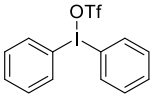		2	**48e**, 71	24	**49e**, 93
6	H	Cl			2	**48f**, 78	16	**49f**, 73
7	Cl	Cl			2	**48g**, 71	16	**49g**, 75

For imidazole ring closing reactions where R = H, the best yields were achieved using the orthoester (Table 3, rows 1; 4–9). Performing this reaction with formic acid we could not prevent hydrolysis at the *C*(6) position. In order to prevent the hydrolysis at the *C*(6) position in reactions with orthoester at elevated temperatures, anhydrous HCl in dioxane was used for the electron-deficient substrates. Imidazole ring formation with orthoester reagents proceeded poorly or not at all when R ≠ H. Aliphatic substituents could be introduced at the *C*(8) position by closing the ring with an anhydride. The trifluoromethyl group was introduced at the *C*(8) position in a two-step process with $(CF_3CO)_2O$ in which trifluoroacetamide was initially formed, and afterwards the cycle was closed at 95 ºC.[67] During the ring closure, hydrolysis occured at the *C*(6) position. To achieve product **50c**, the chlorine at the *C*(6) position was restored by dehydroxychlorination with $POCl_3$.

Table 3

Conditions for Obtaining Substituted 7-arylpurines **50a-i**

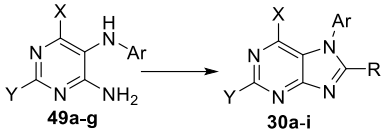

No.	X	Y	R	Ar	Reagent	Solvent	Additive	T (°C)	t(h)	Yield (%)
1	Cl	H	H		$HC(OEt)_3$	DCM	aq. HCl	20	16	**50a**, 96
2	Cl	H	Me		Ac_2O	-	-	120	1	**50b**, 78
3	Cl	H	CF_3		$(CF_3CO)_2O$	1)DCM 2)THF	Py	1)20 2)95	1)16 2)24	**50c**, 70*
4	Cl	H	H	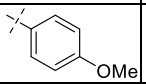	$HC(OEt)_3$	DCM	aq. HCl	40	16	**50d**, 98
5	Cl	H	H	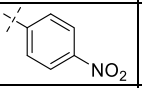	$HC(OEt)_3$	DCE	HCl in dioxane	80	3	**50e**, 91
6	Cl	H	H	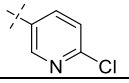	$HC(OEt)_3$	DCE	HCl in dioxane	80	3	**50f**, 82
7	Cl	Me	H		$HC(OEt)_3$	DCM	aq. HCl	20	16	**50g**, 89
8	H	Cl	H		$HC(OEt)_3$	DCM	aq. HCl	20	16	**50h**, 91
9	Cl	Cl	H		$HC(OEt)_3$	DCE	HCl in dioxane	80	16	**50i**, 78

* Overall yield in 2 steps

The scientific publications on the research described in this chapter can be found in Appendices III and V.

2. Photophysical properties and applications of purine derivatives

The research on purine and 6-methylpurine about the properties of this heterocycle in the excited state has shown that the singlet state, which originates during the photoexcitation, is quickly engaged in the intersystem crossing process to form a relatively stable triplet state with a lifetime of 1.7 μs at room temperature or a lifetime of even 1 s at 77 K.[68] The triplet quantum yield of these compounds is 88%.[69] Other studies examined the effect of purine *C*(2) and *C*(6) substituents on the path and rate of excited state relaxation and proposed a relaxation mechanism for 9-methylpurine from an excited singlet state to a triplet through two intermediary states.[70]

Purine derivatives have been employed in OLED structures to perform various functions, but overall, there are very few such examples. One example is the use of a fluorescent purine push-pull system in OLEDs. Devices with purine derivative **51** achieved an external quantum efficiency of 3.1%. The maximum possible efficiency of the fluorescent systems is 25% because the split of excited singlet and triplet states is 1 : 3.[7] In another example, two purines are linked by an aromatic bridge, and depending on the nature of the aromatic cycle, donor-acceptor-donor, acceptor-donor-acceptor, or neutral fluorescent system is formed. Such compounds as **52** have potential applications in OLED or sensors.[6] Adenine and guanine were tested as electron-blocking and hole-transporting layers in the OLED structure. The device with adenine showed the best current conduction and emission efficiency of the tested purines and pyrimidines.[71] Some examples of thermally activated delayed fluorescence are known for purine derivatives linked to electron-rich phenoxazine, where the aromatic systems are twisted out of plane. An OLED with 16% external quantum yield was obtained using purine derivative **53**.[9] Recently, the first phosphorescent iridium complexes **54** with purine ligands have also been published (Fig. 1). Neutral iridium complexes emit light in the orange-red region, while cationic complexes emit light in the yellow-green region.[8]

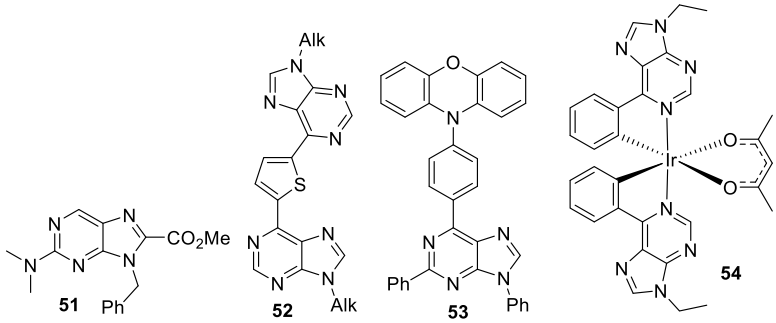

Fig. 1. Purine derivatives known in literature with applications in OLED.[6–9]

OLED consists of two electrodes – cathode and anode, and between them there are several layers of organic materials, which ensure the flow of holes and electrons to the emission layer (EML), where recombination and emission take place (Fig. 2). One or both of the electrodes must be transparent so that the emitted light can exit the device. Examples of commonly used materials for this include LiF/Al cathode and indium tin oxide (ITO) anode.[72] Several auxiliary

layers ensure efficient transport of holes and electrons to the EML and recombination in it. The injection of holes and electrons into the system is controlled by a hole injection layer (HIL), the energy levels of which conform to the anode, and by an electron injection layer (EIL), the energy levels of which conform to the cathode. The hole transport layer (HTL) and the electron transport layer (ETL) are used to match the mobility of electrons and holes, and their energy levels conform to the EML. To promote recombination in EML, an electron blocking layer (EBL) or a hole blocking layer (HBL) are sometimes used, which serve as energy barriers and prevent the flow of electrons or holes to the opposite electrode.[73] The EML consists of an emitter embedded in a host, or in some rare cases this layer is formed solely from the emitter.[74]

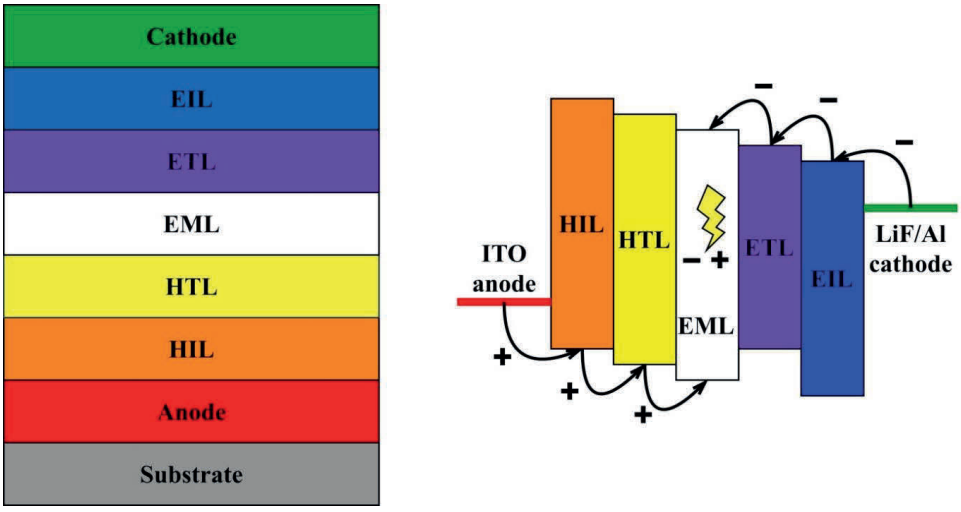

Fig. 2. Representation of structure and working mechanism of OLED.

Far more widely, fluorescent purine derivatives have been used in ion sensors,[75] for fluorescent labeling[76] and marking of cells.[77, 27] Such sensors determine the concentration of ions depending on the intensification or quenching of fluorescence. For substances with applications in cell marking, the most important parameters are biocompatibility, permeability through membranes, cytotoxicity and effect on cell proliferation. Compounds with lower emission quantum yields can also be used for such purposes if only qualitative analysis is required (Fig. 3).

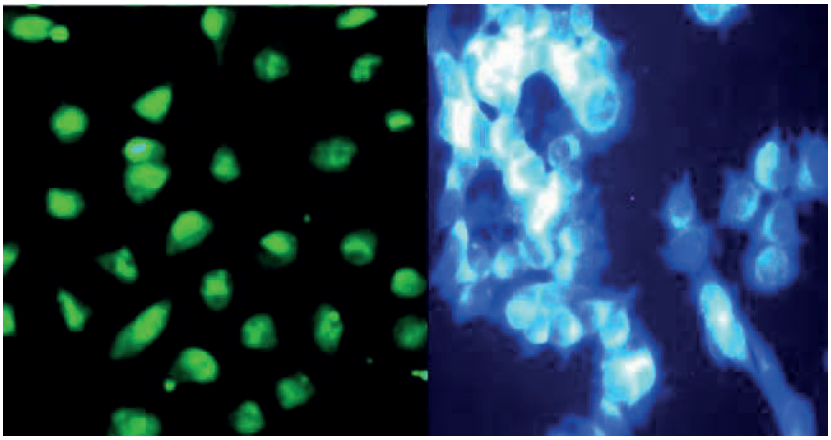

a) b)

Fig. 3. Cell labelling using purine-gold nanoclusters (a)[77b] or push-pull purine derivatives (b).[27]

2.1. Photophysical properties of fluorescent purine derivatives

Organic push-pull fluorescent systems consist of an electron donor and an acceptor connected by a conjugated π system bridge. Transfering energy to such a molecule, for example with UV irradiation, moves it into excited state. In the excited state, the electron has moved from the highest occupied molecular orbital (HOMO) located on and near the electron donor to the lowest unoccupied molecular orbital (LUMO) located on and near the electron acceptor. The excited electron is in the singlet state, so it has an opposite spin compared to the other electron of the pair. To return to the ground state, the excited system returns energy to the environment in the form of a photon – fluorescence occurs. If a molecule capable of fluorescence is excited with electricity, both singlet and triplet excited states are formed. In this case, emission occurs only from the singlet state, but the molecules in triplet state return to the ground state by releasing energy in other ways, most often by heat (Fig. 4).[78] The geometry of the excited state can differ from that of the ground state. The excited state can twist from the initially planar state and fluorescence occurs according to a twisted intramolecular charge transfer (TICT) mechanism.[79] On the other hand, the initially non-planar structure in the excited state may become more planar and fluorescence occurs according to a planar intramolecular charge transfer (PICT) mechanism, which is characterized by a high Stokes shift.[80] The fluorescence quantum yield, fluorescence time, the Stokes shift, and other photophysical properties of the push-pull system can be altered by modifying the electron donor, acceptor, or the π system conjugation.[78] Nitrogen containing heterocycles have been widely explored as electron acceptors in such push-pull systems.[81]

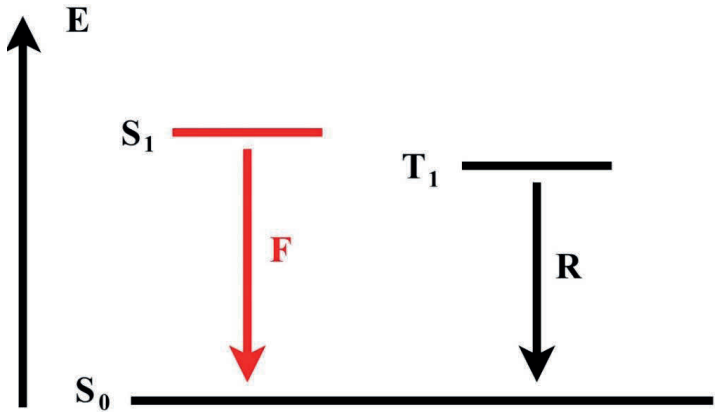

Fig. 4. Schematic representation of fluorescence induced by electricity – fluorescence (F) from singlet state and non-radiative relaxation (R) from triplet state.

The photophysical properties of the purine derivatives obtained in Section 1.2 were measured and experiments were made to test their application in OLEDs. The absorption, emission, quantum yields, energy levels and other data of the compounds were examined.

The obtained compounds **28a-d**, **29a-d**, **36a**,**b** and **41a** possess triphenylmethyl groups, which promote amorphous properties,[61] so that they can be applied using solution methods, which are simpler than vacuum deposition. Experiments with these compounds showed that these compounds indeed form a thin amorphous layer on the glass when applied with solution. DSC measurements on compounds **28a**,**d** and **29a**,**b**,**d** showed that these compounds are amorphous, with glass transition temperatures of 82–102 °C. Compounds containing cyano group possess a higher glass transition temperature. Thermogravimetric analysis of compounds **28d** and **29d** shows that 2-amino-6-triazolylpurines **28** are thermally more stable than 6-amino-2-triazolylpurines **29**, as their decomposition temperatures are 298 and 258 °C.

The obtained push-pull purine derivatives **28a-d**, **29a-d**, **36a**,**b** and **41a**,**c** are fluorescent, and depending on the arrangement of azole and piperidine at the *C*(2) and *C*(6) positions of purine, their maxima of absorption and emission spectra are shifted. For compounds **28a-d**, the lowest energy absorption maximum corresponding to the intramolecular charge transfer is located around 365 nm (Fig. 5), while for compounds **29a-d** this maximum is located around 305 nm (Fig. 6). For compounds **28a**,**b**,**d** the emission maximum is located at 440–450 nm, while for compounds **29a**,**b**,**d** it is located in the near UV region at 390–400 nm. Exceptions are the dimethylamino group containing purine derivatives **28c** and **29c**, whose emission maxima show a batochromic shift by about 60 nm compared to the other derivatives. This was explained by a strong solvatochromy, which is common for compounds containing a dimethylamino group.[82] The absorption and emission spectra of compounds **36a**,**b** and **41a**,**c** differ minimally from the spectra of analogous compounds **29a**,**b**,**d**. In the case of compound **41c**, absorption maxima of carbazole were also observed in the absorption spectrum, as well as maxima in the emission spectra attributed to carbazole (Table 4). Measurements with **8a** and **9a** showed that both regioisomers exhibit positive solvatochromy.

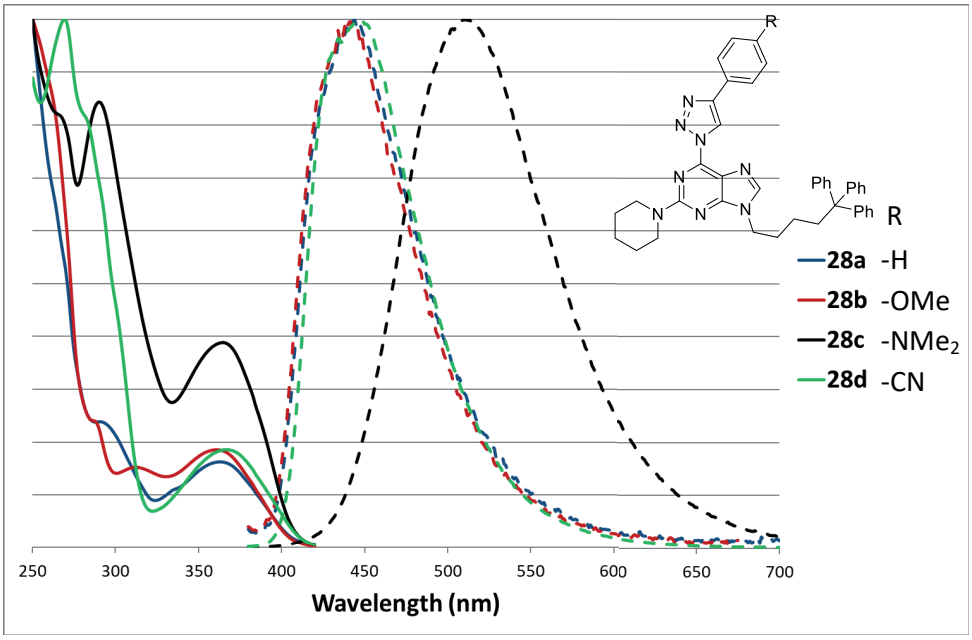

Fig. 5. Normalized absorption(—) and emission(- -) spectra of 2-amino-6-triazolylpurines **28a-d** in DCM solution.

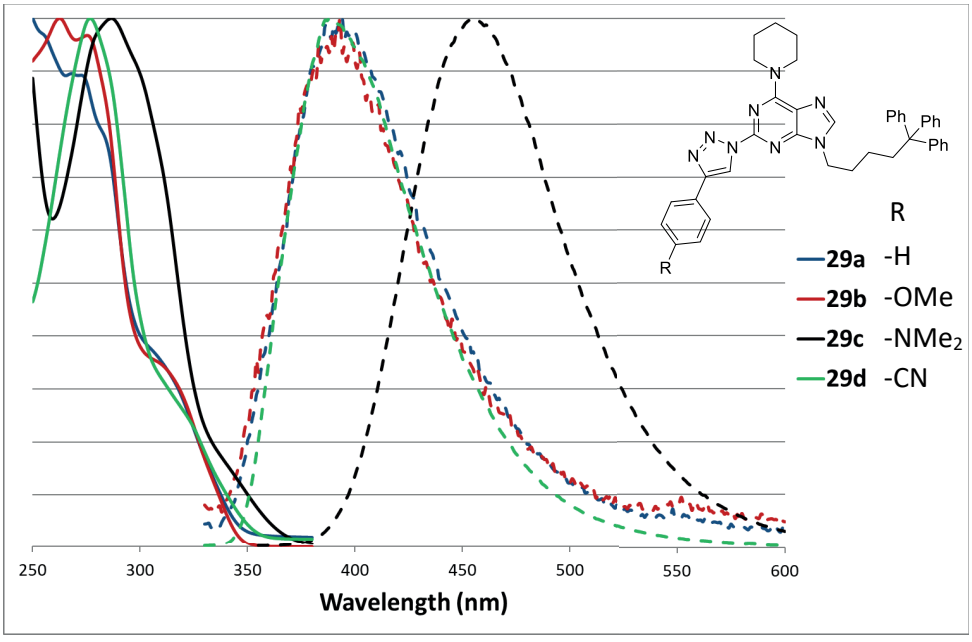

Fig. 6. Normalized absorption(—) and emission(- -) spectra of 6-amino-2-triazolylpurines **29a-d** in DCM solution.

Table 4

Absorption, Emission and Quantum Yield Experimental Data of Purine Derivatives

No.	Compound	$\lambda_{abs\ max}$, (nm)*	$\lambda_{em\ max}$, (nm)*	Φ_{PL} (DCM)	Φ_{PL} (thin layer film)
1	**28a**	364	446	0.91	0.32
2	**28b**	360	439	0.78	0.28
3	**28c**	365	511	0.74	0.03
4	**28d**	367	448	0.90	0.40
5	**29a**	320 (shoulder)	394	0.31	0.22
6	**29b**	320 (shoulder)	399	0.17	0.15
7	**29c**	330 (shoulder)	455	0.30	0.03
8	**29d**	330 (shoulder)	388	0.44	0.20
9	**36a**	305 (shoulder)	356	0.01	0.12
10	**36b**	300 (shoulder)	373	0.07	0.45
11	**41a**	310 (shoulder)	398	0.66	0.42
12	**41c**	292, 323, 338	362, 378, 397	0.51	0.20

*Measured in $5 \cdot 10^{-5}$ M DCM solution

Quantum yields were determined for the fluorescent compounds in DCM solution and in thin layer film, which could be done due to their amorphous properties. Compounds **28a-d**, **29a-d** and **41a**,**c** showed expected results – the quantum yield of fluorescence in solution reached up to 91%, but in thin layer film it was significantly lower, as the molecules are isolated in solution and fluorescence quenching does not occur. For compounds **36a**,**b**, the opposite effect was observed – the fluorescence quantum yield significantly increases in thin layer film. This can be explained by the rotation of aromatic rings in solution, which quenches fluorescence but is reduced in the solid phase. 2-Amino-6-triazolylpurines **28a-d** showed on average higher quantum yields in solution than the reverse regioisomers, but these compounds also showed a larger drop in quantum yield, moving to the solid phase in film (Table 4).

For compounds **28a-d** and **29a-d**, the ionization energy and photoconductivity threshold were determined, and from those the affinity energy was calculated (A. Vembris, ISSP). The measurements revealed that the ionization energy is not much infuenced by the placement of the substituents in the *C*(2) and *C*(6) positions, but changes depending on the donor or acceptor substituent on phenyltriazole. The photoconductivity threshold changes both depending on the arrangement of the substituents and the donor or acceptor moiety. These values are significantly higher for 6-amino-2-triazolylpurines **29a-d** (3.07–3.45 eV) compared to the reverse regioisomers **28a-d** (2.75–2.95 eV).

Triplet energy levels were also determined for these compounds, which are important for potential application in OLEDs as hosts. For compounds **28a-d**, triplet levels are at 2.52–2.54 eV, for compounds **29a**,**b**,**d** 2.87–2.95 eV, and for **29c** 2.75 eV. The properties of compounds **29** are theoretically suitable for application as hosts for blue phosphorescent emitters.

DFT calculations showed that in the case of neutral or electron-withdrawing substituents on phenyltriazole, the HOMO orbitals of compounds **28a**,**d** are centered on purine, while the

LUMO are centered on phenyltriazole, while the HOMO and LUMO orbitals of **29a**,**d** are delocalized throughout the system. This arrangement indicates a more pronounced push-pull character for compounds **29a**,**d** as well as a lower propensity for the excited state to relax without emission. In the case of electron-donating substituents on triazole, compound **28b**,**c** and **29b**,**c** the HOMO orbitals are centered on phenyltriazole, while the LUMO orbitals are centered on purine.

Purine derivatives **28a**,**d** and **29a**,**d** were tested as emitters in OLED, but compound **29b** was tested as a host in OLED with FIrpic emitter. In the case of emitters, no electroluminescence was observed. Whereas in the experiment with the purine derivative **29b** as the host in OLED, the efficiency of the device dropped sharply by increasing voltage, if compared to the control experiment in which the host was polyvinylcarbazole (PVK). These results can be explained by the high current density in the OLED when purine derivative was used. The high charge mobility can be explained by the planar structure and dipole nature of the obtained derivatives. Such compounds could be used as organic field effect transistors in the future.

Research regarding organic field-effect transistors attempts to replace inorganic amorphous silicon in semiconductors. Mechanically flexible electronics, formed by solution methods, can be obtained by using low molecular weight compounds or polymers. For such materials one of the most important parameters is charge mobility, which ensures energy efficiency, operation with low power supply and a stable device temperature. Such devices can be constructed in two ways – with a gate electrode as the top or bottom layer (Fig. 7). If the gate electrode is the top layer, then the polymer substrate is used as the base, otherwise the gate electrode can serve as the base. The other structural elements are input and drain electrodes, an organic semiconductor and an insulator.[83]

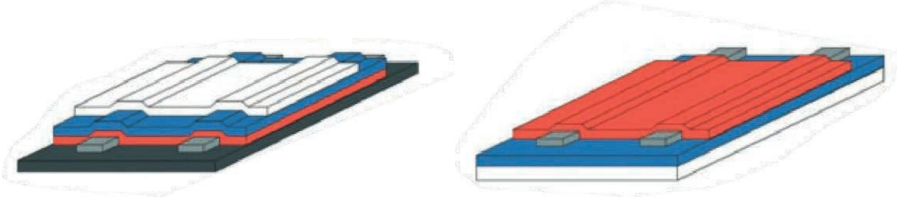

Fig. 7. Schematic representation of organic field effect transistors with gate electrode as the top (left) or bottom (right) layer. Polymer substrate (black), source and drain electrodes (gray), organic semiconductor (orange), ioslator (blue), and gate electrode (white).[83]

The scientific publications on the research described in this chapter can be found in Appendices II and IV.

2.2. Thermally activated delayed fluorescence in purine derivatives

The initial OLED with fluorescent emitters is able to use only 25% of the input energy. This is determined by the fact that during electrical excitation only a quarter of the excited molecules are in the singlet state, which is able to fluoresce, but the rest are in the triplet state, the energy of which is wasted. The situation was improved by phosphorescent metal complexes, which are

able to use all of the input energy, but these complexes are based on expensive and depleting transition metals – most often iridium, sometimes platinum, the use of which should be reduced. Thermally activated delayed fluorescence (TADF) is the field of research that has developed in the past decade and can potentially replace phosphorescent transition metal complexes. TADF looks at compounds that are able to utilize all the input energy through a reverse intersystem crossing (RISC) in which an excited molecule goes from a triplet state to a singlet state. In this case, molecules that are initially excited in the singlet state, produce fluorescence (F), while molecules from the initial triplet state enter the singlet state through RISC and form delayed fluorescence (DF) (Fig. 8).[84]

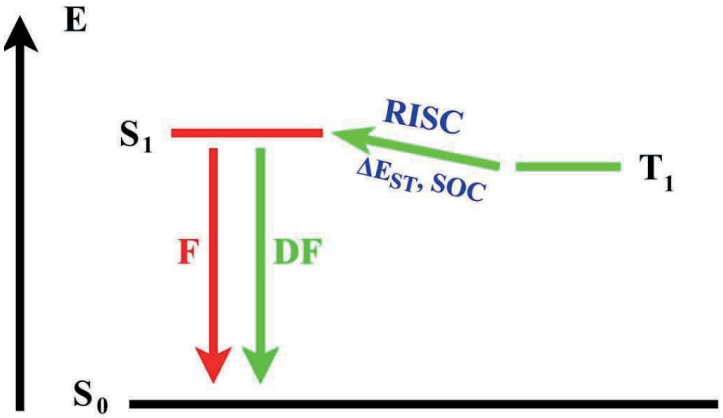

Fig. 8. Schematic representation of TADF emission.

For the RISC process to occur, value of spin-orbit coupling (SOC) must be as high as possible, but the difference between the singlet and triplet levels (ΔE_{ST}) must be sufficiently low. Higher SOC can be achieved with molecules that contain heavy atoms. Low ΔE_{ST} is achieved by reducing the overlap of the HOMO and LUMO orbitals. In molecules with covalently linked donor-acceptor pairs, this is achieved by steric hindrance that interrupts the conjugation between the donor and the acceptor. Another alternative is the use of exciplex systems with separate donor and acceptor components [84] (Fig. 9). Such compounds can be modified to obtain the required physical properties by including the active component in polymers or dendrimers to be used for OLED fabrication by the solution method.[85] The purine ring is characterized by fast intersystem transition process[70] with a high triplet quantum yield,[69] which are relevant parameters for the study of TADF systems. Carbazole has been widely used as the electron donor in TADF emitters and OLED hosts due to its high stability, good hole mobility, and triplet energy levels that are higher than those of fluorene or biphenyl.[86]

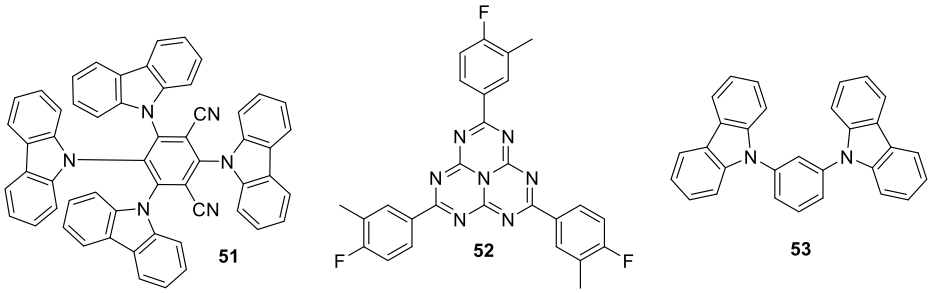

Fig. 9. Examples of sterically hindered compound (**51**) and exciplex pair (**52**+**53**) that can take part in RISC.[84a]

Our initial tests were performed with 6-cyano-9-phenylpurine (**44a**), since the cyano group decreases the electron affinity of the purine, while the phenyl group prevents *N*(9)-*N*(7) tautomerization. Measurements with this compound showed weak fluorescence, yet pronounced phosphorescence at 77 K. This indicates the presence of molecules in the triplet state in sufficient quantity and matches the findings of the theoretical calculations on the energy levels of this system.

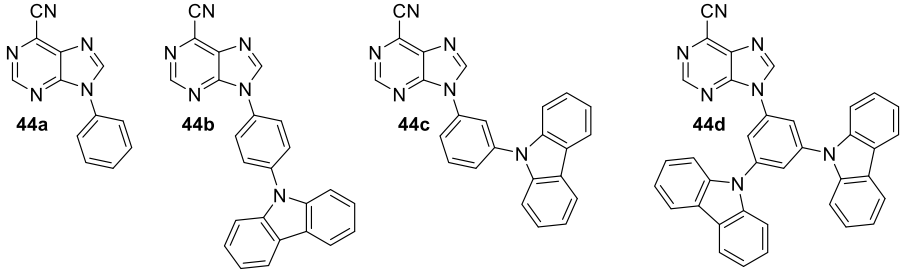

Fig. 10. 6-Cyanopurine component **24a** and covalently bonded conjugates **24b-d**.

Compound **44a** was tested in an exciplex system with PVK and 9-phenylcarbazole (9-PhCbz) due to the matching energy levels of these donors. For physical mixtures, there may be technical problems with molecular arrangement that make the formation of exciplex pairs less likely. An alternative is covalently bonded pairs of exciplexes in which the charge transfer cannot occur intramolecularly. Compounds **44b-d** (Fig. 10) were obtained in which the cyanopurine and carbazole are connected through a benzene ring that is twisted out of hetereocyclic plane. The sterically hindered aromatic fragment interferes with the conjugation of the π-electron system and also works as a donor-donor-acceptor system,[87] which prevents an intramolecular process from occurring. The X-ray structure of the compound **44b** shows that the purine and carbazole are coplanar, but the benzene ring is 50° out of plane (Fig. 11).

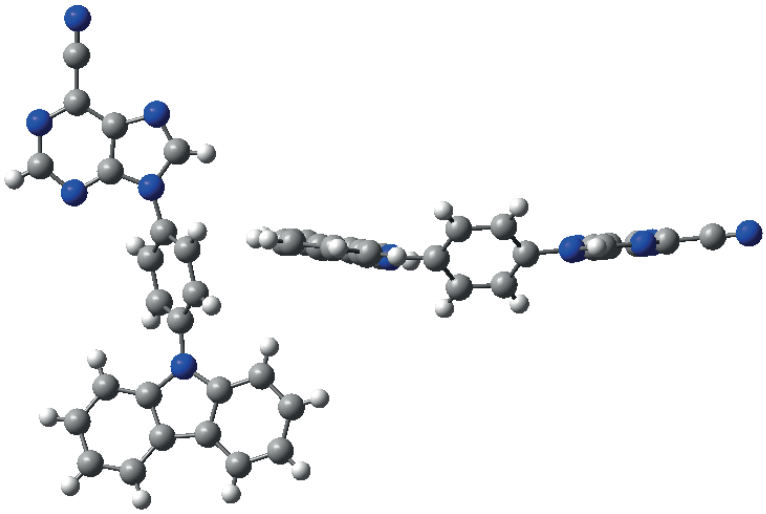

Fig. 11. Compound **44b** XRD structure in two projections with the benzene ring twisted out of plane.

Quenching of the carbazole emission was observed for the physical mixtures of purine and carbazole derivatives in solution, indicating an excited state transfer from carbazole to purine. For the covalently bonded **44b-d**, weak fluorescence was observed at room temperature, but at 77 K the phosphorescence of compounds **44c**,**d** is far more intense than fluorescence, indicating an intermolecular process. On the other hand, the intramolecular process is suppressed by the disrupted conjugation. This observation is also supported by the absorption spectra, which for the covalently bound compounds show a sum of compound **44a** and carbazole component absorption without an additional absorption band for the bonded system. In the case of compound **44b**, fluorescence and phosphorescence of comparable intensity were observed at 77 K, suggesting an increased probability of an intramolecular process.

Measurements in thin layer film (Table 5) showed that emission in the 473–528 nm region occurs from exciplexes with a quantum yield of up to 41% and emission quenching is observed in the presence of oxygen. Decreasing the temperature in the range 300–77 K causes an increase of the quantum yield over most of the range. This observation is in contrast to the expected result for TADF but was explained by the increased stability of the triplet state at low temperatures, which is important in the relaxation of the excited state. This relationship is not linear, and the TADF effect was observed with a local maximum of the quantum yield at 100–180 K. The photoluminescence consists of several components of different durations, which is characteristic to exciplex systems. The fastest component in the samples is 31–55 ns, which is slower than a typical fluorescence, so the delayed emission was observed. At lower temperatures, the fastest component is not much affected, but the next component is extended by about 80 ns, typical to TADF. The fastest and slowest components are caused through different pathways, which is expected in exciplex systems, since the distance between the donor and acceptor component is variable. In two-component systems, the ratio between the slow and fast components can be influenced by changing the donor-acceptor ratio. Experiments with

different concentrations of **44c** in a polymethyl methacrylate host caused an emission shift to the blue region and a decreased quantum yield by increasing dilution of **44c**.

Table 5

Photophysical Properties of Exciplex Systems in Thin Layer Film

No.	System	Λ_{PL}, (nm)[a]	Φ_{PL}	t, (ns)	t, (%)[b]	E_S, (eV)[c]	E_T, (eV)[d]	ΔE_{ST}, (eV)[e]
1	**44a**/ 9-PhCbz (1 : 1)	473	0.25	49	21	2.98	2.95	0.03
				137	56			
				682	16			
2	**44a**/ PVK (1 : 1)	528	0.08	31	12	2.81	2.95	–0.14
				140	56			
				692	32			
3	**44b**	501	0.17	34	21	2.97	2.92	0.05
				149	79			
4	**44c**	502	0.41	54	39	2.82	2.94	–0.12
				246	61			
5	**44d**	497	0.13	55	27	2.85	2.94	–0.09
				183	73			

[a] Emission maximum.

[b] Percentage distribution of photoluminescence components.

[c] Fluorescence activation energy at room temperature.

[d] Phosphorescence activation energy 77 K.

[e] $\Delta E_{ST} = E_S - E_T$

Covalently bonded TADF molecules can have different emission mechanisms depending on the morphology of the solid phase.[88] In measurements with compound **44c**, it was found that the TADF emission discussed above occurs in the amorphous phase, while fluorescence occurs in the crystalline phase with an emission maximum of 471 nm and quantum yield 52%. The change in the emission mechanism in the crystalline phase is explained by a stronger donor-acceptor conjugation, which is facilitated by conformation fixed in the crystal lattice.

The obtained purine derivatives are better suitable for the role of OLED hosts because their photoluminescence is quenched with increasing temperature. OLED tests were performed with compound **44d** because it showed the best charge mobility. An OLED with a green TADF emitter DAcIPN and with compound **44d** as the host was obtained and produced a maximum external quantum yield of 11.6% and brightness above 50000 cd/m^2. An incomplete energy transfer to the emitter was observed when using a low emitter concentration (5%). OLEDs with active matrix **44d** showed higher external quantum yields than previously published results with other hosts known in literature.[89]

The scientific publication of the research described in this chapter can be found in Appendix III.

CONCLUSIONS

1. It is possible to perform the S_NAr reaction with amines at the less reactive atom at *C*(2) position of 2,6-diazidopurine due to the azide-tetrazole equilibrium.

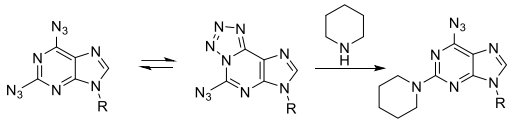

2. The presence of triphenylmethyl groups promotes the amorphous properties of the compounds and enables formation of solution processed amorphous thin layer films of purine derivatives.

3. Imidazole, 1-1*H*-1,2,4-triazole, 1-1*H*-1,2,3-triazole and 2-2*H*-1,2,3-triazole can be introduced at the atom at *C*(2) position using the S_NAr reaction at 160 °C temperature.

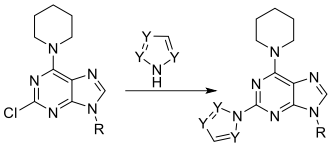

4. Aromatic substituents can be introduced at the nitrogen atom at *N*(9) position of purine using diaryliodanes or the Chan–Lam reaction.

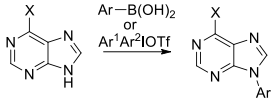

5. *N*(7) Arylpurines can be obtained in high yields from substituted 5-aminopyrimidines via *de novo* synthesis.

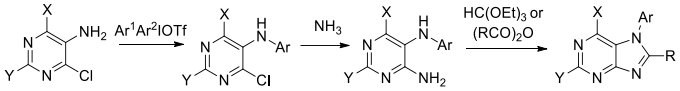

6. 2/6-Amino-2/6-azolylpurines, depending on the substituent placement at the *C*(2) and *C*(6) positions, exhibit fluorescence with emission maxima around 390 or 450 nm. Their quantum yields reach up to 91% in solution and 45% in thin layer film. Such compounds have potential applications as organic field-effect transistors.

7. Both covalently bonded purine-carbazole exciplexes and the mixtures of their analogs exhibit TADF properties. Such compounds and mixtures show emissions of various durations characteristic of exciplexes with the maxima around 500 nm. The emission efficiencies at different temperatures are affected by the stability of the triplet state and the TADF effect. Quantum yields of the products reach up to 41% in the thin layer film. Such compounds have potential applications as hosts in OLEDs.

REFERENCES

1. Seley-Radtke, K. L.; Yates, M. K. *Antiviral Res.* **2018**, *154*, 66.
2. Saito, Y.; Hudson, R. H. E. *J. Photochem. PhotoBiol. C: Photochem. Rev.* **2018**, *36*, 48.
3. Tang, C. W.; VanSlyke, S. A. *Appl. Phys. Lett.* **1987**, *51*, 913.
4. Jou, J.-H.; Kumar, S.; Jou, Y. C. In *Disruptive characteristics and lifetime issues of OLEDs*, Buckley, A., Ed.; Woodhead Publishing, United Kingdom, 2013; pp. 410–442.
5. (a) Jou, J.-H.; Sahoo, S.; Dubey, D. K.; Yadav, R. A. K.; Swayamprabha, S. S.; Chavhan, S.D. *J. Mater. Chem. C* **2018**, *6*, 11492. (b) Chen, H.-W.; Lee, J.-H.; Lin, B.-Y.; Chen, S.; Wu, S. T. *Light Sci. Appl.* **2018**, *7*, 17168.
6. Collier, G. S.; Brown, L. A.; Boone, E. S.; Kaushal, M.; Ericson, M. N.; Walter, M. G.; Long, B. K.; Kilbey II, S. M. *J. Mater. Chem. C* **2017**, *5*, 6891.
7. (a) Butler, R. S.; Cohn, P.; Tenzel, P.; Abboud, K. A.; Castellano, R. K. *J. Am. Chem. Soc.* **2009**, *131*, 623. (b) Yang, Y.; Cohn, P.; Dyer, A. L.; Eom, S.-H.; Reynolds, J. R.; Castellano, R. K.; Xue, J. *Chem. Mater.* **2010**, *22*, 3580. (c) Yang, Y.; Cohn, P.; Eom, S.-H.; Abboud, K. A.; Castellano, R. K.; Xue, J. *J. Mater. Chem. C* **2013**, *1*, 2867.
8. Lorenzo-Aparicio, C.; Gallego, M. R.; de Arellano, C. R.; Sierra, M. A. *Dalton Trans*. **2022**, *51*, 5138.
9. (a) Wang, Z.; Yao, J.; Zhan, L.; Gong, S.; Ma, D.; Yang, C. *Dyes Pigm.* **2020**, *180*, 108437. (b) Wu, Y.; Zhang, Y.; Ran, C.; Lan, J.; Bin, Z.; You, J. *Org. Lett.* **2021**, *23*, 3839.
10. Rosemeyer, H. *Chem. Biodivers.* **2004**, *1*, 361.
11. Cīrule, D.; Ozols, K.; Platnieks, O.; Bizdēna, Ē.; Māliņa, I.; Turks, M. *Tetrahedron* **2016**, *72*, 4177.
12. Singh, B.; Diaz-Gonzalez, R.; Ceballos-Perez, G.; Rojas-Barros, D. I.; Gunaganti, N.; Gillingwater, K.; Martinez-Martinez, M. S.; Manzano, P.; Navarro, M.; Pollastri, M. P. *J. Med. Chem.* **2020**, *63*, 9912.
13. Malínková, V.; Řezníčková, E.; Jorda, R.; Gucký, T.; Kryštof, V. *Bioorg. Med. Chem.* **2017**, *25*, 6523.
14. Novosjolova, I.; Bizdēna, Ē.; Turks, M. *Eur. J. Org. Chem.* **2015**, *2015*, 3629.
15. Zaķis, J. M.; Ozols, K.; Novosjolova, I.; Vilšķērsts, R.; Mishnev, A.; Turks, M. *J. Org. Chem.* **2020**, *85*, 4753.
16. Kania, J.; Gundersen, L.-L. *Eur. J. Org. Chem.* **2013**, *2013*, 2008.
17. Guo, H.-M.; Xin, P.-Y.; Niu, H.-Y.; Wang, D.-C.; Jiang, Y.; Qu, G.-R. *Green Chem.* **2010**, *12*, 2131.
18. Qu, G.-R.; Mao, Z.-J.; Niu, H.-Y.; Wang, D.-C.; Xia, C.; Guo, H.-M. *Org. Lett.* **2009**, *11*, 1745.
19. Parmar, U.; Somvanshi, D.; Kori, S.; Desai, A. A.; Dandela, R.; Maity, D. K.; Kapdi, A. R. *J. Org. Chem.* **2021**, *86*, 8900.
20. Frieden, M.; Aviñó, A.; Eritja, R. *Nucleosides Nucleotides Nucleic Acids* **2003**, *22*, 193.
21. Cīrule, D.; Novosjolova, I.; Bizdēna, Ē.; Turks, M.; *Beilstein J. Org. Chem.* **2021**, *17*, 410.
22. (a) Hocek, M. *Eur. J. Org. Chem.* **2003**, *2003*, 245. (b) Čerňa, I.; Pohl, R.; Klepetářová, B.; Hocek, M. *J. Org. Chem.* **2008**, *73*, 9048. (c) Liu, J.; Robins, M. J. *Org. Lett.* **2004**, *6*, 3421.

23. Wang, D.-C.; Niu, H.-Y.; Qu, G.-R.; Liang, L.; Wei, X.-J.; Zhang, Y.; Guo, H. M. *Org. Biomol. Chem.* **2011**, *9*, 7663.
24. Bhanu Prasad, A. S.; Stevenson, T. M.; Citineni, J. R.; Nyzam, V.; Knochel, P. *Tetrahedron* **1997**, *53*, 7237.
25. Elzein, E.; Palle, V.; Wu, Y.; Maa, T.; Zeng, D.; Zablocki, J. *J. Med. Chem.* **2004**, *47*, 4766.
26. Hocek, M.; Pohl, R.; Císařová, I. *Eur. J. Org. Chem.* **2005**, *2005*, 3026.
27. Šišuļins, A.; Bucevičius, J.; Tseng, Y.-T.; Novosjolova, I.; Traskovskis, K.; Bizdēna, Ē.; Chang, H.-T.; Tumkevičius, S.; Turks, M. *Beilstein J. Org. Chem.* **2019**, *15*, 474.
28. Mahajan, T. R.; Ytre-Arne, M. E.; Strøm-Andersen, P.; Dalhus, B.; Gundersen, L.-L. *Molecules*, **2015**, *20*, 15944.
29. (a) Niu, H.-Y.; Xia, C.; Qu, G.-R.; Zhang, Q.; Jiang, Y.; Mao, R.-Z.; Li, D.-Y.; Guo, H.-M. *Org. Biomol. Chem.* **2011**, *9*, 5039. (b) Csenki, J. T.; Mészáros, Á.; Gonda, Z.; Novák, Z. *Chem. Eur. J.* **2021**, *27*, 15638.
30. Abdoli, M.; Mirjafary, Z.; Saeidian, H.; Kakanejadifard, A. *RSC Adv.* **2015**, *5*, 44371.
31. Traskovskis, K.; Mihailovs, I.; Tokmakovs, A.; Jurgis, A.; Kokars, V.; Rutkis, M. *J. Mater. Chem.* **2012**, *22*, 11268.
32. Tobrman, T.; Štěpnička, P.; Císařová, I.; Dvořák, D. *Eur. J. Org. Chem.* **2008**, *2008*, 2167.
33. Tobrman, T.; Dvořák, D. *Collect. Czech. Chem. Commun.* **2007**, *72*, 1365.
34. Isobe, Y.; Kurimoto, A.; Tobe, M.; Hashimoto, K.; Nakamura, T.; Norimura, K.; Ogita, H.; Takaku, H. *J. Med. Chem.* **2006**, *49*, 2088.
35. Carrera, D.; Angelaud, R.; Sheng, P.; Safina, B.; Li, J. *Org. Process Res. Dev.* **2013**, *17*, 138.
36. Kurimoto, A.; Ogino, T.; Ichii, S.; Isobe, Y.; Tobe, M.; Ogita, H.; Takaku, H.; Sajiki, H.; Hirota, K.; Kawakami, H. *Bioorg. Med. Chem.* **2004**, *12*, 1091.
37. Crestey, F.; Zimdars, S.; Knochel, P. *Synthesis* **2013**, *45*, 3029.
38. Stokes, S. S.; Huynh, H.; Gowravaram, M.; Albert, R.; Cavero-Tomas, M.; Chen, B.; Harang, J.; Loch III, J. T.; Lu, M.; Mullen, G. B.; Zhao, S.; Liu, C.-F.; Mills, S. D. *Bioorg. Med. Chem. Lett.* **2011**, *21*, 4556.
39. Pohl, R.; Hocek, M. *Synthesis* **2004**, *17*, 2869.
40. Hocek, M.; Votruba, I.; Dvořáková, H. *Tetrahedron* **2003**, *59*, 607.
41. Nicolaou, K. C.; Ellery, S. P.; Rivas, F.; Saye, K.; Rogers, E.; Workinger, T. J.; Schallenberger, M.; Tawatao, R.; Montero, A.; Hessell, A.; Romesberg, F.; Carson, D.; Burton, D. *Bioorg. Med. Chem.* **2011**, *19*, 5648.
42. Havelková, M.; Dvořák, D.; Hocek, M. *Synthesis*, **2001**, *11*, 1704.
43. Costanzi, S.; Tikhonova, I. G.; Ohno, M.; Roh, E. J.; Joshi, B. V.; Colson, A.-O.; Houston, D.; Maddileti, S.; Harden, T. K.; Jacobson, K. A. *J. Med. Chem.* **2007**, *50*, 3229.
44. Ibrahim, N.; Chevot, F.; Legraverend, M. *Tetrahedron Lett.* **2011**, *52*, 305.
45. Langli, G.; Gundersen, L.-L.; Rise, F. *Tetrahedron* **1996**, *52*, 5625.
46. Borrmann, T.; Abdelrahman, A.; Volpini, R.; Lambertucci, Alksnis, E.; Gorzalka, S.; Knospe, M.; Schiedel, A. C.; Cristalli, G.; Müller, C. E. *J. Med. Chem.* **2009**, *52*, 5974.

47. (a) Laufer, S. A.; Domeyer, D. M.; Scior, T. R. F.; Albrecht, W.; Hauser, D. R. J. *J. Med. Chem.* **2005**, *48*, 710. (b) Bilbao, N.; Vázquez-González, V.; Aranda, M. T.; González-Rodríguez, D. *Eur. J. Org. Chem.* **2015**, *2015*, 7160.
48. Mahajan, T. R.; Gundersen, L.-L. *Tetrahedron Lett.* **2015**, *56*, 5899.
49. Liang, Y.; Wnuk, S. F. *Molecules*, **2015**, *20*, 4874.
50. Amblard, F.; Nolan, S. P.; Gillaizeau, I.; Agrofoglio, L. A. *Tetrahedron Lett.* **2003**, *44*, 9177.
51. Zhou, P.; Xie, M.-S.; Qu, G.-R.; Li, R.-L.; Guo, H.-M. *Asian J. Org. Chem.* **2016**, *5*, 1100.
52. Horhota, A. T.; Szostak, J. W.; McLaughlin, L. W. *Org. Lett.* **2006**, *8*, 5345.
53. Larsen, A. F.; Ulven, T. *Chem. Commun.* **2014**, *50*, 4997.
54. Khalafi-Nezhad, A.; Zare, A.; Parhami, A.; Navid, M.; Rad, S.; Nejabat, G. R. *Can. J. Chem.* **2006**, *84*, 979.
55. Chen, S.; Graceffa, R. F.; Boezio, A. A. *Org. Lett.* **2016**, *18*, 16.
56. (a) Kotek, V.; Chudíková, N.; Tobrman, T.; Dvořák, D. *Org. Lett.* **2010**, *24*, 5724. (b) Kotek, V.; Tobrman, T.; Dvořák, D. *Synthesis*, **2012**, *44*, 610. (c) Aarhus, T. I.; Fritze, U. F.; Hennum, M.; Gundersen, L.-L. *Tetrahedron Lett.* **2014**, *55*, 5748.
57. Keder, R.; Dvořáková, H.; Dvořák, D. *Eur. J. Org. Chem.* **2009**, *2009*, 1522.
58. (a) Hirota, K.; Kazaoka, K.; Niimoto, I.; Sajiki, H. *Org. Biomol. Chem.* **2003**, *1*, 1354. (b) Biagi, G.; Giorgi, I.; Livi, O.; Pacchini, F.; Salerni, O. L.; Scartoni, V. *J. Heterocycl. Chem.* **2005**, *42*, 743. (c) Guchhait, S. K.; Chaudhary, V. *Org. Biomol. Chem.* **2014**, *12*, 6694. (d) Bollier, M.; Klupsch, F.; Six, P.; Dubuquoy, L.; Azaroual, N.; Millet, R.; Leleu-Chavain, N. *J. Org. Chem.* **2018**, *83*, 422. (e) Tber, Z.; Biteau, N. G.; Agrofoglio, L.; Cros, J.; Goffinont, S.; Castaing, B.; Nicolas, C.; Roy, V. *Eur. J. Org. Chem.* **2019**, *2019*, 5756.
59. (a) Liu, J.; Dang, Q.; Wei, Z.; Shi, F.; Bai, X. *J. Comb. Chem.* **2006**, *8*, 410. (b) Chorvat, R. J.; Bakthavatchalam, R.; Beck, J. P.; Gilligan, P. J.; Wilde, R. G.; Cocuzza, A. J.; Hobbs, F. W.; Cheeseman, R. S.; Curry, M.; Rescinito, J. P.; Krenitsky, P.; Chidester, D.; Yarem, J. A.; Klaczkiewicz, J. D.; Hodge, C. N.; Aldrich, P. E.; Wasserman, Z. R.; Fernandez, C. H.; Zaczek, R.; Fitzgerald, L. W.; Huang, S.-M.; Shen, H. L.; Wong, N.; Chien, B. M.; Quon, C. Y.; Arvanitis, A. *J. Med. Chem.* **1999**, *42*, 833. (c) Gordon, M. R.; Lindell, S. D.; Richards, D. *Synlett* **2018**, *29*, 473. (d) Zelli, R.; Zeinyeh, W.; Haudecouer, R.; Alliot, J.; Boucherle, B.; Callebaut, I.; Décout, J.-L. *Org. Lett.* **2017**, *19*, 6360.
60. (a) Novosjolova, I.; Bizdēna, Ē.; Turks, M. *Tetrahedron Lett.* **2013**, *54*, 6557. (b) Novosjolova, I.; Bizdēna, Ē.; Turks, M. *Phosphorus Sulfur Silicon Relat. Elem.* **2015**, *190*, 1236.
61. Traskovskis, K.; Rudušs, A.; Kokars, V.; Mihailovs, I.; Lesina, N.; Vembris, A. *New J. Chem.* **2019**, *43*, 37.
62. Satoh, Y.; Marcopulos, N. *Tetrahedron Lett.* **1995**, *36*, 1759.
63. Kim, S. H.; Jang, J.; Lee, J. Y. *Appl. Phys. Lett.* **2007**, *90*, 223505.
64. Hong, G.; Gan, X.; Leonhardt, C.; Zhang, Z.; Seibert, J.; Busch, J. M.; Bräse, S. *Adv. Mater.* **2021**, *33*, 2005630.
65. Miyashita, A.; Suzuki, Y.; Ohta, K.; Higashino, T. *Heterocycles* **1994**, *39*, 345.

66. Matsuzaki, K.; Okuyama, K.; Tokunaga, E.; Saito, N.; Shiro, M.; Shibata, N. *Org. Lett.* **2015**, *17*, 3038.
67. Šála, M.; Kögler, M.; Plačková, P.; Mejdrová, I.; Hřebabecký, H.; Procházková, E.; Strunin, D.; Lee, G.; Birkus, G.; Weber, J.; Mertlíková-Kaiserová, H.; Nencka, R. *Bioorg. Med. Chem. Lett.* **2016**, *26*, 2706.
68. Arce, R.; Quiñones, E. *J. Am. Chem. Soc.* **1989**, *111*, 8218.
69. Murgida, D. H.; Bilmes, G. M.; Erra-Balsells, R. *Photochem. Photobiol.* **1996**, *64*, 777.
70. Crespo-Hernández, C. E.; Martínez-Fernández, L.; Rauer, C.; Reichardt, C.; Mai, S.; Pollum, M.; Marquetand, P.; González, L.; Corral, I. *J. Am. Chem. Soc.* **2015**, *137*, 4368.
71. Gomez, E. F.; Venkatraman, V.; Grote, J. G.; Steckl, A. J. *Adv. Mater.* **2015**, *27*, 7552.
72. (a) Wei, Q.; Fei, N.; Islam, A.; Lei, T.; Hong, L.; Peng, R.; Fan, X.; Chen, L.; Gao, P.; Ge, Z. *Adv. Optical Mater.* **2018**, *6*, 1800512. (b) Geffroy, B.; le Roy, P.; Prat, C. *Polym. Int.* **2006**, *55*, 572.
73. Negi, S.; Mittal, P.; Kumar, B. *Microsyst. Technol.* **2018**, *24*, 4981.
74. Godumala, M.; Choi, S.; Cho, M. J.; Choi, D. H. *J. Mater. Chem. C* **2019**, *7*, 2172.
75. (a) Jovaisaite, J.; Cīrule, D.; Jeminejs, A.; Novosjolova, I.; Turks, M.; Baronas, P.; Komskis, R.; Tumkevicius, S.; Jonusauskas, G.; Jursenas, S. *Phys. Chem. Chem. Phys.* **2020**, *22*, 26502. (b) Xu, H.; Chen, W.; Ju, L.; Lu, H. *Spectrochim. Acta A* **2021**, *247*, 119074.
76. Wang, H.-Y.; Yu, K.-K.; Tan, C.-Y.; Li, K.; Liu, Y.-H.; Shi, L.; Lu, K.; Yu, X.-Y. *J. Mater. Chem. C* **2021**, *9*, 2864.
77. (a) Cocca, L. H. Z.; Abegao, L. M. G.; Sciuti, L. F.; Vabre, R.; Siqueira, J. P.; Kamada, K.; Mendonça, C. R.; Piguel, S.; De Boni, L. *J. Phys. Chem. C* **2020**, *124*, 12617. (b) Venkatesh, V.; Shukla, A.; Sivakumar, S.; Verma, S. *ACS Appl. Mater. Interfaces* **2014**, *6*, 2185.
78. Patrizi, B.; Cozza, C.; Pietropaolo, A.; Foggi, P.; de Cumis, M. S. *Molecules*, **2020**, *25*, 430.
79. Sasaki, S.; Drummen, G. P. C.; Konishi, G. *J. Mater. Chem. C* **2016**, *4*, 2731.
80. Patrizi, B.; Iagatti, A.; Abbondanza, L.; Bussotti, L.; Zanardi, S.; Salvalaggio, M.; Fusco, R.; Foggi, P. *J. Phys. Chem. C* **2019**, *123*, 5840.
81. Verbitskiy, E. V.; Rusinov, G. L.; Chupakhin, O. N.; Charushin, V. N. *Dyes Pigm.* **2020**, *180*, 108414.
82. Reichardt, C.; *Chem. Rev.* **1994**, *94*, 2319.
83. (a) Allard, S.; Forster, M.; Souharce, B.; Thiem, H.; Scherf, U. *Angew. Chem. Int. Ed.* **2008**, *47*, 4070. (b) Wang, C.; Zhang, X.; Dong, H.; Chen, X.; Hu, W. *Adv. Energy Mater.* **2020**, *10*, 2000955.
84. (a) Yang, Z.; Mao, Z.; Xie, Z.; Zhang, Y.; Liu, S.; Zhao, J.; Xu, J.; Chi, Z.; Aldred, M. P. *Chem. Soc. Rev.* **2017**, *46*, 915. (b) Chen, X.-K.; Kim, D.; Brédas, J.-L. *Acc. Chem. Res.* **2018**, *51*, 2215.
85. Huang, T.; Jiang, W.; Duan, L. *J. Mater. Chem. C* **2018**, *6*, 5577.
86. Wex, B.; Kaafarani, B. R. *J. Mater. Chem. C* **2017**, *5*, 8622.
87. Auffray, M.; Balijapalli, U.; Ribierre, J.-C.; Tsuchiya, Y.; Adachi, C. *Chem. Lett.* **2020**, *49*, 932.
88. Zhang, D.-D.; Suzuki, K.; Song, X.-Z.; Wada, Y.; Kubo, S.; Duan, L.; Kaji, H. *ACS Appl. Mater. Interfaces* **2019**, *11*, 7192.

89. Skuodis, E.; Bezvikonnyi, O.; Tomkeviciene, A.; Volyniuk, D.; Mimaite, V.; Lazauskas, A.; Bucinskas, A.; Keruckiene, R.; Sini, G.; Grazulevicius, J. V. *Org. Electron.* **2018**, *63*, 29.

PIELIKUMI/APPENDICES

1. pielikums
Appendix I

Sebris, A.; Turks, M.

Recent Investigations and Applications of Azidoazomethine-Tetrazole Tautomeric Equilibrium (Microreview)

Chem. Heterocycl. Compd. **2019**, *55*, 1041.

doi: 10.1007/s10593-019-02574-7

DOI 10.1007/s10593-019-02574-7

Chemistry of Heterocyclic Compounds **2019**, *55*(11), 1041–1043

HETEROCYCLES IN FOCUS

Recent investigations and applications of azidoazomethine-tetrazole tautomeric equilibrium (microreview)

Armands Sebris[1], **Māris Turks**[1]*

[1] *Institute of Technology of Organic Chemistry, Faculty of Materials Science and Applied Chemistry, Riga Technical University, 3 P. Valdena St., Riga LV-1048, Latvia; e-mail: maris.turks@rtu.lv*

Published in Khimiya Geterotsiklicheskikh Soedinenii, 2019, *55*(11), 1041–1043

Submitted August 9, 2019
Accepted September 19, 2019

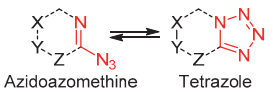

Recent investigations of azidoazomethine-tetrazole (azide-tetrazole) tautomeric equilibrium reported from 2014 to 2019 are summarized. Pyridine, pyrimidine, triazine, azole derivatives and their annulated congeners – purines, quinolines, quinazolines are described.

Introduction

The occurrence of ring-chain tautomerism and understanding the factors affecting the equilibrium and stability of either tetrazole (further in the text T) or azidoazomethine (A) forms are important for reactivity planning. Information covered in recent reviews on synthetic aspects of tetrazole[1] and 1,2,4-triazine[2] chemistry is not discussed here.

2-Azidopyridine-tetrazolo[1,5-*a*]pyridine

Tzschucke group[3] has developed method for conversion of pyridine *N*-oxides to tetrazolopyridines. Products were isolated as tetrazole tautomers, however the existing equilibrium permitted to perform Cu(I)-catalyzed azide–alkyne 1,3-dipolar cycloaddition reactions (CuAAC).

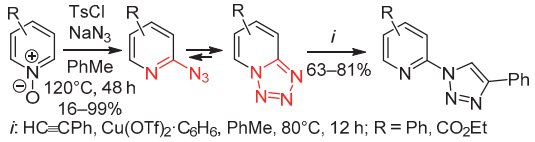

2,6-Diazido-4-methylnicotinonitrile can be selectively reduced to monoamino derivative, which exists as tetrazole tautomer.[4] Introduction of electron-withdrawing acylamino functionality shifts the equilibrium toward the azide form.

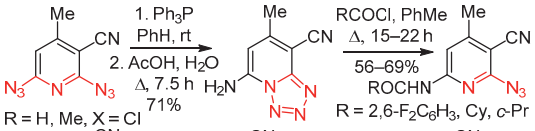

Electron-withdrawing CN group enhances the presence of azide form in compounds **1a**,**b**.[5,6] Introduction of ArNH substituent (compound **1b**) gives rise to azide-tetrazole (**1bA-1bT**) equilibrium.[6] The presence of the azide tautomer permitted S_NAr reactions with amine nucleophiles.[5]

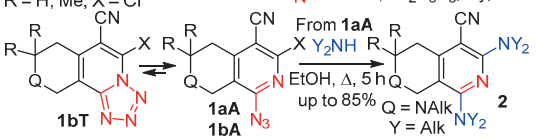

Electron-rich systems of type **3** reveal greater presence of tetrazole tautomer. In both $CDCl_3$ and DMSO solutions ~10% of azido form **3A** is observed and S_NAr reactions with azide leaving group are possible, yet difficult.[5] On the other hand, 5-azido-pyrazolo[3,4-*c*][2,7]naphthyridin-1-amine systems exist solely as tetrazoles and do not undergo S_NAr reactions.[5]

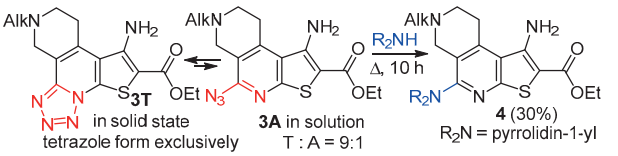

Armands Sebris obtained his MSc in chemical engineering in 2018 from the Riga Technical University. Currently he is working toward PhD thesis under supervision of prof. Māris Turks at the Riga Technical University. His research focuses on reactions of purines and their application in materials science.

Since 2018, professor **Māris Turks** is Dean of the Faculty of Materials Science and Applied Chemistry at the Riga Technical University. His research interests involve applications of liquid sulfur dioxide in organic synthesis and chemistry of triterpenoids, functionalized heterocycles, carbohydrates, and nucleosides.

2-Azidopyrimidine-tetrazolo[1,5-*a*]pyrimidine

Tetrazolopyrimidines are obtained by combining aminotetrazole (**5**) and dicarbonyl compounds (e.g., compound **8**)[7] or their surrogates (e.g., compounds **6**).[8] Electron-rich systems remain as tetrazole tautomers **7T**, but electron-poor cycles prefer the azide form[7,9] (e.g., compound **10**).

Tetrazolopyrimidines can be prepared not only by cyclization with aminotetrazole (**5**),[8,10] other synthetic methods are also available: 1) nitrozation of hydrazines; 2) S_NAr reaction with azides.[10] There is some controversy between the reports by Krivopalov[10] and Martins[8] regarding tautomeric equilibrium of compounds **12** and **14**. A combination of IR and NMR studies in $CDCl_3$ solution permitted to conclude[10] that azides **12A** and **14A** are the dominant tautomers.

Wentrup et al. have shown that tetrazolo[1,5-*a*]pyrimidine upon sublimation can be transformed into 2-azidopyrimidine.[11] Photolysis or flash vacuum thermolysis of the latter produces nitrene which rearranges into a series of interesting ring opening products. Similar transformations are possible with pyridine, pyridazine, phthalazine, quinoline and quinazoline derivatives.[11b] It should be noted that an energetic compound – 2,4,6-triazidopyrimidine-5-carbonitrile exists solely in the triazide form.[12]

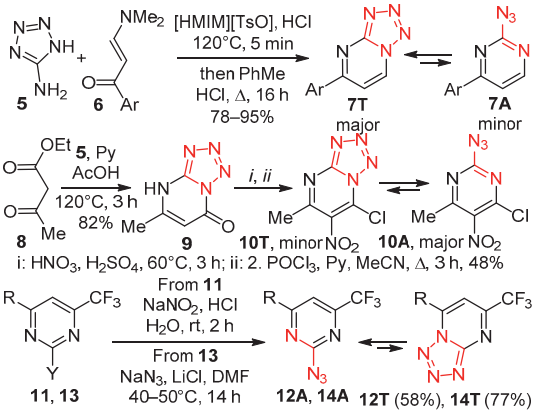

4-Azidopyrimidine-tetrazolo[1,5-*c*]pyrimidine

Electron-withdrawing or sterically demanding groups provide the azide form, compound **15A**, whereas strongly electron-donating substituents ensure formation of tetrazole **15T**.[13] If the equilibrium is possible, CuAAC reaction proceeds with productive outcome providing triazoles **16**. However, 4-azidopyrimidin-2-one exists solely as tetrazole.

Fully substituted tetrazolopyrimidines containing nitroamino substituent were obtained in 54–62% yield from pyrimidin-4-ones and bis(4-nitrophenyl)phosphoryl azide in the presence of DBU.[14]

Pleshkova et al. have studied thermodynamic and kinetic parameters of the tautomeric equilibrium of 2,6-disubstituted 4-azidopyrimidines in detail.[15] It was suggested that MeCN particularly coordinates N_3 group thus favoring azide tautomer. Polycyclic structures containing azidopyrimidine fragments[16] behave identically – electron-poor systems and nonpolar solvents favor azide, but electron-rich systems and polar solvents favor tetrazole formation.

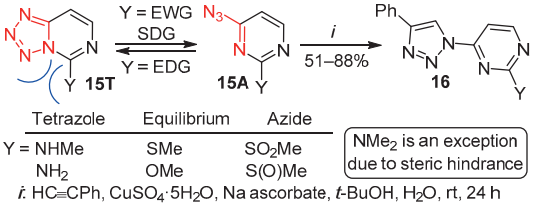

Azido(deaza)purines-tetrazolo(deaza)purines

Diazidopurines **17A** (X = N) exist solely in diazide form in solid state and in $CHCl_3$, however in DMSO, small amounts of tetrazoles **17T** are observed.[17] Experiments with diazido-7-deazapurines (X = CH) in various solvents showed a slightly higher amount of tetrazole form **17T**.[18] Apparently, due to the higher reactivity of tautomer **17T**, S_NAr reactions with amine and thiol nucleophiles occur with unusual C-2 selectivity. If compared with starting materials **17**, EDG-containing products **18** exhibit higher presence of tetrazole tautomer, however **18A**↔**18T** equilibrium is sufficient to produce 1,2,3-triazoles from compound **18A** in CuAAC reaction.[17b,c]

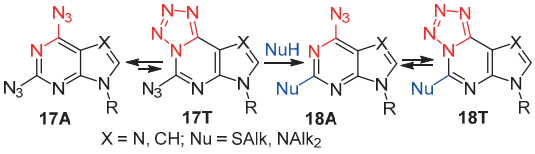

Azidotriazine-tetrazolotriazine

Deprotonation of *N*-nitroamine **19A** makes the triazine system sufficiently electron rich to stabilize the tetrazole ring in tautomer **19T**.[19] ^{15}N-Labelled tetrazolo[5,1-*c*][1,2,4]-triazine **20T1** was obtained by acid-promoted cyclization of intermediate **21**, which was obtained from diazotized ^{15}N-labeled aminotetrazole (**5**). Ring-chain tautomerism provided the most stable isomer – tetrazolo[1,5-*b*][1,2,4]-triazin-7-one (**20T2**).[20]

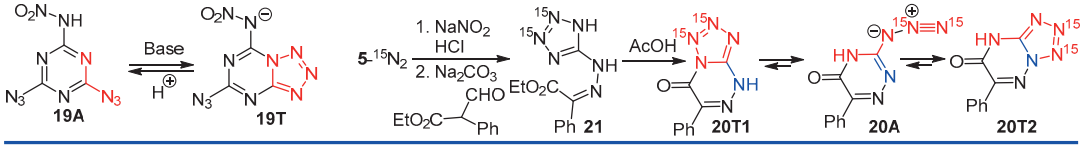

Miscellaneous

2,4-Diazidoquinazoline does not exist in diazide form, but is rather described by forms **22TT/22AT**. It undergoes S_NAr reaction to produce amine **23**, which can be further transformed into triazole derivative **24**.[21]

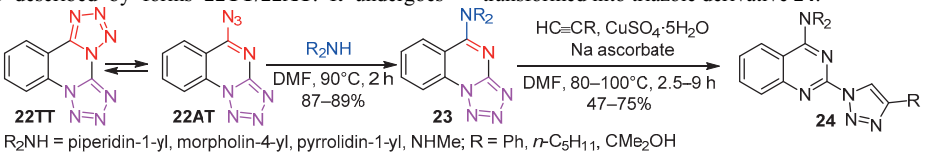

R_2NH = piperidin-1-yl, morpholin-4-yl, pyrrolidin-1-yl, NHMe; R = Ph, *n*-C_5H_{11}, CMe_2OH

Recently, ultrasound-assisted multicomponent process involving Groebke–Blackburn–Bienaymé reaction / S_NAr / azide-tetrazole tautomerisation strategy was reported to produce imidazo[2,1-*b*]thiazole-tetrazoloquinoline conjugates.[22]

Tetrazolo[5,1-*b*][1,3,4]thiadiazine systems were obtained in two-step one-pot process of hydrazinylthiadiazine synthesis and their further nitrosation.[23]

DFT calculations of N_3 group rotation and the azide-tetrazole ring-chain tautomeric equilibrium were performed for 2-azido-1,3-azoles,[24] azidobenzothiazoles,[25] and 5-azido-1,2,4-triazoles.[26] Tetrazole ring formation is favored if there is sufficient π-electron delocalization (azidothiazole: X = S, Z = C) and a highly polar medium to stabilize higher dipole moment of tetrazole tautomer.[24] Formation of additional tetrazole aromatic ring in the equilibrium 3-azido-1,2,4-triazole ↔ [1,2,4]triazolo[4,3-*d*]tetrazole increases stability of the system.[26]

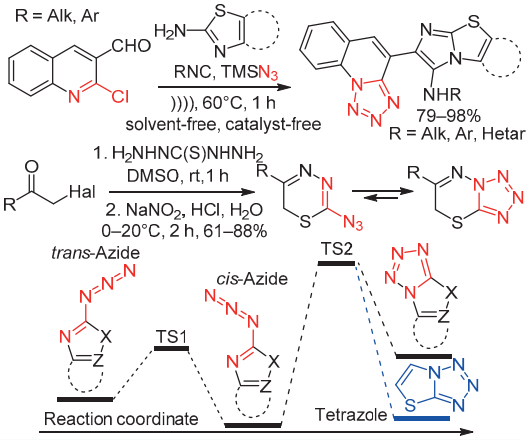

Conclusions

Azide moiety can be introduced into heterocyclic systems by 1) S_NAr reactions, 2) nitrosation of hydrazinyl moiety, 3) heterocyclization with aminotetrazole fragment followed by ring-chain tautomerism. There are prerequisites for the azide-tetrazole tautomeric equilibrium shift toward one of the forms.

Factor	Azide	Tetrazole
Nature of heterocyclic core, substituent effects	Electron-poor	Electron-rich
Solvent polarity	↓	↑
Temperature	↑	↓
Sterical hindrance in the proximity of tetrazole ring closing	Yes	No

Authors thank Latvian-Ukrainian coproject No. W3956 for financial support.

References

1. Ostrovskii, V. A.; Popova, E. A.; Trifonov, R. E. *Adv. Heterocycl. Chem.* **2017**, *123*, 1.
2. Deev, S. L.; Shestakova, T. S.; Charushin, V. N.; Chupakhin, O. N. *Chem. Heterocycl. Compd.* **2017**, *53*, 963. [*Khim. Geterotsikl. Soedin.* **2017**, *53*, 963.]
3. Liu, S.; Lentz, D.; Tzschucke, C. C. *J. Org. Chem.* **2014**, *79*, 3249.
4. Dyadyuchenko, L. V.; Dmitrieva, I. G.; Aksenov, N. A.; Dotsenko, V. V. *Chem. Heterocycl. Compd.* **2018**, *54*, 964. [*Khim. Geterotsikl. Soedin.* **2018**, *54*, 964.]
5. Sirakanyan S. N.; Spinelli, D.; Geronikaki, A.; Hovakimyan, A. A.; Noravyan, A. S. *Tetrahedron* **2014**, *70*, 8648.
6. Paronikyan, E. G.; Dashyan, Sh. Sh.; Minasyan, N. S.; Stepanyan, G. M. *Russ. J. Org. Chem.* **2017**, *53*, 941. [*Zh. Org. Khim.* **2017**, *53*, 925.]
7. Savateev, K. V.; Fedotov, V. V.; Ulomskiy, E. N.; Rusinov, V. L. *Chem. Heterocycl. Compd.* **2018**, *54*, 197. [*Khim. Geterotsikl. Soedin.* **2018**, *54*, 197.]
8. Scapin, E.; Salbego, P. R. S.; Bender, C. R.; Meyer, A. R.; Pagliari, A. B.; Orlando, T.; Zimmer, G. C.; Frizzo, C. P.; Bonacorso, H. G.; Zanatta, N.; Martins, M. A. P. *Beilstein J. Org. Chem.* **2017**, *13*, 2396.
9. Goryaeva, M. V.; Burgart, Ya. V.; Ezhikova, M. A.; Kodess, M. I.; Saloutin, V. I. *Beilstein J. Org. Chem.* **2015**, *11*, 385.
10. Nikolaenkova, E. B.; Aleksandrova, N. V.; Mamatyuk, V. I.; Krivopalov, V. P. *Russ. Chem. Bull., Int. Ed.* **2018**, *67*, 893. [*Izv. Akad. Nauk, Ser. Khim.* **2018**, *67*, 893.]
11. (a) Torker, S.; Kvaskoff, D.; Wentrup, C. *J. Org. Chem.* **2014**, *79*, 1758. (b) Wentrup, C. *Chem. Rev.* **2017**, *117*, 4562.
12. (a) Chapyshev, S. V.; Korchagin, D. V.; Chernyak, A. V.; Garanin, V. A. *ARKIVOC* **2018**, (v), 39. (b) Chapyshev, S. V. *Molecules* **2015**, *20*, 19142.
13. Thomann, A.; Zapp, J.; Hutter, M.; Empting, M.; Hartmann, R. W. *Org. Biomol. Chem.* **2015**, *13*, 10620.
14. Novakov, I. A.; Babushkin, A. S.; Brunilina, L. L.; Navrotskii, M. B.; Orlinson, B. S.; Robinovich, M. D.; Yablokov, A. S. *Russ. J. Gen. Chem.* **2017**, *87*, 219. [*Zh. Obshch. Khim.* **2017**, *87*, 242.]
15. Pleshkova, N. V.; Nikolaenkova, E. B.; Krivopalov, V. P.; Mamatyuk, V. I. *Russ. Chem. Bull., Int. Ed.* **2017**, *66*, 2095. [*Izv. Akad. Nauk, Ser. Khim.* **2017**, *66*, 2095.]
16. Sirakanyan, S. N.; Spinelli, D.; Geronikaki, A.; Kartsev, V. G.; Panosyan, H. A.; Ayvazyan, A. G.; Tamazyan, R. A.; Frenna, V.; Hovakimyan, A. A. *Tetrahedron* **2016**, *72*, 1919.
17. (a) Ozols, K.; Cīrule, D.; Novosjolova, I.; Stepanovs, D.; Liepinsh, E.; Bizdēna, Ē.; Turks, M. *Tetrahedron Lett.* **2016**, *57*, 1174. (b) Novosjolova, I.; Bizdēna, Ē.; Turks, M. *Tetrahedron Lett.* **2013**, *54*, 6557. (c) Šišuļins, A.; Bucevičius, J.; Tseng, Y.-T.; Novosjolova, I.; Traskovskis, K.; Bizdēna, Ē.; Chang, H.-T.; Tumkevičius, S.; Turks, M. *Beilstein J. Org. Chem.* **2019**, *15*, 474.
18. (a) Bucevičius, J.; Tumkevičius, S. *Chemija* **2015**, *26*, 126. (b) Bucevicius, J.; Turks, M.; Tumkevicius, S. *Synlett* **2018**, 525.
19. (a) Chapyshev, S. V.; Korchagin, D. V. *Chem. Heterocycl. Compd.* **2017**, *53*, 791. [*Khim. Geterotsikl. Soedin.* **2017**, *53*, 791.] (b) Chapyshev, S. V.; Ushakov, E. N. *Phys. Chem. Chem. Phys.* **2015**, *17*, 17296.
20. Deev, S. L.; Paramonov, A. S.; Shestakova, T. S.; Khalymbadzha, I. A. Chupakhin, O. N.; Subbotina, J. O.; Eltsov, O. S.; Slepukhin, P. A.; Rusinov, V. L.; Arseniev, A. S.; Shenkarev, Z. O. *Beilstein J. Org. Chem.* **2017**, *13*, 2535.
21. Kalniņa, A.; Bizdēna, Ē.; Kiselovs, G.; Mishnev, A.; Turks, M. *Chem. Heterocycl. Compd.* **2014**, *49*, 1667. [*Khim. Geterotsikl. Soedin.* **2013**, *49*, 1797.]
22. Claudio-Catalán, M. Á.; Pharande, S. G.; Quezada-Soto, A.; Kishore, K. G.; Rentería-Gómez, A.; Padilla-Vaca, F.; Gámez-Montaño, R. *ACS Omega*, **2018**, *3*, 5177.
23. Kulikov, A. S.; Epishina, M. A.; Fershtat, L. L.; Romanova, A. A.; Makhova, N. N. *Tetrahedron Lett.* **2017**, *58*, 3998.
24. Karakus, N.; Demirel, M. *J. Mol. Struct.* **2015**, *1093*, 65.
25. Abu-Eittah, R. H.; El-Taher, S.; Hassan, W. M. I.; Noamaan, M. A. *Comput. Theor. Chem.* **2014**, *1033*, 52.
26. Yang, J.; Gong, X.; Wang, G. *RSC Adv.* **2015**, *5*, 9503.

2. pielikums
Appendix II

Sebris, A.; Traskovskis, K.; Novosjolova, I.; Turks, M.

Synthesis and Photophysical Properties of 2-Azolyl-6-piperidinylpurines

Chem. Heterocycl. Compd. **2021**, *57*, 560.

doi: 10.1007/s10593-021-02943-1

Chemistry of Heterocyclic Compounds **2021**, *57*(5), 560–567

Synthesis and photophysical properties of 2-azolyl-6-piperidinylpurines

Armands Sebris[1], Kaspars Traskovskis[1], Irina Novosjolova[1]*, Māris Turks[1]*

[1] *Faculty of Materials Science and Applied Chemistry, Riga Technical University, 3 Paula Valdena St., Riga LV-1048, Latvia; e-mail: irina.novosjolova@rtu.lv, maris.turks@rtu.lv*

Published in Khimiya Geterotsiklicheskikh Soedinenii, 2021, *57*(5), 560–567

Submitted January 15, 2021
Accepted February 24, 2021

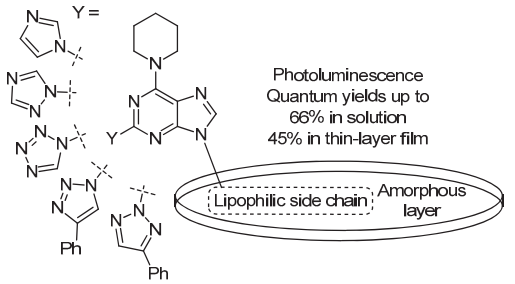

A synthesis of novel fluorescent 2-azolyl-6-piperidinylpurine derivatives was designed. Azolyl substituent at purine C-2 atom was introduced *via* nucleophilic aromatic substitution or in the case of tetrazolyl and 1,2,3-triazolyl substituents *via* a ring formation on a pre-installed amine or azide moiety, respectively. The obtained purine intermediates were functionalized at N-9 position using Mitsunobu reaction conditions to achieve amorphous compounds, which form thin-layer films of good quality. The synthesized push-pull systems exhibited fluorescence with emission in range of 360–400 nm and quantum yields up to 66% in CH_2Cl_2 solution and up to 45% in the thin-layer film.

Keywords: azoles, purines, fluorescence, nucleophilic aromatic substitution, ring formation.

For decades, purine derivatives have been extensively studied due to their wide spectrum of biological activities.[1–4] Purine cycle is known as the most common nitrogen heterocycle in nature.[5,6] Fluorescence properties exhibited by certain purine derivatives are often used in cell imaging.[7–11] On the contrary, materials science applications of fluorescent purine derivatives are poorly studied. Lately Castellano's group has developed organic light emitting diodes (OLEDs) with purine emitters[12,13] and Yang's group obtained the first thermally activated delayed fluorescence (TADF) emitter using purine ring as the electron-accepting group.[14]

Applications of organic compounds in materials science are often limited by complicated and expensive processes, for example, vacuum deposition, which is used for creating thin substance layers. The alternative is a solution processing, which requires compounds that form stable amorphous phase and possess good solubility. These properties can be achieved by introducing a trityl moiety in the molecule.[15,16]

Expanding the previous work of our group,[11] we developed a synthesis of 2-azolyl-6-piperidinylpurine derivatives as push-pull systems with different substituents at the N-9 atom. While there is a wide range of information on introduction of various azoles at purine C-6 position,[17–21] transformations at purine C-2 position are less common, as C-6 position is more reactive and preliminary functionalization of C-6 position deactivates substitution at C-2 position.[6] The known examples represent pyrazole ring construction on hydrazine,[23] imidazole ring introduction *via* an oxidated intermediate of 8-oxoadenine and 8-oxohypoxanthine,[23] and substituted benzimidazole introduction using Buchwald–Hartwig cross coupling[24,25] or a S_NAr reaction.[26]

The initial synthetic approach to the target compounds included N^9-functionalization using Mitsunobu reaction between 2,6-dichloropurine (**1**) and 2-hydroxyethyl 3,3,3-tri-

Scheme 1. Attempted synthesis of 2-[2-(1*H*-imidazol-1-yl)-6-(piperidin-1-yl)-9*H*-purin-9-yl]ethyl 3,3,3-triphenylpropanoates

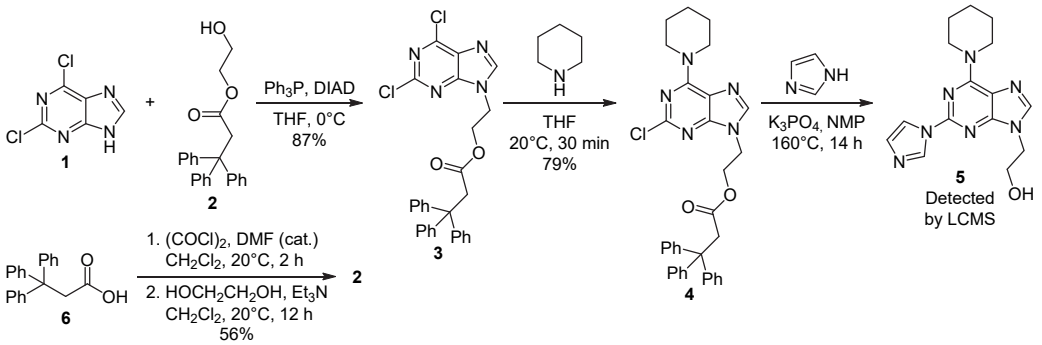

phenylpropanoate (**2**)[27] (Scheme 1). The selected side chain is foreseen to ensure the amorphous properties of otherwise crystalline heterocycles. Compound **2** containing trityl group was obtained by esterification of commercially available or readily prepared[28] acid **6**. Next, a S_NAr reaction of adduct **3** at C-6 position with piperidine produced intermediate **4** under mild conditions (20°C, 30 min). Then the next S_NAr reaction was tried for the introduction of imidazole at C-2 position.[24] At 160°C in the presence of K_3PO_4 as a base, we observed the S_NAr process at the C-2 atom. However, these conditions were too harsh, and the ester moiety was cleaved at the N-9 side chain producing compound **5** regardless of its relatively high stability which arises due to sterical hindrance.

To avoid the ester cleavage of substituent at N-9 position we decided to perform firstly the S_NAr reaction with piperidine at C-6 and then with imidazole at C-2 position of N^9-unsubstituted purine. Again, the second S_NAr process did not provide the desired product, most likely due to the presence of a negative charge on the purine ring arising from its deprotonation.

Then a thermally stable and base-resistant tetrahydropyranyl (THP) protecting group was introduced at N-9 position, and product **7**[29] was obtained in 73% yield starting from 2,6-dichloropurine (**1**) (Scheme 2). Compound **7** reacted smoothly with piperidine at C-6 position (20°C, 30 min) providing the key intermediate **8**[30,31] in 95% yield. The latter underwent S_NAr reactions at C-2 position with azole nucleophiles such as imidazole, 1,2,4-triazole, and 4-phenyl-1,2,3-triazole.

Although relatively harsh reaction conditions have been applied (K_3PO_4, *N*-methylpyrrolidone (NMP), 160°C) the S_NAr substitution process in compound **8** proceeded with good yields (51–68%). S_NAr reaction with 1,2,4-triazole selectively gave 1*H*-1,2,4-triazol-1-ylpurine **9b**, and no 1,2,4-triazol-4-yl derivative was observed. Reaction with 4-phenyl-1,2,3-triazole yielded a 1:1 mixture of 2-(1*H*-1,2,3-triazol-1-yl)purine and 2-(2*H*-1,2,3-triazol-2-yl)purine derivatives **9c**,**d** with isolated yields 35 and 32%, respectively (Scheme 2). The identity of compound **9c** was confirmed by an alternative synthetic pathway, in which the 1*H*-1,2,3-triazol-1-yl substituent was installed by Cu(I)-catalyzed

Scheme 2. Synthesis of 2-[2-azolyl-6-(piperidin-1-yl)-9*H*-purin-9-yl]ethyl 3,3,3-triphenylpropanoates **11a**,**b**

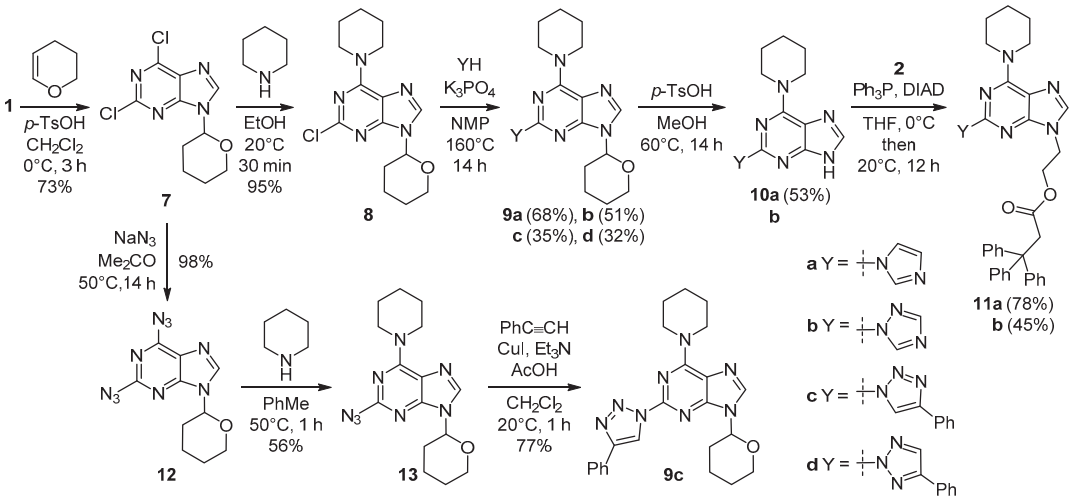

Scheme 3. Synthesis of 9-alkylated 6-(piperidin-1-yl)-2-(1*H*-tetrazol-1-yl)-9*H*-purine derivatives **18a**–**c**

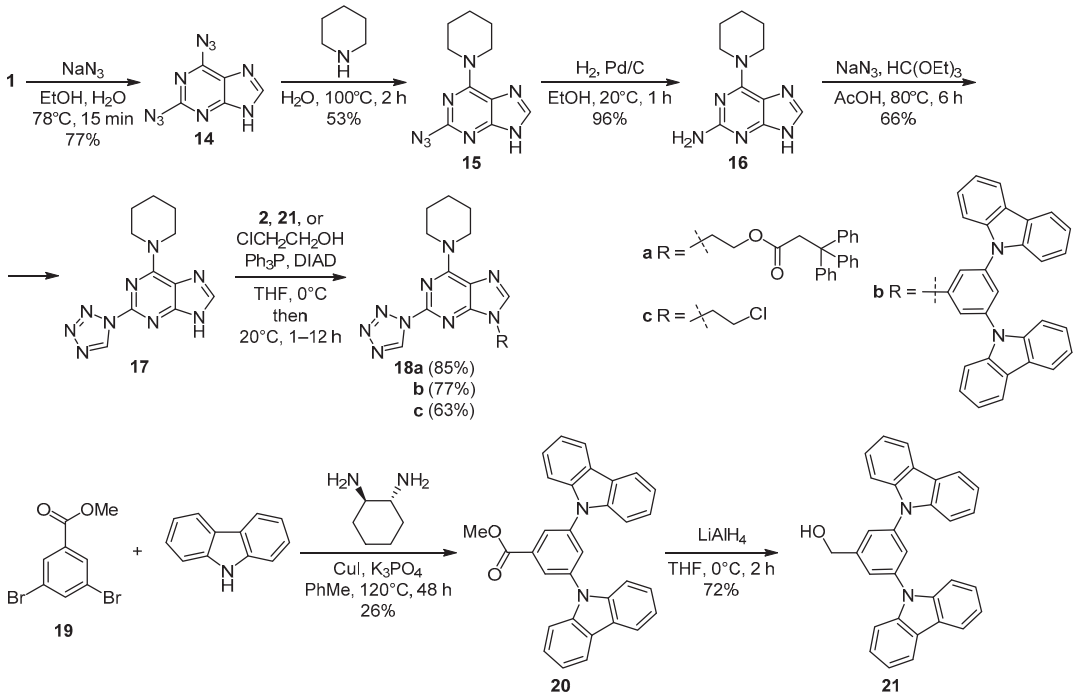

azide-alkyne cycloaddition reaction of azide derivative **13**. The latter was obtained by a S_NAr reaction of 2,6-diazidopurine **12**. Toluene as relatively nonpolar solvent and slightly elevated temperature ensured the C-6 reactivity due to the prevalence of 6-azido form of the substrate, which can enter azide-tetrazole tautomeric equilibrium.[11,32–35]

THP deprotection of compounds **9a**,**b** yielded azolylpurines **10a**,**b**, which were further functionalized at N-9 position *via* Mitsunobu reaction with diisopropyl azodicarboxylate (DIAD) to give compounds **11a**,**b** (Scheme 2). Deprotected compound **10b** exhibited extremely poor solubility in DMF, DMSO, THF, and various alcohols, thus preventing compound characterization. It was, therefore, telescoped into the Mitsunobu reaction giving compound **11b**.

Attempts to introduce a tetrazole ring at C-2 position of purine **6** by the S_NAr process of 2-chloropurine derivative **8** did not provide the desired product. Since tetrazole is rather acidic (pK_a 4.9), its deprotonated form is a weak nucleophile. Aiming to obtain the desired product we switched to a ring construction on 2-aminopurine derivative **16** (Scheme 3).[36] The latter was synthesized starting from 2,6-dichloropurine (**1**). Firstly, 2,6-diazidopurine (**14**)[37] was obtained. Subsequent S_NAr reaction with piperidine yielded adduct **15**.[38] The remaining 2-azido group was catalytically reduced to amino group. The obtained 2-aminopurine **16**[39] was used in ring formation with NaN_3 and $HC(OEt)_3$ and gave the expected 2-tetrazolylpurine derivative **17** in 66% yield. Similarly to 9*H*-purine derivatives **10a**,**b**, also intermediate **17** underwent selective alkylation at N-9 atom under Mitsunobu conditions yielding compounds **18a**–**c** in 63–85% yields (Scheme 3). Alcohols such as 2-hydroxyethyl 3,3,3-triphenylpropanoate (**2**), [3,5-di(9*H*-carbazol-9-yl)phenyl]methanol (**21**), and 2-choroethanol were used. The latter provides compound **18c**, the chloroethyl substituent of which can serve as a "sticky end" for further modifications of the side chain. Reagent **21** for the introduction of the dicarbazolylphenyl moiety was synthesized from compound **19** using copper-catalyzed N-arylation to give compound **20**,[40] followed by ester reduction with $LiAlH_4$ to compound **21**.

Photophysical properties of compounds **11a**,**b** and **18a**,**b** were investigated in $5 \cdot 10^{-5}$ M CH_2Cl_2 solution and in the thin films (Figs. 1, 2 and Table 1). For compounds **11a**,**b** and **18a**, the lowest energy absorption bands correspond to intramolecular charge transfer transition (ICT) of purine chromophores indicated by shoulders in the 300–310 nm range. For compound **18b**, the ICT band overlaps with carbazole absorption as indicated by characteristic maxima λ_{abs} at 323 and 338 nm. The emission maxima λ_{em} for compounds **11a**,**b** and **18a** were in the 356–401 nm range, which corresponds to near UV and purple light. The increase of number of nitrogen atoms in the azole ring resulted in a higher electron deficiency, which caused a bathochromic shift in emission maxima.[41] The 3,5-dicarbazolylphenyl moiety in compound **18b** was intended to improve hole transfer capabilities for potential use in OLEDs.[42] In the case of purine derivative **18b** we observed

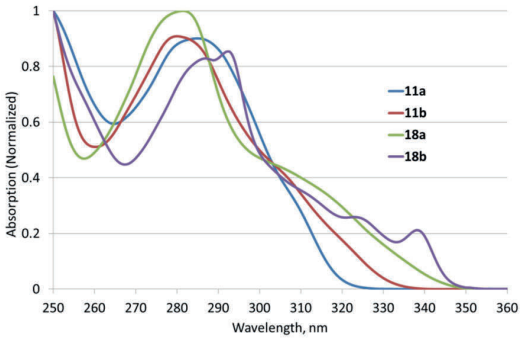

Figure 1. Absorption spectra of 2-azolyl-6-piperidinylpurines **11a**,**b** and **18a**,**b** in $5\cdot10^{-5}$ M CH_2Cl_2 solution.

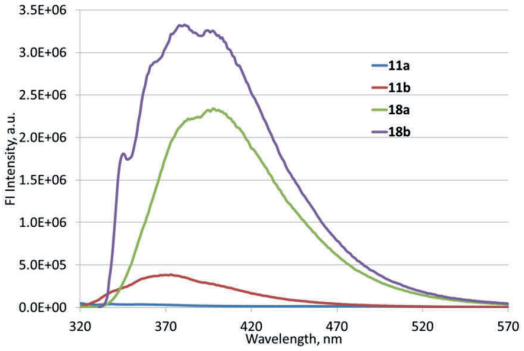

Figure 2. Emission spectra of 2-azolyl-6-piperidinylpurines **11a**,**b** and **18a**,**b** in $5\cdot10^{-5}$ M CH_2Cl_2 solution.

an emission spectrum, which is a combination of emission from 6-piperdinyl-2-tetrazolylpurine and 3,5-dicarbazolylphenyl moieties. We explain this by similar lowest energy singlet levels for carbazole and purine chromophores. Onset of absorption for both **18a**,**b** which contain the same purine moiety is at 350 nm. Characteristic maxima of carbazole emission are also distinguishable in PL band (362, 378, 397 nm: entry 7, Table 1).

Unlike tetrazole-substituted derivatives **18a**,**b**, compounds **11a**,**b** showed better quantum yield in the thin-layer film than in the CH_2Cl_2 solution. This is unusual, since typically quantum yields in the thin-layer films are lowered due to an intermolecular quenching, which is reduced in solution. Compounds **11b** and **18a** showed the best quantum yields in the thin-layer films, 0.45 and 0.42 respectively.

To conclude, we have developed several approaches for the introduction of various azolyl moieties at C-2 position of purine ring system containing an electron-donating piperidinyl substituent at its C-6 position. S_NAr reactions were used for the introduction of imidazolyl, 1*H*-1,2,4-triazol-1-yl, and 2*H*-1,2,3-triazol-2-yl substituents at the purine C-2 position. On the other hand, selective construction of 1*H*-1,2,3-triazol-1-yl group on 2-azidopurine derivative was carried out by Cu(I)-catalyzed azide-alkyne cycloaddition reaction, and a tetrazolyl substituent was introduced by three-component assembling on 2-aminopurine derivative. The developed synthetic pathways allowed a late stage N^9-functionalization of the obtained heterocyclic assemblies to achieve amorphous states of the desired push-pull purines for potential materials science applications in the future. An introduction of 2-chloroethyl side chain at N-9 position will serve as a functionalization site for possible chemical modifications in future. The obtained conjugates exhibited emission in the near UV region in both solution (up to 66% quantum yield) and in the thin-layer films (up to 45% quantum yield).

Experimental

UV-Vis absorption spectra were recorded with a PerkinElmer Lambda 35 spectrometer. Films for optical measurements were prepared using spin-coating technique with a Laurell WS-400B-6NPP/LITE spin-coater on glass slides, using 30 mg/ml THF solutions. After the coating, all films were dried in oven at 100°C for 2 h. Emission spectra and quantum yields for solutions and thin films were recorded using a QuantaMaster 40 steady state spectrofluorometer (Photon Technology International, Inc.) equipped with a 6 inch integrating sphere by LabSphere, using the software package provided by the manufacturer. ^{1}H and ^{13}C NMR spectra were recorded on a Bruker 300 (300 and 75 MHz, respectively) spectrometer. Internal standard – residual non-deuterated solvent peak for ^{1}H nuclei (7.26 ppm in $CDCl_3$, 2.50 ppm in DMSO-d_6) and deuterated solvent peak for ^{13}C nuclei (77.2 ppm in $CDCl_3$, 39.5 ppm in DMSO-d_6). Nontrivial peak assignments were confirmed with ^{1}H–^{13}C HSQC and/or ^{1}H–^{13}C HMBC spectra. High-resolu-

Table 1. Photophysical properties of 2-azolyl-6-piperidinylpurines **11a**,**b** and **18a**,**b**

Entry	Compound	State	λ_{abs}, nm	λ_{em}, nm	Emission quantum yield
1	**11a**	CH_2Cl_2 solution	284, 305 (shoulder)	356	0.01
2	**11a**	Thin-layer film	286, 300 (shoulder)	366	0.12
3	**11b**	CH_2Cl_2 solution	280, 300 (shoulder)	373	0.07
4	**11b**	Thin-layer film	283, 310 (shoulder)	373	0.45
5	**18a**	CH_2Cl_2 solution	281, 310 (shoulder)	398	0.66
6	**18a**	Thin-layer film	285, 310 (shoulder)	401	0.42
7	**18b**	CH_2Cl_2 solution	292, 323, 338	362, 378, 397	0.51
8	**18b**	Thin-layer film	295, 326, 340	401, 422	0.20

tion mass spectra (ESI) were recorded on a Waters Q-TOF Micromass spectrometer. Melting points were determined on a Fisher Digital Melting Point Analyzer Model 355. HPLC analysis was performed using an Agilent Technologies 1200 Series system equipped with XBridge C18 column, 4.6 × 150 mm, particle size 3.5 μm, with flow rate of 1 ml/min, using 0.1% aqueous TFA (A) and MeCN (B) for mobile phase; wavelength of detection was 260 nm; eluent: gradient 30–95% B in A for 5 min, 95% B for 5 min, 95–30% B for 2 min. All reactions were followed by TLC on E. Merck Kieselgel 60 F_{254} plates with detection by UV light. Silica gel (60 Å, 40–63 μm, ROCC) was used for flash chromatography.

Commercially available reagents were used as received. Starting materials **1**, **6**, and **19** are commercially available. Compounds **2**,[27] **3**,[27] **7**,[29] **8**,[30,31] **14**,[37] **15**,[38] and **16**[39] are known from literature.

2-[2-Chloro-6-(piperidin-1-yl)-9*H*-purin-9-yl]ethyl 3,3,3-triphenylpropanoate (4). Piperidine (0.57 ml, ρ 0.86 g/cm^3, 5.79 mmol, 3.0 equiv) was added to a solution of compound **3** (1.0 g, 1.93 mmol, 1.0 equiv) in THF (30 ml), and the reaction mixture was stirred at 20°C for 30 min. Then the reaction mixture was evaporated, dissolved in CH_2Cl_2 (30 ml), and washed with aqueous KH_2PO_4 solution (3 × 20 ml), saturated $NaHCO_3$ solution (20 ml), and brine (10 ml). The organic phase was dried over anhydrous Na_2SO_4, filtered, and evaporated. Yield 865 mg (79%), colorless solid. R_f 0.32 (CH_2Cl_2–MeCN, 20:1). HPLC: t_R 8.22 min. ^{1}H NMR spectrum ($CDCl_3$, 50°C), δ, ppm: 1.63–1.81 (6H, m, 3CH_2); 3.72 (2H, s, CH_2); 4.03–4.14 (4H, m, 2CH_2); 4.10–4.34 (4H, m, 2CH_2); 7.12–7.31 (15H, m, H Ph); 7.40 (1H, s, H-8). ^{13}C NMR spectrum ($CDCl_3$, 50°C), δ, ppm: 24.8; 26.3; 42.5; 46.4; 46.7; 56.1; 62.3; 118.8; 126.5; 128.0; 129.3; 138.5; 146.5; 152.5; 154.2; 154.3; 170.5. Found, *m*/*z*: 566.2328 $[M+H]^+$. $C_{33}H_{33}ClN_5O_2$. Calculated, *m*/*z*: 566.2317.

2-(1*H*-Imidazol-1-yl)-6-(piperidin-1-yl)-9-(tetrahydro-2*H*-pyran-2-yl)-9*H*-purine (9a). Anhydrous K_3PO_4 (1.38 g, 6.52 mmol, 3.0 equiv) was added to a solution of compound **8** (700 mg, 2.17 mmol, 1.0 equiv), imidazole (222 mg, 3.26 mmol, 1.5 equiv) in dry NMP (3.5 ml) under Ar, and the reaction mixture was stirred at 160°C for 14 h. Then the reaction mixture was poured into H_2O (30 ml) and extracted with PhMe (3 × 20 ml). The organic phase was washed with brine (3 × 20 ml), H_2O (2 × 20 ml), and again with brine (10 ml), dried over anhydrous Na_2SO_4, filtered, and evaporated. Silica gel column chromatography (eluent CH_2Cl_2 in MeOH, gradient 0–5%) of the residue provided product **9a**. Yield 523 mg (68%), colorless solid. R_f 0.41 (CH_2Cl_2–MeOH, 20:1). HPLC: t_R 4.75 min. ^{1}H NMR spectrum ($CDCl_3$, 50°C), δ, ppm (*J*, Hz): 1.57–2.15 (12H, m, 6CH_2); 3.76 (1H, td, ^2J = ^3J = 11.2, ^3J = 2.8) and 4.15 (1H, d, ^2J = 11.2, CH_2O); 4.10–4.36 (4H, m, 2CH_2); 5.66 (1H, dd, ^3J = 9.8, ^3J = 2.4, NCHO); 7.09 (1H, s, H imidazole); 7.85 (1H, s, H imidazole); 7.87 (1H, s, H-8); 8.54 (1H, s, H imidazole). ^{13}C NMR spectrum ($CDCl_3$, 50°C), δ, ppm: 23.0; 24.8; 25.0; 26.2; 31.8; 46.6; 68.9; 81.8; 117.0; 118.2; 129.7; 136.0; 136.3; 149.7; 151.1; 153.8. Found, *m*/*z*: 354.2033 $[M+H]^+$. $C_{18}H_{24}N_7O$. Calculated, *m*/*z*: 354.2037.

6-(Piperidin-1-yl)-9-(tetrahydro-2*H*-pyran-2-yl)-2-(1*H*-1,2,4-triazol-1-yl)-9*H*-purine (9b) was prepared analogously to compound **9a** from compound **8** (700 mg, 2.17 mmol, 1.0 equiv), 1,2,4-triazole (225 mg, 3.26 mmol, 1.5 equiv), dry NMP (3.5 ml), anhydrous K_3PO_4 (1.38 g, 6.52 mmol, 3.0 equiv). Yield 388 mg (51%), colorless solid. R_f 0.39 (CH_2Cl_2–MeOH, 20:1). HPLC: t_R 5.43 min. ^{1}H NMR spectrum ($CDCl_3$, 50°C), δ, ppm (*J*, Hz): 1.57–2.16 (12H, m, 6CH_2); 3.78 (1H, td, ^2J = ^3J = 11.3, ^3J = 2.7) and 4.12 (1H, d, ^2J = 11.3, CH_2O); 4.11–4.38 (4H, m, 2CH_2); 5.82 (1H, dd, ^3J = 10.2, ^3J = 1.9, NCHO); 7.94 (1H, s, H-8); 8.09 (1H, s, H triazole); 9.12 (1H, s, H triazole). ^{13}C NMR spectrum ($CDCl_3$, δ, ppm: 22.8; 24.7; 25.0; 26.2; 32.4; 46.5; 68.8; 81.3; 118.8; 136.6; 143.8; 149.4; 150.9; 153.1; 153.8. Found, *m*/*z*: 355.1998 $[M+H]^+$. $C_{17}H_{23}N_8O$. Calculated, *m*/*z*: 355.1989.

2-(4-Phenyl-1*H*-1,2,3-triazol-1-yl)-6-(piperidin-1-yl)-9-(tetrahydro-2*H*-pyran-2-yl)-9*H*-purine (9c) and 2-(4-phenyl-2*H*-1,2,3-triazol-2-yl)-6-(piperidin-1-yl)-9-(tetrahydro-2*H*-pyran-2-yl)-9*H*-purine (9d), 1:1 mixture, were prepared analogously to compound **9a** from compound **8** (296 mg, 0.92 mmol, 1.0 equiv), 4-phenyl-1*H*-1,2,3-triazole (200 mg, 1.38 mmol, 1.5 equiv), dry NMP (2 ml), anhydrous K_3PO_4 (585 mg, 2.76 mmol, 3.0 equiv). Products **9c**,**d** were separated by silica gel column chromatography (eluent PhMe in MeCN, gradient 0–10%).

Compound 9c. Yield 137 mg (35%), colorless solid. R_f 0.28 (CH_2Cl_2–MeCN, 10:1). HPLC: t_R 6.87 min. ^{1}H NMR spectrum ($CDCl_3$, 50°C), δ, ppm (*J*, Hz): 1.57–2.23 (12H, m, 6CH_2); 3.82 (1H, td, ^2J = ^3J = 11.2, ^3J = 2.7) and 4.17 (1H, d, ^2J = 11.2, CH_2O); 4.15–4.55 (4H, m, 2CH_2); 5.85 (1H, dd, ^3J = 10.2, ^3J = 2.2, NCHO); 7.35 (1H, t, ^3J = 7.5, H Ar); 7.45 (2H, t, ^3J = 7.6, H Ar); 7.93–8.01 (3H, m, H Ar, H-8); 8.69 (1H, s, H triazole). ^{13}C NMR spectrum ($CDCl_3$, 50°C), δ, ppm: 23.0; 24.9; 25.2; 26.3; 32.4; 46.8; 68.9; 81.9; 118.9; 119.3; 126.3; 128.3; 128.9; 130.9; 136.9; 147.5; 149.6; 151.2; 154.1. Found, *m*/*z*: 431.2332 $[M+H]^+$. $C_{23}H_{27}N_8O$. Calculated, *m*/*z*: 431.2302.

Compound 9d. Yield 125 mg (32%), colorless solid. R_f 0.20 (PhMe–MeCN, 10:1). HPLC: t_R 6.78 min. ^{1}H NMR spectrum ($CDCl_3$, 50°C), δ, ppm (*J*, Hz): 1.55–2.11 (11H, m) and 2.15 (1H, d, ^2J = 11.2, 6CH_2); 3.83 (1H, td, ^2J = ^3J = 11.4, ^3J = 2.8) and 4.15 (1H, d, ^2J = 11.2, CH_2O); 4.23–4.48 (4H, m, 2CH_2); 5.93 (1H, dd, ^3J = 10.1, ^3J = 2.3, NCHO); 7.39 (1H, tt, ^3J = 7.5, ^4J = 1.5, H Ar); 7.47 (2H, t, ^3J = 7.6, H Ar); 7.93–8.01 (3H, m, H Ar, H-8); 8.15 (1H, s, H triazole). ^{13}C NMR spectrum ($CDCl_3$, 50°C), δ, ppm: 23.0; 24.9; 25.2; 26.4; 32.6; 46.8; 68.9; 81.5; 119.1; 126.8; 129.0; 129.1; 130.3; 133.9; 136.8; 149.8; 151.1; 151.4; 154.3. Found, *m*/*z*: 431.2275 $[M+H]^+$. $C_{23}H_{27}N_8O$. Calculated, *m*/*z*: 431.2302.

Alternative method for the synthesis of compound 9c. Phenylacetylene (251 μl, ρ 0.93 g/cm^3, 2.29 mmol, 1.5 equiv) was added to a solution of compound **13** (500 mg, 1.52 mmol, 1.0 equiv), CuI (58 mg, 0.30 mmol, 0.20 equiv), AcOH (95 μl, ρ 1.05 g/cm^3, 1.67 mmol, 1.1 equiv), and Et_3N (230 μl, ρ 0.73 g/cm^3, 1.67 mmol, 1.1 equiv) in CH_2Cl_2 (15 ml). The reaction mixture was stirred isolated from daylight for 1 h at 20°C. Then the reaction mixture was poured into H_2O

(30 ml) and extracted with CH_2Cl_2 (3 × 20 ml). The combined organic phase was washed with aqueous $NaHSO_3$ (15 ml) and saturated NaCl (15 ml), dried over anhydrous Na_2SO_4, filtered, and evaporated. Silica gel column chromatography (eluent CH_2Cl_2 in MeCN, gradient 0–10%) of the residue provided product **9c** as a colorless solid. Yield 506 mg (77%).

2-(1*H*-Imidazol-1-yl)-6-(piperidin-1-yl)-9*H*-purine (10a). *p*-TsOH·H_2O (429 mg, 2.49 mmol, 2.2 equiv) was added to a solution of compound **9a** (400 mg, 1.13 mmol, 1.0 equiv) in MeOH (12 ml), and the reaction mixture was stirred for 14 h at 60°C. Then the reaction mixture was evaporated, the residue was suspended in 0.5 M solution of K_2CO_3 in H_2O–MeOH, 10:1 (20 ml) and filtered off. Recrystallization of the precipitate from EtOH provided product **10a**. Yield 161 mg (53%), colorless solid, mp 272–274°C (decomp., EtOH). R_f 0.23 (CH_2Cl_2–MeOH, 20:1). HPLC: t_R 3.71 min. ^{1}H NMR spectrum (DMSO-d_6, 60°C), δ, ppm: 1.55–1.80 (6H, m, $3CH_2$); 4.12–4.39 (4H, m, $2CH_2$); 7.05 (1H, s, H imidazole); 7.85 (1H, s, H imidazole); 8.04 (1H, s, H-8); 8.46 (1H, s, H imidazole); 13.00 (1H, br. s, NH). ^{13}C NMR spectrum (DMSO-d_6, 60°C), δ, ppm: 24.2; 25.7; 45.8; 116.8; 117.2; 129.4; 135.5; 138.1; 148.8; 152.0; 153.0. Found, *m*/*z*: 270.1450 $[M+H]^+$. $C_{13}H_{16}N_7$. Calculated, *m*/*z*: 270.1462.

2-[2-(1*H*-Imidazol-1-yl)-6-(piperidin-1-yl)-9*H*-purin-9-yl]ethyl 3,3,3-triphenylpropanoate (11a). DIAD (0.09 ml, ρ 1.03 g/cm^3, 0.45 mmol, 1.2 equiv) was added over 15 min to a solution of compound **9a** (100 mg, 0.37 mmol, 1.0 equiv), Ph_3P (117 mg, 0.45 mmol, 1.2 equiv), and 2-hydroxyethyl 3,3,3-triphenylpropanoate (**2**) (154 mg, 0.45 mmol, 1.2 equiv) in dry THF (5 ml) at 0°C, followed by stirring for 12 h at 20°C. Then the reaction mixture was evaporated, the residue was suspended in MeOH (15 ml) and H_2O (1 ml) and cooled at –10°C for 30 min. The formed precipitate was filtered off and washed with cold MeOH (2 × 5 ml) to give compound **11a**. Yield 173 mg (78%), colorless solid. R_f 0.39 (CH_2Cl_2–MeOH, 20:1). HPLC: t_R 6.64 min. ^{1}H NMR spectrum ($CDCl_3$, 50°C), δ, ppm: 1.64–1.88 (6H, m, $3CH_2$); 3.71 (2H, s, CH_2); 4.04–4.18 (4H, m, $2CH_2$); 4.14–4.42 (4H, m, $2CH_2$); 7.06–7.32 (16H, m, H Ph, H imidazole); 7.43 (1H, s, H-8); 7.84 (1H, s, H imidazole); 8.53 (1H, s, H imidazole). ^{13}C NMR spectrum ($CDCl_3$, 50°C), δ, ppm: 24.8; 26.3; 42.4; 46.2; 46.5; 55.9; 62.1; 117.1; 118.2; 126.5; 128.0; 129.2; 129.9; 136.4; 138.4; 146.3; 149.8; 151.6; 153.9; 170.6. Found, *m*/*z*: 598.2930 $[M+H]^+$. $C_{36}H_{36}N_7O_2$. Calculated, *m*/*z*: 598.2925.

2-[6-(Piperidin-1-yl)-2-(1*H*-1,2,4-triazol-1-yl)-9*H*-purin-9-yl]ethyl 3,3,3-triphenylpropanoate (11b). *p*-TsOH·H_2O (283 mg, 1.49 mmol, 2.2 equiv) was added to a solution of compound **9b** (240 mg, 0.68 mmol, 1.0 equiv) in MeOH (10 ml), and the reaction mixture was stirred for 14 h at 60°C. Then the reaction mixture was evaporated and suspended in 0.5 M K_2CO_3 solution in H_2O–MeOH, 10:1 (20 ml), and filtered. The crude 9*H*-deprotected compound **10b** (100 mg, 0.37 mmol, 1.0 equiv) was used for the synthesis of compound **11b**, using 2-hydroxyethyl 3,3,3-triphenylpropanoate (**2**) (154 mg, 0.45 mmol, 1.2 equiv), Ph_3P (117 mg, 0.45 mmol, 1.2 equiv), DIAD (0.09 ml, ρ 1.03 g/cm^3, 0.45 mmol, 1.2 equiv), and THF (5 ml) according to the procedure for the synthesis of compound **11a**. Yield 185 mg (45%), colorless solid. R_f 0.46 (CH_2Cl_2–MeOH, 20:1). HPLC: t_R 7.33 min. ^{1}H NMR spectrum ($CDCl_3$, 50°C), δ, ppm: 1.66–1.90 (6H, m, $3CH_2$); 3.75 (2H, s, CH_2); 4.10–4.24 (4H, m, $2CH_2$); 4.08–4.54 (4H, m, $2CH_2$); 7.08–7.35 (15H, m, H Ph); 7.50 (1H, s, H-8); 8.10 (1H, s, H triazole); 9.13 (1H, s, H triazole). ^{13}C NMR spectrum ($CDCl_3$, 50°C), δ, ppm: 24.7; 26.2; 42.4; 46.1; 46.4; 55.9; 62.4; 118.8; 126.4; 128.0; 129.1; 139.0; 143.8; 146.3; 149.4; 151.5; 153.1; 153.8; 170.5. Found, *m*/*z*: 599.2879 $[M+H]^+$. $C_{35}H_{35}N_8O_2$. Calculated, *m*/*z*: 599.2878.

2,6-Diazido-9-(tetrahydro-2*H*-pyran-2-yl)-9*H*-purine (12). NaN_3 (2.38 g, 36.63 mmol, 4.0 equiv) was added to a solution of compound **7**[27] (2.50 g, 9.16 mmol, 1.0 equiv) in Me_2CO (60 ml), and the reaction mixture was stirred in dark for 14 h at 50°C. Then the reaction mixture was evaporated, the residue was suspended in H_2O (50 ml), filtered off, and washed with H_2O (3 × 20 ml) to give compound **12**. Yield 2.58 g (98%), colorless solid. R_f 0.26 (CH_2Cl_2–MeOH, 20:1). HPLC: t_R 5.74 min. ^{1}H NMR spectrum ($CDCl_3$), δ, ppm (*J*, Hz): 1.58–2.16 (6H, m, $3CH_2$); 3.75 (1H, td, $^2J = {}^3J = 11.3$, $^3J = 2.6$) and 4.16 (1H, d, $^2J = 11.3$, CH_2O); 5.68 (1H, dd, $^3J = 10.1$, $^3J = 2.2$, NCHO); 8.10 (1H, s, H-8). ^{13}C NMR spectrum ($CDCl_3$), δ, ppm: 22.7; 24.9; 31.9; 68.9; 82.1; 121.4; 141.5; 153.2; 153.7; 156.0. Found, *m*/*z*: 287.1121 $[M+H]^+$. $C_{10}H_{11}N_{10}O$. Calculated, *m*/*z*: 287.1112.

2-Azido-6-(piperidin-1-yl)-9-(tetrahydro-2*H*-pyran-2-yl)-9*H*-purine (13). Piperidine (2.59 ml, ρ 0.86 g/cm^3, 26.2 mmol, 3.0 equiv) was added to a solution of compound **12** (2.5 g, 8.74 mmol, 1.0 equiv) in PhMe (30 ml). The reaction mixture was stirred in dark for 1 h at 50°C. Then the reaction mixture was evaporated, and the residue was purified by silica gel column chromatography (eluent CH_2Cl_2 in MeCN, gradient 0–10%). Yield 1.61 g (56%), pale-yellow solid. R_f 0.45 (CH_2Cl_2–MeOH, 20:1). HPLC: t_R 7.20 min. ^{1}H NMR spectrum ($CDCl_3$, 50°C), δ, ppm (*J*, Hz): 1.55–2.11 (12H, m, $6CH_2$); 3.73 (1H, td, $^2J = {}^3J = 11.4$, $^3J = 2.4$) and 4.12 (1H, d, $^2J = 11.4$, CH_2O); 4.09–4.35 (4H, m, $2CH_2$); 5.64 (1H, dd, $^3J = 10.0$, $^3J = 2.0$, NCHO); 7.82 (1H, s, H-8). ^{13}C NMR spectrum ($CDCl_3$, 50°C), δ, ppm: 23.0; 24.8; 25.0; 26.2; 32.0; 46.5; 68.9; 81.4; 117.3; 135.5; 151.7; 153.8; 156.2. Found, *m*/*z*: 329.1835 $[M+H]^+$. $C_{15}H_{21}N_8O$. Calculated, *m*/*z*: 329.1833.

6-(Piperidin-1-yl)-2-(1*H*-tetrazol-1-yl)-9*H*-purine (17). $HC(OEt)_3$ (240 mg, ρ 0.89 g/cm^3, 11.75 mmol, 1.6 equiv) was added to a solution of compound **16** (1.60 g, 7.34 mmol, 1.0 equiv) and NaN_3 (716 mg, 11.02 mmol, 1.5 equiv) in AcOH (40 ml), and the reaction mixture was stirred for 6 h at 80°C. Then the reaction mixture was evaporated and suspended in saturated aqueous $NaHCO_3$ solution (40 ml). The precipitate was filtered off, washed with saturated aqueous $NaHCO_3$ solution (2 × 10 ml), H_2O (2 × 10 ml), and dried to provide product **17**. Yield 1.31 g (66%), colorless solid. R_f 0.39 (CH_2Cl_2–MeOH, 20:1). HPLC: t_R 4.48 min. ^{1}H NMR spectrum (DMSO-d_6, 60°C), δ, ppm: 1.54–1.80 (6H, m, $3CH_2$); 4.19–4.39 (4H, m, $2CH_2$); 8.17 (1H, s, H-8); 9.97 (1H, s, H tetrazole). ^{13}C NMR spectrum (DMSO-d_6, 60°C), δ, ppm: 24.1: 25.7; 45.8 (br); 118.3;

139.3; 142.9; 146.8; 151.7; 152.9. Found, *m*/*z*: 272.1003 $[M+H]^+$. $C_{11}H_{14}N_9$. Calculated, *m*/*z*: 272.1367.

2-[6-(Piperidin-1-yl)-2-(1*H*-tetrazol-1-yl)-9*H*-purin-9-yl]ethyl 3,3,3-triphenylpropanoate (18a) was prepared analogously to compound **11a** from compound **17** (300 mg, 1.12 mmol, 1.0 equiv), 2-hydroxyethyl 3,3,3-triphenylpropanoate (**2**) (465 mg, 1.34 mmol, 1.2 equiv), Ph_3P (352 mg, 1.34 mmol, 1.2 equiv), and DIAD (0.27 ml, ρ 1.03 g/cm^3, 1.34 mmol, 1.2 equiv) in THF (10 ml) for 12 h at 20°C. Yield 570 mg (85%), colorless solid. R_f 0.38 (CH_2Cl_2–MeCN, 10:1). HPLC: t_R 7.48 min. ^{1}H NMR spectrum ($CDCl_3$, 50°C), δ, ppm: 1.67–1.89 (6H, m, $3CH_2$); 3.72 (2H, s, CH_2); 4.10–4.22 (4H, m, $2CH_2$); 4.02–4.62 (4H, m, $2CH_2$); 7.12–7.30 (15H, m, H Ph); 7.52 (1H, s, H-8); 9.38 (1H, s, H tetrazole). ^{13}C NMR spectrum ($CDCl_3$, 50°C), δ, ppm: 24.6; 26.2; 42.5; 46.0; 46.4; 55.8; 62.0; 119.3; 126.4; 127.9; 129.0; 139.4; 141.7; 146.2; 147.4; 151.1; 153.7; 170.4. Found, *m*/*z*: 600.2823 $[M+H]^+$. $C_{34}H_{34}N_9O_2$. Calculated, *m*/*z*: 600.2830.

9,9'-(5-{[6-(Piperidin-1-yl)-2-(1*H*-tetrazol-1-yl)-9*H*-purin-9-yl]methyl}-1,3-phenylene)bis(9*H*-carbazole) (18b) was prepared analogously to compound **11a** from compound **17** (118 mg, 0.44 mmol, 1.0 equiv), [3,5-di(9*H*-carbazol-9-yl)-phenyl]methanol (**21**) (212 mg, 0.48 mmol, 1.1 equiv), Ph_3P (138 mg, 0.53 mmol, 1.2 equiv), and DIAD (0.11 ml, ρ 1.03 g/cm^3, 0.53 mmol, 1.2 equiv) in THF (5 ml) for 1 h at 20°C. Yield 233 mg (77%), colorless solid. R_f 0.75 (CH_2Cl_2–MeCN, 10:1). HPLC: t_R 9.57 min. ^{1}H NMR spectrum ($CDCl_3$, 50°C), δ, ppm (*J*, Hz): 1.62–1.93 (6H, m, $3CH_2$); 3.91–4.67 (4H, m, $2CH_2$); 5.60 (2H, s, CH_2); 7.28 (4H, t, ^3J = 7.5, H Ar); 7.37 (4H, t, ^3J = 7.5, H Ar); 7.45 (4H, d, ^3J = 7.5, H Ar); 7.64 (2H, s, H Ar); 7.79 (1H, s, H Ar); 7.93 (1H, s, H-8); 8.10 (4H, d, ^3J = 7.5, H Ar); 9.36 (1H, s, H tetrazole). ^{13}C NMR spectrum ($CDCl_3$, 50°C), δ, ppm: 24.7; 26.3; 46.8; 47.2; 109.7; 119.8; 120.7; 120.9; 124.0; 124.6; 125.1; 126.4; 138.9; 139.6; 140.5; 140.6; 141.8; 148.1; 151.7; 154.2. Found, *m*/*z*: 692.2542 $[M+H]^+$. $C_{42}H_{34}N_{11}$. Calculated, *m*/*z*: 692.2993.

9-(2-Chloroethyl)-6-(piperidin-1-yl)-2-(1*H*-tetrazol-1-yl)-9*H*-purine (18c) was prepared analogously to compound **11a** from compound **17** (400 mg, 1.48 mmol, 1.0 equiv), 2-chloroethanol (0.11 ml, ρ 1.20 g/cm^3, 1.63 mmol, 1.1 equiv), Ph_3P (466 mg, 1.78 mmol, 1.2 equiv), and DIAD (0.35 ml, ρ 1.03 g/cm^3, 1.78 mmol, 1.2 equiv) in THF (8 ml) for 3 h at 20°C. The product was purified by silica gel column chromatography (eluent CH_2Cl_2 in MeCN, gradient 0–6%). Yield 312 mg (63%), colorless solid. R_f 0.15 (CH_2Cl_2–MeCN, 20:1). HPLC: t_R 5.14 min. ^{1}H NMR spectrum ($CDCl_3$, 50°C), δ, ppm (*J*, Hz): 1.67–1.88 (6H, s, $3CH_2$); 3.96 (2H, t, ^3J = 5.7, CH_2); 4.10–4.50 (4H, m, $2CH_2$); 4.57 (2H, t, ^3J = 5.7, CH_2); 7.88 (1H, s, H-8); 9.41 (1H, s, H tetrazole). ^{13}C NMR spectrum ($CDCl_3$, 50°C), δ, ppm: 24.7; 26.3; 42.5; 46.0; 47.0; 119.8; 139.9; 141.9; 147.8; 151.4; 154.1. Found, *m*/*z*: 334.1268 $[M+H]^+$. $C_{13}H_{17}ClN_9$. Calculated, *m*/*z*: 334.1290.

Methyl 3,5-di(9*H*-carbazol-9-yl)benzoate (20).[43] (1*R*,2*R*)-Cyclohexane-1,2-diamine (0.96 ml, ρ 0.95 g/cm^3, 7.96 mmol, 0.6 equiv) was added to a solution of methyl 3,5-dibromobenzoate (**19**) (3.90 g, 13.27 mmol, 1.0 equiv), CuI (756 mg, 3.98 mmol, 0.3 equiv), 9*H*-carbazole (5.54 g, 33.18 mmol, 2.5 equiv), and anhydrous K_3PO_4 in dry PhMe (100 ml). The reaction mixture was stirred at 120°C for 48 h. Then the reaction mixture was centrifuged, the supernatant was extracted with H_2O (3 × 40 ml) and brine (10 ml). The organic phase was evaporated, and silica gel column chromatography (eluent hexane in MTBE, gradient 0–20%), followed by precipitation from MeOH (50 ml) and washing with cold MeOH (3 × 20 ml), provided product **20**. Yield 1.61 g (26%), colorless solid. R_f 0.79 (CH_2Cl_2). HPLC: t_R 10.26 min. ^{1}H NMR spectrum ($CDCl_3$), δ, ppm (*J*, Hz): 4.00 (3H, s, CH_3); 7.34 (4H, t, ^3J = 7.5, H Ar); 7.46 (4H, t, ^3J = 7.5, H Ar); 7.54 (4H, d, ^3J = 7.5, H Ar); 8.04 (1H, t, ^4J = 1.9, H Ar); 8.17 (4H, d, ^3J = 7.5, H Ar); 8.39 (2H, d, ^4J = 1.9, H Ar). ^{13}C NMR spectrum ($CDCl_3$), δ, ppm: 52.9; 109.7; 120.7; 120.8; 123.9; 126.5; 126.8; 129.4; 134.0; 139.9; 140.5; 168.5. Found, *m*/*z*: 467.1772 $[M+H]^+$. $C_{32}H_{23}N_2O_2$. Calculated, *m*/*z*: 467.1754.

[3,5-Di(9*H*-carbazol-9-yl)phenyl]methanol (21).[44] A solution of $LiAlH_4$ (406 mg, 10.20 mmol, 5.0 equiv) in dry THF (20 ml) was stirred at 0°C for 30 min, then a solution of compound **20** (1.00 g, 2.14 mmol, 1.0 equiv) in dry THF (10 ml) was added dropwise, and the reaction mixture was stirred at 0°C for 2 h. Then the reaction mixture was evaporated, suspended in CH_2Cl_2 (20 ml), and centrifuged. Silica gel column chromatography (CH_2Cl_2) provided product **21**. Yield 676 mg (72%), colorless solid. R_f 0.36 (CH_2Cl_2). HPLC: t_R 8.41 min. ^{1}H NMR spectrum ($CDCl_3$), δ, ppm (*J*, Hz): 1.99 (1H, br. s, OH), 4.95 (2H, s, CH_2); 7.33 (4H, t, ^3J = 7.5, H Ar); 7.46 (4H, t, ^3J = 7.5, H Ar); 7.56 (4H, d, ^3J = 7.5, H Ar); 7.73 (2H, s, H Ar); 7.76 (1H, s, H Ar); 8.17 (4H, d, ^3J = 7.5, H Ar). ^{13}C NMR spectrum ($CDCl_3$), δ, ppm: 64.6; 109.8; 120.5; 120.6; 123.8; 123.9; 124.3; 126.3; 139.7; 140.7; 144.9. Found, *m*/*z*: 439.1835 $[M+H]^+$. $C_{31}H_{23}N_2O$. Calculated, *m*/*z*: 439.1805.

Supplementary information file containing experimental procedures for compounds **2**, **8**, **14**–**16** and ^{1}H and ^{13}C NMR spectra of compounds **4**, **9a**–**d**, **10a**, **11a**,**b**, **12**, **13**, **17**, **18a**–**c**, **20**, and **21**, is available at the journal website http://hgs.osi.lv.

This work was supported by the ERDF 1.1.1.1 activity project No. 1.1.1.1/16/A/131 "Design and Investigation of Light Emitting and Solution Processable Organic Molecular Glasses".

References

1. Rosemeyer, H. *Chem. Biodiversity* **2004**, *1*, 361.
2. Legraverend, M. *Tetrahedron* **2008**, *64*, 8585.
3. Arsenyan, P.; Vasiljeva, P.; Domracheva, I.; Kanepe-Lapsa, I. *Chem. Heterocycl. Compd.* **2020**, *56*, 776. [*Khim. Geterotsikl. Soedin.* **2020**, *56*, 776.]
4. Musiyak, V. V.; Gruzdev, D. A.; Kravchenko, M. A.; Vakhrusheva, D. V.; Levit, G. L.; Krasnov, V. P.; Charushin, V. N. *Mendeleev Commun.* **2019**, *29*, 11.
5. Manvar, A.; Shah, A. *Tetrahedron* **2013**, *69*, 8105.
6. Novosjolova, I.; Bizdena, E.; Turks, M. *Eur. J. Org. Chem.* **2015**, 3629.
7. Saito, Y.; Hudson, R. H. E. *J. Photochem. Photobiol. C* **2018**, *36*, 48.

8. Xu, W.; Chan, K. M.; Kool, E. T. *Nat. Chem.* **2017**, *9*, 1043.
9. Matarazzo, A.; Hudson, R. H. E. *Tetrahedron* **2015**, *71*, 1627.
10. Dumas, A.; Luedtke, N. W. *Chem.–Eur. J.* **2012**, *18*, 245.
11. Šišuļins, A.; Bucevičius, J.; Tseng, Y.; Novosjolova, I.; Traskovskis, K.; Bizdēna, Ē.; Chang, H.; Tumkevičius, S.; Turks, M. *Beilstein J. Org. Chem.* **2019**, *15*, 474.
12. Yang, Y.; Cohn, P.; Dyer, A. L.; Eom, S. H.; Reynolds, J. R.; Castellano, R. K.; Xue, J. *Chem. Mater.* **2010**, *22*, 3580.
13. Yang, Y.; Cohn, P.; Eom, S.-H.; Abboud, K. A.; Castellano, R. K.; Xue, J. *J. Mater. Chem. C* **2013**, *1*, 2867.
14. Wang, Z.; Yao, J.; Zhan, L.; Gong, S.; Ma, D.; Yang, C. *Dyes Pigm.* **2020**, *180*, 108437.
15. Traskovskis, K.; Mihailovs, I.; Tokmakovs, A.; Kokars, V.; Rutkis, M. *Proc. SPIE* **2012**, *8434*, 84341P.
16. Traskovskis, K.; Ruduss, A.; Kokars, V.; Mihailovs, I.; Lesina, N.; Vembris, A. *New J. Chem.* **2019**, *43*, 37.
17. Brændvang, M.; Gundersen, L. L. *Bioorg. Med. Chem.* **2005**, *13*, 6360.
18. Lagisetty, P.; Russon, L. M.; Lakshman, M. K. *Angew. Chem., Int. Ed.* **2006**, *45*, 3660.
19. Qu, G. R.; Zhang, H. L.; Niu, H. Y.; Xue, Z. K.; Lv, X. X.; Guo, H. M. *Green Chem.* **2012**, *14*, 1877.
20. Wang, S. Ben; Jin, P.; Li, F. N.; Quan, Z. S. *Eur. J. Med. Chem.* **2014**, *84*, 574.
21. Zhong, M.; Nowak, I.; Cannon, J. F.; Robins, M. J. *J. Org. Chem.* **2006**, *71*, 4216.
22. Elzein, E.; Palle, V.; Wu, Y.; Maa, T.; Zeng, D.; Zablocki, J. *J. Med. Chem.* **2004**, *47*, 4766.
23. Nilov, D. I.; Komarov, D. Y.; Panov, M. S.; Karabaeva, K. E.; Mereshchenko, A. S.; Tarnovsky, A. N.; Wilson, R. M. *J. Am. Chem. Soc.* **2013**, *135*, 3423.
24. Safina, B. S.; Sweeney, Z. K.; Li, J.; Chan, B. K.; Bisconte, A.; Carrera, D.; Castanedo, G.; Flagella, M.; Heald, R.; Lewis, C.; Murray, J. M.; Nonomiya, J.; Pang, J.; Price, S.; Reif, K.; Salphati, L.; Seward, E. M.; Wei, B.; Sutherlin, D. P. *Bioorg. Med. Chem. Lett.* **2013**, *23*, 4953.
25. Murray, J. M.; Sweeney, Z. K.; Chan, B. K.; Balazs, M.; Bradley, E.; Castanedo, G.; Chabot, C.; Chantry, D.; Flagella, M.; Goldstein, D. M.; Kondru, R.; Lesnick, J.; Li, J.; Lucas, M. C.; Nonomiya, J.; Pang, J.; Price, S.; Salphati, L.; Safina, B.; Savy, P. P. A.; Seward, E. M.; Ultsch, M.; Sutherlin, D. P. *J. Med. Chem.* **2012**, *55*, 7686.
26. Carrera, D. E.; Sheng, P.; Safina, B. S.; Li, J.; Angelaud, R. *Org. Proc. Res. Dev.* **2013**, *17*, 138.
27. Kapilinskis, Z.; Novosjolova, I.; Turks, M. *Molbank* **2018**, M1024.
28. Hellerman, L. *J. Am. Chem. Soc.* **1927**, *49*, 1735.
29. Huang, R.; Xie, C.; Huang, L.; Liu, J. *Tetrahedron* **2013**, *69*, 577.
30. Bhakuni, D. S.; Gupta, P. K.; Chowdhury, B. L. *Indian J. Chem., Sect. B*: *Org. Chem. Incl. Med. Chem.* **1984**, *23B*, 1286.
31. Li, J. J.; Gui, X. X. *Chin. Chem. Lett.* **2014**, *25*, 1341.
32. Sebris, A.; Turks, M. *Chem. Heterocycl. Compd.* **2019**, *55*, 1041. [*Khim. Geterotsikl. Soedin.* **2019**, *55*, 1041.]
33. Zaķis, J. M.; Ozols, K.; Novosjolova, I.; Vilšķērsts, R.; Mishnev, A.; Turks, M. *J. Org. Chem.* **2020**, *85*, 4753.
34. Ozols, K.; Cīrule, D.; Novosjolova, I.; Stepanovs, D.; Liepinsh, E.; Bizdena, E.; Turks, M. *Tetrahedron Lett.* **2016**, *57*, 1174.
35. Novosjolova, I.; Bizdēna, Ē.; Turks, M. *Tetrahedron Lett.* **2013**, *54*, 6557.
36. Satoh, Y.; Marcopulos, N. *Tetrahedron Lett.* **1995**, *36*, 1759.
37. Kovaļovs, A.; Novosjolova, I.; Bizdēna, Ē.; Bižāne, I.; Skardziute, L.; Kazlauskas, K.; Jursenas, S.; Turks, M. *Tetrahedron Lett.* **2013**, *54*, 850.
38. Smirnova, N. B.; Postovskii, I. Y. *Zh. Vses. Khim. O-va im. D. I. Mendeleeva* **1964**, *9*(6), 711.
39. Huang, L. K.; Cherng, Y. C.; Cheng, Y. R.; Jang, J. P.; Chao, Y. L.; Cherng, Y. J. *Tetrahedron* **2007**, *63*, 5323.
40. Kwon, T. H.; Kim, M. K.; Kwon, J.; Shin, D. Y.; Park, S. J.; Lee, C. L.; Kim, J. J.; Hong, J. I. *Chem. Mater.* **2007**, *19*, 3673.
41. Vabre, R.; Legraverend, M.; Piguel, S. *Dyes Pigm.* **2014**, *105*, 145.
42. Grigalevicius, S.; Tavgeniene, D.; Krucaite, G.; Griniene, R.; Li, W. C.; Luo, D.; Chang, C. H. *Dyes Pigm.* **2018**, *152*, 100.
43. Feng, K.; Zuniga, C.; Zhang, Y.-D.; Kim, D.; Barlow, S.; Marder, S. R.; Brédas, J. L.; Weck, M. *Macromolecules* **2009**, *42*, 6855.
44. Yoon, S. H.; Shin, J.; Um, H. A.; Lee, T. W.; Cho, M. J.; Kim, Y. J.; Son, Y. H.; Yang, J. H.; Chae, G.; Kwon, J. H.; Choi, D. H. *J. Polym. Sci., Part A: Polym. Chem.* **2014**, *52*, 707.

3. pielikums
Appendix III

Traskovskis, K.; Sebris, A.; Novosjolova, I.; Turks, M. Guzauskas, M.; Volyniuk, D.; Bezvikonnyi, O.; Grazulevicius, J.; Mishnev, A.; Grzibovskis, R.; Vembris, A.

All-organic Fast Intersystem Crossing Assisted Exciplexes Exhibiting Sub-Microsecond Thermally Activated Delayed Fluorescence

J. Mater. Chem. C **2021**, *9*, 4532.

doi: 10.1039/D0TC05099G

Journal of Materials Chemistry C

ROYAL SOCIETY OF CHEMISTRY

PAPER

Cite this: J. Mater. Chem. C, 2021, 9, 4532

All-organic fast intersystem crossing assisted exciplexes exhibiting sub-microsecond thermally activated delayed fluorescence†

Kaspars Traskovskis, *[a] Armands Sebris,[a] Irina Novosjolova,[a] Māris Turks, *[a] Matas Guzauskas,[b] Dmytro Volyniuk, [b] Oleksandr Bezvikonnyi,[b] Juozas V. Grazulevicius, [b] Anatoly Mishnev,[c] Raitis Grzibovskis [d] and Aivars Vembris[d]

Received 28th October 2020, Accepted 1st March 2021

DOI: 10.1039/d0tc05099g

rsc.li/materials-c

A novel strategy is presented towards acquisition of exciplex systems exhibiting thermally activated delayed fluorescence (TADF) with a high reverse intersystem crossing (RISC) rate (exceeding 10^7 s^{-1}). This approach involves constructing exciplex donor–acceptor molecular pairs, where the acceptor molecule possesses the ability to undergo fast and efficient intersystem crossing (ISC). With the use of 6-cyano-9-phenylpurine (PCP) acceptor and carbazole-based donor molecules, exciplexes were obtained, where the excitation is contained on PCP and undergoes fast ISC to form a local excited triplet state (^3LE_A). The controlled excitation transfer to the ^3LE_A level provides an optimal reverse intersystem crossing pathway, enabling TADF with a sub-microsecond emission lifetime. The side-effect of such an emissive mechanism is an unusual thermal photoluminescence quenching, caused by the limited PCP triplet state stability under room temperature conditions. PCP-carbazole dyads were obtained, which, in neat solid films, form intermolecular TADF-active exciplexes between donor and acceptor fragments of the neighbouring molecules. These compounds show balanced bipolar charge transport ability and were used as emissive layer host materials. The obtained organic light emitting diode (OLED) with an exciplex-forming host and a TADF emitter showed an external quantum efficiency exceeding 10% and low efficiency roll-off.

Introduction

The mainstream adoption of organic light emitting diode (OLED) technology is driving the ever-increasing demand for improved emissive materials.[1,2] Following an electrical excitation pathway, the spin statistics reveal that the injected electrons and holes recombine into singlet (S) and triplet (T) excitons with a ratio of 1 : 3.[3] This sets a limitation on OLED emitters, as the emission from triplet excited states needs to be realized. Organic molecules exhibiting thermally activated delayed fluorescence (TADF) have received great attention from the research community as a potential substitution for costly transition metal-containing materials.[4–6] In contrast to the phosphorescent organometallic complexes, where the presence of a heavy metal atom induces spin–orbit coupling (SOC), giving rise to a mixed character of S and T states, the TADF process is determined by a thermal energy assisted reverse intersystem crossing (RISC) between the lowest lying T_1 and S_1 levels.[7]

To stimulate the $T_1 \rightarrow S_1$ conversion, the energy gap between T_1 and S_1 states (ΔE_{ST}) needs to be minimized. This can be achieved by limiting an overlap between hole and electron wavefunctions.[8] In practical terms this involves synthesizing conjugated donor–acceptor (D–A) molecules, where the highest occupied molecular orbital (HOMO) and the lowest unoccupied molecular orbital (LUMO) are confined on separate molecular fragments. A large variety of TADF emitters has been explored, giving a fairly good understanding about structure–property correlations.[9–11] Besides conventional TADF molecules, where emission can be associated with an intramolecular charge transfer state, an alternative approach exists, where

[a] Faculty of Materials Science and Applied Chemistry, Riga Technical University, P. Valdena Str. 3, LV-1048, Riga, Latvia. E-mail: kaspars.traskovskis@rtu.lv, maris.turks@rtu.lv

[b] Department of Polymer Chemistry and Technology, Kaunas University of Technology, Barsausko 39, LT-51423, Kaunas, Lithuania

[c] Latvian Institute of Organic Synthesis, Aizkraukles Str. 21, Riga LV-1006, Latvia

[d] Institute of Solid State Physics, University of Latvia, Kengaraga Str. 8, LV-1063, Riga, Latvia

† Electronic supplementary information (ESI) available. CCDC 1988182. For ESI and crystallographic data in CIF or other electronic format see DOI: 10.1039/d0tc05099g

TADF originates from exciplex systems.[12–14] In this case the first molecule acts as an electron donor and the second as an electron acceptor. Because of the involvement of two separate moieties, the overlap between HOMO and LUMO wavefunctions is minimal and a very small ΔE_{ST} value can be attained.[15] In addition to a reduced structural complexity, the exciplex systems theoretically allow a simpler emission colour tuning through matching D and A components with appropriate energy levels. Despite the apparent advantages, the theory-guided development of such emitting materials is currently limited due to a relatively low number of known exciplex-forming molecular pairs, unclear structures of the emissive molecular dyad[16] and unsatisfactory photoluminescence quantum yields (Φ_{PL}) of many exciplex systems.

The generally accepted kinetic pathway of exciplex formation between two molecules (D and A) involves three steps.[17] First, one of the molecules is promoted to its excited state (D* or A*), then a complex between the closely situated excited and ground-state species forms (D*A or DA*). In the case of a favourable electronic configuration of the components, where both the ionization potential (IP) and electron affinity (EA) values of A are higher than those of D, the electron transfer process takes place from D to A and an excited intermolecular charge transfer state (ICT) is formed ($[D^+A^-]$*). The overall exciplex structure is defined as the combination of the involved resonance forms: D*A ↔ DA* ↔ $[D^+A^-]$*, where the first two are denoted as locally excited (LE) states, but the last one is denoted as the charge transfer excited state.[18] Regarding the development of TADF-active exciplex systems, LE states play a crucial role. Closely lying singlet ^{1}ICT and triplet ^{3}LE levels are mandatory for substantial SOC, enabling the RISC process and ensuring triplet-harvesting in OLEDs. Such a process is favourable in comparison to the coupling between ^{1}ICT and ^{3}ICT, as SOC is expected to be zero for S and T states with a similar spatial confinement of the involved molecular orbitals.[19]

In this paper we propose a novel structural approach towards TADF exciplex systems. It is based on the introduction of an acceptor molecule, which possesses an inherent fast intersystem system crossing (FISC) ability, *i.e.* the rate of ^3LE_A population ($^1LE \rightarrow {}^3LE$) greatly outpaces the emissive or non-radiative relaxation from ^{1}LE to the ground state S_0 ($^1LE \rightarrow S_0$). For such emitting systems the dominant emissive pathway would involve a RISC process between $^3LE_A \rightarrow {}^1$ICT states and a sequential radiative relaxation in the form of the delayed fluorescence ($^1ICT \rightarrow S_0$). The favourable coupling between ^{3}LE and ^{1}ICT states is expected to enhance SOC, resulting in a reduced lifetime of the delayed emission (Fig. 1). Other apparent advantages of such exciplex systems would be the elimination of competing emission processes such as fluorescence from LE states.[20,21] Increased colour purity would make such TADF exciplex systems more suitable for OLED display integration.[22]

Among potentially suitable FISC-capable molecules, our attention was drawn to the purine heterocycle. The extensive investigation of this naturally occurring DNA building block has shown that upon photoexcitation it undergoes a rapid (on a scale of a few hundred ps) ISC process[23] with a relatively high

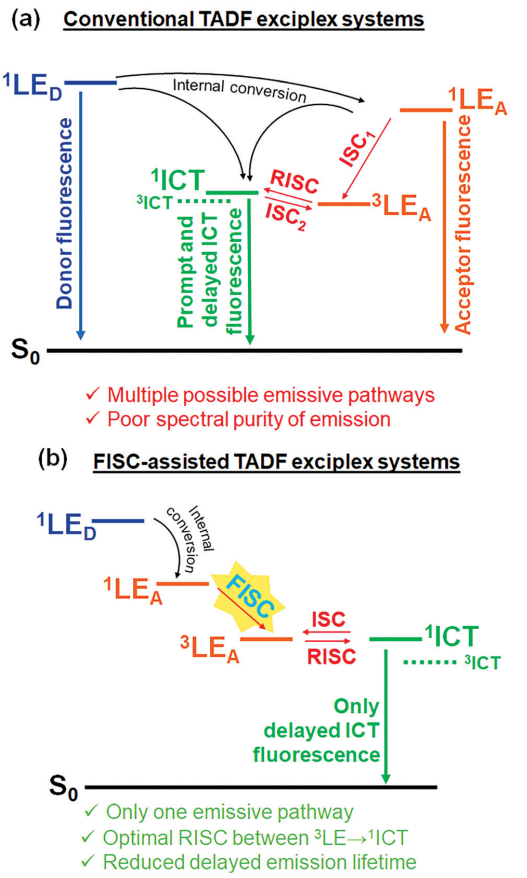

Fig. 1 Schematic representation of the emission processes for conventional (a) and FISC-assisted TADF exciplex systems (b).

triplet quantum yield of 0.88.[24] The generated triplet state is moderately stable and in a solution persists for about 1.7 μs.[25] Besides a suitable excited state kinetics, purine-based materials have been successfully used in OLEDs as charge transporting materials,[26] marking these compounds as an appropriate building block for FISC-assisted TADF exciplex systems. Here we report the development and photophysical properties of a suitable purine derivative and its further integration in exciplex systems with carbazole-based donor components, employing approaches with physical mixing and covalent bonding. The OLED integration of the materials was attempted employing them as the charge transporting host material for the emissive layer (EML).

Results and discussion

Development of a FISC-capable purine acceptor

In accordance to El-Sayed's rule the ISC process is forbidden, if the transition proceeds between S and T states with a similar

electronic configuration.[27] For purine this limitation is overcome by an interplay of molecular orbitals with an unlike electronic spatial distribution, namely, n orbitals related to lone electron pairs of the nitrogen atoms and π orbitals of the aromatic ring system. As a result, ISC becomes possible between the nπ* and ππ* excited states.[23] Our initial attempts to obtain emissive exciplex systems by using unfunctionalized purine and common donor molecules were not successful. In order to reduce the small intrinsic EA value of the purine, enable excitation transfer from the donor and increase the probability of exciplex formation, a cyano group was introduced at its 6 position.[28] Further modification of the purine involved an arylation of the 9-position with a phenyl group to prevent the possible tautomerization. Accordingly, compound 6-cyano-9-phenylpurine (PCP) was obtained (Scheme 1).

The absorption and photoluminescence (PL) spectra of PCP in THF solution are given in Fig. 2a. The compound shows an absorption band with a maximum at 294 nm. Upon photoexcitation a weak fluorescence can be detected with a band maximum at 431 nm and a PL quantum yield (Φ_{PL}) below 0.01. In contrast, under low temperature conditions (77K, 2-MeTHF) the compound exhibits a strong, long-lived bluish-green phosphorescence, as indicated by time-resolved emission measurements (Fig. 2b and c). The pronounced dominance of the triplet state emission over fluorescence is a clear indication of a rapidly populated T_1 state.

To gain a deeper insight into excited state kinetics, time-dependent density-functional theory (TD-DFT) calculations were employed. Optimized S_0, S_1 and T_1 state geometries of PCP were examined to account for the vertical and adiabatic states (Fig. 3a). Similarly to the non-functionalized purine, the lowest energy transitions of PCP are associated with an electron transfer from either the occupied n or π-type molecular orbitals to the unoccupied π* orbital (Fig. S1, ESI†). For the ground state (GS) geometry the excitation process is dominated by $^1\pi\pi^*$ transition with an oscillator strength (f_{osc}) of 0.20. However, two other transitions ($^1\pi_{Ph}\pi^*$ and $^1n\pi^*$) are predicted at lower energies as they show much smaller f_{osc} values of 0.07 and 0.0014. In such a way the experimentally observed featureless absorption band at 294 nm can be mainly attributed to the $^1\pi\pi^*$ transition, as the weaker bands cannot be resolved in the UV-Vis spectra due the overlap.

The optimized S_1 geometry of the compound corresponds to the relaxed $^1n\pi^*$ excited state, while the T_1 structural configuration equates to the $^3\pi\pi^*$ state. According to El-Sayed's rule,

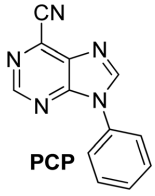

Scheme 1 Structure of the purine-derived acceptor.

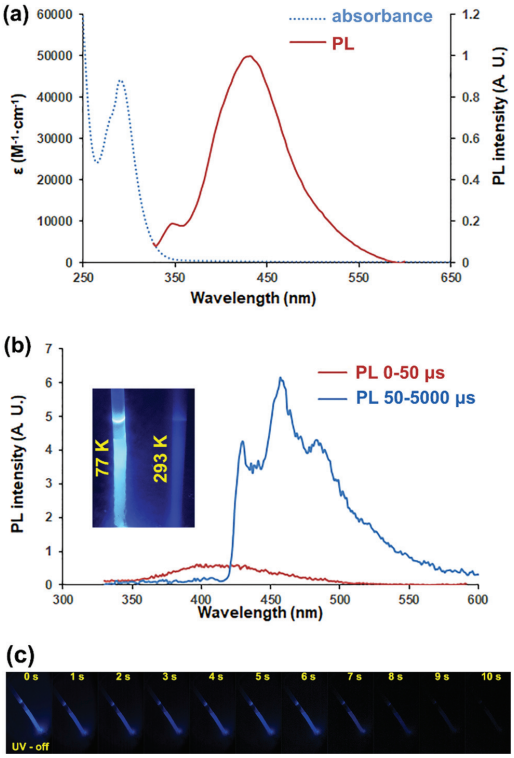

Fig. 2 (a) Absorption and PL spectra of PCP in THF solution. (b) Fluorescence (0–50 μs) and phosphorescence (50–5000 μs) emission bands of PCP, measured in 2-MeTHF at 77 K. The inset shows a photograph of UV-irradiated (365 nm) PCP solution in 2-MeTHF at 293 and 77 K. (c) Photographs of the same sample at 77K, taken at different time intervals after UV irradiation is turned off.

such an orbital arrangement of the S_1 and T_1 states is favourable for the ISC process. To provide further evidence for this assumption, the theoretical ISC rate (k_{ISC}) was calculated between the aforementioned excited states by employing the excited state dynamics (ESD) module in the Orca program (Fig. 3b).[29] A considerable SOC matrix element (SOCME) between $^1n\pi^*$ and $^3\pi\pi^*$ levels is predicted, amounting to 1.23 cm^{-1}. The corresponding ISC rate $k_{ISC} = 4.4 \times 10^8\ s^{-1}$ was obtained. While being relatively fast, such a k_{ISC} value potentially allows a close competition between ISC and fluorescence processes. Because of this, the fluorescence rate ($k_{fluor.}$) for $^1n\pi^*$ was also calculated to account for the radiative depopulation of the lowest energy singlet excited state. Value $k_{fluor.} = 1.8 \times 10^6\ s^{-1}$ was obtained, suggesting that the radiative process is slow, presumably due to the low oscillator strength of the $^1n\pi^*$ transition. The theoretical predictions are in good agreement with the experimental observations. While a weak fluorescence is observed for PCP, the Φ_{PL} of this radiative pathway is below 0.01 and the low-temperature emission is dominated by

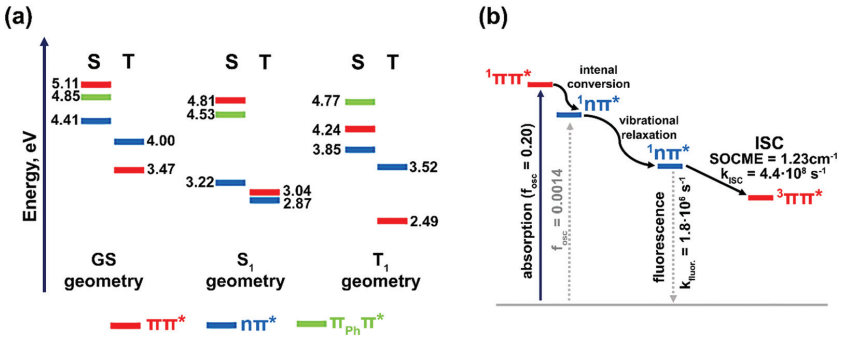

Fig. 3 (a) Calculated lowest lying singlet and triplet excited state energies of PCP (CAM-B3LYP/def2-TZVP). (b) Proposed photoexcitation mechanism of PCP. Calculated ISC and fluorescence rates are given for the relaxed S_1 ($^1n\pi^*$) state.

phosphorescence. Such behaviour is consistent with the ISC rate being about two orders of magnitude higher than the competing fluorescence process. Overall, despite the attachment of the –CN group, the calculated excited state energy level configuration and photophysical behaviour of PCP are almost identical to those of the FISC-capable parent compound – purine.[23]

Investigation of FISC-assisted exciplex systems

In order to evaluate the possibilities of a practical realization of FISC-assisted TADF exciplexes two distinctive structural approaches were investigated. Generally, exciplex systems are prepared as physical mixtures of donor and acceptor molecules. Electron rich aromatic amines are usually employed as the donor component due to appropriate energy level placement and excellent hole-transporting ability.[30] Accordingly, carbazole (Cbz) was chosen as the donor. In order to overcome the strong crystallization tendency of Cbz, its structural modifications, 9-phenylcarbazole (9-PhCbz) and poly(9-vinylcarbazole) (PVK), were used for the preparation of the physical mixtures (Scheme 2).

While the use of separate donor and acceptor molecules provides a simple way to prepare functional materials, the application of such exciplex systems as TADF-active hosts is met with technological challenges. Mainly this is related to a poor control over the molecular packing patterns in multi-molecular mixtures, making the formation of exciplex molecular pairs less likely. As a solution for this problem, the development of intramolecular exciplex systems is proposed, where the donor and acceptor molecules are covalently bound.[31] Structurally such compounds are often designed as donor–donor′–acceptor (D–D′–A) molecules, where through bond conjugation between D–A fragments is prevented.[32,33] Accordingly, we prepared three covalently bound molecular dyads PCbz(1–3) (Scheme 2), where PCP and Cbz are connected through a phenyl ring. The D–A bridge in these molecules features a phenylenediamine motif, which is expected to obstruct the through bond D–A electron transfer process. A single crystal X-ray structure was obtained for compound PCbz-2 (Fig. S2, ESI†). The molecule assumes a conformation,

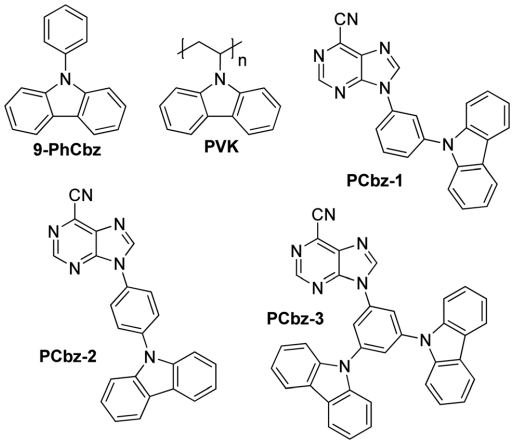

Scheme 2 Chemical structures of the donor fragments 9-PhCbz and PVK and covalently bound acceptor-donor dyads PCbz-1, PCbz-2, and PCbz-3.

where purine and Cbz ring systems are coplanar, but the central benzene ring is twisted out of the D–A fragment plane by approximately 50°. In addition to pseudo-D–D′–A structural composition the twisted bridging fragment additionally obstructs the π-electron conjugation between D and A fragments. Consequently, as it is later shown by TD-DFT calculations only the through-space charge transfer process can take place between purine and Cbz fragments.

The IP and EA values for the investigated compounds are given in Fig. 4a. Our experimental setup was not able to directly assess EA of PCP. Instead, for PCP this parameter is estimated to be around 3.20 eV, by assigning the EA value of PCbz dyads to the weakly conjugated acceptor fragment. Consequently, the energy levels of donor–acceptor pairs allow the exciplex formation, as for PCP both EA and IP (6.15 eV for PCP) are higher than the representative values for the donor compounds.

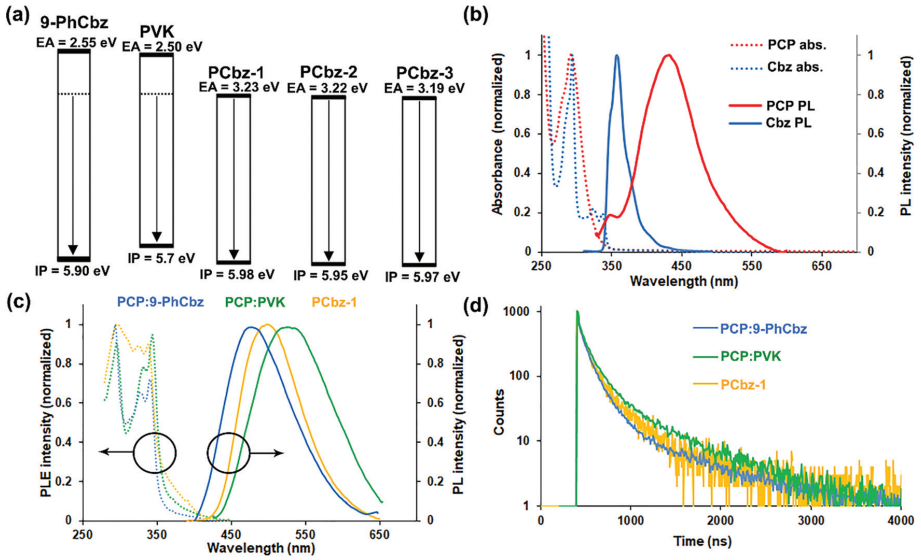

Fig. 4 (a) IP and EA values of the investigated compounds. (b) Absorption and emission spectra of Cbz and PCP in THF solution. (c) PLE and PL spectra of exciplex systems in amorphous films. (d) PL decay of exciplex systems.

Photophysical properties in solution

The absorption and emission spectra of PCP and Cbz in THF solution are given in Fig. 4b. The emission band of PCP is significantly redshifted in comparison to Cbz. In such a way the excitation transfer $^1LE_D \rightarrow {}^1LE_A$ is expected for the corresponding bimolecular system. This is further supported by the fact that the emission of Cbz is quenched in the presence of PCP. The measured T_1 energy levels of the Cbz and PCP are, accordingly, 3.09 and 2.95 eV (Fig. S3, ESI†). A deeper insight into the photo-physical processes for the investigated D–A molecular pairs can be gained from the investigation of the synthesized dyads. In solution PCbz (1–3) show broad emission bands with maxima at 523–544 nm. These bands are considerably redshifted in comparison to PCP and Cbz emission (Fig. S4a, ESI†), thus indicating formation of emissive intramolecular charge transfer (CT) states. The emission is weak, with Φ_{PL} below 0.01. The PL lifetime values fall in the range of several nanoseconds, pointing to a purely fluorescence emission process (Fig. S4b, ESI†).

Low temperature PL measurements were performed to determine the T_1 level of the compounds in the dissolved state (Fig. S5, ESI†). In all the cases phosphorescence originates from the PCP fragment. For PCbz-1 and PCbz-3 the intensity of phosphorescence is several times stronger than CT fluorescence, similarly to the situation observed for the unmodified acceptor fragment. This lets us assume that for the closely located PCP and Cbz pairs the photoexcitation kinetics are favourable for FISC-assisted exciplex formation, as the excitation mainly relaxes to the local triplet state of the acceptor fragment. The origin of the observed CT emission is attributed to a competing slower emissive relaxation pathway, which, in contrast to the situation observed for PCP, now originates from the ^1CT state. While a complete excitation transfer $^1LE_A \rightarrow {}^1CT$ is expected to take place in a conjugated molecule due to the internal conversion being a much faster process than ISC, for PCbz-1 and PCbz-3 this seems to be prevented by a weak coupling between the D and A fragments. Such an assumption is supported by the UV-Vis absorption spectral data of the PCbz series (Fig. S6, ESI†), where the absorption of the molecular dyads can be interpreted as a sum of PCP and Cbz absorption bands, with no apparent formation of the CT state. On the other hand, low temperature fluorescence and phosphorescence, in terms of intensity, become almost identical for PCbz-2. This suggests an increased ground-state CT character for the compound, probably caused by the alternative intermolecular D–A bounding pattern.

To interpret these results, TD-DFT calculations were performed for PCbz (1–3) (Table S1, ESI†). The lowest energy singlet state arises from the through-space CT transition between the Cbz and PCP fragments (Fig. S7, ESI†). Oscillator strength values of this transition are small, indicating a weak D–A coupling. Though, in comparison to other compounds, this value is about 8 times larger for PCbz-2. This result is consistent with the low-temperature emission data in solution, where a stronger CT character and less pronounced ISC are assumed for the compound due to comparable phosphorescence and fluorescence intensities (Fig. S4, ESI†). The lowest energy excited triplet state of the D–A dyads is the local triplet of the 6-cyanopurine acceptor. The T_2 state is the CT triplet, located closely below ^1CT ($\Delta E = 0.01$ to 0.10 eV). Due to the deep

^3LE_A level, the intramolecular TADF process is not expected, as the energy gap between ^3LE_A and ^1CT states exceeds 0.24 eV. This correlates well with the experimental data in 2-MeTHF solution, where this energy gap is estimated at around 0.20 eV.

Photophysical properties in films

The emission properties of the exciplex systems were investigated in spin-coated thin films. The samples featuring a physical mixture of the components were prepared by mixing PCP and 9-PhCbz at a 1 : 1 molar ratio. To prevent the crystallization and phase separation of the individual components the resulting mixture was dispersed in poly(methyl methacrylate) (PMMA) with a mass ratio between the exciplex forming molecular pair and polymer host being set at 50 : 50 wt%. The second exciplex system was prepared by mixing PCP and PVK at an approximately 1 : 1 molar ratio. The rest of the tested samples were neat amorphous films of PCbz(1–3).

In all the cases broad charge-transfer emission bands were observed with maxima in the range of 473–528 nm (Fig. 4c and Fig. S8, ESI;† Table 1). System PCP:PVK shows significantly redshifted ICT emission due to PVK possessing a lower IP value than the other donor components (Fig. 4a). The photoluminescence excitation (PLE) spectra are consistent with the exciplex formation, as emission originates from the photoexcitation of D and A components and no direct CT or ICT transitions can be detected (Fig. 4c). Slight PL quenching in the presence of oxygen was detected for the samples (Fig. S9, ESI†).

The PL lifetime measurements reveal multiexponential decay dynamics. This is a characteristic behaviour for exciplex systems due to the involvement of molecular pairs with poorly defined spatial configuration (Fig. 4d and Fig. S10, ESI;† Table 1).[34] The fitted lifetime values indicate that the emission process involves contribution from triplet states, as long-lived emission components of up to 0.69 μs can be measured. In contrast to the conventional TADF emitters, no clear distinction between prompt and delayed emissions can be made. The fastest component of the multiexponential decays varies in the range of 31–54 ns, exceeding the typical fluorescence lifetime values of organic fluorophores.[35] This observation supports the proposed FISC-assisted exciplex formation, as the realization of such a mechanism should yield predominantly delayed emission. The shape and position of PL spectral bands show no transformations with time (Fig. S11, ESI†), again suggesting that all the occurring emission processes originate from a single excited state. In terms of Φ_{PL} the highest value of 0.41 was measured for PCbz-1. For other compounds this parameter is notably lower, in the range of 0.08–0.25. The least efficient emission is observed for the PCP:PVK system. Such a quantum yield drop is characteristic for the exciplex systems bearing polymeric donor components, because the formation of exciplex molecular pairs is obstructed due to steric effects of polymer chains.[36] The TADF nature of the compounds is additionally supported by the linear dependency of the delayed emission intensity on laser flux, with the resulting slope coefficient of 1 (Fig. S12, ESI†). In the case of triplet–triplet annihilation a slope of 2 is expected.[37]

Temperature-dependent PL measurements were conducted for PCP:9-PhCbz and PCbz(1–3) exciplex systems. Upon cooling in 300–77 K interval PL decays reveal minimal temperature-induced changes (Fig. S13, ESI†). Generally, a slight emission intensification across the whole decay curve can be observed (Fig. 5a). This is a contrasting behaviour in comparison to conventional TADF emitters, for which cooling leads to a substantial intensity drop for the delayed emission component.[38] Direct measurements of PL intensity reveal a more pronounced temperature dependence (Fig. 5b and Fig. S14, ESI†). All examined samples show notable PL intensification upon cooling. This is particularly apparent for PCbz-1, where, upon cooling to 77 K, the PL quantum yield increases from 0.41 to 0.69 (Fig. 5c). This intensification is not linear and at about 150–180 K a local maximum can be resolved in PL efficiency-temperature correlation curve.

Previous observations provide evidence for FISC-assisted TADF exciplex formation. Assuming a complete excitation transfer to the ^3LE_A state, triplet stability is expected to become a significant factor for the excited state relaxation process. The triplet lifetime of PCP is predicted to not exceed 1.7 μs under room temperature conditions (experimentally determined value for purine). Accordingly, the rates of RISC-mediated radiative relaxation from ^1CT state and non-radiative local triplet relaxation are similar and the both processes occur on a comparable timescale. Thus, the observed gradual intensification of the emission with the cooling can be considered as a consequence of PCP triplet state stabilization. The observed local emission efficiency maxima at about 100–180 K, on other hand, can be related to the manifestation of TADF (Fig. 5c), as it indicates the thermal activation process. Assuming the FISC-assisted emissive mechanism, ΔE_{ST} gaps of the examined exciplex systems are assigned as the energy difference between local PCP triplet and ^1CT singlet energies (Table 1). The ^3LE_A

Table 1 Photo-physical properties of the investigated exciplex systems

Exciplex system	λ_{PL}[a] [nm]	Φ_{PL}	τ_1, τ_2, (τ_3) [ns]	$\tau_1 : \tau_2$ (: τ_3)[b] [%]	E_S[c] [eV]	E_T[d] [eV]	ΔE_{ST}[e] [eV]
PCP:9-PhCbz	473	0.25	49, 137, 682	21 : 56 : 16	2.98	2.95	0.03
PCP:PVK	528	0.08	31, 140, 692	12 : 56 : 32	2.81	2.95	−0.14
PCbz-1	502	0.41	54, 246	39 : 61	2.82	2.94	−0.12
PCbz-2	501	0.17	34, 149	21 : 79	2.97	2.92	0.05
PCbz-3	497	0.13	55, 183	27 : 73	2.85	2.94	−0.09

[a] Emission band maxima. [b] Relative contribution of multi-exponential PL decay components. [c] Onset energy of fluorescence at room temperature. [d] Onset energy of PCP or PCbz(1–3) phosphorescence in 2-MeTHF at 77 K. [e] $\Delta E_{ST} = E_S - E_T$.

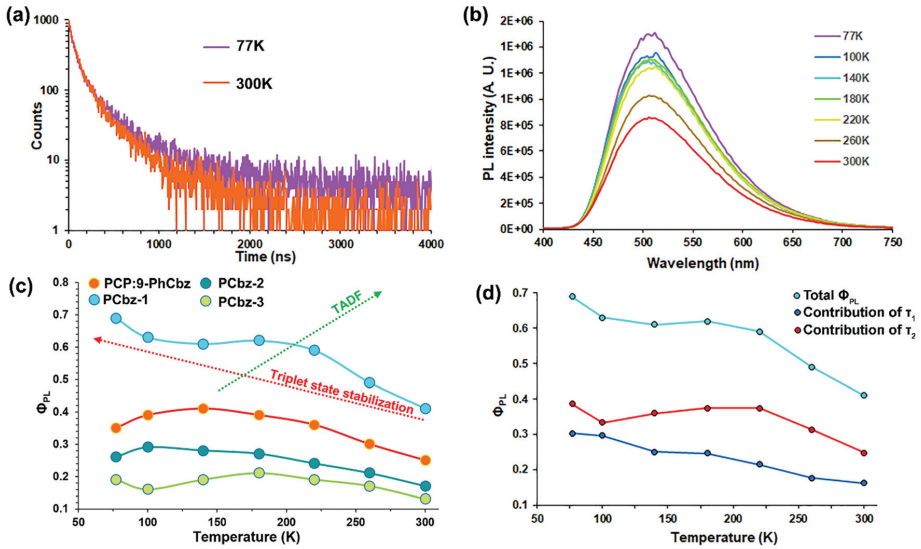

Fig. 5 (a) PL decay of the PCbz-1 neat amorphous film recorded at 300 and 77 K temperature. (b) Temperature-dependent PL intensity changes of PCbz-1 measured in a neat amorphous film. (c) Temperature-induced Φ_{PL} changes in neat films of PCbz(1–3) and the PCP:9-PhCBz/PMMA mixture. Arrowed lines illustrate the proposed photo-physical processes. (d) Contribution of τ_1 (~50 ns) and τ_2 (~150–200 ns) PL components towards cooling-induced Φ_{PL} changes for PCbz-1.

level of the exciplex systems is placed at 0.09–0.14 eV above the emissive singlet level, with the exception of PCP:9-PhCbz and PCbz-2, where the local triplet is the lowest lying excited state. In such a way, the most probable thermally activated radiative process should involve internal upconversion $^3CT \rightarrow {}^3LE_A$, followed by RISC between $^3LE_A \rightarrow {}^1CT$ levels or only RISC between $^3LE_A \rightarrow {}^1CT$ levels, if the local triplet is the lowest level.[39] While the manifestation of TADF is expected to result in a gradual intensity increase of the delayed PL component across the whole 77–300 K range, starting from 200 K the thermal activation is likely undermined by the rapidly decreasing triplet state population of the PCP acceptor.

PL lifetimes were fitted for the neat PCbz-1 film across the 300–77 K cooling range. Throughout the temperature range the PL decay can be approximated with a biexponential fit, yielding lifetimes $\tau_1 \approx 50$ ns and $\tau_2 \approx 300$ ns. The impact of cooling on τ_1 is negligible, while for τ_2 a gradual increase by about 80 ns can be observed (Fig. S15, ESI†). Increasing lifetime of τ_2 indicates a reduction in the radiative rate thus suggesting the TADF emission mechanism. The contribution of each decay component towards total Φ_{PL} is plotted in Fig. 5d. As it can be seen a cooling-induced PL efficiency increase can be observed for both the components. The fastest component shows almost linear intensity increase across the temperature range. At the same time, the behaviour of τ_2 is closer to typical TADF emitters, with a clearly resolvable thermal activation, which peaks at around 225 K. Since both the decay components are temperature-dependent their origin can be attributed to the triplet (^3LE_A) state.[40]

A deeper insight into the emission mechanism is provided by the analysis of dilution effects on PL characteristics in a PCbz-1:PMMA guest–host system (Fig. 6 and Table S2, ESI†). The PL bands of the samples show a steady redshift from 468 to 502 nm, as the concentration of PCbz-1 increases from 1 to 100 wt%. This linear concentration-induced redshift of the PL band is a clear indication of exciplex formation. The ^1CT energy of the exciplex can be directly correlated with the distance between the involved D and A fragments, where more closely situated molecular pairs possess a lower energy S_1 state.[41] In the studied case the distance between D and A fragments decreases with the emitter concentration, causing the observed PL redshift. At a PCbz-1 concentration of 1 wt% it is expected that a significant contribution to the total emission originates from the intramolecular through-space charge transfer process, as the PCbz-1 molecules become more isolated. Because no apparent changes in band shape or PL kinetics are observed in comparison to more concentrated samples the emission in this case is still attributed to the exciplex formation mechanism.[31,42,43]

The shift of the ^1CT band to lower wavelengths is accompanied by emission efficiency increase, as Φ_{PL} rises from 0.18 to 0.41 (Table S2, ESI†). This can be explained by the relative placement of ^1CT and ^3LE_A levels. For 1 and 10 wt% samples the ^1CT level (measured at the PL onset) is placed significantly above T_1 of the PCP fragment (ΔE_{ST} = 0.34 and 0.15 eV). By assuming almost complete excitation transfer to the ^3LE_A state, the large energy gap between the local triplet and the emissive singlet forbids the RISC process for a significant population of

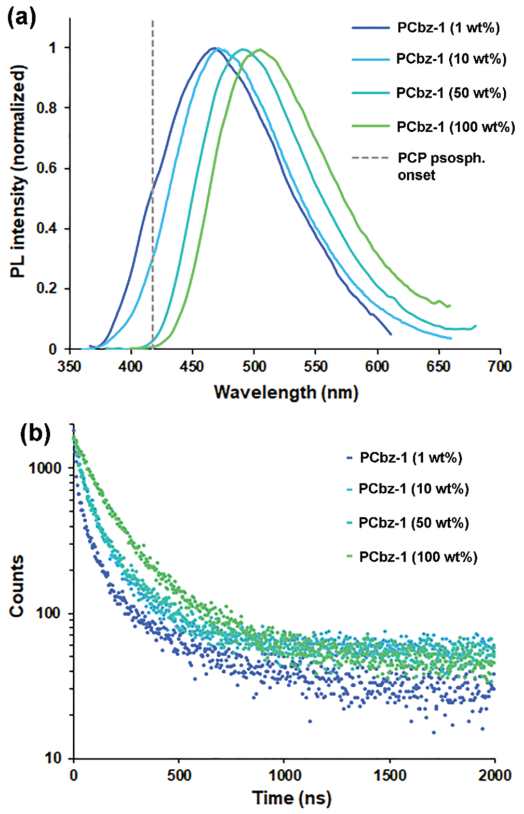

Fig. 6 (a) PL spectra of PCbz-1:PMMA films with different emitter concentrations. Phosphorescence onset of PCP is given to mark the ^3LE_A energy level. (b) PL decays of the aforementioned samples.

D/A pairs (LE state energy is not affected by the composition of the D/A mixture). Coincidently, for 50 and 100 wt% samples a substantial Φ_{PL} increase is observed, as the ^3LE_A level now matches the ^1CT onset (Fig. 6a). The difference between the studied samples is also apparent, when PL decays are compared (Fig. 6b). Namely, the intensity of delayed emission increases with PCbz-1 concentration. This provides another evidence for substantial excitation trapping by the dark ^3LE_A state in the more diluted PMMA films.

Because of the notable intensity decrease for delayed emission in a 1 wt% sample, a prompt emission can be resolved in PL decay. Accordingly, the fit with three decay components can be obtained (Table S2, ESI†), showing prompt fluorescence with 6.9 ns lifetime that accounts for 7% of the total emission. Expressed in Φ_{PL} this amounts to 0.01, a value that is identical to the measured PL quantum yield in the PCP:PMMA (5 wt%) film. Accordingly, the prompt emission can be interpreted as a result of direct energy transfer from the ^1LE_A to ^1CT state, whereas the rest of the emission is a result of an initial ISC process to the ^3LE_A state, followed by TADF. The detection of prompt and delayed emission components allows calculation of the photophysical rate constants for the emissive system.[44] Accordingly, a k_{ISC} value of 1.35×10^8 s^{-1} was obtained, which is comparable to the theoretically calculated value for PCP. At the same time the relatively slow prompt fluorescence rate $k_{fluor.} = 1.83 \times 10^6$ s^{-1} determines a high ISC quantum yield (Φ_{ISC}) of 0.92. Because of the two delayed emission components being present, the rate constants for each were determined separately. The slowest component (τ = 368 ns) possesses a k_{RISC} of 6.12×10^6 s^{-1}, a delayed fluorescence rate k_{DF} of 2.49×10^5 s^{-1} and a nonradiative rate k_{nr} of 2.47×10^6 s^{-1}. For the fastest component (τ = 63 ns) these parameters are $k_{RISC} = 2.85 \times 10^7$ s^{-1}, $k_{DF} = 1.17 \times 10^6$ s^{-1} and $k_{nr} = 1.47 \times 10^7$ s^{-1}. As it can be seen rate constants vary significantly between the two cases, indicating slightly different upconversion mechanisms. This is expected for exciplex systems, where large variation in distance between D and A fragments results in dispersion in the relative placement of ^1CT, ^3CT and ^3LE levels.[41] In particular, two cases can be distinguished. If the energy levels of the involved states overlap ($^1CT \approx {}^3CT \approx {}^3LE$), an optimal situation is created, where both SOC ($^3LE \rightarrow {}^1CT$) and hyperfine coupling ($^3CT \rightarrow {}^1CT$) contribute to the RISC process.[41] When ^3LE energetically departs from ^1CT and ^3CT levels, the upconversion proceeds mainly through vibronic coupling with an energetically higher placed ^3LE state.[45] We attribute the fastest delayed emission component to the first case. The optimal energy level placement provides an exceptionally fast k_{RISC} of 2.85×10^7 s^{-1}. Such systems can possess a very small ΔE_{ST} gap, below 5 meV,[15] thus explaining the lack of apparent thermal activation in the cooling range up to 77 K. The longer lifetime decay component, on the other hand, can be attributed to the exciplex pairs, where the ^1CT level is placed below ^3LE_A and thermal activation is needed for the RISC process. The significantly higher nonradiative rate is calculated for the fastest delayed component. By assuming that the limited triplet lifetime of PCP is the main factor causing nonradiative relaxation to the ground state, this can be explained by the relative energy level placement. By assuming the level configuration, where $^1CT \approx {}^3CT \approx {}^3LE$, a significant fraction of the excited states is located on the PCP fragment, causing increased nonradiative decay. For the longer lifetime emission this is partly overcome, as excitation is mainly located on the deeper ^3CT level.

Interestingly, the prevalence of one or the other triplet upconversion mechanism can be forced by the composition of the D/A system, as shown by the analysis of PCP : 9-PhCbz mixtures composed of 1 : 2 and 2 : 1 molar ratios (Fig. S16, ESI†). Like in the case of the equimolar sample, the components were mixed in PMMA (50 wt%). Similarly to PCbz-1, PCP : 9-PhCbz (1 : 2) shows a biexponential decay with 50 ns (τ_1) and 150–250 ns (τ_2) components (Fig. S16a, ESI†). The contribution of τ_2 towards total PL is much larger and at 180 K, where the sample shows most intense emission, it reaches 80%. At the same time PCP : 9-PhCbz (2 : 1) possesses monoexponential PL decay, for which only the faster component ($\tau_1 \approx$ 50 ns) is present (Fig. S16b, ESI†). Characteristically, this delayed emission also shows no apparent temperature-induced

PL intensity maxima and lifetime changes. It can be speculated that this difference in emission properties is caused by relative PCP mass content. Since a large concentration of PCP can enable more efficient triplet exciton transfer to lower energy states through the Dexter mechanism,[46] this can aid ^3LE_A and ^1CT energy level matching. For systems where PCP molecules are more diluted the ^3LE_A level stabilization is less likely and internal conversion to lower energy ^3CT states is expected to dominate.

Emission mechanisms in covalently bound acceptor-donor dyads

TADF-active molecules featuring a covalently bound, but weakly interacting donor–acceptor pair, are known to exhibit multiple emissive mechanisms depending on the solid-state morphology.[47,48] Similar behaviour is observed for compound PCbz-1.

The photo-physical properties of PCbz-1 in the neat amorphous film and crystalline powder are outlined in Fig. 7. The comparison of UV-Vis absorption spectra in different media (Fig. 7a) reveals that in its crystalline state the compound starts to exhibit a well-resolved absorption band in the 350–550 nm range, indicating the formation of the CT state. PL measurements show a substantial emission band displacement (Fig. 7b), as PL in crystalline powder (λ_{max} = 471 nm) is notably blueshifted in comparison to the amorphous film (502 nm). In terms of Φ_{PL}, crystalline powder shows a slightly increased emission efficiency value of 0.52. As can be predicted from UV-Vis absorption data, PLE spectra affirm CT character for the crystalline form, as emission originates mainly from the direct excitation of the CT band, with the maximum at 430 nm. For the amorphous film emission proceeds through the excitation of D/A fragments, indicating the formation of an exciplex. The obtained PL decays reveal major differences in the excited state relaxation pathways (Fig. 7c). As previously discussed, the emission in the amorphous film originates from the formation of a TADF-active exciplex. In stark contrast, the crystalline form exhibits a strictly fluorescent nature, with a monoexponential PL decay, characterized with 27 ns lifetime and a radiative rate of $1.93 \times 10^7\ s^{-1}$. This radiative rate is by an order of magnitude higher than the prompt component of the TADF-active PCbz-1 exciplex and can be attributed to increased oscillator strength of the CT state in the crystalline sample. The strengthening of the D–A conjugation in this case is attributed to the conformational locking of the molecular fragments due to the lattice hardening in crystals. A deliberate conformational locking is a well-known strategy for induction of the CT state in otherwise weakly conjugated fluorophores.[49] Because no ISC to the triplet state takes place for the crystalline form, it shows a higher Φ_{PL} value despite the ^1CT energy level being well above the PCP triplet.

By assuming similar crystal packing patterns for PCbz(1–3), the acquired single crystal X-ray structure of PCbz-2 gives indication for the existence of two distinctive emissive forms. The intermolecular distance between donor and acceptor moieties in the crystal is 6.78 Å (Fig. S2c, ESI†). For a typical TADF-active exciplex system the distance between D and A molecules below 5 Å is expected.[16] For the neat amorphous sample the

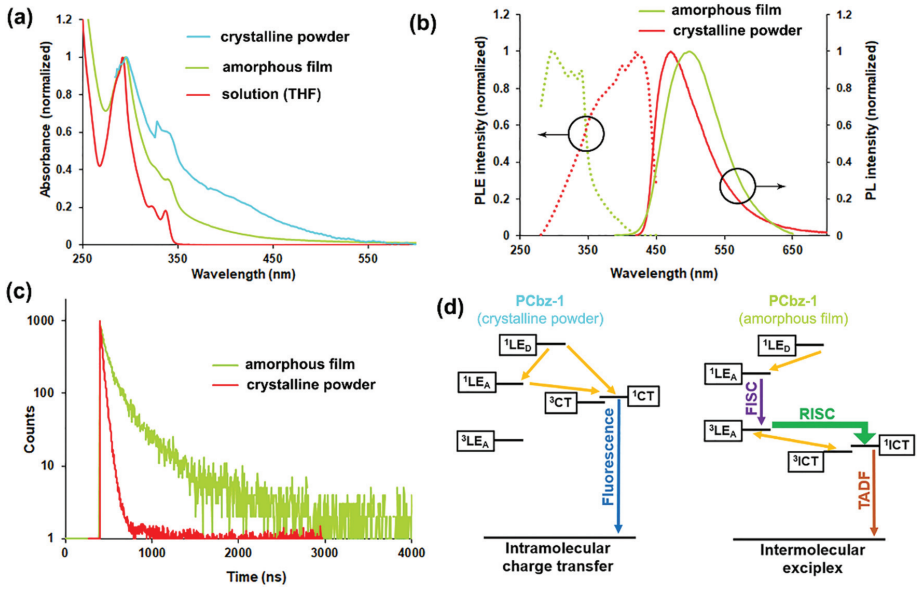

Fig. 7 (a) UV-Vis absorption spectra of PCbz-1 in different media. (b) PLE and PL spectra of different solid-state forms of PCbz-1. (c) PL decays of different solid state forms of PCbz-1. (d) Proposed mechanisms for emission processes.

emission is expected to arise from the intermolecular ^{1}ICT state, which forms due to more closely situated (<5 Å) donor and acceptor pairs of neighbouring molecules.[47] Because the energy of the ^{1}ICT state in exciplexes becomes more stabilized, as the distance between components decreases,[41,50] the ΔE_{ST} gap between ^{1}CT and ^{3}LE levels becomes small enough for enabling TADF. Since the ^{1}ICT state cannot be directly excited, the emission mechanism proceeds through the FISC-assisted pathway (Fig. 7d).

Electronic properties of exciplex systems

To evaluate the practical application viability, charge transporting properties and OLED performance were investigated for the acquired exciplex systems. Because of higher Φ_{PL} values and easier device preparation compounds PCbz(1–3) were chosen for the studies. Charge-transporting properties in vacuum deposited layers of PCbz(1–3) were examined by the time of flight (TOF) method (Fig. 8a and Fig. S17, Table S3, ESI†). Bipolar charge transport with relatively strong dispersity was observed, with the electron and hole mobilities exceeding 10^{-4} cm^2 V^{-1} s^{-1} at high electric fields. The balanced charge transportation together with triplet harvesting ability marks the investigated compounds as promising candidates for applications in organic optoelectronic devices. Though, the observed thermal PL quenching for the investigated compounds makes them more suited for the role of charge-transporting host materials.

Exciplex-based hosts can be exploited to obtain OLEDs with the power efficiency higher than 100 lm W^{-1} due to the pn-active heterojunction.[51] However, it is difficult to deposit three-component light emitting layers due to the issues with the compound concentration control. This can be overcome by the use of covalently bound exciplex-forming materials. Accordingly, compound PCbz-3 with the best charge mobilities was applied as an exciplex-based host for the green TADF emitter 4,6-di(9,9-dimethylacridan-10-yl)isophthalonitrile (DAcIPN). PCbz-3 with the HOMO (−5.97 eV) and LUMO (−3.19 eV) is an energetically suitable charge transporting material for DAcIPN: HOMO (−5.65 eV) and LUMO (−3.3 eV).[52] Using the light-emitting layer DAcIPN(x wt%):PCbz-3, where x was 5, 10 or 20 wt%, respectively, the devices A1, B1, and C1 were fabricated with structure ITO/HAT-CN(10 nm)/NPB(40 nm)/mCP(4 nm)/DAcIPN(x wt%):PCbz-3 (24 nm)/TSPO1(4 nm)/TPBi(40 nm)/LiF:Al. The commercially available compounds hexaazatriphenylenehexacarbonitrile (HATCN), *N*,*N*′-di(1-naphthyl)-*N*,*N*′-diphenyl-(1,1′-biphenyl)-4,4′-diamine (NPB), 1,3-bis(9-carbazolyl)benzene (mCP), diphenyl-4-triphenylsilyl-phenylphosphineoxide (TSPO1) and 1,3,5-tris(1-phenyl-1*H*-benzimidazol-2-yl)benzene (TPBi) were used as the functional materials. Selection of conventional hole-injecting (HAT-CN), hole-transporting (NPB), exciton-blocking (mCP and TSPO1), electron-transporting (TPBi), and electron-injecting (LiF) layers allowed the containment of the hole-electron recombination zone within the light-emitting layer. The maximum brightness

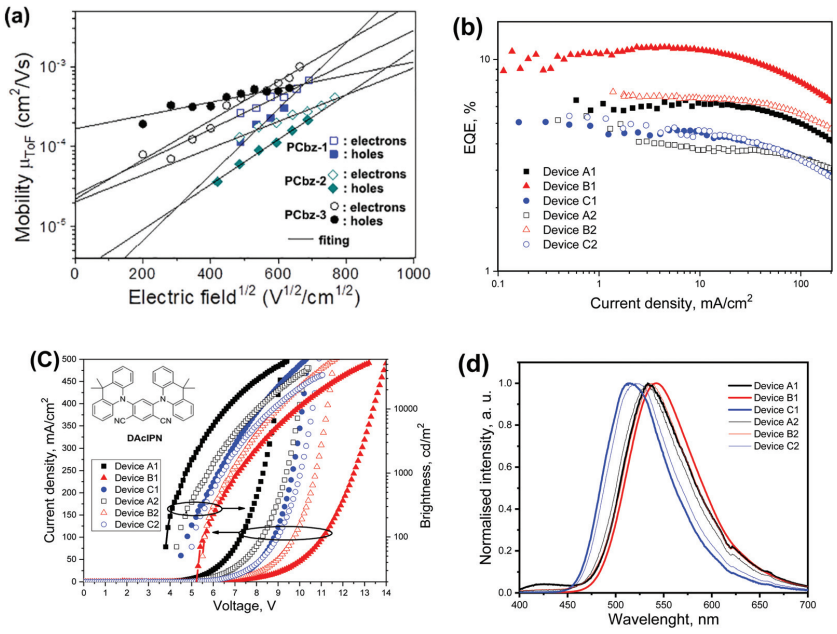

Fig. 8 (a) Hole and electron mobilities *versus* electric fields for the layers of PCbz(1–3), (b) plots of EQE *versus* current density, (c) current density and brightness *versus* voltage (inset: Chemical structure of DAcIPN), and (d) EL spectra recorded at 7 V.

exceeding 50 000 cd m^{-2} and the maximum external quantum efficiency (EQE) of 11.6% with low roll-off efficiency were obtained for device B1, demonstrating the potential of the host PCbz-3 (Fig. 8b and c).

Complete host–guest energy transfer was achieved in devices B1 and C1 (Fig. 8d). The measured EL spectra fully originated from DAcIPN and the emission was stable with an increase of electric field (Fig. 8d and Fig. S18, ESI†). In contrast, the low-intensity emission band was observed in the range of 410–450 nm in EL spectra of device A1 indicating that the energy transfer from PCbz-3 to DAcIPN did not completely occur at low concentration (5 wt%) of the emitter in the light-emitting layer. This observation can apparently be attributed to the lower EQEs of device A1 in comparison to those of device C1 and the previously reported device with the emitting layer of the molecular dispersion of DAcIPN (5 wt%) in TCz1.[52]

It should be noted that the EL spectrum of device C1 was blue shifted in comparison to the EL spectra of devices A1 and B1. The blue shift resulted from complicated aggregation effects of emitter DAcIPN which were discussed elsewhere (Fig. 8d and Fig. S18, ESI†).[52] Due to the aggregation effects of DAcIPN, slight blue-shifts can be recognized in the EL spectra of the fabricated devices compared to the PL spectra of the corresponding vacuum deposited light-emitting layers (Fig. S19, ESI†). The concentration of DAcIPN also has a considerable effect on the charge-transporting properties of the light-emitting layer of DAcIPN:PCbz-3, resulting in different turn-on voltages of devices A1, B1 and C1 (3.9, 4.6, and 5.3 V, respectively) despite the same device structure being used (Fig. 8c). The similar trends were observed for the output characteristics of devices A2, B2 and C2, for which slightly thinner emitting layers were used (20 *vs.* 24 nm) (Fig. 8b–d). Lower EQEs of devices A2, B2 and C2 than those of devices A1, B1 and C1 can be attributed to different charge transport balance and alternating distribution of exciton recombination zones within the light-emitting layers. Such differences are caused by the strong sensitivity of emitter DAcIPN to the hosting media.[44] It is important to note that OLEDs containing host PCbz-3 showed higher EQEs (5.4% for device C1 and 5.1% for device C2) than previously published devices based on the known hosts TCz1, mCP, and bis[2-(diphenylphosphino)phenyl] ether oxide (DPEPO) (4.8, 2, and 2.8%, respectively).[52] This result proves the potential of the reported intermolecular exciplex-forming compounds as OLED host materials.

Conclusions

We have successfully demonstrated that molecules possessing fast intersystem crossing ability can be purposely used as building blocks for TADF exciplex systems. The ability to contain the excitation on ^3LE_A state forces an optimal RISC pathway, in such a way that the emission lifetime is reduced to a sub-microsecond level. The apparent drawback for the examined exciplex systems is the observed heat-induced decrease in emission efficiency. This effect is caused by the short room-temperature triplet lifetime of the chosen purine acceptor. To overcome this, alternative organic molecules with fast ISC can be proposed from the large variety of known room-temperature phosphorescent compounds with long-lived triplet states.[53–56] We believe that our approach can be used to enable a novel rational design guided strategy towards efficient emissive TADF materials for their use in OLEDs both as emitters and host materials.

Conflicts of interest

There are no conflicts of interest to declare.

Acknowledgements

This work is supported by the ERDF 1.1.1.1. activity project No 1.1.1.1/16/A/131. M. G. and D. V. acknowledge the Research Council of Lithuania (''PolyTADFer'', No. P-LLT-19-14). Support for the research was also provided by the Institute of Solid State Physics, University of Latvia as the Center of Excellence which has received funding from the European Union's Horizon 2020 Framework Programme H2020-WIDESPREAD-01-2016-2017-Teaming Phase 2 under grant agreement No. 739508, project CAMART^2.

References

1 H.-W. Chen, J.-H. Lee, B.-Y. Lin, S. Chen and S.-T. Wu, *Light Sci. Appl.*, 2018, **7**, 17168.
2 J.-H. Jou, S. Sahoo, D. K. Dubey, R. A. K. Yadav, S. S. Swayamprabha and S. D. Chavhan, *J. Mater. Chem. C*, 2018, **6**, 11492–11518.
3 H. Yersin, A. F. Rausch, R. Czerwieniec, T. Hofbeck and T. Fischer, *Coord. Chem. Rev.*, 2011, **255**, 2622–2652.
4 Q. Zhang, B. Li, S. Huang, H. Nomura, H. Tanaka and C. Adachi, *Nat. Photonics*, 2014, **8**, 326–332.
5 Q. Zhang, D. Tsang, H. Kuwabara, Y. Hatae, B. Li, T. Takahashi, S. Y. Lee, T. Yasuda and C. Adachi, *Adv. Mater.*, 2015, **27**, 2096–2100.
6 Z. Yang, Z. Mao, Z. Xie, Y. Zhang, S. Liu, J. Zhao, J. Xu, Z. Chi and M. P. Aldred, *Chem. Soc. Rev.*, 2017, **46**, 915–1016.
7 T. J. Penfold, F. B. Dias and A. P. Monkman, *Chem. Commun.*, 2018, **54**, 3926–3935.
8 A. Köhler and D. Beljonne, *Adv. Funct. Mater.*, 2004, **14**, 11–18.
9 M. Y. Wong and E. Zysman-Colman, *Adv. Mater.*, 2017, **29**, 1605444.
10 Y. Liu, C. Li, Z. Ren, S. Yan and M. R. Bryce, *Nat. Rev. Mater.*, 2018, **3**, 18020.
11 M. Godumala, S. Choi, M. J. Cho and D. H. Choi, *J. Mater. Chem. C*, 2019, **7**, 2172–2198.
12 K. Goushi, K. Yoshida, K. Sato and C. Adachi, *Nat. Photonics*, 2012, **6**, 253–258.
13 X.-K. Liu, Z. Chen, C.-J. Zheng, C.-L. Liu, C.-S. Lee, F. Li, X.-M. Ou and X.-H. Zhang, *Adv. Mater.*, 2015, **27**, 2378–2383.

14 M. Chapran, P. Pander, M. Vasylieva, G. Wiosna-Salyga, J. Ulanski, F. B. Dias and P. Data, *ACS Appl. Mater. Interfaces*, 2019, **11**, 13460–13471.
15 D. Graves, V. Jankus, F. B. Dias and A. Monkman, *Adv. Funct. Mater.*, 2014, **24**, 2343–2351.
16 T.-C. Lin, M. Sarma, Y.-T. Chen, S.-H. Liu, K.-T. Lin, P.-Y. Chiang, W.-T. Chuang, Y.-C. Liu, H.-F. Hsu, W.-Y. Hung, W.-C. Tang, K.-T. Wong and P.-T. Chou, *Nat. Commun.*, 2018, **9**, 3111.
17 in *The Exciplex*, ed. M. Gordon and W. Ware, Academic Press, New York, 1975.
18 M. Cocchi, D. Virgili, C. Sabatini and J. Kalinowski, *Chem. Phys. Lett.*, 2006, **421**, 351–355.
19 X.-K. Chen, D. Kim and J.-L. Brédas, *Acc. Chem. Res.*, 2018, **51**, 2215–2224.
20 P. L. dos Santos, F. B. Dias and A. P. Monkman, *J. Phys. Chem. C*, 2016, **120**, 18259–18267.
21 M. Colella, A. Danos and A. P. Monkman, *J. Phys. Chem. Lett.*, 2019, **10**, 793–798.
22 J. Adachi, H. Kakizoe, P. K. D. Tsang and A. Endo, *SID Symp. Dig. Tech. Pap.*, 2019, **50**, 95–98.
23 C. E. Crespo-Hernández, L. Martínez-Fernández, C. Rauer, C. Reichardt, S. Mai, M. Pollum, P. Marquetand, L. González and I. Corral, *J. Am. Chem. Soc.*, 2015, **137**, 4368–4381.
24 D. H. Murgida, G. M. Bilmes and R. Erra-Balsells, *Photochem. Photobiol.*, 1996, **64**, 777–784.
25 E. Quinones and R. Arce, *J. Am. Chem. Soc.*, 1989, **111**, 8218–8223.
26 E. F. Gomez, V. Venkatraman, J. G. Grote and A. J. Steckl, *Adv. Mater.*, 2015, **27**, 7552–7562.
27 M. A. El-Sayed, *J. Chem. Phys.*, 1963, **38**, 2834–2838.
28 A. Casey, S. D. Dimitrov, P. Shakya-Tuladhar, Z. Fei, M. Nguyen, Y. Han, T. D. Anthopoulos, J. R. Durrant and M. Heeney, *Chem. Mater.*, 2016, **28**, 5110–5120.
29 F. Neese, *Wiley Interdiscip. Rev.: Comput. Mol. Sci.*, 2018, **1**, e1327.
30 S. Shahnawaz, S. Sudheendran Swayamprabha, M. R. Nagar, R. A. K. Yadav, S. Gull, D. K. Dubey and J.-H. Jou, *J. Mater. Chem. C*, 2019, **7**, 7144–7158.
31 J.-A. Lin, S.-W. Li, Z.-Y. Liu, D.-G. Chen, C.-Y. Huang, Y.-C. Wei, Y.-Y. Chen, Z.-H. Tsai, C.-Y. Lo, W.-Y. Hung, K.-T. Wong and P.-T. Chou, *Chem. Mater.*, 2019, **31**, 5981–5992.
32 K.-L. Woon, C.-L. Yi, K.-C. Pan, M. K. Etherington, C.-C. Wu, K.-T. Wong and A. P. Monkman, *J. Phys. Chem. C*, 2019, **123**, 12400–12410.
33 M. Auffray, U. Balijapalli, J.-C. Ribierre, Y. Tsuchiya and C. Adachi, *Chem. Lett.*, 2020, **49**, 932–935.
34 S. A. Jenekhe and J. A. Osaheni, *Science*, 1994, **265**, 765–768.
35 M. Y. Berezin and S. Achilefu, *Chem. Rev.*, 2010, **110**, 2641–2684.
36 M. Chapran, R. Lytvyn, C. Begel, G. Wiosna-Salyga, J. Ulanski, M. Vasylieva, D. Volyniuk, P. Data and J. V. Grazulevicius, *Dyes Pigm.*, 2019, **162**, 872–882.
37 X. Qiao and D. Ma, *Mater. Sci. Eng., R*, 2020, **139**, 100519.
38 H. Uoyama, K. Goushi, K. Shizu, H. Nomura and C. Adachi, *Nature*, 2012, **492**, 234–238.
39 J. U. Kim, I. S. Park, C.-Y. Chan, M. Tanaka, Y. Tsuchiya, H. Nakanotani and C. Adachi, *Nat. Commun.*, 2020, **11**, 1765.
40 K.-H. Kim, S.-J. Yoo and J.-J. Kim, *Chem. Mater.*, 2016, **28**, 1936–1941.
41 C.-K. Moon, J.-S. Huh, J.-M. Kim and J.-J. Kim, *Chem. Mater.*, 2018, **30**, 5648–5654.
42 H. Tsujimoto, D.-G. Ha, G. Markopoulos, H. S. Chae, M. A. Baldo and T. M. Swager, *J. Am. Chem. Soc.*, 2017, **139**, 4894–4900.
43 S. Shao, J. Hu, X. Wang, L. Wang, X. Jing and F. Wang, *J. Am. Chem. Soc.*, 2017, **139**, 17739–17742.
44 F. B. Dias, T. J. Penfold and A. P. Monkman, *Methods Appl. Fluoresc.*, 2017, **5**, 012001.
45 J. Gibson, A. P. Monkman and T. J. Penfold, *ChemPhysChem*, 2016, **17**, 2956–2961.
46 O. V. Mikhnenko, P. W. M. Blom and T.-Q. Nguyen, *Energy Environ. Sci.*, 2015, **8**, 1867–1888.
47 R. Skaisgiris, T. Serevičius, K. Kazlauskas, Y. Geng, C. Adachi and S. Juršėnas, *J. Mater. Chem. C*, 2019, **7**, 12601–12609.
48 D. Zhang, K. Suzuki, X. Song, Y. Wada, S. Kubo, L. Duan and H. Kaji, *ACS Appl. Mater. Interfaces*, 2019, **11**, 7192–7198.
49 X. Tang, L.-S. Cui, H.-C. Li, A. J. Gillett, F. Auras, Y.-K. Qu, C. Zhong, S. T. E. Jones, Z.-Q. Jiang, R. H. Friend and L.-S. Liao, *Nat. Mater.*, 2020, **19**, 1332–1338.
50 Y. Wada, H. Nakagawa, S. Matsumoto, Y. Wakisaka and H. Kaji, *Nat. Photonics*, 2020, **14**, 643–649.
51 D. Chen, K. Liu, L. Gan, M. Liu, K. Gao, G. Xie, Y. Ma, Y. Cao and S.-J. Su, *Adv. Mater.*, 2016, **28**, 6758–6765.
52 E. Skuodis, O. Bezvikonnyi, A. Tomkeviciene, D. Volyniuk, V. Mimaite, A. Lazauskas, A. Bucinskas, R. Keruckiene, G. Sini and J. V. Grazulevicius, *Org. Electron.*, 2018, **63**, 29–40.
53 S. Hirata, *Adv. Opt. Mater.*, 2017, **5**, 1700116.
54 Kenry, C. Chen and B. Liu, *Nat. Commun.*, 2019, **10**, 2111.
55 L. Xiao and H. Fu, *Chem. – Eur. J.*, 2019, **25**, 714–723.
56 M. Hayduk, S. Riebe and J. Voskuhl, *Chem. – Eur. J.*, 2018, **24**, 12221–12230.

4. pielikums
Appendix IV

Sebris, A.; Novosjolova, I.; Traskovskis, K.; Kokars, V.; Tetervenoka, N.; Vembris, A.; Turks, M.

Photophysical and Electrical Properties of Highly Luminescent 2/6-Triazolyl-Substituted Push–Pull Purines

ACS Omega **2022**, *7*, 5242.

doi: 10.1021/acsomega.1c06359

ACS OMEGA

http://pubs.acs.org/journal/acsodf

Article

Photophysical and Electrical Properties of Highly Luminescent 2/6-Triazolyl-Substituted Push−Pull Purines

Armands Sebris, Irina Novosjolova,* Kaspars Traskovskis,* Valdis Kokars, Natalija Tetervenoka, Aivars Vembris, and Māris Turks*

Cite This: *ACS Omega* 2022, 7, 5242−5253

Read Online

ACCESS | Metrics & More | Article Recommendations | Supporting Information

ABSTRACT: New push−pull *N*(9)-alkylated 6-piperidino-2-triazolylpurine and 2-piperidino-6-triazolylpurine derivatives are synthesized, and their optical and optoelectronic properties are comprehensively characterized with experimental and computational methods. The compounds possess intense violet or blue fluorescence with fluorescence quantum yields of up to 91% in solution and 40% in host-free films. Depending on their structural composition, the compounds have ionization energy in the range of 5.25−6.04 eV, electron affinity of 2.18−3.15 eV, and triplet energy of 2.52−2.95 eV. Due to the presence of hole-transporting purine and electron-transporting triazole fragments, compounds exhibit bipolar charge-transportation ability. Despite the favorable emissive properties of the studied push−pull purines, their electroluminescence in thin films is quenched owing to large current densities that are present even at a moderate driving voltage. This marks application directions related to a predominantly charge-transportation functionality as the most suitable for this compound class.

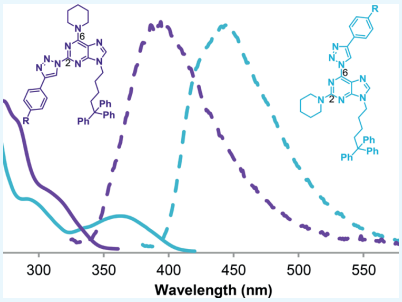

INTRODUCTION

DNA nucleobases have been successfully incorporated in electron-blocking or hole-transporting layers of organic light-emitting diodes (OLEDs) due to their large band gap (E_g) values and suitable energy levels.[1,2] Additionally, carbazole-functionalized DNA has been used as a charge-transporting co-host material in the active emissive layer (EML), consequently showing performance improvements in comparison to some conventional host materials.[3] Nucleobases or their derivatives have also been used in organic field-effect transistors (OFETs), mainly as the dielectrics.[4,5]

Recent studies have shown that chemical modifications of one of the nucleobase cores, the purine heterocycle, by an introduction of electron donor and acceptor fragments, provide highly emissive push−pull-type compounds, whose fluorescence (FL) quantum yield (Φ_{FL}) can reach unity.[6−11] While the fluorescent nature of these compounds limits the potentially attainable efficiency of the corresponding purine-based OLEDs, singlet harvesting compounds still find a practical use in blue light-emitting devices due to the poor chemical stability of the triplet harvesting alternatives.[12] Several early reports of OLEDs showing electroluminescence in the important deep-blue and violet parts of the spectrum have been demonstrated using purine-based emitters.[13,14] In addition, it was recently reported that 9-methylpurine-based derivatives containing phenoxazine groups in the para-position of the phenyl substituent at C6 or C2 and C6 positions of purine possess thermally activated delayed fluorescence, further underlining the potential prospects of the compound class for the application in organic electronic devices.[15] On the other hand, purine derivatives containing phenoxazine or phenothiazine groups in the meta-position of the phenyl substituent synthesized by us reached only up to 15% quantum yields in PMMA-based films.[16]

In 2021, we designed TADF-active exciplexes based on 6-cyano-9-phenylpurine-carbazole dyads, studied their photophysical properties in the solution, film, and crystalline phase and successfully used them as host materials for the emissive layer in OLEDs.[17] In this paper, we investigate the practical application feasibility and possible limitations of fluorescent push−pull purines containing triazolyl moieties, focusing on the compound integration in solution-processed films with electroluminescent or charge-transporting functionality and studying the optical and optoelectronic properties of synthesized purine derivatives. A series of *N*(9)-alkylated 6(or 2)-piperidino-2(or 6)-triazolylpurine push−pull-type molecules were acquired for the purpose of the study. The photophysical and thermal properties of the compounds and their energy level configuration were experimentally determined. The experimental data were supplemented with quantum-chemical calculations. The

Received: November 11, 2021
Accepted: January 13, 2022
Published: February 2, 2022

https://doi.org/10.1021/acsomega.1c06359
ACS Omega 2022, 7, 5242−5253

Scheme 1. General Synthetic Routes for the Synthesis of Triazolylpurines 5a−d and 9a−d

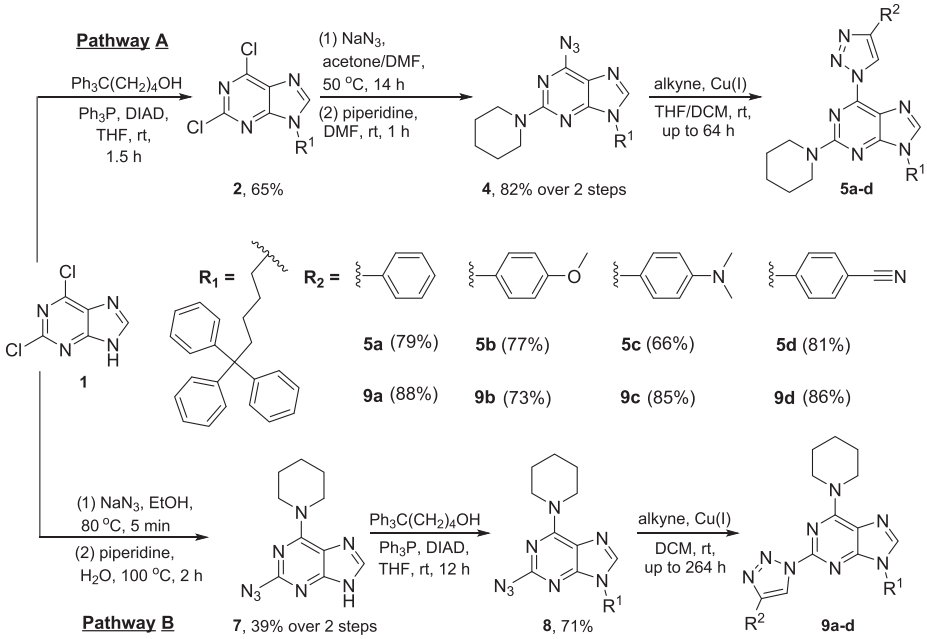

results indicate that the compounds exhibit excellent charge-transporting ability, which is detrimental to the electroluminescence process but can be potentially exploited in purely charge-transportation-related areas of organic electronics.

RESULTS AND DISCUSSION

Material Design and Synthesis. The newly synthesized materials were based on a known highly emissive molecular scaffold,[18−23] where 2- or 6-amino-substituted purines are functionalized with electron-deficient 1,2,3-triazole moieties at the corresponding unoccupied 2- or 6-position. It has been shown that natural 2- or 6-amino-substituted purine derivatives, guanine and adenine, possess good hole-transporting ability.[1] The presence of 1,2,3-triazole moieties, on the other hand, is shown to enhance the electron transport properties of the molecule.[24] It was predicted that the suggested bipolar composition of the target molecules would facilitate balanced charge-transporting properties. To better understand correlations between the structure and photophysical properties of the compounds, differently substituted phenyl groups were attached to the triazole cycle. The poor solubility and inherent crystallinity of the corresponding purine derivatives were overcome with the introduction of 5,5,5-triphenylpentyl groups. Triphenylmethane-based derivatives are known to promote amorphous phase formation for otherwise crystalline polar molecules.[25]

For the synthesis of the desired compounds, we used two different approaches (Pathway A and B), yielding compound series **5a−d** and **9a−d** (Scheme 1). The commercially available 2,6-dichloropurine **1** was used as the starting material. For the synthesis of compound **5**, first, we introduced a triphenylpentyl group at the *N*(9) position of purine using DIAD, Ph_3P, and corresponding alcohol under the Mitsunobu conditions.[26,27] Then, we substituted chlorine atoms at C(2) and C(6) positions with azido groups and next introduced piperidine as a donating group. For *N*(9)-alkylated substrates, substitution with piperidine took place at the C(2) position and subsequently the triazolyl ring was introduced at the C(6) position via Cu(I)-catalyzed cycloaddition reactions with different alkynes. Previously reported methods have been used for the copper-(I)-catalyzed alkyne-azide cycloaddition (CuAAC) reactions to produce triazole moieties.[19,28] Products **5a−d** were obtained with 66−81% yields (Scheme 1).

On the other hand, series **9** were obtained using the same reaction conditions but in a reverse sequence (Scheme 1). First, unprotected 2,6-dichloropurine **1** was treated with NaN_3 followed by an S_NAr reaction with piperidine. In the case of *N*(9)-H 2,6-diazidopurine, the S_NAr reaction with piperidine took place regioselectively at the C(6) position, which is opposite to *N*(9)-alkylated substrates. Next, product **7** was alkylated at the *N*(9) position and products **8** were cyclized with different alkynes to target products **9a−d**. These 1,3-dipolar cycloaddition reactions required longer times compared to previous ones but still produced products **9a−d** with 73−88% yields. For example, a reaction with 4-dimethylaminophenylacetylene required 264 hours to be completed. An increase of the temperature to accelerate the cycloaddition was impossible due to the instability of azido starting materials. Moreover, all of the steps, where the azido group was involved, were performed while being covered from the day light. All azido compounds (**4**, **7**, **8**) should be stored at temperature ≤ -20 °C to prevent degradation.

Phase Behavior and Thermal Characteristics. With the introduction of triphenylpentyl groups that enhance solubility and promote the formation of an amorphous phase, the synthesized compounds were primarily designed as being suitable for solution-based processing methods. The resulting purine derivatives are highly soluble in moderate polarity

https://doi.org/10.1021/acsomega.1c06359
ACS Omega 2022, 7, 5242−5253

solvents ($CHCl_3$, DCM, THF) and form amorphous films upon spin-coating from the corresponding solutions. To closely investigate the solid-state phase behavior, the selected compounds **5a**, **5d**, **9a**, **9b**, and **9d** were studied by employing differential scanning calorimetry (DSC). From this series, only compound **9d** showed the presence of a crystalline state upon the first heating cycle (melting temperature 176.0 °C). In the case of other compounds, glass transition temperature (T_g) was detected as the only phase transition. DSC plots of the second heating cycle for the purine derivatives are given in Figure 1. The

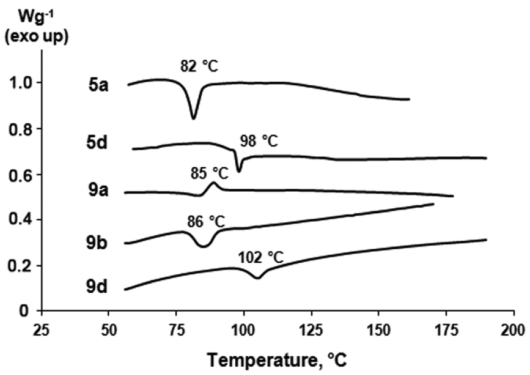

Figure 1. DSC plots during the second heating for selected push−pull purine derivatives.

obtained T_g values vary in the range of 82−102 °C. These parameters are sufficient to ensure the structural integrity and to prevent phase transition processes in optoelectronic devices under typical device operation conditions. For comparison, T_g of a conventional charge-transporting host material as 4,4′-bis(*N*-carbazolyl)-1,1′-biphenyl (CBP) is 62 °C.[29] Structural correlations among the series of the synthesized compounds reveal that T_g increase in the range of 13−20 °C can be linked with the presence of the cyanophenyl group (compounds **5d**, **9d**). As it is indicated by DFT calculations, which evaluate the ground state dipole moment (μ) values of **5d** and **9d** at μ = 11.9 and 10.5 D (Table S1), these molecules are the most polar among the examined series. Further discussion concerning molecular orbital placement relates this to an increased spatial separation of electron-rich and poor regions of the molecules. Since μ can be associated with a strong amplification in the force of solid-state intermolecular interactions,[30] the consequential rigidification of the glassy lattice manifests in increased T_g for **5d** and **9d**. The same explanation can be given for the outlier crystallization tendency for compound **9d**, which is also caused by the high polarity of the compound.

The presence of *N*-heterocyclic molecular fragments has often been linked to a reduced thermal and chemical stability of the corresponding molecules.[31,32] Thermogravimetric analysis was performed to evaluate the thermal stability of the compounds **5d** and **9d** (Figure S1). The results show that both the molecules possess good thermal stability with the corresponding decomposition temperatures of 298 and 258 °C. A notable increase in stability can be observed for a purine derivative with a 2-amino-6-triazolyl substitution pattern in comparison to a 2-triazolyl-6-amino counterpart.

Photophysical Characterization. The synthesized materials were initially characterized employing UV−vis absorption and photoluminescence (PL) spectroscopy. The obtained absorption and emission bands are given in Figure 2, and band maxima values are outlined in Table 1. Taking into account the structural impact on the photophysical properties, the placement of substituents at the purine ring in either 2-amino-6-triazolyl (series **5**) or 2-triazolyl-6-amino (series **9**) arrangement has the most notable impact on electronic transitions. In the case of **5**, UV−vis absorption spectra feature intense bands in the 250−300 nm range that can be attributed predominantly to the local excitation (LE) of the purine aromatic system.[33,34] The lowest energy bands with maxima at 360−367 nm, on the other hand, correspond to intramolecular charge-transfer (ICT) transitions. The FL spectra of **5** exhibit wide featureless emission bands in the blue spectral region (maxima at 439−448 nm). Considering the aromatic substituents at the 1,2,3-triazole ring, only the introduction of *N*,*N*-dimethylaniline (**5c**) causes a notable deviation in emissive properties, redshifting the FL band by approximately 60 nm. We relate this observation to a stronger solvatochromic response of the compound and the resulting stabilization of the excited state energy level. This is presumably caused by the presence of nitrogen lone pair, which may enhance specific solute−solvent interactions, such as hydrogen bonding.[35] Because of this, dialkyl substituted amines are common structural fragments met in strongly solvatochromic dyes.[36] Φ_{FL} values for **5** vary in the range of 0.74−0.91 in solution. Generally, the introduction of electron-donating groups at 1,2,3-triazole can be associated with reduced Φ_{FL}. In spin-coated amorphous films, the compounds retain fairly large emission efficiency (Φ_{FL} = 0.40−0.28), indicating a moderate extent of solid-state quenching,[37,38] with the exception of **5c**, which shows a dramatic emission efficiency drop to 0.03.

For the 2-triazolyl-6-amino purine series (**9a**−**d**), the lowest energy absorption and FL bands show a substantial hypsochromic shift in comparison to the structural analogues from the 6-triazolyl-2-amino purine series (**5a**−**d**). ICT absorption bands ($\lambda_{abs\ max}$ 300−305 nm) now partly overlap with LE transitions, while emission has shifted to the violet part of the spectrum ($\lambda_{em\ max}$ 388−455 nm). Analogous to the previously observed behavior, only the introduction of the *N*,*N*-dimethylaniline fragment to the 1,2,3-triazole moiety causes a notable redshift of absorption and FL bands. Φ_{FL} values in solution for **9a**−**d** (0.17−0.44) are notably lower than those measured for **5**. On the other hand, in amorphous films, series **9** show a relatively lesser FL efficiency drop (0.15−0.22), with the exception of *N*,*N*-dimethylaniline-substituted **9c**.

All compounds show monoexponential emission decay curves, associable with a fluorescence process (Figure S2). Lifetime values vary in the range of 11−13 ns for series **5**, while for compounds **9**, the emissive relaxation to the ground state proceeds substantially faster, in the range of 2−8 ns (Table 1). The corresponding radiative (k_r) and nonradiative (k_{nr}) decay rates (Table S2) indicate that k_r is somewhat comparable among all compounds, but k_{nr} is notably increased for series **9**. It is worth noting that the FL lifetime of the compounds is longer than typical values for purine-based emitters.[6] As shown by Collier et al., the emission rate in such emitters decreases as the π-conjugation system of the emitter expands and the charge-transfer process is not confined to the purine moiety but assumes an intramolecular charge-transfer character.[9] A similar situation is observed for our compounds, where the emissive process involves charge transfer between different aromatic fragments.

All of the studied compounds show a positive solvatochromic response for FL bands, without notable band shape trans-

https://doi.org/10.1021/acsomega.1c06359
ACS Omega 2022, 7, 5242−5253

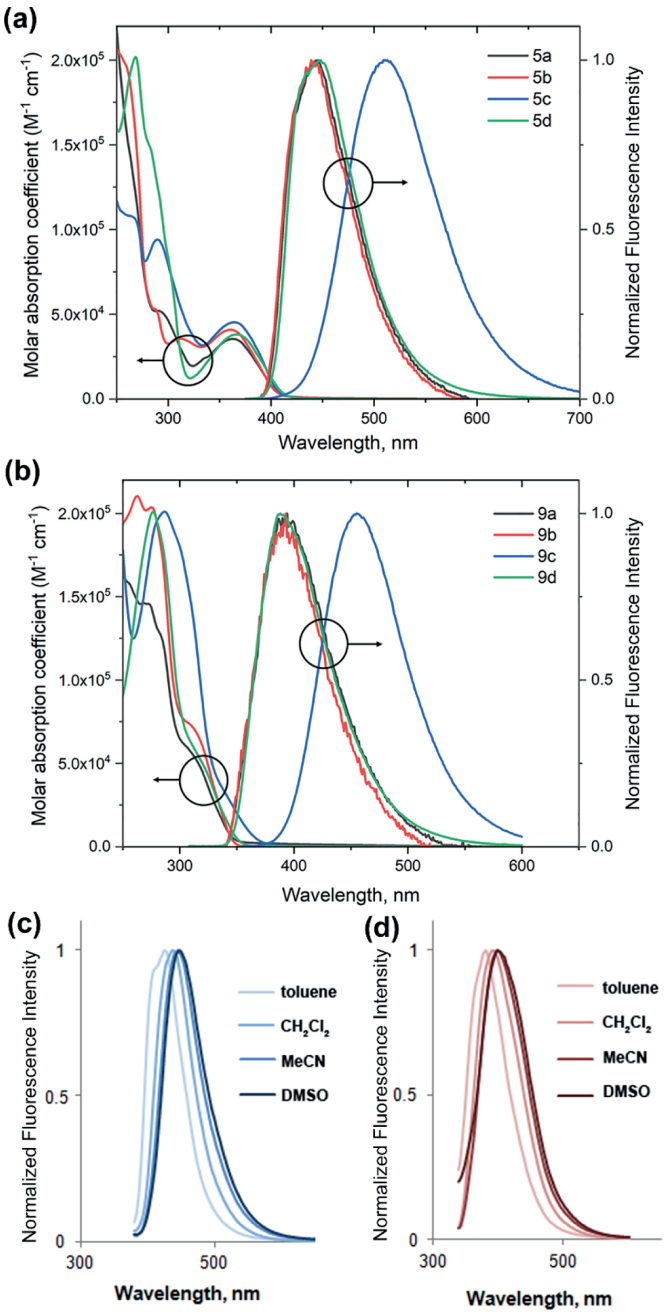

Figure 2. Absorption and emission spectra for compound series **5** (a) and **9** (b) measured in CH_2Cl_2. Solvatochromic response for emission bands of **5a** (c) and **9a** (d).

formations (see Figure 2c,d for the solvatochromic response of **5a** and **9a**). This indicates a dipole moment increase of the molecules upon the excitation process and points to the ICT character of the excited states.[36]

Characterization of Electronic Levels. The configuration of electronic levels for optoelectronic materials determines whether compounds are compatible with an incorporated emitter, host material, or neighboring layers of the charge-transporting materials or electrodes. The electronic levels in thin

https://doi.org/10.1021/acsomega.1c06359
ACS Omega 2022, 7, 5242−5253

Table 1. Experimental and Calculated Photophysical Parameters and Energy Levels for Compounds 5a−5d and 9a−9d

	experimental								calculations			
compound	$\lambda_{abs.ma}$, nm[a]	$\lambda_{em.\ max}$, nm[a]	Φ_{PL}[b]	τ, ns[a]	E_T, eV[c]	I_E, eV[d]	A_E, eV[e]	E_{th}, eV[f]	HOMO, eV	LUMO, eV	ΔE_{S0-S1}, eV[g]	ΔE_{S0-T1}, eV[h]
5a	364	446	0.91/0.32	13	2.53	5.80	2.85	2.95	−5.61	−1.63	3.57	2.75
5b	360	439	0.78/0.28	11	2.54	5.86	3.07	2.79	−5.45	−1.56	3.51	2.76
5c	365	511	0.74/0.03	12	2.52	5.25	2.47	2.78	−4.86	−1.45	3.06	2.61
5d	367	448	0.90/0.40	12	2.54	5.90	3.15	2.75	−5.79	−1.96	3.42	2.69
9a	320	394	0.31/0.22	3.6	2.93	5.76	2.31	3.45	−5.73	−1.23	4.09	3.19
9b	320	399	0.17/0.15	2.0	2.95	5.85	2.59	3.26	−5.41	−1.16	3.87	3.08
9c	330	455	0.30/0.03	7.9	2.75	5.25	2.18	3.07	−4.86	−1.05	3.44	2.88
9d	330	388	0.44/0.20	3.9	2.87	6.04	2.89	3.15	−5.99	−1.75	3.81	3.08

[a]Measured in CH_2Cl_2. [b]Values in CH_2Cl_2 solution and films. [c]Triplet energy levels, determined in 2-MeTHF at 77 K. [d]I_E − ionization energy. [e]A_E − affinity energy. [f]E_{th} − photoconductivity threshold value. [g]Calculated lowest singlet excitation energy. [h]Calculated lowest triplet excitation energy.

spin-coated amorphous films of the synthesized compounds were determined by photoemission yield spectroscopy, to find ionization energy (I_E), and photoconductivity measurements, to determine the photoconductivity threshold value (E_{th}). The electron affinity level (E_A) was then calculated as the difference between I_E and E_{th}. The obtained values are outlined in Table 1. In agreement with the previously discussed results of photophysical characterization, the electronic level measurements confirm a clear distinction between compounds **5** and **9**. E_{th} of **5** (2.75−2.95 eV) are lower than for **9** (3.07−3.45 eV), indicating notably higher band gap values for the latter series of compounds. Several structure−property relationships can be observed. First, among the structurally comparable compound pairs that contain identical aryl substituents at the 1,2,3-triazole ring, the I_E value is almost not influenced by the attachment pattern of amino and triazole substituents at the purine ring. This energy level is only affected by the substituents at the 1,2,3-triazole-attached phenyl ring. The A_E level placement, on the other hand, is affected by both these structural variations. In general, the introduction of the *N*,*N*-dimethylaminophenyl fragment at 1,2,3-triazole causes destabilization of I_E and A_E levels. This could be explained by the resulting donor−acceptor−donor (D−A−D) type configuration of the resulting conjugated molecules that reduce delocalization energy of the push−pull system. In contrast, the presence of the electron-deficient cyanophenyl group causes stabilization of I_E and A_E, as the molecules form an extended D−A system now. The compounds that contain an electronically neutral phenyl group show the largest E_{th} values, as the lack of electron-accepting or -donating groups reduces their overall push−pull character.

The determination of triplet energy levels (E_T) is crucial for host materials that are being designed for triplet harvesting emitters. If E_T of the charge-transporting material is higher than that for the emissive compound, exothermic excited triplet state migration proceeds to the emitter. If the situation is reversed, the triplet states largely stay on the host molecules, negatively affecting the corresponding OLED efficiency.[39] E_T of the synthesized compounds was determined by employing low-temperature phosphorescence measurements in a frozen 2-methyltetrahydrofuran matrix at 77 K. Triplet energies were assigned at the highest energy phosphorescence band maxima (see Figures 3 and S3). For series **5**, E_T values vary in the range of 2.52−2.54 eV (Table 1), but for **9a**, **b**, **d**, they are 2.87−2.95 eV, with **9c** being an outlier at 2.75 eV. These values suggest that compounds **9** can be potentially used as host materials for blue-phosphorescent compounds.

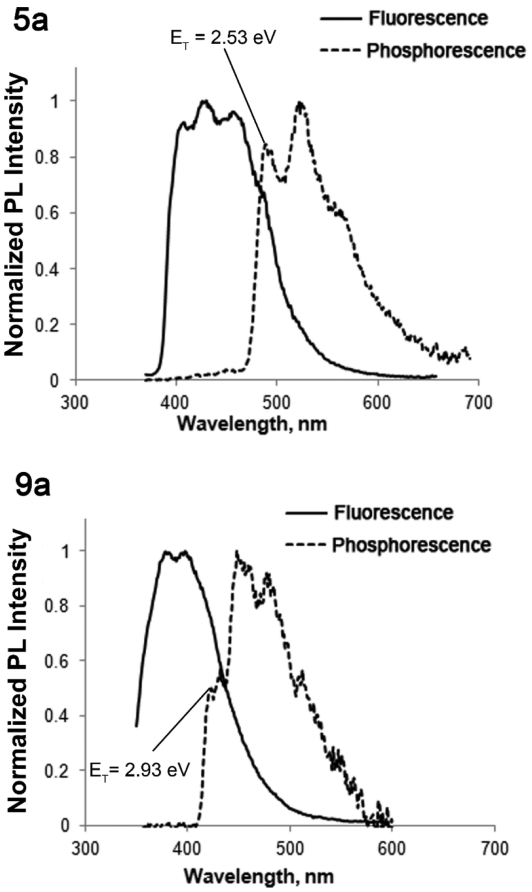

Figure 3. Fluorescence and phosphorescence spectra of **5a** and **9a** in the 2-MeTHF matrix at 77 K.

Quantum-Chemical Calculations. DFT calculations for the synthesized compounds were performed to better explain the correlations between the synthesized structures and their photophysical properties. The numerical values of the highest occupied molecular orbital (HOMO), lowest unoccupied molecular orbital (LUMO) energy levels, and singlet and triplet excitation energies are outlined in Table 1, but the visualizations

https://doi.org/10.1021/acsomega.1c06359
ACS Omega 2022, 7, 5242−5253

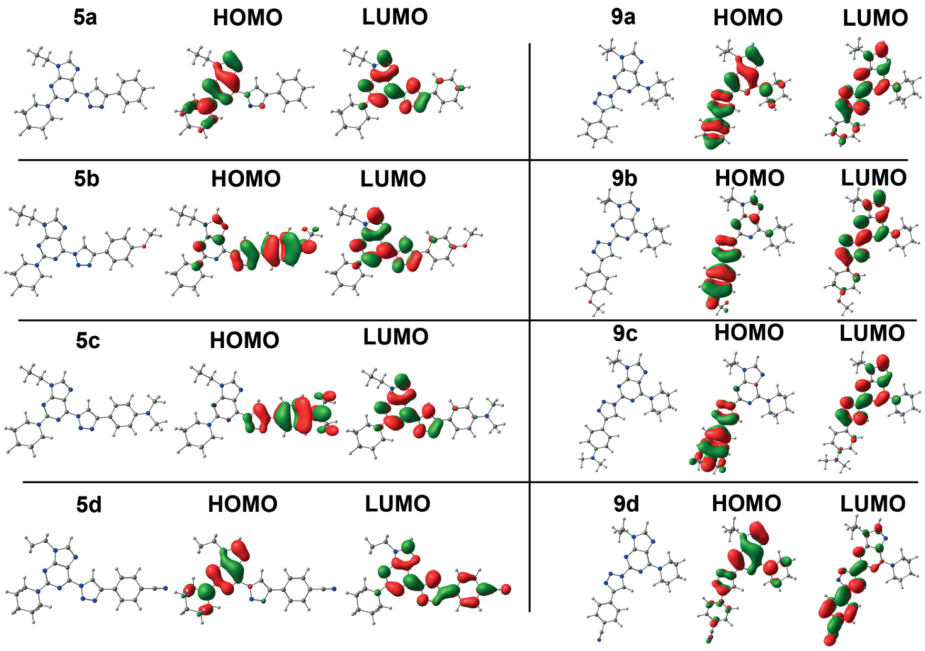

Figure 4. Calculated geometries and HOMO/LUMO distribution for compounds **5a**−**d** and **9a**−**d**.

of the orbitals are given in Figure 4. The optimized structures of the compounds assume conformations, where all of the present aromatic ring systems are coplanar, indicating that π-electrons are delocalized in a conjugated system and no sterical overcrowding effects take place that would result in a twisted geometry. Generally, a good agreement between the experimental and DFT values can be found, as the calculated HOMO and LUMO energy level values correlate well with the measured ionization potentials and electron affinities.

As it can be concluded from the previously discussed experimental results, regarding the substitution pattern at 2- and 6-positions, the photophysical and electronic characteristics of the compounds change drastically. This discrepancy between **5** and **9** is partly explained by the molecular orbital configuration of the compounds. In the case of **5a**, purine-centered HOMO and triazole-centered LUMO are much more spatially separated than for **9a**, where these frontal orbitals are delocalized all over the conjugated ring system and largely overlap. This points to a more pronounced push−pull characteristic for **5a** and its analogues. The assumption is additionally supported by the calculated band gap values that show a substantial drop in $\Delta E_{\mathrm{HOMO-LUMO}}$ for **5** in comparison to **9**. The differing nature of the molecular orbital configuration may also explain the detected drastic variations in nonradiative excitation decay rates (k_{nr}) between the two compound subsets. The less contained molecular orbitals for series **9** compounds would result in the excited states that are delocalized across multiple aromatic ring systems, thus increasing the susceptibility to relaxation pathways through vibrational or conformational motion processes.

The introduction of electron-donating groups at the 1,2,3-triazole fragment drastically changes the molecular orbital configuration for the compounds, as HOMO then localizes on the corresponding electron-rich aryltriazole moiety, while LUMO is mostly confined to the purine fragment. Despite this transformation of the electronic system, in terms of molecular orbital energy values, this causes no major deviations in regard to other synthesized compounds. For **5d** and **9d**, the presence of the electron-accepting cyanophenyl group enhances the spatial separation between the purine-centered HOMO and the triazole-based LUMO by shifting the LUMO to the corresponding electron-deficient benzene ring and the cyano group. Such increased push−pull characteristic is considered as the origin for the experimentally observed stabilization of I_{E} and A_{E} levels in comparison to the rest of the synthesized compounds. This also reflects in the increased calculated ground state dipole moment values of the compounds.

Optoelectronic Properties. The evaluation of the synthesized compounds for use in optoelectronic devices was initially carried out by the preparation of OLEDs, where solution-processed EMLs consisted only of the synthesized purine derivatives. Purines with the highest fluorescence quantum yield were chosen for OLED preparation, namely, **5a**, **5d**, **9a**, and **9d**. In all of the cases, no electroluminescence originating from purine derivatives was observed. At the same time, the prepared OLEDs showed relatively large current densities, as the values exceeding 100 mA/cm^2 were measured at a driving voltage of 5−7 V (Figure S4). High current can be proposed as the main reason for the lack of detectable emission. Polaron concentration in EML at such current levels is high and, most likely, an extensive polaron-exciton quenching takes place. In addition, high current promotes a current leakage. The prevalence of nonradiative exciton recombination pathways under such conditions results in excessive heating that can further reduce the performance parameters of light-emitting diodes.[40] An unbalanced charge carrier injection in the devices

https://doi.org/10.1021/acsomega.1c06359
ACS Omega 2022, 7, 5242−5253

was proposed as another possible cause for the lack of measurable emission.

After unsuccessful attempts to use the purines as the emitting compounds, these compounds were tested as potential charge-transporting host materials for phosphorescent triplet emitters. Based on its highest measured triplet energy value, compound **9b** was chosen as the most suitable material for such a purpose. Tentative OLEDs with EML composed of conventional iridium(III) blue emitter FIrpic (10 wt %) and **9b** were prepared. Unfortunately, an identical result as in purine-only samples was obtained since devices exhibited no electroluminescence. To better understand the possible cause for this poor OLED performance, a multi-host device with ITO/PEDOT:PSS/EML/BPhen/LiF/Al architecture was prepared, where EML consisted of FIrpic/**9b**/CBP (10:30:60 wt %) (Figure 5). In this case, a measurable amount of luminance was

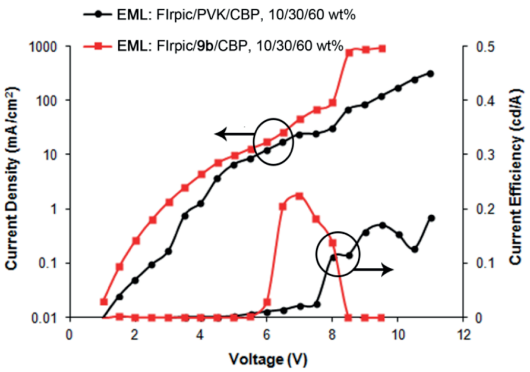

Figure 5. Current density and current efficiency-voltage dependencies for multi-host OLEDs.

detected, originating from the phosphorescent host. In comparison with a reference device with FIrpic/PVK/CBP (10:30:60 wt %) EML, the purine bearing OLED showed a notable increase in current density, indicating improved charge transport properties. The device also showed improved efficiency parameters at the voltage range slightly above the luminance onset mark. The further driving voltage increase, however, resulted in a sharp decrease in luminance, while the reference device experienced a steady rise in current efficiency. Such behavior indicates a better charge carrier density and balance at turn-on voltage levels in a purine-containing device, but a further voltage increase causes a rapid deterioration in the operational stability. Two possible reasons could be mentioned for the steep OLED efficiency decrease. Although better-balanced charge carries in the system, there is still high leaked current (around 10 mA/cm^2 at turn-on voltage) so that exciton quenching by polarons takes place at higher driving voltages. Second, the prepared emitter layer consists of only small molecules that could lead to higher FIrpic emitter aggregation compared to the system with an added polymer host (PVK). Consequently, exciton−exciton annihilation will be observed and will result in efficiency roll-off. The roll-off could be decreased by optimizing the ratio between **9b** and CBP. At a voltage of 8 V, a partial current shortage was observed that destroyed the OLED and no electroluminescence was observed.

Finally, single charge carrier devices were prepared using architectures ITO/LiF/purine **5d** or **9d**/LiF/Al for electron-only or ITO/MoO_3/purine **5d** or **9d** /MoO_3/Cu for hole-only transport measurement purposes (Figure 6). The obtained

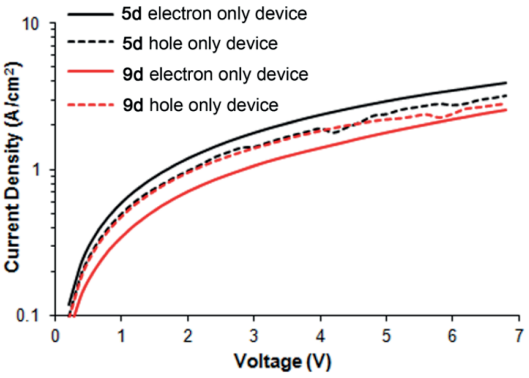

Figure 6. Current density−voltage characteristics for electron-only and hole-only devices of **5d** and **9d**.

results indicate that the compounds possess bipolar charge-transporting properties, as the hole and electron-only devices have similar voltage−charge density dependencies. At the same time, both compounds show very high current levels. Even at voltages as low as 2 V, the current density exceeds 1 A/cm^2 and this parameter reaches the 3 A/cm^2 mark with a voltage increase to 7 V. These current density values are more than an order of magnitude greater than those measured for readily applied OLED charge-transporting host materials.[41,42] This result confirms that the large current density in EML is the main reason for the poor OLED performance of the studied push−pull purines. The good charge-transporting ability of the acquired triazolyl functionalized purines can be attributed to their planar geometry and dipolar nature. Our previous investigation of closely similar structures has revealed that in the crystalline state these compounds tend to form highly ordered vertical stacks that are determined by dipolar $\pi-\pi$ interactions between the electron-rich purine and electron-deficient triazolyl ring systems.[43] Taking into account the good charge-transporting ability of the synthesized push−pull purines, their use as semiconductors in organic field-effect transistors (OFETs) or other devices with purely charge-transporting functionality can be proposed as the most promising application directions.

Interestingly, slight variations can be observed between charge transport properties for 2-amino-6-triazolyl (**5d**) and 2-triazolyl-6-amino (**9d**) configured compounds. While both compounds show almost overlapping current density−voltage dependency in the hole-only mode, **5d** exhibits vaguely better electron transportation ability. At the same time, **9d** is more prone to hole transport. The calculated distribution of frontier molecular orbitals for the corresponding compounds (Figure 4) shows that the HOMO in both cases similarly lies on the purine ring system, explaining the almost identical hole-transporting properties. The LUMO, on the other hand, is located mainly on the cyanophenyl ring for **9d** but is delocalized over the whole purine−triazole−phenyl system for **5d**. Increased LUMO delocalization seems to be beneficial for the overall electron-transporting ability of the push−pull purines.

https://doi.org/10.1021/acsomega.1c06359
ACS Omega 2022, 7, 5242−5253

CONCLUSIONS

The optical and optoelectronic properties of push−pull *N*(9)-alkylated 6-piperidino-2-triazolylpurine and 2-piperidino-6-triazolylpurine derivatives have been investigated. The interchangeable 2/6-substitution pattern of the studied compounds provides a molecular platform in which frontier molecular orbital energy levels can be greatly modified. This allows obtaining molecules with ionization energy in the range of 5.25−6.04 eV, electron affinity of 2.18−3.15 eV, and triplet energy of 2.52−2.95 eV. The compounds also exhibit strong fluorescence in violet and blue spectral regions, with the measured Φ_{FL} in solutions reaching 0.91. The functionalization of purines with phase modifying groups prevents crystallization of compounds and reduces solid-state emission quenching, allowing the preparation of amorphous spin-coated host-free films with Φ_{FL} of up to 0.40. While the emissive properties and high triplet energy levels could mark the synthesized compounds as promising candidates for either emitter or host materials in the emissive layers of OLEDs, no electroluminescence was observed in the corresponding devices. This can be attributed to an excessive charge-transporting ability of the compounds that leads to either current leakage or strong emission quenching due to the large current density in the emissive layer. On the other hand, the bipolar character and good charge-transporting ability of the investigated compounds can potentially be exploited to provide materials in other areas of organic electronics, such as organic field-effect transistors.

EXPERIMENTAL PART

General Information. ^{1}H- and ^{13}C-NMR spectra were recorded on Bruker Avance at 300 and 75.5 MHz, respectively. The proton signals for residual nondeuterated solvents (δ 7.26 for $CDCl_3$, δ 2.50 for DMSO-d_6) and carbon signals (δ 77.1 for $CDCl_3$, δ 39.5 for DMSO-d_6) were used as an internal reference for ^{1}H- and ^{13}C-NMR spectra, respectively.

Analytical thin-layer chromatography (TLC) was performed on Merck 60 Å silica gel F_{254} plates. Column chromatography was performed on Merck 40−60 μm 60 Å silica gel. Anhydrous methylene chloride, dimethylformamide, and acetonitrile were obtained by distillation over CaH_2, tetrahydrofuran was obtained by distillation over sodium. Commercial reagents were used as received. The infrared spectra were recorded on Perkin Elmer Spectrum BX. Wavelengths are given in cm^{-1}. For HPLC analysis, we used *A*gilent Technologies 1200 Series chromatograph equipped with an Agilent XDB-C18 (4.6 × 50 mm, 1.8 μm) column and a Phenomenex Gemini NX (4.6 × 100 mm, 3 μm) column. Eluent A: 0.01 M KH_2PO_4 solution with 6% v/v MeCN added; eluent B: 0.1% TFA solution with 5% v/v MeCN added; and eluent C: MeCN.

Optical measurements of solutions were carried out at a typical material concentration of 1×10^{-5} mol L^{-1}. The UV−vis absorption spectra were recorded with a Perkin Elmer Lambda 35 spectrometer. Films for optical measurements were prepared using a spin-coating technique with a Laurell WS-400B-6NPP/LITE spin-coater on glass slides, using $CHCl_3$ solutions with a material concentration of 30 mg/mL. After the preparation, all films were dried in an oven at 100 °C for 2 h. Emission spectra, Φ_{FL}, and lifetime values in solutions or thin films were measured using a QuantaMaster 40 steady-state spectrofluorometer (Photon Technology International, Inc.) equipped with a 6-inch integrating sphere by LabSphere, using the software package provided by the manufacturer. For lifetime measurements, excitation at 365 nm was used, while emission was detected at the respective band maxima. Low-temperature emission measurements were carried out by cooling the cuvettes in a liquid nitrogen-filled quartz Dewar. Phosphorescence spectra were recorded using time-gated detection by collecting emission in a 50−5000 μs interval after the excitation. Differential scanning calorimetry (DSC) thermograms were acquired using a Mettler Toledo DSC-1/200W apparatus. The samples were heated from 50 to 190 °C at a rate of 10 °C min^{-1} and isothermally aged for 5 min, then cooled to 50 °C at a rate of 10 °C min^{-1} and isothermally aged for 5 min. The cycle was repeated 3 times. Decomposition temperatures were obtained using a Perkin Elmer STA 6000 thermal analyzer.

The molecular ionization energy in a thin film (I_E) and photoconductivity measurements (E_{th}) were carried out on a self-made experimental system using a method described in our previous work.[44] The values of electron affinity energies in thin film (A_E) were calculated using the difference of experimentally determined values of E_{th} and I_E.

Density functional theory (DFT) calculations were performed using the ORCA[45] program package. For auxiliary tasks, the Avogadro program[46] was used. The geometry optimizations for all compounds were obtained using nonlocal functional B3LYP with a 6-311G**[47] basis set. Ground state dipole moment (μ) values were calculated at the same theory level. Initial atomic coordinates were chosen based on X-ray analysis data of closely related structures.[43] For TDDFT calculations, def2-TZVP basis, def2/J auxiliary basis, and the RIJCOSX approximation were used. To reduce the computational cost, the structures were simplified by substituting triphenylpentyl moieties with ethyl groups.

Sandwich-type samples with the pixel size of 16 mm^2 were prepared for the OLED, electron-only, and hole-only devices. Indium tin oxide (ITO) glass (Präzisions Glas & Optik GmbH) with a sheet resistivity of 50 Ω^2 was used as a substrate in all cases. A 12 mm wide ITO strip line was made by wet etching at the middle of the substrate. ITO substrates were cleaned by the following method: sonicated in $CHCl_3$; sonicated in acetone; rinsed two times with deionized (DI) water; sonicated in water with 3 vol % of Hellmanex II detergent; rinsed with DI water; and sonicated in DI water and isopropyl alcohol.

OLEDs with structure ITO/PEDOT:PSS(40 nm)/EML(60 nm)/TPBi(20 nm)/LiF(1 nm)/Al(120 nm) or ITO/PEDOT:PSS(40 nm)/EML(60 nm)/BPhen(20 nm)/LiF(1 nm)/Al(120 nm) were prepared. Poly (3,4-ethylenedioxythiophene)-poly (styrenesulfonate) (PEDOT:PSS), 2,2′,2″-(1,3,5-benzinetriyl)-tris(1-phenyl-1-*H*-benzimidazole) (TPBi), and LiF were used as hole-injection, electron transport, and electron-injection layers, respectively. Before deposition of PEDOT:PSS, the ITO glass (50 Ω^2) was blown dry with nitrogen and treated with UV-ozone for 20 min. The ITO layer was covered with PEDOT:PSS (from H.C. Starck, Al4083) using a spin-coater Laurell WS650. The rotation lasted for 1 min with a speed of 2000 rpm. The sample was moved into a glovebox and heated at 150 °C for 30 min. The solution of emitting layer compounds with a concentration of 7 mg/mL in tetrahydrofuran was spin-coated on the PEDOT:PSS layer with 2000 rpm for 40 s and heated at 120 °C for 15 min afterward. The following EMLs were used in different devices: pure push−pull purines; **9b** and bis[2-(4,6-difluorophenyl)pyridinato-C2,N](picolinato)iridium (FIrpic; Ossila) 90:10 wt %; FIrpic/**9b**/4,4′-bis(*N*-carbazolyl)-1,1′-biphenyl (CBP) (10:30:60 wt %); and FIrpic/poly(9-vinylcarbazole) (PVK)/CBP (10:30:60

https://doi.org/10.1021/acsomega.1c06359
ACS Omega 2022, 7, 5242−5253

wt %). Furthermore, the samples were moved from the glovebox to a vacuum chamber, without exposure to air, for thermal evaporation of electron transport TPBi (Sigma Aldrich 806781) or BPhen (Sigma Aldrich 11880), electron-injection LiF (Sigma Aldrich 449903), and electrodes at the pressure 6×10^{-6} Torr. The deposition speed was 1, 0.1, and 5 Å/s for TPBi, LiF, and Al, respectively. The current−voltage characteristics of the OLEDs were measured using a Keithley 2450 SourceMeter. The electroluminescence brightness was measured by Konica Minolta Luminance and Color Meter CS-150. The structure of hole-only device was ITO/MoO_3(10 nm)/compound(60 nm)/MoO_3(10 nm)/Al(100 nm) and the electron-only device was ITO/LiF(1 nm)/compound(60 nm)/ LiF(1 nm)/Al(100 nm). Layer preparation parameters were the same as for OLED.

*General Procedures and Characterization of Products. 9-(5,5,5-Triphenylpentyl)-2,6-dichloro-9H-purine (**2**).* Under an argon atmosphere, diisopropyl azodicarboxylate (DIAD) (7.88 mL, ρ = 1.03 g/cm^3, 40.02 mmol, 1.5 equiv.) was added dropwise to a cooled solution of 2,6-dichloropurine **1** (5.00 g, 26.46 mmol, 1.0 equiv.), 5,5,5-triphenylpentanol[48] (8.79 g, 27.79 mmol, 1.1 equiv.), and Ph_3P (10.21 g, 38.93 mmol, 1.5 equiv.) in absolute THF (40 mL) over 15 min. The reaction mixture was stirred for 1.5 h at 20 °C, controlled by HPLC, then evaporated, the residue was dissolved in EtOH (20 mL), and cooled to −10 °C for 30 min. Formed precipitates were filtered and washed with cold EtOH (2 × 5 mL). The filtrate was evaporated and purified by silica gel column chromatography (DCM/MeCN, gradient 0 → 10%). Yield 8.36 g, 65%. Colorless amorphous solid, R_f = 0.49 (DCM/MeCN = 20/1). HPLC: t_R = 7.63 min. IR (FT-IR): 3081, 2938, 1597, 1558 cm^{-1}. ^{1}H-NMR (300 MHz, $CDCl_3$) δ (ppm): 7.92 (s, 1H, H-C(8)), 7.32−7.14 (m, 15H, H-C(Ph)), 4.15 (t, 2H, ^3J = 7.2 Hz, ($-CH_2-$)), 2.68−2.55 (m, 2H, ($-CH_2-$)), 1.91 (quintet, 2H, ^3J = 7.5 Hz, ($-CH_2-$)), 1.22−1.06 (m, 2H, ($-CH_2-$)). ^{13}C-NMR (75.5 MHz, $CDCl_3$) δ (ppm): 153.2, 152.9, 151.8, 147.0, 145.7, 130.7, 129.1, 128.0, 126.1, 56.7, 44.5, 39.7, 30.5, 22.9. HRMS (ESI): calcd for $[C_{28}H_{24}Cl_2N_4 + H^+]$ 487.1451, found 487.1446.

*2,6-Diazido-9-(5,5,5-triphenylpentyl)-9H-purine (**3**).* NaN_3 (0.20 g, 3.08 mmol, 2.4 equiv.) was added to a solution of alkylated 2,6-dichloropurine **2** (0.62 g, 1.27 mmol, 1.0 equiv.) in acetone (10 mL), stirred for 14 h at 50 °C, covered from the light, controlled by HPLC, evaporated, and suspended in water (30 mL). The formed precipitates were filtered and washed with water (3 × 10 mL) and dried in a vacuum. Yield 0.63 g, 99%. Colorless amorphous solid, R_f = 0.57 (DCM/MeCN = 20/1). HPLC: t_R = 7.73 min. IR (FT-IR): 2154, 2134, 1598, 1577 cm^{-1}. ^{1}H-NMR (300 MHz, $CDCl_3$) δ (ppm): 7.73 (s, 1H, H-C(8)), 7.33−7.12 (m, 15H, H-C(Ph)), 4.07 (t, 2H, ^3J = 7.2 Hz, ($-CH_2-$)), 2.68−2.55 (m, 2H, ($-CH_2-$)), 1.88 (quintet, 2H, ^3J = 7.5 Hz, ($-CH_2-$)), 1.24−1.07 (m, 2H, ($-CH_2-$)). ^{13}C-NMR (75.5 MHz, $CDCl_3$) δ (ppm): 156.0, 153.9, 153.7, 147.1, 143.5, 129.1, 128.0, 126.1, 121.1, 56.7, 44.0, 39.8, 30.5, 22.9. HRMS (ESI): calcd for $[C_{28}H_{24}N_{10} + H^+]$ 501.2258, found 501.2240.

*6-Azido-9-(5,5,5-triphenylpentyl)-2-(piperidin-1-yl)-9H-purine (**4**).* Piperidine (0.60 mL, ρ = 0.86 g/cm^3, 5.99 mmol, 3.0 equiv.) was added to a solution of compound **3** (1.00 g, 1.99 mmol, 1.0 equiv.) in DMF (20 mL) and stirred for 1 h at 20 °C, covered from the light, controlled by HPLC. The reaction mixture was evaporated and purified by silica gel column chromatography (DCM/MeCN, gradient 0 → 10%). Yield 899 mg, 83%. Light yellow amorphous solid, R_f = 0.38 (DCM/MeCN = 10:1). HPLC: t_R = 9.46 min. IR (FT-IR): 2934, 2852, 2119, 1618, 1567 cm^{-1}. ^{1}H-NMR (300 MHz, $CDCl_3$) δ (ppm): 7.44 (s, 1H, H-C(8)), 7.30−7.06 (m, 15H, H-C(Ph)), 3.96 (t, 2H, ^3J = 7.2 Hz, ($-CH_2-$)), 3.83−3.72 (m, 4H, 2 × ($-CH_2-$)), 2.68−2.54 (m, 2H, ($-CH_2-$)), 1.85 (quintet, 2H, ^3J = 7.4 Hz, ($-CH_2-$)), 1.74−1.50 (m, 6H, 3 × ($-CH_2-$)), 1.11 (m, 2H, ($-CH_2-$)). ^{13}C-NMR (75.5 MHz, $CDCl_3$) δ (ppm): 158.6, 154.8, 152.6, 147.3, 140.5, 129.2, 127.9, 126.0, 117.1, 56.7, 45.4, 42.9, 39.8, 30.5, 25.9, 25.0, 22.8. HRMS (ESI): calcd for $[C_{33}H_{34}N_8 + H^+]$ 543.2979, found 543.2986.

*2-Azido-6-(piperidin-1-yl)-9H-purine (**7**).*[49] To a solution of 2,6-dichloropurine (**1**) (3.00 g, 15.90 mmol, 1.0 equiv.) in EtOH (30 mL), a solution of NaN_3 (4.13 g, 63.60 mmol, 4.0 equiv.) in water (15 mL) was added and the reaction mixture was stirred at 100 °C temperature for 30 min, then it was cooled and a colorless precipitate was formed, which was filtered and recrystallized from EtOH (100 mL) to give 2.46 g (w = 75%) of product **6** as a colorless solid. Then, piperidine (4 mL) was added to a suspension of 2,6-diazido-9*H*-purine (**6**) (2.46 g, 12.18 mmol, 1.0 equiv.)[19,50] in water (10 mL) and was stirred at 100 °C temperature for 2.5 h. Then, the reaction mixture was cooled to room temperature and AcOH was added while the pH of the solution reached 7. The mixture was kept in the fridge for 3 h. The precipitate was filtered and washed with cold EtOH (30 mL) and recrystallized from EtOH (75 mL) to give product **7** as a colorless solid. Yield 2.03 g, 52%. mp = 215 °C (decompose). HPLC: t_R = 4.41 min. IR (FT-IR): 3059, 2931, 2819, 2125 (N3), 1603, 1579, 1367 cm^{-1}. ^{1}H-NMR (300 MHz, DMSO-d_6) δ (ppm): 12.76 (brs, 1H, H-N), 7.96 (s, 1H, H-C(8)), 4.27−4.05 (m, 4H, 2 × ($-CH_2-$)), 1.76−1.53 (m, 6H, 3 × ($-CH_2-$)). ^{13}C-NMR (75.5 MHz, DMSO-d_6) δ (ppm): 154.8, 153.1, 152.7, 137.6, 116.4, 45.4, 25.6, 24.1.

*2-Azido-9-(5,5,5-triphenylpentyl)-6-(piperidin-1-yl)-9H-purine (**8**).* Under an argon atmosphere, DIAD (0.41 mL, ρ = 1.03 g/cm^3, 2.10 mmol, 1.1 equiv.) was added over 15 min to a cooled solution of 2-azido-6-(piperidin-1-yl)-9*H*-purine (**7**) (460 mg, 1.90 mmol, 1.0 equiv.), 5,5,5-triphenylpentanol (633 mg, 2.00 mmol, 1.05 equiv.), and Ph_3P (550 mg, 2.10 mmol, 1.1 equiv.) in THF (15 mL) and stirred for 12 h at 20 °C, controlled by HPLC, filtered, evaporated, diluted with MeCN (5 mL), and cooled to −10 °C for 30 min. The formed precipitates were filtered and washed with cold MeCN (2 × 3 mL) and dried in a vacuum. Yield 730 mg, 71%. Colorless amorphous solid, R_f = 0.80 (DCM/MeCN = 40:1). HPLC: t_R = 9.18 min. IR (FT-IR): 2938, 2853, 2126, 1588, 1486, 1360, 1339, 1250, 997 cm^{-1}. ^{1}H-NMR (300 MHz, $CDCl_3$) δ (ppm): 7.47 (s, 1H, H-C(8)), 7.32−7.12 (m, 15H, H-C(Ph)), 4.44−4.04 (m, 4H, 2 × ($-CH_2-$)), 3.99 (t, 2H, ^3J = 7.4 Hz, ($-CH_2-$)), 2.64−2.54 (m, 2H, ($-CH_2-$)), 1.84 (quintet, 2H, ^3J = 7.4 Hz, ($-CH_2-$)), 1.83−1.64 (m, 6H, 3 × ($-CH_2-$)), 1.20−1.07 (m, 2H, ($-CH_2-$)). ^{13}C-NMR (75.5 MHz, $CDCl_3$) δ (ppm): 156.1, 153.9, 152.5, 147.2, 137.6, 129.2, 128.0, 126.0, 117.5, 56.7, 46.3 (assigned from the HSQC spectrum at 50 °C temperature), 43.5, 39.9, 30.7, 26.2, 24.9, 23.0. HRMS (ESI): calcd for $[C_{33}H_{34}N_8 + H^+]$ 543.2979, found 543.2980.

*Synthesis of 2-(Piperidin-1-yl)-6-triazolyl-9-alkylpurines **5**. 6-(4-(4-Methoxyphenyl)-1H-1,2,3-triazol-1-yl)-9-(5,5,5-triphenylpentyl)-2-(piperidin-1-yl)-9H-purine (**5b**).* 10% AcOH solution in water (1.0 mL), sodium ascorbate (85 mg, 0.43 mmol, 0.9 equiv.), and $CuSO_4 \cdot 5H_2O$ (51 mg, 0.20 mmol, 44 mol %) were added to a solution of compound **4** (250 mg, 0.46 mmol, 1.0 equiv.) and 4-methoxyphenylacetylene (0.15 mL, ρ = 1.02 g/cm^3, 1.16 mmol, 2.5 equiv.) in THF (10 mL) and stirred for 4 h at 20 °C. The reaction mixture was evaporated, the

https://doi.org/10.1021/acsomega.1c06359
ACS Omega 2022, 7, 5242−5253

residue was dissolved in DCM (20 mL), and washed with NaHS solution (3 × 5 mL). The DCM layer was dried over anhydrous Na_2SO_4, filtered, evaporated, and purified by silica gel column chromatography (DCM/MeCN = 5/1). Yield 240 mg, 77%. Yellow amorphous solid, R_f = 0.76 (DCM/MeCN = 5:1). HPLC: t_R = 8.75 min, purity 97%. IR (FT-IR): 2933, 2851, 1718, 1628, 1565 cm^{-1}. ^{1}H-NMR (300 MHz, $CDCl_3$) δ (ppm): 9.00 (s, 1H, H-C(triazole)), 7.95 (d, 2H, ^3J = 8.6 Hz, Ar), 7.68 (s, 1H, H-C(8)), 7.24−7.09 (m, 15H, Ar), 7.01 (d, 2H, ^3J = 8.6 Hz, Ar), 4.05 (t, 2H, ^3J = 7.1 Hz, (−CH_2−)), 3.92−3.80 (m, 7H, 2 × (−CH_2−), (−CH_3)), 2.70−2.58 (m, 2H, (−CH_2−)), 1.90 (quintet, 2H, ^3J = 7.1 Hz, (−CH_2−)), 1.76−1.56 (m, 6H, 3 × (−CH_2−)), 1.23−1.08 (m, 2H, (−CH_2−)). ^{13}C-NMR (75.5 MHz, $CDCl_3$) δ (ppm): 160.0, 158.4, 156.9, 147.5, 147.2, 145.1, 142.5, 129.2, 128.0, 127.7, 126.1, 123.1, 118.5, 115.5, 114.4, 56.7, 55.5, 45.6, 43.1, 39.8, 30.5, 25.9, 24.9, 22.8. HRMS (ESI): calcd for [$C_{42}H_{42}N_8O$ + H^+] 675.3554, found 675.3545.

General Synthetic Procedure for 1,3-Dipolar Cycloaddition Reaction for 5a, 5c, 5d, and ***9a*****−*****d*****.** DIPEA (104 μL, ρ = 0.74 g/cm^3, 0.61 mmol, 1.1 equiv.), AcOH (37 μL, ρ = 1.05 g/cm^3, 0.61 mmol, 1.1 equiv.), and CuI (21 mg, 0.11 mmol, 0.2 equiv.) were added to a solution of 2-amino-6-azidopurine **4** or 6-amino-2-azidopurine **8** (300 mg, 0.55 mmol, 1.0 equiv.) and alkyne (1.5 equiv.) in DCM (9 mL) and stirred for 14−264 h at 20 °C, covered from the light, and controlled by HPLC. The reaction mixture was poured into the water (20 mL) and extracted with DCM (3 × 10 mL). Organic layers were combined and washed with diluted NaHS solution (10 mL), filtered through Celite, separated, and washed with brine (10 mL), dried over anhydrous Na_2SO_4, filtered, evaporated, and purified by silica gel column chromatography (DCM/MeCN, gradient 0 → 25%).

*6-(4-Phenyl-1H-1,2,3-triazol-1-yl)-9-(5,5,5-triphenylpentyl)-2-(piperidin-1-yl)-9H-purine (****5a****).* Reaction time: 14 h. Yield 282 mg, 79%. Light yellow amorphous solid, R_f = 0.23 (DCM/MeCN = 10:1). HPLC: t_R = 8.49 min. IR (FT-IR): 3055, 2932, 2851, 1628, 1565, 1533, 1446, 1009 cm^{-1}. ^{1}H-NMR (300 MHz, $CDCl_3$) δ (ppm): 9.07 (s, 1H, H-C(triazole)), 7.99 (d, 2H, ^3J = 7.3 Hz, H-C(Ph)), 7.80 (s, 1H, H-C(8)), 7.47 (t, 2H, ^3J = 7.3 Hz, H-C(Ph)), 7.37 (t, 1H, ^3J = 7.3 Hz, H-C(Ph)), 7.25−7.08 (m, 15H, H-C(Ph)), 4.07 (t, 2H, ^3J = 7.0 Hz, (−CH_2−)), 3.92−3.82 (m, 4H, 2 × (−CH_2−)), 2.70−2.59 (m, 2H, (−CH_2−)), 1.91 (quintet, 2H, ^3J = 7.0 Hz, (−CH_2−)), 1.76−1.56 (m, 6H, 3 × (−CH_2−)), 1.24−1.08 (m, 2H, (−CH_2−)). ^{13}C-NMR (75.5 MHz, $CDCl_3$) δ (ppm): 158.3, 156.7, 147.5, 147.1, 144.9, 142.6, 130.3, 129.1, 128.9, 128.4, 127.9, 126.2, 126.0, 119.2, 115.2, 56.6, 45.5, 43.0, 39.7, 30.4, 25.8, 24.8, 22.7. HRMS (ESI): calcd for [$C_{41}H_{40}N_8$ + H^+] 645.3449, found 645.3443.

*9-(5,5,5-Triphenylpentyl)-6-(4-(4-(N,N-dimethylamino)-phenyl)-1H-1,2,3-triazol-1-yl)-2-(piperidin-1-yl)-9H-purine (****5c****).* Reaction time: 64 h. Yield 249 mg, 66%. Yellow amorphous solid, R_f = 0.26 (DCM/MeCN = 10:1). HPLC: t_R = 7.59 min. IR (FT-IR): 2932, 2856, 1622, 1561, 1561, 1538, 1491, 1445, 1410, 1359, 1020 cm^{-1}. ^{1}H-NMR (300 MHz, $CDCl_3$) δ (ppm): 8.95 (s, 1H, H-C(triazole)), 7.88 (d, 2H, ^3J = 8.7 Hz, H-C(Ar)), 7.67 (s, 1H, H-C(8)), 7.26−7.10 (m, 15H, H-C(Ph)), 6.82 (d, 2H, ^3J = 8.7 Hz, H-C(Ar)), 4.05 (t, 2H, ^3J = 7.1 Hz, (−CH_2−)), 3.92−3.82 (m, 4H, 2 × (−CH_2−)), 3.01 (s, 6H, $(Me)_2$N−), 2.69−2.60 (m, 2H, (−CH_2−)), 1.90 (quintet, 2H, ^3J = 7.1 Hz, (−CH_2−)), 1.74−1.58 (m, 6H, 3 × (−CH_2−)), 1.24−1.08 (m, 2H, (−CH_2−)). ^{13}C-NMR (75.5 MHz, $CDCl_3$) δ (ppm): 158.4, 156.8, 150.6, 148.0, 147.2, 145.2, 142.3, 129.2, 127.9, 127.3, 126.0, 118.7, 117.6, 115.5, 112.6, 56.7, 45.6, 43.0, 40.7, 39.8, 30.5, 25.9, 24.9, 22.8. HRMS (ESI): calcd for [$C_{43}H_{45}N_9$ + H^+] 688.3871, found 688.3888.

*6-(4-(4-Cyanophenyl)-1H-1,2,3-triazol-1-yl)-9-(5,5,5-triphenylpentyl)-2-(piperidin-1-yl)-9H-purine (****5d****).* Reaction time: 14 h. Silica gel column chromatography (DCM/MeCN, gradient 0 → 10%). Yield 298 mg, 81%. Light yellow amorphous solid, R_f = 0.40 (DCM/MeCN = 10:1). HPLC: t_R = 8.15 min. IR (FT-IR): 2934, 2852, 2225, 1630, 1564, 1534, 1491, 1446, 1412, 1232, 1010 cm^{-1}. ^{1}H-NMR (300 MHz, $CDCl_3$) δ (ppm): 9.21 (s, 1H, H-C(triazole)), 8.13 (d, 2H, ^3J = 8.4 Hz, H-C(Ar)), 7.76 (d, 2H, ^3J = 8.4 Hz, H-C(Ar)), 7.71 (s, 1H, H-C(8)), 7.24−7.10 (m, 15H, H-C(Ph)), 4.07 (t, 2H, ^3J = 7.2 Hz, (−CH_2−)), 3.92−3.83 (m, 4H, 2 × (−CH_2−)), 2.69−2.59 (m, 2H, (−CH_2−)), 1.91 (quintet, 2H, ^3J = 7.2 Hz, (−CH_2−)), 1.74−1.58 (m, 6H, 3 × (−CH_2−)), 1.22−1.10 (m, 2H, (−CH_2−)). ^{13}C-NMR (75.5 MHz, $CDCl_3$) δ (ppm): 158.4, 157.0, 147.2, 145.8, 144.6, 142.8, 134.8, 132.8, 129.2, 128.0, 126.7, 126.1, 120.7, 118.9, 115.4, 111.9, 56.7, 45.6, 43.2, 39.8, 30.4, 25.9, 24.9, 22.8. HRMS (ESI): calcd for [$C_{42}H_{39}N_9$ + H^+] 670.3401, found 670.3406.

Synthesis of 6-(Piperidin-1-yl)-2-triazolyl-9-alkylpurines ***9****. 2-(4-Phenyl-1H-1,2,3-triazol-1-yl)-6-(piperidin-1-yl)-9-(5,5,5-triphenylpentyl)-9H-purine (****9a****).* Reaction time: 72 h. Yield 314 mg, 88%. Colorless amorphous solid, R_f = 0.27 (DCM/MeCN = 20:1). HPLC: t_R = 9.42 min. IR (FT-IR): 3055, 2934, 2853, 1595, 1492, 1437, 1251, 1017 cm^{-1}. ^{1}H-NMR (300 MHz, $CDCl_3$) δ (ppm): 8.64 (s, 1H, H-C(triazole)), 7.95 (d, 2H, ^3J = 7.2 Hz, H-C(Ph)), 7.63 (s, 1H, H-C(8)), 7.46 (t, 2H, ^3J = 7.2 Hz, H-C(Ph)), 7.36 (t, 1H, ^3J = 7.2 Hz, H-C(Ph)), 7.24−7.06 (m, 15H, H-C(Ph)), 4.42−4.24 (m, 4H, 2 × (−CH_2−)), 4.15 (t, 2H, ^3J = 7.2 Hz, (−CH_2−)), 2.67−2.58 (m, 2H, (−CH_2−)), 1.92 (quintet, 2H, ^3J = 7.2 Hz, (−CH_2−)), 1.82−1.72 (m, 6H, 3 × (−CH_2−)), 1.28−1.15 (m, 2H, (−CH_2−)). ^{13}C-NMR (75.5 MHz, $CDCl_3$) δ (ppm): 153.9, 151.7, 149.3, 147.4, 147.2, 138.7, 130.7, 129.2, 128.9, 128.3, 128.0, 126.2, 126.0, 119.0, 118.8, 56.7, 46.7 (assigned from the HSQC spectrum at 50 °C temperature), 43.7, 39.9, 30.8, 26.3, 24.8, 23.0. HRMS (ESI): calcd for [$C_{41}H_{40}N_8$ + H^+] 645.3449, found 645.3439.

*2-(4-(4-Methoxyphenyl)-1H-1,2,3-triazol-1-yl)-6-(piperidin-1-yl)-9-(5,5,5-triphenylpentyl)-9H-purine (****9b****).* Reaction time: 240 h. Yield 274 mg, 73%. Colorless amorphous solid, R_f = 0.23 (DCM/MeCN = 20:1). HPLC: t_R = 8.57 min. IR (FT-IR): 3053, 2934, 2853, 1594, 1567, 1492, 1445, 1249, 1020 cm^{-1}. ^{1}H-NMR (300 MHz, $CDCl_3$) δ (ppm): 8.56 (s, 1H, H-C(triazole)), 7.87 (d, 2H, ^3J = 8.8 Hz, H-C(Ar)), 7.63 (s, 1H, H-C(8)), 7.25−7.08 (m, 15H, H-C(Ph)), 6.99 (d, 2H, ^3J = 8.8 Hz, H-C(Ar)), 4.45−4.20 (m, 4H, 2 × (−CH_2−)), 4.15 (t, 2H, ^3J = 7.2 Hz, (−CH_2−)), 3.87 (s, 3H, H_3C-O), 2.66−2.58 (m, 2H, (−CH_2−)), 1.92 (quintet, 2H, ^3J = 7.2 Hz, (−CH_2−)), 1.82−1.71 (m, 6H, 3 × (−CH_2−)), 1.29−1.14 (m, 2H, (−CH_2−)). ^{13}C-NMR (75.5 MHz, $CDCl_3$) δ (ppm): 159.8, 153.9, 151.7, 149.3, 147.2 (2C) (assigned from the HMBC spectrum), 138.7, 129.2, 127.9, 127.5, 126.0, 123.4, 119.0, 117.9, 114.3, 56.7, 55.5, 46.7 (assigned from the HSQC spectrum at 50 °C temperature), 43.7, 39.9, 30.7, 26.3, 24.8, 23.1. HRMS (ESI): calcd for [$C_{42}H_{42}N_8O$ + H^+] 675.3554, found 675.3566.

*9-(5,5,5-Triphenylpentyl)-2-(4-(4-(N,N-dimethylamino)-phenyl)-1H-1,2,3-triazol-1-yl)-6-(piperidin-1-yl)-9H-purine (****9c****).* Reaction time: 264 h. Yield 320 mg, 85%. Beige amorphous solid, R_f = 0.68 (DCM/MeCN = 10:1). HPLC: t_R = 7.55 min. IR (FT-IR): 2934, 2853, 1594, 1571, 1492, 1443, 1356, 1251, 1024 cm^{-1}. ^{1}H-NMR (300 MHz, $CDCl_3$) δ (ppm): 8.51 (s, 1H, H-C(triazole)), 7.81 (d, 2H, ^3J = 8.7 Hz, H-C(Ar)), 7.60 (s, 1H, H-

https://doi.org/10.1021/acsomega.1c06359
ACS Omega 2022, 7, 5242−5253

C(8)), 7.24−7.09 (m, 15H, H-C(Ph)), 6.82 (d, 2H, ^3J = 8.7 Hz, H-C(Ar)), 4.42−4.24 (m, 4H, 2 × (−CH_2−)), 4.14 (t, 2H, ^3J = 7.3 Hz, (−CH_2−)), 3.01 (s, 6H, (($Me)_2$N−)), 2.66−2.57 (m, 2H, (−CH_2−)), 1.92 (quintet, 2H, ^3J = 7.3 Hz, (−CH_2−)), 1.81−1.71 (m, 6H, 3 × (−CH_2−)), 1.28−1.14 (m, 2H, (−CH_2−)). ^{13}C-NMR (75.5 MHz, $CDCl_3$) δ (ppm): 153.9, 151.7, 150.6, 149.4, 147.8, 147.2, 138.6, 129.2, 127.9, 127.1, 125.9, 119.0, 118.9, 117.2, 112.6, 56.7, 46.6 (assigned from the HSQC spectrum at 50 °C temperature), 43.7, 40.6, 39.9, 30.7, 26.3, 24.8, 23.1. HRMS (ESI): calcd for [$C_{43}H_{45}N_9$ + H^+] 688.3871, found 688.3878.

*2-(4-(4-Cyanophenyl)-1H-1,2,3-triazol-1-yl)-9-(5,5,5-triphenylpentyl)-6-(piperidin-1-yl)-9H-purine (**9d**).* Reaction time: 144 h. Yield 317 mg, 86%. Colorless amorphous solid, R_f = 0.85 (DCM/MeCN = 10:1). HPLC: t_R = 8.41 min. IR (FT-IR): 2937, 2856, 2226, 1597, 1571, 1493, 1445, 1251, 1025 cm^{-1}. ^{1}H-NMR (300 MHz, $CDCl_3$) δ (ppm): 8.73 (s, 1H, H-C(triazole)), 8.05 (d, 2H, ^3J = 8.4 Hz, H-C(Ar)), 7.73 (d, 2H, ^3J = 8.4 Hz, H-C(Ar)), 7.63 (s, 1H, H-C(8)), 7.24−7.08 (m, 15H, H-C(Ph)), 4.44−4.24 (m, 4H, 2 × (−CH_2−)), 4.15 (t, 2H, ^3J = 7.3 Hz, (−CH_2−)), 2.67−2.58 (m, 2H, (−CH_2−)), 1.92 (quintet, 2H, ^3J = 7.3 Hz, (−CH_2−)), 1.83−1.70 (m, 6H, 3 × (−CH_2−)), 1.27−1.12 (m, 2H, (−CH_2−)). ^{13}C-NMR (75.5 MHz, $CDCl_3$) δ (ppm): 153.9, 151.6, 149.1, 147.2, 145.6, 138.9, 135.1, 132.8, 129.2, 128.0, 126.5, 126.1, 120.0, 119.3, 119.0, 111.7, 56.7, 46.6 (assigned from the HSQC spectrum at 50 °C temperature), 43.7, 39.9, 30.8, 26.3, 24.8, 23.1. HRMS (ESI): calcd for [$C_{42}H_{39}N_9$ + H^+] 670.3401, found 670.3383.

■ ASSOCIATED CONTENT

Supporting Information

The Supporting Information is available free of charge at https://pubs.acs.org/doi/10.1021/acsomega.1c06359.

Supporting Information file contains figures of thermogravimetric analysis of compounds **9a** and **9b**, emission lifetime measurements for compounds **5a−d** and **9a−d**, fluorescence and phosphorescence spectra of **5b−c** and **9b−c** in the 2-MeTHF matrix at 77 K, current density−voltage dependencies for purine-only and purine host-FIrpic OLEDs, calculated dipole momentum values of the compounds, radiative and nonradiative decay rates of the compounds, and NMR spectra of compounds **2**, **3**, **4**, **7**, **8**, **5a−d**, and **9a−d** (PDF)

■ AUTHOR INFORMATION

Corresponding Authors

Irina Novosjolova − *Faculty of Materials Science and Applied Chemistry, Riga Technical University, LV-1048 Riga, Latvia;* orcid.org/0000-0002-9607-2222; Email: irina.novosjolova@rtu.lv

Kaspars Traskovskis − *Faculty of Materials Science and Applied Chemistry, Riga Technical University, LV-1048 Riga, Latvia;* orcid.org/0000-0003-1416-7533; Email: kaspars.traskovskis@rtu.lv

Māris Turks − *Faculty of Materials Science and Applied Chemistry, Riga Technical University, LV-1048 Riga, Latvia;* orcid.org/0000-0001-5227-0369; Email: maris.turks@rtu.lv

Authors

Armands Sebris − *Faculty of Materials Science and Applied Chemistry, Riga Technical University, LV-1048 Riga, Latvia*

Valdis Kokars − *Faculty of Materials Science and Applied Chemistry, Riga Technical University, LV-1048 Riga, Latvia*

Natalija Tetervenoka − *Institute of Solid State Physics, University of Latvia, LV-1063 Riga, Latvia*

Aivars Vembris − *Institute of Solid State Physics, University of Latvia, LV-1063 Riga, Latvia*

Complete contact information is available at: https://pubs.acs.org/10.1021/acsomega.1c06359

Notes

The authors declare no competing financial interest.

■ ACKNOWLEDGMENTS

This work is supported by the ERDF 1.1.1.1. activity project No. 1.1.1.1/16/A/131. The authors thank Dr. sc. ing. Jānis Zicāns and Dr. sc. ing. Remo Merijs Meri for DSC analyses.

■ REFERENCES

(1) Gomez, E. F.; Venkatraman, V.; Grote, J. G.; Steckl, A. J. DNA Bases Thymine and Adenine in Bio-Organic Light Emitting Diodes. *Sci. Rep.* **2014**, *4*, No. 7105.

(2) Gomez, E. F.; Venkatraman, V.; Grote, J. G.; Steckl, A. J. Exploring the Potential of Nucleic Acid Bases in Organic Light Emitting Diodes. *Adv. Mater.* **2015**, *27*, 7552−7562.

(3) Cho, M. J.; Lee, U. R.; Kim, Y. S.; Shin, J.; Kim, Y. M.; Park, Y. W.; Ju, B.-K.; Jin, J.-I.; Choi, D. H. Organic Soluble Deoxyribonucleic Acid (DNA) Bearing Carbazole Moieties and Its Blend with Phosphorescent Ir (III) Complexes. *J. Polym. Sci., Part A: Polym. Chem.* **2010**, *48*, 1913−1918.

(4) Irimia-Vladu, M.; Troshin, P. A.; Reisinger, M.; Shmygleva, L.; Kanbur, Y.; Schwabegger, G.; Bodea, M.; Schwödiauer, R.; Mumyatov, A.; Fergus, J. W.; et al. Biocompatible and Biodegradable Materials for Organic Field-Effect Transistors. *Adv. Funct. Mater.* **2010**, *20*, 4069−4076.

(5) Kim, Y. S.; Jung, K. H.; Lee, U. R.; Kim, K. H.; Hoang, M. H.; Jin, J.-I.; Choi, D. H. High-Mobility Bio-Organic Field Effect Transistors with Photoreactive DNAs as Gate Insulators. *Appl. Phys. Lett.* **2010**, *96*, No. 103307.

(6) Butler, R. S.; Myers, A. K.; Bellarmine, P.; Abboud, K. A.; Castellano, R. K. Highly Fluorescent Donor-Acceptor Purines. *J. Mater. Chem.* **2007**, *17*, 1863−1865.

(7) Butler, R. S.; Cohn, P.; Tenzel, P.; Abboud, K. A.; Castellano, R. K. Synthesis, Photophysical Behavior, and Electronic Structure of Push-Pull Purines. *J. Am. Chem. Soc.* **2009**, *131*, 623−633.

(8) Vabre, R.; Legraverend, M.; Piguel, S. Synthesis and Evaluation of Spectroscopic Properties of Newly Synthesized Push-Pull 6-Amino-8-styryl Purines. *Dyes Pigm.* **2014**, *105*, 145−151.

(9) Collier, G. S.; Brown, L. A.; Boone, E. S.; Kaushal, M.; Ericson, M. N.; Walter, M. G.; Long, B. K.; Kilbey, S. M. Linking Design and Properties of Purine-Based Donor-Acceptor Chromophores as Optoelectronic Materials. *J. Mater. Chem. C* **2017**, *5*, 6891−6898.

(10) Zucolotto Cocca, L. H.; Abegaõ, L. M. G.; Sciuti, L. F.; Vabre, R.; De Paula Siqueira, J.; Kamada, K.; Mendonca, C. R.; Piguel, S.; De Boni, L. Two-Photon Emissive Dyes Based on Push-Pull Purines Derivatives: Toward the Development of New Photoluminescence Bioprobes. *J. Phys. Chem. C* **2020**, *124*, 12617−12627.

(11) Pelosi, A. G.; Zucolotto Cocca, L. H.; Abegão, L. M. G.; Sciuti, L. F.; Piguel, S.; De Boni, L.; Mendonça, C. R. Influence of Electron-Withdrawing Groups in Two-Photon Absorption of Imidazopyridines Derivatives. *Dyes Pigm.* **2022**, *198*, No. 109972.

(12) Jacquemin, D.; Escudero, D. The Short Device Lifetimes of Blue PhOLEDs: Insights into the Photostability of Blue Ir(III) Complexes. *Chem. Sci.* **2017**, *8*, 7844−7850.

(13) Yang, Y.; Cohn, P.; Eom, S.-H.; Abboud, K. A.; Castellano, R. K.; Xue, J. Ultraviolet-Violet Electroluminescence from Highly Fluorescent Purines. *J. Mater. Chem. C* **2013**, *1*, 2867−2874.

(14) Yang, Y.; Cohn, P.; Dyer, A. L.; Eom, S.-H.; Reynolds, J. R.; Castellano, R. K.; Xue, J. Blue-Violet Electroluminescence from a Highly Fluorescent Purine. *Chem. Mater.* **2010**, *22*, 3580−3582.
(15) Wang, Z.; Yao, J.; Zhan, L.; Gong, S.; Ma, D.; Yang, C. Purine-Based Thermally Activated Delayed Fluorescence Emitters for Efficient Organic Light-Emitting Diodes. *Dyes Pigm.* **2020**, *180*, No. 108437.
(16) Sebris, A.; Traskovskis, K.; Novosjolova, I.; Turks, M. Synthesis and Photophysical Properties of Purine-Phenoxazine and Purine-Phenothiazine Conjugates. *Key Eng. Mater.* **2021**, *903*, 155−161.
(17) Traskovskis, K.; Sebris, A.; Novosjolova, I.; Turks, M.; Guzauskas, M.; Volyniuk, D.; Bezvikonnyi, O.; Grazulevicius, J. V.; Mishnev, A.; Grzibovskis, R.; et al. All-Organic Fast Intersystem Crossing Assisted Exciplexes Exhibiting Sub-Microsecond Thermally Activated Delayed Fluorescence. *J. Mater. Chem. C* **2021**, *9*, 4532−4543.
(18) Novosjolova, I.; Bizdēna, Ē.; Turks, M. Synthesis and Applications of Azolylpurine and Azolylpurine Nucleoside Derivatives. *Eur. J. Org. Chem.* **2015**, *2015*, 3629−3649.
(19) Kovaļovs, A.; Novosjolova, I.; Bizdēna, Ē.; Bižāne, I.; Skardziute, L.; Kazlauskas, K.; Jursenas, S.; Turks, M. 1,2,3-Triazoles as Leaving Groups in Purine Chemistry: A Three-Step Synthesis of N6-Substituted-2-triazolyl-adenine Nucleosides and Photophysical Properties Thereof. *Tetrahedron Lett.* **2013**, *54*, 850−853.
(20) Ozols, K.; Cīrule, D.; Novosjolova, I.; Stepanovs, D.; Liepinsh, E.; Bizdēna, Ē.; Turks, M. Development of N6-Methyl-2-(1,2,3-triazol-1-yl)-2′-deoxyadenosine as a Novel Fluorophore and Its Application in Nucleotide Synthesis. *Tetrahedron Lett.* **2016**, *57*, 1174−1178.
(21) Cīrule, D.; Ozols, K.; Platnieks, O.; Bizdēna, Ē.; Māliņa, I.; Turks, M. Synthesis of Purine Nucleoside-Amino Acid Conjugates and Their Photophysical Properties. *Tetrahedron* **2016**, *72*, 4177−4185.
(22) Šišuļins, A.; Bucevičius, J.; Tseng, Y.-T.; Novosjolova, I.; Traskovskis, K.; Bizdēna, Ē.; Chang, H.-T.; Tumkevičius, S.; Turks, M. Synthesis and Fluorescent Properties of N(9)-Alkylated 2-Amino-6-triazolylpurines and 7-Deazapurines. *Beilstein J. Org. Chem.* **2019**, *15*, 474−489.
(23) Sebris, A.; Traskovskis, K.; Novosjolova, I.; Turks, M. Synthesis and Photophysical Properties of 2-Azolyl-6-piperidinylpurines. *Chem. Heterocycl. Compd.* **2021**, *57*, 560−567.
(24) Kim, M. K.; Kwon, J.; Kwon, T.-H.; Hong, J.-I. A Bipolar Host Containing 1, 2, 3-Triazole for Realizing Highly Efficient Phosphorescent Organic Light-Emitting Diodes. *New J. Chem.* **2010**, *34*, 1317−1322.
(25) Traskovskis, K.; Ruduss, A.; Kokars, V.; Mihailovs, I.; Lesina, N.; Vembris, A. Thiphenylmethane Based Structural Fragments as Building Blocks Towards Solution-Processable Heteroleptic Iridium(III) Complexes for OLED Use. *New J. Chem.* **2019**, *43*, 37−47.
(26) Toyota, A.; Katagiri, N.; Kaneko, C. Mitsunobu Reactions for the Synthesis of Carbocyclic Analogues of Nucleosides: Examination of the Regioselectivity. *Synth. Commun.* **1993**, *23*, 1295−1305.
(27) Manvar, A.; Shah, A. Diversity Oriented Efficient Access of Trisubstituted Purines via Sequential Regioselective Mitsunobu Coupling and S_NAr Based C6 Functionalizations. *Tetrahedron* **2013**, *69*, 680−691.
(28) Bucevicius, J.; Turks, M.; Tumkevicius, S. Easy Access to Isomeric 7-Deazapurine−1,2,3-Triazole Conjugates via S_NAr and CuAAC Reactions of 2,6-Diazido-7-deazapurines. *Synlett* **2018**, *29*, 525−529.
(29) Tsai, M.-H.; Hong, Y.-H.; Chang, C.-H.; Su, H.-C.; Wu, C.-C.; Matoliukstyte, A.; Simokaitiene, J.; Grigalevicius, S.; Grazulevicius, J. V.; Hsu, C.-P. 3-(9-Carbazolyl)carbazoles and 3,6-Di(9-carbazolyl)-carbazoles as Effective Host Materials for Efficient Blue Organic Electrophosphorescence. *Adv. Mater.* **2007**, *19*, 862−866.
(30) Karle, J.; Huang, L. The Glue That Holds Crystals Together: A Review. *J. Mol. Struct.* **2003**, *647*, 9−16.
(31) Wang, X.-J.; You, J.-Z. Study on the Molecular Structure and Thermal Stability of Purine Nucleoside Analogs. *J. Anal. Appl. Pyrolysis* **2015**, *111*, 1−14.
(32) Boelke, A.; Vlasenko, Y. A.; Yusubov, M. S.; Nachtsheim, B. J.; Postnikov, P. S. Thermal Stability of N-Heterocycle-Stabilized Iodanes − a Systematic Investigation. *Beilstein J. Org. Chem.* **2019**, *15*, 2311−2318.
(33) Crespo-Hernández, C. E.; Martínez-Fernández, L.; Rauer, C.; Reichardt, C.; Mai, S.; Pollum, M.; Marquetand, P.; González, L.; Corral, I. Electronic and Structural Elements That Regulate the Excited-State Dynamics in Purine Nucleobase Derivatives. *J. Am. Chem. Soc.* **2015**, *137*, 4368−4381.
(34) Traskovskis, K.; Sebris, A.; Novosjolova, I.; Turks, M.; Guzauskas, M.; Volyniuk, D.; Bezvikonnyi, O.; Grazulevicius, J. V.; Mishnev, A.; Grzibovskis, R.; et al. All-Organic Fast Intersystem Crossing Assisted Exciplexes Exhibiting Sub-microsecond Thermally Activated Delayed Fluorescence. *J. Mater. Chem. C* **2021**, *9*, 4532−4543.
(35) Taft, R. W.; Kamlet, M. J. The Solvatochromic Comparison Method. 2. The Alpha-Scale of Solvent Hydrogen-Bond Donor (HBD) Acidities. *J. Am. Chem. Soc.* **1976**, *98*, 2886−2894.
(36) Reichardt, C. Solvatochromic Dyes as Solvent Polarity Indicators. *Chem. Rev.* **1994**, *94*, 2319−2358.
(37) Lee, J.; Aizawa, N.; Numata, M.; Adachi, C.; Yasuda, T. Versatile Molecular Functionalization for Inhibiting Concentration Quenching of Thermally Activated Delayed Fluorescence. *Adv. Mater.* **2017**, *29*, No. 1604856.
(38) Royakkers, J.; Minotto, A.; Congrave, D. G.; Zeng, W.; Hassan, A.; Leventis, A.; Cacialli, F.; Bronstein, H. Suppressing Solid-State Quenching in Red-Emitting Conjugated Polymers. *Chem. Mater.* **2020**, *32*, 10140−10145.
(39) Reineke, S.; Baldo, M. A. Recent Progress in the Understanding of Exciton Dynamics within Phosphorescent OLEDs. *Phys. Status Solidi A* **2012**, *209*, 2341−2353.
(40) Wiesmann, C.; Bergenek, K.; Linder, N.; Schwarz, U. T. Photonic Crystal LEDs - Designing Light Extraction. *Laser Photonics Rev.* **2009**, *3*, 262−286.
(41) Zhang, T.; He, S. J.; Wang, D. K.; Jiang, N.; Lu, Z. H. A Multi-Zoned White Organic Light-Emitting Diode with High CRI and Low Color Temperature. *Sci. Rep.* **2016**, *6*, No. 20517.
(42) Lin, M. S.; Yang, S. J.; Chang, H. W.; Huang, Y. H.; Tsai, Y. T.; Wu, C. C.; Chou, S. H.; Mondal, E.; Wong, K. T. Incorporation of a CN Group into MCP: A New Bipolar Host Material for Highly Efficient Blue and White Electrophosphorescent Devices. *J. Mater. Chem.* **2012**, *22*, 16114−16120.
(43) Novosjolova, I.; Bizdēna, Ē.; Belyakov, S.; Turks, M. The Synthesis and X-Ray Studies of 6-Pyrrolidinyl-2-triazolyl Purine Arabinonucleoside. *Mater. Sci. Appl. Chem.* **2013**, *28*, 39−44.
(44) Latvels, J.; Grzibovskis, R.; Pudzs, K.; Vembris, A.; Blumberga, D. Photoelectrical Properties of Indandione Fragment Containing Azobenzene Compounds. *Org. Photonics VI* **2014**, *9137*, No. 91371G.
(45) Neese, F. The ORCA Program System. *Wiley Interdiscip. Rev. Comput. Mol. Sci.* **2012**, *2*, 73−78.
(46) Hanwell, M. D.; Curtis, D. E.; Lonie, D. C.; Vandermeerschd, T.; Zurek, E.; Hutchison, G. R. Avogadro: An Advanced Semantic Chemical Editor, Visualization, and Analysis Platform. *J. Cheminform.* **2012**, *4*, No. 17.
(47) Krishnan, R.; Binkley, J. S.; Seeger, R.; Pople, J. A. Self-consistent Molecular Orbital Methods. XX. A Basis Set for Correlated Wave Functions. *J. Chem. Phys.* **1980**, *72*, 650−654.
(48) Jensen, F. R.; Bedard, R. L. Cleavage of Tetrahydrofuran by Triphenylmethylmagnesium Bromide. *J. Org. Chem.* **1959**, *24*, 874−875.
(49) Smirnova, N. B.; Postovskii, I. Y. Some Purine Azides. *Zh. Vsesoyuznogo Khim. Obs. im. D.I. Mendeleeva* **1964**, *9*, 711−712.
(50) Temple, C.; Kussner, C. L.; Montgomery, J. A. Studies on the Azidoazomethine-Tetrazole Equilibrium. V. 2- and 6-Azidopurines 1. *J. Org. Chem.* **1966**, *31*, 2210−2215.

https://doi.org/10.1021/acsomega.1c06359
ACS Omega 2022, 7, 5242−5253

5. pielikums
Appendix V

Sebris, A.; Novosjolova, I.; Turks, M.

Synthesis of 7-Arylpurines from Substituted Pyrimidines

Synthesis **2022**, *54*, 5529.

doi: 10.1055/a-1898-9675

Publikācijas pielikums pieejams bez maksas Thieme mājaslapā

The Supporting Information is available free of charge on the Thieme Website

www.thieme.com

SYNTHESIS
Reviews and Full Papers in Chemical Synthesis

Publishing House and Copyright:
© 2022 by
Georg Thieme Verlag KG
Rüdigerstraße 14
70469 Stuttgart
ISSN 0039-7881

Thieme

Synthesis A. Sebris et al. Paper

Synthesis of 7-Arylpurines from Substituted Pyrimidines

Armands Sebris
Irina Novosjolova*
Māris Turks*

Institute of Technology of Organic Chemistry, Faculty of Materials Science and Applied Chemistry, Riga Technical University, Paula Valdena Str. 3, Riga 1048, Latvia
irina.novosjolova@rtu.lv
maris.turks@rtu.lv

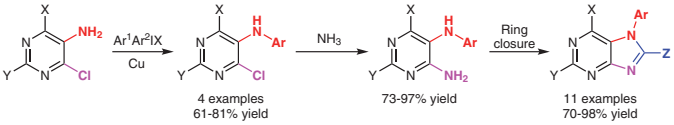

Received: 09.06.2022
Accepted after revision: 13.07.2022
Published online: 13.07.2022 (Accepted Manuscript), 13.09.2022 (Version of Record)
DOI: 10.1055/a-1898-9675; Art ID: SS-2022-06-0280-OP

Abstract A simple three-step approach for the synthesis of substituted *N*7-arylpurines with an overall yield of the whole sequence from 40% to 71% is described. *N*7-Arylpurines were constructed by *de novo* synthesis from commercially available substituted 4-chloropyrimidine-5-amines. Different substituents at purine *C*2 and *C*6 were obtained by changing the corresponding substituents of the starting pyrimidine. Further, heteroaromatic, electron-deficient, and electron-rich aromatic groups were attached to the exocyclic amino group by iodane reagents under copper catalysis. This moiety is prepared to become purine *N*7 position after the ring closure. Finally, purine *C*8 substitution was varied during the last step of the developed sequence by employing different reagents for the purine ring closing reactions or post functionalization.

Key words purines, pyrimidines, copper-catalyzed arylation, iodanes, *de novo* synthesis, imidazole ring closing

There is a significant interest in the synthesis of various purine derivatives due to their biological activity and potential application as new drugs. Purine derivatives are widely employed for treating viral diseases and cancer.[1] Many drugs containing or mimicking purine moiety are either made of heterocyclic systems with displaced nitrogen atoms or possess purine substitution pattern, which is rarely observed in nature.[2] In this context synthetic methods for purine *N*7-substitution remain topical in a toolbox of medicinal chemists. There is also rising interest towards nitrogen heterocycles as ligands for transition metals and fluorescent purines in materials science.[3]

*N*7-Alkylation of purines is known, but it often occurs as the minor process along with the major *N*9-alkylation. Also in the cases when the selectivity is switched towards *N*7-product, it still might be necessary to separate it from the *N*9-alkylated counterpart.[4] Alternatively, *N*7-alkylated isomers can be selectively prepared over at least 4 steps.[5]

On the other hand, the methods for *N*7 arylation are far fewer, and the ones that exist, have their limitations. One synthetic pathway is a *de novo* synthesis from aryl-substituted imidazoles, closing the pyrimidine ring. This pathway requires specifically prefunctionalized imidazoles to close the ring. The ring closure proceeds with yields from 9 to 85%, when preparing 7-arylhypoxanthines and up to 46% for other derivatives.[6] Another method provides 7-arylpurines in a single step from arylaminoacetonitriles and formamidine acetate.[7] This method only affords purines without substitution at *C*2, *C*6 and *C*8 in yields from 26 to 70%. Also substituted 1,2-benzoquinones can be introduced at *N*7 by the Michael addition, which is specific to 1,2-quinone derivatives.[8] A method for *N*7 arylation of protected adenine and guanine has been developed, employing Chan–Lam coupling, which proceeds with moderate yields. This method still produces a *N*7/*N*9 mixture, ratio of which varies widely depending on the substituents on the aryl group.[9] Also a method executing *N*7 arylation via C–H activation of thiophene with Selectfluor and Cu(II) catalyst is reported as a single case among other substrates.[10] Another recent article presents a single example of *N*7 arylation with mesitylene using electrophotocatalysis.[11]

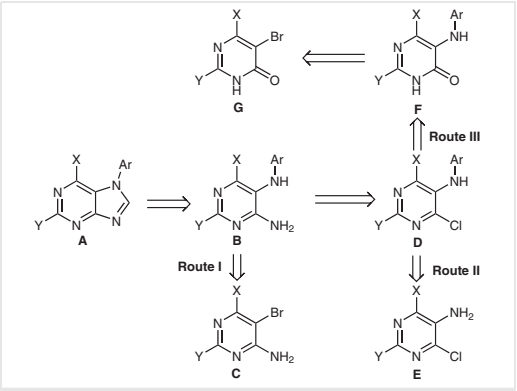

Scheme 1 Retrosynthetic analysis

In light of the aforementioned facts, there is room for improvement for synthetic pathways towards *N*7-arylpurines. Hence, we report here a straightforward approach towards *N*7-arylpurines via *de novo* synthesis from substituted pyrimidines. We tested various synthetic approaches to find the best method of introducing the aromatic moiety in the necessary position and selected the most efficient one to prepare *N*7-arylpurines.

Several synthetic pathways were initially planned (Scheme 1, Route I–III) in order to determine the optimal pyrimidine substation pattern, which would be suitable for installing *C*5-arylamino substituent before the purine ring closure. Routes I and III were designed for introduction of arylamino moiety on **C** and **G**, while Route II was designed for arylation of an amino group of **E** at pyrimidine *C*5. Route I was initially preferred since it required only 2 steps, while Route II was only slightly inferior, since we expected that the transformation from **D** to **B** would bring only a negligible reduction to the overall yield. Route III was the longest and it was unclear how well the dehydroxychlorination step would proceed.

Our first attempts were at introduction of the arylamino moiety at pyrimidine *C*5 (Route I) of **C** using S_NAr reaction or Buchwald–Hartwig cross coupling with aniline. In the S_NAr reaction product, **B** was never observed as increased

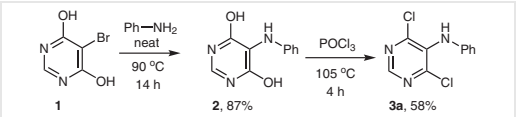

Scheme 2 Initial attempts toward intermediate **D** by retrosynthetic route **C**

temperature only caused degradation of pyrimidine. Neither the tested cross-coupling conditions between bromide **C** and anilines gave product **B**, and this route was abandoned. Similarly, our initial attempts at palladium-catalyzed cross coupling of **E** with iodobenzene were unsuccessful (Route II).

Then, inspired by a published precedent of a successful S_NAr reaction at pyrimidine *C*5 with aniline,[12] we started the sequence from compound **1** (equals to **G** in route III). The S_NAr reaction in neat aniline proceeded with up to 87% yield and the following dehydroxychlorination of compound **2** with $POCl_3$ provided compound **3a** in a 58% yield (Scheme 2).

The S_NAr reaction **1** → **2** was performed using aniline as a reagent and solvent (20 equiv) but doing so with more complicated anilines would be undesirable. Reducing the

Table 1 Optimization Studies for Arylation of Substrate **4a** with Ph_2IOTf

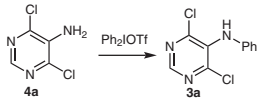

Entry	Catalyst	Base	Solvent	Temp (°C)	Time (h)	Ph_2IOTf (equiv)	Conversion to product **3a**
1	–	K_2CO_3, 1.1 equiv	Toluene	110	4	1.1	0
2	–	–	DMF	130	16	1.1	0
3	$Cu(OAc)_2$	K_3PO_4, 2.0 equiv	THF	40	16	2	0
4	CuI	K_2CO_3, 2.0 equiv	DCM	40	16	1.3	54
5	Cu_2O						0
6	CuI	Et_3N, 2.0 equiv	DCM	40	16	1.3	52
7			DCE	80			52
8		K_2CO_3, 2.0 equiv	DCE	80			55
9			NMP	80			20
10	Cu (powder)	–	NMP	80	2	1.3	55
11					2	3	85
12					2	4	100
13		Et_3N, 4.0 equiv	NMP	80	2	4	0
14		–	NMP	20	16	2	58
15				50	8	2	67
16			DMF	80	2	4	58
17			THF	60	8	4	0

amount of aniline in the reaction mixture led to solidifying of reaction mixture and incomplete conversion, which greatly complicated purification. The use of a mechanical stirrer led to reaction mixture solidifying on the stirrer and gave no improvement to conversion. Attempts to use any solvent and aniline as a reagent lead to a reduction of reactivity and only moderate conversion to compound **2** could be achieved. Here described technical issues with the S_NAr reaction might be solved by technologies used in mechanochemistry, but that will be a basis for another technological report.

Dehydroxychlorination reaction between the intermediate **2** and $POCl_3$ gave plenty of unidentified by-products. However, attempts with other dehydroxychlorination reagents, which are known for pyrimidine chlorination[13] – PCl_5, $SOCl_2$, $COCl_2$, and triphosgene – gave either degradation or a lower yield. These reactivity/selectivity problems might be due to the presence of the adjacent NH moiety,[13b] which is inherent to the structure. Given these issues, we decided to test other methods of arylation of strategic staring material **E** (Route II, Scheme 1).

Our attention was caught by several reports of heteroaromatic NH arylation that use iodine(III) reagents, including purine exocyclic NH arylation, which shares structural elements with aminopyrimidines.[14] Those examples and a report, which showed compatibility of iodine(III) reagent with our substrates,[15] encouraged us to investigate *N*-arylation with diaryliodanes in detail.

The initial attempts to perform uncatalyzed arylation using diphenyl-λ^3-iodanyl triflate[16] (Ph_2IOTf) with base[17] or without it[18] did not produce compound **3a** and left the starting material unchanged (Table 1, entries 1, 2). While the experiment with Cu(II) catalysis[19] gave no conversion to product **3a**, Cu(I) catalysis[20] showed a 54% conversion to the desired product (entry 4). Using different sources of Cu(I) (or full optimization, see table in SI) showed almost no difference, except for Cu_2O, which did not result in conversion of starting material. Optimization attempts by changing the base, solvent, and temperature, did not improve the conversion. Adding more catalyst, base, and Ph_2IOTf after the reaction had stalled, did not restart it. Using chromatography, we observed some degradation products of Ph_2IOTf, however, there was sufficiently large amount of it left intact in the reaction mixture. It should be noted that also degradation of **4a** was not observed.

Table 2 Copper-Catalyzed Arylation of 5-Aminopyrimidines **4a–d** with Diaryliodanes

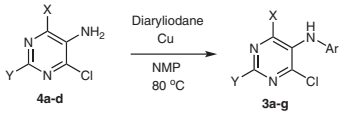

Entry	X	Y	Diaryliodane	Ar	Time (h)	Yield of product **3a–g** (%)
1	Cl	H	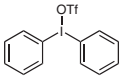		2	**3a**, 81
2	Cl	H	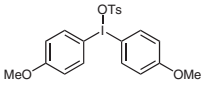	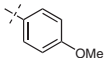	2	**3b**, 65
3	Cl	H	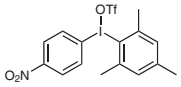	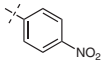	48	**3c**, 66
4	Cl	H	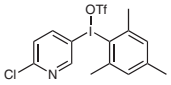		48	**3d**, 61
5	Cl	Me	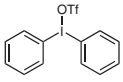		2	**3e**, 71
6	H	Cl			2	**3f**, 78
7	Cl	Cl			2	**3g**, 71

To achieve full conversion with copper catalysis, we performed an experiment using Cu(0) powder as a catalyst.[21] The initial experiment showed promising conversion and fully consumed Ph_2IOTf, so the amount of Ph_2IOTf was increased until full conversion, which was achieved at 4 equivalents of the reagent. An experiment with an added nitrogen base, which could also complex the copper source, stopped the reaction. Since it was found that a sacrificial excess of iodane reagent should be used and a part of it degrades under reaction, we attempted longer experiments at lower temperatures with a smaller excess of iodane, however, full conversion to **3a** could not be achieved this way. Using DMF instead of NMP impaired the reaction, while no conversion was observed in THF. That could be explained by a need for a highly polar solvent to dissolve the active Cu component as this reaction looks to be homogenous.

Finally, we decided to use 4 equivalents of iodane reagent for the optimized reaction conditions of *N*-arylation, as they always provided full conversion of aminopyrimidine starting materials **4a–d**. Thus, compound **3a**, for which the optimization was performed, was isolated in good 81% yield (Table 2, entry 1). Compound **3b** was synthesized to show the ability of this method to introduce aromatic groups with electron-donating groups. Bis(4-methoxyphenyl)-λ^3-iodanyl tosylate[22] can be transformed to triflate, but we were delighted to see that reaction also proceeds with tosylate in a 65% yield. It should be noted that the electronic properties of the diaryliodane had an impact on this reaction – electron-donating groups made this iodane more prone to degradation[23] and full conversion of **4a** was not achieved even with 4 equivalents of this iodane reagent. On the contrary, mesityl(4-nitrophenyl)-λ^3-iodanyl triflate,[24] which we used to introduce an electron-accepting 4-nitrophenyl moiety, was far more stable in the reaction conditions. As a consequence, it was also less reactive, requiring 48 hours to reach a satisfactory conversion and 66% isolated yield of product **3c**. Next, we planned to introduce a chloropyridine moiety to check whether the proposed synthetic approach can be performed with functionalized heteroaromatics. (6-Chloropyridin-3-yl)mesityl-λ^3-iodanyl triflate[25] was used for the N7-arylation and the electron-deficient nature of pyridine slowed down the reaction similarly to the synthesis of nitro derivative **3c**. Nevertheless, pyridyl product **3d** was isolated in a good 61% yield. To achieve differently *C*2- and *C*6-substituted purines at the end of the sequence, we performed the *N*-arylation on different pyrimidine substrates and prepared compounds **3e–g**, all with isolated yields over 70%. On the other hand, arylation of 4-chloropyrimidin-5-amine produced only degradation of this pyrimidine. It was the only pyrimidine substrate from the tested ones, which degraded under the reaction conditions. Experiments to introduce a mesityl group using bismesityl-λ^3-iodanyl triflate[16] showed no conversion, possibly due to steric hinderance.

The next step is an introduction of an amine moiety at pyrimidine *C*4 (Table 3). This was achieved by an S_NAr reaction with NH_3. For this purpose, we have used saturated NH_3 in *i*PrOH to reduce the odds of receiving hydrolysis byproducts. After a brief optimization using **3a**, we determined that the optimal temperature for a single substitution in a reasonable time is 80 °C. Compounds **5a–c** and **5e** were obtained in excellent 90–97% yields as Cl atoms at *C*4 and *C*6 are symmetrical. In the case of starting material **3d**, a small amount of a competing S_NAr product at pyridyl moiety was observed (LC-MS analysis), which slightly diminished the yield of product **5d** to 80%. In the case of products **5f** and **5g**, the chlorine atoms at *C*2 are not symmetrical to those at *C*4[26] and C6, so it is possible to get the undesired regioisomer. Fortunately, pyrimidine *C*2 position is less reactive than *C*4 and *C*6 so only small amounts of the undesired isomers were detected by LCMS and **5f** and **5g** were isolated in yields over 70%. We also observed that the S_NAr reaction proceeds more slowly in more electron-rich systems. Thus, transformation towards **5b** and **5e** required a longer reaction time for full conversion.

Table 3 S_NAr Substitution of Chloropyrimidine **3a–g** with Ammonia

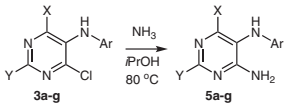

3a-g 5a-g

Entry	X	Y	Ar	Time (h)	Yield of product **5a–g** (%)
1	Cl	H		16	**5a**, 91
2	Cl	H	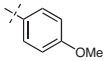	48	**5b**, 90
3	Cl	H	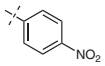	16	**5c**, 97
4	Cl	H		16	**5d**, 80
5	Cl	Me		24	**5e**, 93
6	H	Cl		16	**5f**, 73
7	Cl	Cl		16	**5g**, 75

The final step of the proposed synthetic sequence is the ring-closing reaction (Table 4). From initial experiments with **5a**, we picked ring-closing reaction conditions using $HC(OEt)_3$ under acid catalysis.[27] In this way, the reaction proceeded without any by-product formation and compound **6a** was isolated in a 96% yield. Closing ring to a *C*8-

Table 4 Purine Ring Closing Reaction of Compound **5a–g**

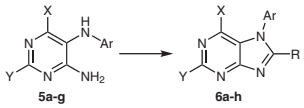

Entry	X	Y	R	Ar	Reagent	Solvent	Additive	Temp (°C)	Time (h)	Yield of product **6a–h** (%)
1	Cl	H	H		$HC(OEt)_3$	DCM	cat. aq HCl	20	16	**6a**, 96
2	Cl	H	Me		$CH_3C(OEt)_3$	DCE	cat. HCl in 1,4-dioxane	140	16	**6b**, 14
3					Ac_2O	–	–	120	1	**6b**, 78
4	Cl	H	H	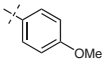	HCO_2H	$HC(OEt)_3$	$MgSO_4$	100	16	**6c**, 52
5					$HC(OEt)_3$	DCM	cat. aq HCl	40	16	**6c**, 98
6	Cl	H	H	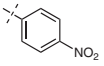	HCO_2H	$HC(OEt)_3$	$MgSO_4$	100	16	**6d**, 65
7					$HC(OEt)_3$	DCE	cat. HCl in 1,4-dioxane	80	3	**6d**, 91
8	Cl	H	H		HCO_2H	$HC(OEt)_3$	$MgSO_4$	100	16	**6e**, 44
9					$HC(OEt)_3$	DCE	cat. HCl in 1,4-dioxane	80	3	**6e**, 82
10	Cl	Me	H		$HC(OEt)_3$	DCM	cat. aq HCl	20	16	**6f**, 89
11	H	Cl	H		$HC(OEt)_3$	DCM	cat. aq HCl	20	16	**6g**, 91
12	Cl	Cl	H		$HC(OEt)_3$	DCE	cat. HCl in 1,4-dioxane	80	16	**6h**, 78

substituted purine was also considered, however $CH_3C(OEt)_3$ turned out to be far less reactive, showing some conversion to the required product only at 140 °C, at which a considerable degradation was also observed. Another method with Ac_2O as a solvent and reagent worked remarkably better,[28] giving compound **6b** in a 78% yield. We also tested this transformation with benzoic anhydride but failed to introduce two aromatic rings next to each other, most likely due to steric hinderance.

Initial attempts to perform ring closing with $HC(OEt)_3$ at 20 °C for **5b–d** did not show any conversion. Then, upon testing other methods, we found that the imidazole ring can also be formed with formic acid.[29] The downside of this method is the formation of 2 equivalents of water, which at elevated temperatures give a large amount of hydrolysis byproduct, drastically reducing the yield. The hydrolysis reaction is only moderately curtailed by an excess of added $MgSO_4$. Seeing these yields as insufficient, we returned to the initial method and by utilizing higher temperatures, DCE instead of DCM and anhydrous HCl in 1,4-dioxane to avoid heating the reaction in the presence of water, we managed to isolate **6c–e** in 82–98% yields. Compounds **6f** and **6g** were prepared at 20 °C in 89 and 91% yields, while **5g** required heating at 80 °C to provide **6h** in a 78% yield.

A specific case was the ring closure to a *C*8 trifluoromethyl-substituted purine **8** (Scheme 3). It is a two-step reaction, initially forming trifluoroacetamide, which at elevated temperatures eliminates water and forms the imidazole ring.[30] In our case, the formed trifluoromethyl-substituted purine is so electron-deficient and thus reactive under S_NAr conditions. The latter resulted in full hydrolysis (79% yield of compound **7**) with 1 equivalent of water, which is formed *in situ*. We were delighted to see that the dehydroxychlorination of intermediate **7** with $POCl_3$ proceeded well and provided target product **8** in an 88% yield. Thus, the overall yield of 70% was achieved for the whole sequence **5a** → **7** → **8** as indicated in Scheme 3.

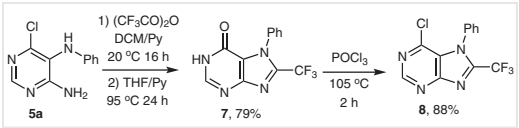

Scheme 3 Introduction of trifluoromethyl group at purine *C*8

After the imidazole ring is formed, its *C*8 position can be functionalized with chlorine atom to obtain compound **9**. Thus, deprotonation of acidic H-C8 with LDA followed by an electrophilic chlorine source (Scheme 4) gave the expected product **9**. In the case of TsCl,[31] product **9** was formed in a 58% yield, but C_2Cl_6[32] gave a higher yield of 76%.

It is important to note that the chlorine substituents also can be removed under reductive conditions. Since the *N*-arylation of 4-chloropyrimidin-5-amine failed, we could not prepare **10**[7c] directly using the above-described synthetic approach. However, the chlorine from compound **6a**

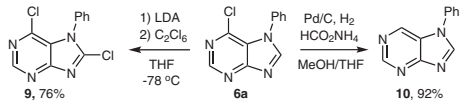

Scheme 4 Chlorination and chlorine reduction of compound **6a**

can be easily reduced giving product **10** in a 92% yield (Scheme 4). Even if the arylation of the respective pyrimidine had worked, the advantage to prepare purine **10** this way, is the lower price of the commercially available starting material **4a** compared to the corresponding 4-chloropyrimidin-5-amine.

In conclusion, we have developed a three-step approach for the *de novo* synthesis of *N*7-arylpurines from substituted pyrimidines. The best method to introduce an aromatic group at the necessary position was arylation of 5-aminopyrimidines using diaryliodanes. The further S_NAr reaction of chloropyrimidines with ammonia is a common reaction, which was performed with high yields even in cases, where regioisomers could form. Of the several ways to close the imidazole ring, orthoformate reaction with acid catalysis showed the best results for *C*8 unsubstituted purines, while *C*8-alkyl substituted purines were prepared using the corresponding anhydrides. Functional groups, which do not interfere with the reaction sequence, were located at purine *C*2 and *C*6 by choosing the appropriate pyrimidine starting material. We have prepared 6-chloro, 2-chloro, and 2,6-dichlorosubstituted purines, which can be readily functionalized to modified nucleobases, used in cross-coupling reactions or other transformations. Chlorine substituent at *C*8 position can be introduced after imidazole ring closure for more possibilities of further functionalization. Purine derivatives are well accepted privileged structures in medicinal chemistry and their application start to emerge also in the materials science. The developed synthetic approach to 7-arylpurines will be a valuable addition to the toolbox of purine ring modifications.

Commercial reagents (Acros, Alfa Aesar, Fluorochem, BLD Pharm) were used as received. Reactions and purity of the synthesized compounds were monitored by TLC using silica gel 60 F_{254} aluminum plates precoated with a 0.25 mm layer of silica gel (Merck). Visualization was accomplished by UV light. Column chromatography was performed using silica gel 60 (0.040–0.063 mm) (Upasil). Yields refer to chromatographically and spectroscopically homogeneous materials (with purity ≥95%).

NMR spectra were recorded on Bruker Avance 500 spectrometers. ^{1}H NMR spectra were recorded at 500 MHz, with internal references from residual nondeuterated solvents (δ = 7.26 for $CDCl_3$, δ = 2.50 for DMSO-d_6 and 3.31 for CD_3OD). ^{13}C NMR spectra were recorded at 125.7 MHz with internal references from solvent carbon signals (δ = 77.16 for $CDCl_3$, δ = 39.52 for DMSO-d_6 and 49.00 for CD_3OD). ^{19}F NMR spectra were recorded at 470.5 MHz with no internal reference. Coupling constants are reported in Hz and chemical shifts of signals are given in ppm and standard abbreviations were used for multiplicity assignments. The IR spectra were recorded in hexachlorobutadiene (4000–2000 cm^{-1}) and paraffin oil (2000–450 cm^{-1}) with an FTIR PerkinElmer Spectrum 100 spectrometer.

For HPLC analyses Agilent Technologies 1200 Series system was used (XBridge C18 column, 4.6 × 150 mm, particle size 3.5 µm). Eluent A: 0.1% aq TFA/CH_3CN (95:5, v/v), eluent B: CH_3CN. Gradient: 30–95% B 5 min, 95% B 5 min, 95–30% B 2 min. Flow rate: 1 mL/min. Wavelength of detection was set to 260 nm.

HRMS analysis was performed on an Agilent 1290 Infinity series UPLC system, connected to Agilent 6230 TOF LC/MS mass spectrometer; column Extend C18 RRHD 2.1 × 50 mm, 1.8 µm. Eluents: formic acid in CH_3CN (0.1%) and aq 0.1% formic acid.

5-(Phenylamino)pyrimidine-4,6-diol (2)

Aniline (36.5 mL, ρ = 1.02 g/cm^3, 0.4 mol, 20.0 equiv) was added to 5-bromopyrimidine-4,6-diol (**1**; 3.82 g, 20.0 mmol, 1.0 equiv) under argon atmosphere and the resulting reaction mixture was stirred at 90 °C for 16 h. Next, the reaction mixture was diluted with EtOAc (100 mL) and kept at 0 °C for 1 h. The precipitate was then filtered, washed with EtOH (3 × 50 mL) and dried in vacuo; yield 3.53 g (87%); colorless solid; R_f = 0.22 (DCM/EtOH 1:1); mp 205–220 °C (dec.).

IR (hexachlorobutadiene/paraffin oil): 3066, 2600, 1647, 1555, 1444, 1293, 1232 cm^{-1}.

^{1}H NMR (500 MHz, DMSO-d_6): δ = 12.50–11.00 (br s, 2 H, HO), 7.92 (s, 1 H, HC2), 7.04 (t, ^3J = 7.7 Hz, 2 H, C_6H_5), 6.72–6.54 (br s, 1 H, HN), 6.58 (t, ^3J = 7.7 Hz, 1 H, C_6H_5), 6.51 (d, ^3J = 7.7 Hz, 2 H, C_6H_5).

^{13}C NMR (125.7 MHz, DMSO-d_6): δ = 161.7, 146.2, 144.8, 128.2, 116.6, 113.8, 106.5.

HRMS (ESI): *m*/*z* [M + H]$^+$ calcd for $C_{10}H_{10}N_3O_2$: 204.0773; found: 204.0780.

4-Chloro-*N*-arylpyrimidin-5-amines 3a–g; General Procedure

Anhydrous NMP was added to a mixture of substituted 4-chloro-5-aminopyrimidine **4** (1.0 equiv), diaryliodane (4.0 equiv), and Cu (0.1 equiv). The resulting reaction mixture was stirred under argon atmosphere at 80 °C for the designated time (Table 2). The mixture was then poured into H_2O (150 mL) and extracted with a 1:1 toluene/EtOAc mixture (3 × 150 mL). The combined organic phases were then washed with sat. aq $NaHCO_3$ (150 mL), H_2O (150 mL) and brine (50 mL), dried (anhyd Na_2SO_4), filtered, and evaporated. The crude product was purified by silica gel column chromatography using either pure DCM or DCM/MeCN, as indicated by the R_f values.

4,6-Dichloro-*N*-phenylpyrimidin-5-amine (3a)

Prepared from 4,6-dichloropyrimidin-5-amine (**4a**; 1.00 g, 6.1 mmol), diphenyliodonium triflate (10.54 g, 24.5 mmol), Cu (39 mg, 0.61 mmol), and NMP (12 mL); yield: 1.19 g (81%); off-white solid; R_f = 0.45 (DCM); mp 100–104 °C.

Alternative Preparation of Compound 3a (Scheme 2)

$POCl_3$ (15 mL) was added to compound **2** (1.02 g, 5.0 mmol, 1.0 equiv) under argon atmosphere, and the reaction mixture was stirred at 105 °C for 2 h. The mixture was then evaporated, suspended in H_2O (50 mL), and extracted with EtOAc (3 × 30 mL). The combined organic phases were washed with sat. aq $NaHCO_3$ (30 mL), H_2O (30 mL) and brine (20 mL), dried (anhyd Na_2SO_4), filtered, and evaporated. The product was purified by silica gel column chromatography (DCM) and dried in vacuo; yield: 698 mg (58%).

IR (hexachlorobutadiene/paraffin oil): 3379, 1603, 1518, 1498, 1400, 1376, 1226 cm^{-1}.

^1H NMR (500 MHz, $CDCl_3$): δ = 8.52 (s, 1 H, HC2), 7.30 (t, ^3J = 7.7 Hz, 2 H, C_6H_5), 7.06 (t, ^3J = 7.7 Hz, 1 H, C_6H_5), 6.79 (d, ^3J = 7.7 Hz, 2 H, C_6H_5), 5.96–5.84 (br s, 1 H, HN).

^{13}C NMR (125.7 MHz, $CDCl_3$): δ = 154.2, 151.0, 140.7, 132.9, 129.2, 123.1, 118.4.

HRMS (ESI): *m*/*z* [M + H]$^+$ calcd for $C_{10}H_8Cl_2N_3$: 240.0095; found: 240.0100.

4,6-Dichloro-*N*-(4-methoxyphenyl)pyrimidin-5-amine (3b)

Prepared from 4,6-dichloropyrimidin-5-amine (**4a**; 732 mg, 4.5 mmol), di(4-methoxyphenyl)iodonium tosylate (9.15 g, 17.9 mmol), Cu (29 mg, 0.45 mmol), and NMP (10 mL); yield: 782 mg (65%); orange solid; R_f = 0.71 (DCM/MeCN 20:1); mp 66–68 °C.

IR (hexachlorobutadiene/paraffin oil): 3267, 1507, 1398, 1369, 1226, 1028 cm^{-1}.

^1H NMR (500 MHz, $CDCl_3$): δ = 8.43 (s, 1 H, HC2), 6.88–6.80 (m, 4 H, C_6H_4), 5.88–5.79 (br s, 1 H, HN), 3.80 (s, 3 H, OCH_3).

^{13}C NMR (125.7 MHz, $CDCl_3$): δ = 156.6, 152.0, 149.7, 134.3, 133.9, 122.1, 114.5, 55.7.

HRMS (ESI): *m*/*z* [M + H]$^+$ calcd for $C_{11}H_{10}Cl_2N_3O$: 270.0201; found: 270.0197.

4,6-Dichloro-*N*-(4-nitrophenyl)pyrimidin-5-amine (3c)

Prepared from 4,6-dichloropyrimidin-5-amine (**4a**; 1.09 g, 6.6 mmol), (2,4,6-trimethylphenyl)(4-nitrophenyl)iodonium triflate (12.61 g, 26.5 mmol), Cu (42 mg, 0.66 mmol), and NMP (12 mL). Different purification: The quenched reaction mixture was extracted with 1:1 toluene/hexane mixture (2 × 100 mL) and the combined organic phases were discarded. The aqueous phase was extracted with a 1:1 toluene/EtOAc mixture (3 × 150 mL), which was then washed with 5% aq NaOH (2 × 100 mL), H_2O (150 mL) and brine (50 mL), dried (anhyd Na_2SO_4), filtered, and evaporated. The crude mixture was suspended in Et_2O (30 mL) by ultrasonication, filtered, washed with Et_2O (2 × 5 mL) and dried in vacuo; yield: 1.25 g (66%); brown solid; R_f = 0.65 (DCM/EtOH 20:1); mp 214–218 °C.

IR (hexachlorobutadiene/paraffin oil): 3302, 1597, 1498, 1385, 1321, 1306, 1110 cm^{-1}.

^1H NMR (500 MHz, DMSO-d_6): δ = 9.45–9.38 (br s, 1 H, HN), 8.87 (s, 1 H, HC2), 8.09 (d, ^3J = 9.2 Hz, 2 H, C_6H_4), 6.82 (d, ^3J = 9.2 Hz, 2 H, C_6H_4).

^{13}C NMR (125.7 MHz, DMSO-d_6): δ = 159.3, 155.0, 149.9, 139.2, 130.6, 125.7, 113.8.

HRMS (ESI): *m*/*z* [M + H]$^+$ calcd for $C_{10}H_7Cl_2N_4O_2$: 284.9446; found: 284.9954.

4,6-Dichloro-*N*-(6-chloropyridin-3-yl)pyrimidin-5-amine (3d)

Prepared from 4,6-dichloropyrimidin-5-amine (**4a**; 1.00 g, 6.1 mmol), (2,4,6-trimethylphenyl)(6-chloropyrid-3-yl)iodonium triflate (12.40 g, 24.5 mmol), Cu (39 mg, 0.61 mmol), and NMP (12 mL); yield: 1.03 g (61%); colorless solid; R_f = 0.24 (DCM/MeCN 20:1); mp 174–178 °C.

IR (hexachlorobutadiene/paraffin oil): 3166, 1521, 1484, 1461, 1410, 1389, 1240, 1109 cm^{-1}.

^1H NMR (500 MHz, $CDCl_3$): δ = 8.60 (s, 1 H, HC2), 7.99 (s, 1 H, C5NClH$_3$), 7.25 (d, ^3J = 8.5 Hz, 1 H, C5NClH$_3$), 7.01 (d, ^3J = 8.5 Hz, 1 H, C5NClH$_3$), 5.94–5.82 (br s, 1 H, HN).

^{13}C NMR (125.7 MHz, $CDCl_3$): δ = 155.0, 152.4, 144.9, 139.7, 136.6, 131.7, 127.7, 124.3.

HRMS (ESI): *m*/*z* [M + H]$^+$ calcd for $C_9H_6Cl_3N_4$: 274.9658; found: 274.9669.

4,6-Dichloro-2-methyl-*N*-phenylpyrimidin-5-amine (3e)

Prepared from 4,6-dichloro-2-methylpyrimidin-5-amine (**4b**; 1.00 g, 5.6 mmol), diphenyliodonium triflate (9.66 g, 22.5 mmol), Cu (36 mg, 0.56 mmol), and NMP (12 mL); yield: 1.01 g (71%); off-white solid; R_f = 0.50 (DCM); mp 72–74 °C.

IR (hexachlorobutadiene/paraffin oil): 3375, 1601, 1515, 1476, 1429, 1368, 1315 cm^{-1}.

^1H NMR (500 MHz, DMSO-d_6): δ = 8.12–8.04 (br s, 1 H, HN), 7.16 (t, ^3J = 7.2 Hz, 2 H, C_6H_5), 6.78 (t, ^3J = 7.2 Hz, 1 H, C_6H_5), 6.62 (d, ^3J = 7.2 Hz, 2 H, C_6H_5), 2.60 (s, 3 H, CH_3).

^{13}C NMR (125.7 MHz, $CDCl_3$): δ = 162.7, 155.6, 141.7, 129.8, 129.4, 122.4, 117.4, 25.1.

HRMS (ESI): *m*/*z* [M + H]$^+$ calcd for $C_{11}H_{10}Cl_2N_3$: 254.0252; found: 254.0257.

2,4-Dichloro-*N*-phenylpyrimidin-5-amine (3f)

Prepared from 2,4-dichloropyrimidin-5-amine (**4c**; 1.00 g, 6.1 mmol), diphenyliodonium triflate (10.54 g, 24.5 mmol), Cu (39 mg, 0.61 mmol), and NMP (12 mL); yield: 1.14 g (78%); orange solid; R_f = 0.65 (DCM); mp 62–64 °C.

IR (hexachlorobutadiene/paraffin oil): 3225, 1564, 1497, 1440, 1387, 1192 cm^{-1}.

^1H NMR (500 MHz, $CDCl_3$): δ = 8.40 (s, 1 H, HC6), 7.41 (t, ^3J = 7.7 Hz, 2 H, C_6H_5), 7.23–7.15 (m, 3 H, C_6H_5), 6.08–5.92 (br s, 1 H, HN).

^{13}C NMR (125.7 MHz, $CDCl_3$): δ = 148.5, 147.9, 143.7, 138.5, 135.7, 130.2, 125.4, 121.8.

HRMS (ESI): *m*/*z* [M + H]$^+$ calcd for $C_{10}H_8Cl_2N_3$: 240.0095; found: 240.0097.

2,4,6-Trichloro-*N*-phenylpyrimidin-5-amine (3g)

Prepared from 2,4,6-trichloropyrimidin-5-amine (**4d**; 967 mg, 4.9 mmol), diphenyliodonium triflate (8.40 g, 19.5 mmol), Cu (31 mg, 0.49 mmol), and NMP (12 mL); yield: 957 mg (71%); off-white solid; R_f = 0.78 (DCM); mp 80–82 °C.

IR (hexachlorobutadiene/paraffin oil): 3398, 1600, 1496, 1478, 1434, 1375, 1216 cm^{-1}.

^1H NMR (500 MHz, $CDCl_3$): δ = 7.31 (t, ^3J = 7.2 Hz, 2 H, C_6H_5), 7.08 (t, ^3J = 7.2 Hz, 1 H, C_6H_5), 6.79 (d, ^3J = 7.2 Hz, 2 H, C_6H_5), 5.90–5.78 (br s, 1 H, H-N).

^{13}C NMR (125.7 MHz, $CDCl_3$): δ = 155.4, 151.4, 140.5, 131.9, 129.4, 123.5, 118.6.

HRMS (ESI): *m*/*z* [M + H]$^+$ calcd for $C_{10}H_7Cl_3N_3$: 273.9706; found: 273.9701.

N^5-Arylpyrimidin-4,5-diamines 5a–g; General Procedure

Saturated NH_3 solution in *i*-PrOH (5 mL per mmol of substrate **3**) was added to substituted 4-chloro-5-aminopyrimidine **3** and the resulting reaction mixture was stirred in a pressure flask at 80 °C for the designated time (Table 3). The reaction mixture was then evaporated, and the residue was suspended in H_2O and kept at 0 °C for 1 h. The product was isolated by filtration, washed on the filter with H_2O and dried in vacuo.

6-Chloro-N^5-phenylpyrimidine-4,5-diamine (5a)

Yield: 1.41 g (91% from 1.68 g, 7.0 mmol of compound **3a**); colorless solid; R_f = 0.38 (DCM/EtOH 20:1); mp 151–153 °C.

IR (hexachlorobutadiene/paraffin oil): 3383, 3090, 1651, 1563, 1497, 1473, 1351, 1271 cm^{-1}.

^{1}H NMR (500 MHz, DMSO-d_6): δ = 8.11 (s, 1 H, HC2), 7.40–6.55 (br s, 2 H, -NH$_2$), 7.38–7.28 (br s, 1 H, HN), 7.13 (t, ^3J = 7.7 Hz, 2 H, C$_6$H$_5$), 6.69 (t, ^3J = 7.7 Hz, 1 H, C$_6$H$_5$), 6.49 (d, ^3J = 7.7 Hz, 2 H, C$_6$H$_5$).

^{13}C NMR (125.7 MHz, DMSO-d_6): δ = 162.9, 155.7, 154.7, 144.9, 128.9, 118.0, 115.6, 113.5.

HRMS (ESI): m/z [M + H]$^+$ calcd for $C_{10}H_{10}ClN_4$: 221.0594; found: 221.0604.

6-Chloro-N^5-(4-methoxyphenyl)pyrimidine-4,5-diamine (5b)

Yield: 451 mg (90% from 540 mg, 2.0 mmol of compound **3b**); off-white solid; R_f = 0.38 (DCM/EtOH); mp 137–139 °C.

IR (hexachlorobutadiene/paraffin oil): 3372, 3121, 1637, 1561, 1509, 1473, 1277, 1240 cm^{-1}.

^{1}H NMR (500 MHz, $CDCl_3$): δ = 8.22 (s, 1 H, HC2), 6.82 (d, ^3J = 8.2 Hz, 2 H, C$_6$H$_4$), 6.65 (d, ^3J = 8.2 Hz, 2 H, C$_6$H$_4$), 5.38–5.12 (br s, 3 H, HN, NH$_2$), 3.77 (s, 3 H, OCH$_3$).

^{13}C NMR (125.7 MHz, $CDCl_3$): δ = 160.1, 155.0, 154.0, 153.9, 135.6, 118.0, 117.6, 115.1, 55.8.

HRMS (ESI): m/z [M + H]$^+$ calcd for $C_{11}H_{12}ClN_4O$: 251.0700; found: 251.0704.

6-Chloro-N^5-(4-nitrophenyl)pyrimidine-4,5-diamine (5c)

Yield: 519 mg (97% from 570 mg, 2.0 mmol of compound **3c**); brown solid; R_f = 0.23 (DCM/EtOH 20:1); mp 219–221 °C.

IR (hexachlorobutadiene/paraffin oil): 3450, 3325, 1643, 1590, 1476, 1300, 1267, 1109 cm^{-1}.

^{1}H NMR (500 MHz, CD_3OD): δ = 8.17 (s, 1 H, HC2), 8.09 (d, ^3J = 8.8 Hz, 2 H, C$_6$H$_4$), 6.63 (d, ^3J = 8.8 Hz, 2 H, C$_6$H$_4$).

^{13}C NMR (125.7 MHz, CD_3OD): δ = 164.5, 158.3, 157.0, 152.6, 140.7, 127.0, 115.6, 113.8.

HRMS (ESI): m/z [M + H]$^+$ calcd for $C_{10}H_9ClN_5O_2$: 266.0445; found: 266.0452.

6-Chloro-N^5-(6-chloropyridin-3-yl)pyrimidine-4,5-diamine (5d)

Yield: 412 mg (80% from 552 mg, 2.0 mmol of compound **3d**); colorless solid; R_f = 0.15 (DCM/EtOH 20:1); mp 143–145 °C.

IR (hexachlorobutadiene/paraffin oil): 3460, 3200, 1622, 1569, 1538, 1464, 1350, 1287 cm^{-1}.

^{1}H NMR (500 MHz, $CDCl_3$): δ = 8.32 (s, 1 H, HC2), 7.90 (s, 1 H, C5NClH$_3$), 7.19 (d, ^3J = 8.5 Hz, 1 H, C5NClH$_3$), 6.85 (d, ^3J = 8.5 Hz, 1 H, C5NClH$_3$), 5.38–5.18 (br. s, 1 H, HN, NH$_2$).

^{13}C NMR (125.7 MHz, $CDCl_3$): δ = 161.2, 156.9, 155.9, 143.0, 138.7, 137.0, 124.7, 124.5, 115.3.

HRMS (ESI): m/z [M + H]$^+$ calcd for $C_9H_8Cl_2N_5$: 256.0157; found: 256.0161.

6-Chloro-2-methyl-N^5-phenylpyrimidine-4,5-diamine (5e)

Yield: 656 mg (93% from 762 g, 3.0 mmol of compound **3e**); colorless solid; R_f = 0.35 (DCM/EtOH 20:1); mp 172–174 °C.

IR (hexachlorobutadiene/paraffin oil): 3468, 3074, 1649, 1601, 1550, 1488, 1423, 1299 cm^{-1}.

^{1}H NMR (500 MHz, DMSO-d_6): δ = 7.50–6.50 (br s, 2 H, NH$_2$), 7.24–7.16 (br s, 1 H, HN), 7.11 (t, ^3J = 7.2 Hz, 2 H, C$_6$H$_5$), 6.67 (t, ^3J = 7.2 Hz, 1 H, C$_6$H$_5$), 6.47 (d, ^3J = 7.2 Hz, 2 H, C$_6$H$_5$), 2.33 (s, 3 H, CH$_3$).

^{13}C NMR (125.7 MHz, DMSO-d_6): δ = 163.8, 162.9, 155.9, 145.4, 128.9, 117.7, 113.3, 112.9, 24.8.

HRMS (ESI): m/z [M + H]$^+$ calcd for $C_{11}H_{12}ClN_4$: 235.0750; found: 235.0752.

2-Chloro-N^5-phenylpyrimidine-4,5-diamine (5f)

Yield: 486 mg (73% from 720 g, 3.0 mmol of compound **3f**); off-white solid; R_f = 0.40 (DCM/EtOH 20:1); mp 189–191 °C.

IR (hexachlorobutadiene/paraffin oil): 3283, 3117, 1667, 1578, 1494, 1386, 1273, 1248 cm^{-1}.

^{1}H NMR (500 MHz, DMSO-d_6): δ = 7.89 (s, 1 H, HC2), 7.31–7.03 (br s, 2 H, NH$_2$), 7.26–7.18 (br s, 1 H, HN), 7.19 (t, ^3J = 7.2 Hz, 2 H, C$_6$H$_5$), 6.83–6.74 (m, 3 H, C$_6$H$_5$).

^{13}C NMR (125.7 MHz, DMSO-d_6): δ = 160.3, 152.9, 147.3, 144.2, 129.2, 120.9, 119.3, 115.5.

HRMS (ESI): m/z [M + H]$^+$ calcd for $C_{10}H_{10}ClN_4$: 221.0594; found: 221.0596.

2,6-Dichloro-N^5-phenylpyrimidine-4,5-diamine (5g)

Yield: 574 mg (75% from 825 mg, 3.0 mmol of compound **3g**); colorless solid; R_f = 0.53 (DCM/EtOH 20:1); mp 157–159 °C.

IR (hexachlorobutadiene/paraffin oil): 3467, 3287, 1650, 1602, 1548, 1492, 1366, 1005 cm^{-1}.

^{1}H NMR (500 MHz, DMSO-d_6 + D_2O): δ = 7.13 (t, ^3J = 7.2 Hz, 2 H, C$_6$H$_5$), 6.71 (t, ^3J = 7.2 Hz, 1 H, C$_6$H$_5$), 6.50 (d, ^3J = 7.2 Hz, 2 H, C$_6$H$_5$).

^{13}C NMR (125.7 MHz, DMSO-d_6 + D_2O): δ = 164.3, 156.2, 154.9, 144.8, 129.6, 119.1, 115.6, 114.1.

HRMS (ESI): m/z [M + H]$^+$ calcd for $C_{10}H_9Cl_2N_4$: 255.0204; found: 255.0203.

7-Arylpurines 6a–h; General Procedure

The required orthoester (4.0 equiv) and one drop of additive (Table 4) were added to substituted 4,5-diaminopyrimidine **5** (1.0 equiv) in the indicated solvent. The resulting reaction mixture was stirred for the designated time and temperature (Table 4). The reaction mixture was diluted with DCM (20 mL per mmol of substrate **5**) and washed with sat. aq $NaHCO_3$ (10 mL per mmol of substrate **5**), H_2O (10 mL per mmol of substrate **5**) and brine (5 mL per mmol of substrate **5**), dried (anhyd Na_2SO_4), filtered, and evaporated. If necessary, the products **6e**,**h** were purified using silica gel column chromatography by eluents indicated with the R_f values.

7-Arylpurines 6c–e; Alternative Procedure

HCO_2H (2.0 equiv) and anhyd $MgSO_4$ (10 equiv) were added to substituted 4,5-diaminopyrimidine **5** (250 mg, 1.0 equiv) in triethyl orthoformate (5 mL). The resulting reaction mixture was stirred for 16 h at 100 °C. The mixture was then filtered, and the inorganic material was washed with acetone (2 × 20 mL), which was evaporated. The product was purified by silica gel column chromatography.

6-Chloro-7-phenyl-7*H*-purine (6a)

Prepared from compound **5a** (884 mg, 4.0 mmol), triethyl orthoformate (2.7 mL, ρ = 0.89 g/cm^3, 16.0 mmol), aq HCl, and DCM (40 mL) at 20 °C for 16 h; yield: 882 mg (96%); off-white solid; R_f = 0.15 (DCM/MeCN 10:1); mp 203–205 °C.

IR (hexachlorobutadiene/paraffin oil): 1595, 1536, 1498, 1402, 1343, 1210, 961 cm^{-1}.

^1H NMR (500 MHz, $CDCl_3$): δ = 8.97 (s, 1 H, HC2), 8.97 (s, 1 H, HC8), 7.64–7.56 (m, 3 H, C_6H_5), 6.65 (d, ^3J = 7.2 Hz, 2 H, C_6H_5).

^{13}C NMR (125.7 MHz, $CDCl_3$): δ = 162.0, 152.9, 149.0, 143.8, 134.5, 130.3, 129.7, 127.4, 123.2.

HRMS (ESI): *m*/*z* [M + H]$^+$ calcd for $C_{11}H_8ClN_4$: 231.0437; found: 231.0441.

6-Chloro-8-methyl-7-phenyl-7*H*-purine (6b)

Prepared from compound **5a** (221 mg, 1.0 mmol), triethyl orthoacetate (0.73 mL, ρ = 0.89 g/cm^3, 4.0 mmol), HCl in 1,4-dioxane, DCE (10 mL) at 140 °C for 16 h; yield: 34 mg (14%).

Alternative Preparation of 6b Using Ac_2O

Ac_2O (6 mL) was added to compound **5a** (221 mg, 1.0 mmol, 1.0 equiv) and the resulting reaction mixture was stirred at 120 °C for 1 h. The mixture was poured into H_2O (70 mL) and extracted with DCM (3 × 40 mL). The combined organic phases were washed with sat. aq $NaHCO_3$ (3 × 30 mL), H_2O (30 mL) and brine (20 mL), dried (anhyd Na_2SO_4), filtered, and evaporated. The product was purified by silica gel column chromatography (DCM/EtOH 0 → 3%) and dried in vacuo; yield: 191 mg (78%); colorless solid; R_f = 0.38 (DCM/EtOH 20:1); mp 184–186 °C.

IR (hexachlorobutadiene/paraffin oil): 1595, 1545, 1501, 1442, 1408, 1239, 1159 cm^{-1}.

^1H NMR (500 MHz, $CDCl_3$): δ = 8.86 (s, 1 H, HC2), 7.65–7.55 (m, 3 H, C_6H_5), 6.65 (d, ^3J = 6.7 Hz, 2 H, C_6H_5), 2.52 (s, 3 H, CH_3).

^{13}C NMR (125.7 MHz, $CDCl_3$): δ = 161.4, 159.5, 152.6, 142.3, 134.6, 130.5, 129.9, 128.4, 124.5, 14.9.

HRMS (ESI): *m*/*z* [M + H]$^+$ calcd for $C_{12}H_{10}ClN_4$: 245.0594; found: 245.0602.

6-Chloro-7-(4-methoxyphenyl)-7*H*-purine (6c)

Prepared from compound **5b** (251 mg, 1.0 mmol), triethyl orthoformate (0.67 mL, ρ = 0.89 g/cm^3, 4.0 mmol), aq HCl, and DCM (10 mL) at 40 °C for 16 h; yield: 255 mg (98%); colorless solid; R_f = 0.40 (DCM/EtOH 20:1); mp 218–222 °C.

Alternative Procedure: Prepared from compound **5b** (250 mg, 1.0 mmol), HCO_2H (75 μL, ρ = 1.22 g/cm^3, 2.0 mmol), and $MgSO_4$ (1.2 g, 10.0 mmol); yield: 137 mg (52%).

IR (hexachlorobutadiene/paraffin oil): 1597, 1535, 1512, 1447, 1342, 1249, 1205, 1172 cm^{-1}.

^1H NMR (500 MHz, $CDCl_3$): δ = 8.94 (s, 1 H, HC2), 8.29 (s, 1 H, HC8), 7.36 (d, ^3J = 8.4 Hz, 2 H, C_6H_4), 7.06 (d, ^3J = 8.4 Hz, 2 H, C_6H_4), 3.91 (s, 3 H, OCH_3).

^{13}C NMR (125.7 MHz, $CDCl_3$): δ = 161.9, 161.0, 152.9, 149.3, 143.9, 128.7, 127.1, 123.4, 114.7, 55.9.

HRMS (ESI): *m*/*z* [M + H]$^+$ calcd for $C_{12}H_{10}ClN_4O$: 261.0543; found: 261.0552.

6-Chloro-7-(4-nitrophenyl)-7*H*-purine (6d)

Prepared from compound **5c** (265 mg, 1.0 mmol), triethyl orthoformate (0.67 mL, ρ = 0.89 g/cm^3, 4.0 mmol), HCl in 1,4-dioxane, and DCE (10 mL) at 80 °C for 3 h; yield: 251 mg (91%); yellow solid; R_f = 0.40 (DCM/EtOH 20:1); mp 243–245 °C.

Alternative Procedure: Prepared from compound **5c** (250 mg, 0.94 mmol), HCO_2H (71 μL, ρ = 1.22 g/cm^3, 1.9 mmol), and $MgSO_4$ (1.1 g, 9.4 mmol); yield: 169 mg (65%).

IR (hexachlorobutadiene/paraffin oil): 1590, 1520, 1497, 1401, 1343, 1206 cm^{-1}.

^1H NMR (500 MHz, DMSO-d_6): δ = 9.09 (s, 1 H, HC8), 8.94 (s, 1 H, HC2), 8.48 (d, ^3J = 8.5 Hz, 2 H, C_6H_4), 8.03 (d, ^3J = 8.5 Hz, 2 H, C_6H_4).

^{13}C NMR (125.7 MHz, DMSO-d_6): δ = 161.9, 152.2, 150.7, 147.8, 142.5, 139.7, 128.9, 124.4, 122.8.

HRMS (ESI): *m*/*z* [M + H]$^+$ calcd for $C_{11}H_7ClN_5O_2$: 276.0288; found: 276.0285.

6-Chloro-7-(6-chloropyridin-3-yl)-7*H*-purine (6e)

Prepared from compound **5d** (179 mg, 0.7 mmol), triethyl orthoformate (0.46 mL, ρ = 0.89 g/cm^3, 2.8 mmol), HCl in 1,4-dioxane, DCE (7 mL) at 80 °C for 3 h; yield: 153 mg (82%); colorless solid; R_f = 0.33 (DCM/EtOH 20:1); mp 176–178 °C.

Alternative Procedure: Prepared from compound **5d** (250 mg, 0.98 mmol), HCO_2H (71 μL, ρ = 1.22 g/cm^3, 1.9 mmol), and $MgSO_4$ (1.2 g, 9.8 mmol); yield: 116 mg (44%).

IR (hexachlorobutadiene/paraffin oil): 1597, 1536, 1475, 1406, 1343, 1313, 1214, 1108 cm^{-1}.

^1H NMR (500 MHz, $CDCl_3$): δ = 9.01 (s, 1 H, HC2), 8.59 (s, 1 H, $C5NClH_3$), 8.33 (s, 1 H, HC8), 7.81 (d, ^3J = 8.5 Hz, 1 H, $C5NClH_3$), 7.61 (d, ^3J = 8.5 Hz, 1 H, $C5NClH_3$).

^{13}C NMR (125.7 MHz, $CDCl_3$): δ = 162.2, 153.6, 153.4, 148.5, 147.6, 143.6, 137.3, 130.5, 125.1, 123.1.

HRMS (ESI): *m*/*z* [M + H]$^+$ calcd for $C_{10}H_6Cl_2N_5$: 266.0000; found: 266.0006.

6-Chloro-2-methyl-7-phenyl-7*H*-purine (6f)

Prepared from compound **5e** (353 mg, 1.5 mmol), triethyl orthoformate (1.0 mL, ρ = 0.89 g/cm^3, 6.0 mmol), aq HCl, and DCM (15 mL) at 20 °C for 16 h; yield: 328 mg (89%); colorless solid; R_f = 0.43 (DCM/EtOH 20:1); mp 268–270 °C.

IR (hexachlorobutadiene/paraffin oil): 3051, 1607, 1537, 1495, 1474, 1397, 1339, 1229 cm^{-1}.

^1H NMR (500 MHz, $CDCl_3$): δ = 8.26 (s, 1 H, HC8), 7.62–7.55 (m, 3 H, C_6H_5), 7.47–7.42 (m, 2 H, C_6H_5).

^{13}C NMR (125.7 MHz, $CDCl_3$): δ = 163.1, 162.8, 148.9, 143.3, 134.7, 130.1, 129.6, 127.3, 121.1, 25.8.

HRMS (ESI): *m*/*z* [M + H]$^+$ calcd for $C_{12}H_{10}ClN_4$: 245.0594; found: 245.0592.

2-Chloro-7-phenyl-7*H*-purine (6g)

Prepared from compound **5f** (332 mg, 1.5 mmol), triethyl orthoformate (1.0 mL, ρ = 0.89 g/cm^3, 6.0 mmol), aq HCl, and DCM (15 mL) at 20 °C for 16 h; yield 316 mg (91%); off-white solid; R_f = 0.20 (DCM/MeCN 10:1); mp 210–220 °C (dec.).

IR (hexachlorobutadiene/paraffin oil): 1605, 1555, 1501, 1416 1389, 1336, 1181 cm^{-1}.

^1H NMR (500 MHz, $CDCl_3$): δ = 8.90 (s, 1 H, HC6), 8.48 (s, 1 H, HC8), 7.67 (t, ^3J = 7.5 Hz, 2 H, C_6H_5), 7.59 (t, ^3J = 7.5 Hz, 1 H, C_6H_5), 7.52 (d, ^3J = 7.5 Hz, 2 H, C_6H_5).

^{13}C NMR (125.7 MHz, $CDCl_3$): δ = 163.4, 155.5, 148.3, 142.5, 134.7, 130.9, 129.8, 124.6, 123.7.

HRMS (ESI): m/z [M + H]$^+$ calcd for $C_{11}H_8ClN_4$: 231.0437; found: 231.0439.

2,6-Dichloro-7-phenyl-7*H*-purine (6h)

Prepared from compound **5g** (383 mg, 1.5 mmol), triethyl orthoformate (1.0 mL, ρ = 0.89 g/cm^3, 6.0 mmol), HCl in 1,4-dioxane, DCE (15 mL) at 80 °C for 16 h; yield: 312 mg (78%); off-white solid; R_f = 0.24 (DCM/MeCN 20:1); mp 240–242 °C.

IR (hexachlorobutadiene/paraffin oil): 1594, 1495, 1403, 1338, 1228, 1212, 999 cm^{-1}.

^{1}H NMR (500 MHz, $CDCl_3$): δ = 8.34 (s, 1 H, HC8), 7.67–7.57 (m, 3 H, C_6H_5), 7.52 (d, ^3J = 7.2 Hz, 2 H, C_6H_5).

^{13}C NMR (125.7 MHz, $CDCl_3$): δ = 163.6, 153.7, 150.3, 144.7, 134.1, 130.6, 129.8, 127.3, 122.4.

HRMS (ESI): m/z [M + H]$^+$ calcd for $C_{11}H_7Cl_2N_4$: 265.0048; found: 265.0056.

7-Phenyl-8-trifluoromethyl-7*H*-hypoxanthine (7)

Trifluoracetic anhydride (0.28 mL, ρ = 1.51 g/cm^3, 2.0 mmol, 2.0 equiv) was added to a solution of compound **5a** (221 mg, 1.0 mmol, 1.0 equiv) in a mixture of DCM (10 mL) and pyridine (1.3 mL). The resulting reaction mixture was stirred at 20 °C for 16 h. Then the mixture was evaporated to dryness and the residue was transferred to a pressure vial by resuspending it in anhyd THF (10 mL) and pyridine (1.7 mL). The resulting mixture was stirred at 95 °C for 24 h. Then it was evaporated, and the residue was suspended in H_2O (20 mL) and filtered. The precipitate was washed with H_2O (2 × 20 mL) and dried in vacuo; yield: 221 mg (79%); colorless solid; R_f = 0.23 (DCM/EtOH 20:1); mp >300 °C.

IR (hexachlorobutadiene/paraffin oil): 1682, 1506, 1409, 1291, 1164, 1152 cm^{-1}.

^{1}H NMR (500 MHz, DMSO-d_6): δ = 13.50–11.75 (br. s, 1 H, H-N), 8.15 (s, 1 H, HC2), 7.63–7.50 (m, 5 H, C_6H_5).

^{13}C NMR (125.7 MHz, DMSO-d_6): δ = 154.4, 153.7, 146.6, 139.1 (q, $^2J_{C,F}$ = 38 Hz), 134.2, 130.1, 128.8, 127.5, 119.1, 118.3 (q, $^1J_{C,F}$ = 272 Hz).

^{19}F NMR (470.5 MHz, DMSO-d_6): δ = –59.4.

HRMS (ESI): m/z [M + H]$^+$ calcd for $C_{12}H_8F_3N_4O$: 281.0650; found: 281.0651.

6-Chloro-7-phenyl-8-trifluoromethyl-7*H*-purine (8)

$POCl_3$ (8 mL) was added to compound **7** (221 mg, 0.8 mmol, 1.0 equiv) under argon atmosphere and the resulting reaction mixture was stirred at 105 °C for 2 h. The mixture was evaporated, and the residue purified by silica gel column chromatography (DCM/MeCN 0 → 4%); yield: 207 mg (88%); colorless solid; R_f = 0.56 (DCM/MeCN 10:1); mp 190–193 °C.

IR (hexachlorobutadiene/paraffin oil): 1586, 1514, 1449, 1416, 1287, 1217, 1165, 1151, 1141 cm^{-1}.

^{1}H NMR (500 MHz, $CDCl_3$): δ = 9.04 (s, 1 H, HC2), 7.68 (t, ^3J = 7.5 Hz, 1 H, C_6H_5), 7.60 (t, ^3J = 7.5 Hz, 2 H, C_6H_5), 7.45 (d, ^3J = 7.5 Hz, 2 H, C_6H_5).

^{13}C NMR (125.7 MHz, $CDCl_3$): δ = 158.7, 154.0, 146.6 (q, $^2J_{C,F}$ = 40 Hz), 145.6, 133.0, 131.4, 129.7, 128.5, 125.3 118.1 (q, $^1J_{C,F}$ = 274 Hz).

^{19}F NMR (470.5 MHz, $CDCl_3$): δ = –61.1.

HRMS (ESI): m/z [M + H]$^+$ calcd for $C_{12}H_7ClF_3N_4$: 299.0311; found: 299.0312.

6,8-Dichloro-7-phenyl-7*H*-purine (9)

A solution of BuLi in hexanes (2.4 M, 0.42 mL, 1 mmol, 2.0 equiv) was dropwise added to a solution of *i*-Pr_2NH (0.15 mL, ρ = 0.72 g/cm^3, 1.05 mmoL, 2.1 equiv) in anhyd THF (5 mL) at –78 °C under argon atmosphere. The resulting LDA solution was stirred at –78 °C for 30 min. A solution of compound **6a** (115 mg, 0.5 mmol, 1.0 equiv) in anhyd THF (5 mL) was then dropwise added and the freshly formed solution of LDA and the formed mixture was stirred at –78 °C for 1 h. A solution of hexachloroethane (237 mg, 1.0 mmol, 2.0 equiv) in anhyd THF (5 mL) was then dropwise added and the reaction mixture was stirred at –78 °C for 1 h. Upon completion, the mixture was diluted with sat. aq NH_4Cl and stirred until it warmed up to 20 °C. The neutralized mixture was extracted with EtOAc (3 × 50 mL), the combined organic phases were washed with H_2O (30 mL) and brine (20 mL), dried (anhyd Na_2SO_4), filtered, and evaporated. The product was purified by silica gel column chromatography (DCM/MeCN 0 → 8%) and dried in vacuo; yield: 101 mg (76%); colorless solid; R_f = 0.30 (DCM/MeCN 10:1); mp 212–214 °C.

IR (hexachlorobutadiene/paraffin oil): 1586, 1541, 1439, 1400, 1349, 1234, 982 cm^{-1}.

^{1}H NMR (500 MHz, $CDCl_3$): δ = 8.90 (s, 1 H, HC2), 7.68–7.57 (m, 3 H, C_6H_5), 7.45 (d, ^3J = 7.4 Hz, 2 H, C_6H_5).

^{13}C NMR (125.7 MHz, $CDCl_3$): δ = 159.9, 153.2, 149.3, 142.7, 133.3, 131.1, 129.8, 128.7, 125.1.

HRMS (ESI): m/z [M + H]$^+$ calcd for $C_{11}H_7Cl_2N_4$: 265.0048; found: 265.0048.

7-Phenyl-7*H*-purine (10)[7c]

HCO_2NH_4 (252 mg, 4.0 mmol, 4.0 equiv) and 10 w% Pd/C (23 mg, 10 w%) were added to a solution of compound **6a** (231 mg, 1.0 mmol, 1.0 equiv) in a 1:1 THF/EtOH mixture (40 mL). Then a mild H_2 bubbling was applied to the resulting stirred reaction mixture for 30 min. Next, the bubbling was stopped and the mixture was stirred under H_2 atmosphere for 16 h (rubber balloon containing H_2, which ensures ambient pressure). The mixture was then filtered through Celite and washed with EtOH (2 × 20 mL). The combined filtrates were evaporated and the product was dried in vacuo; yield: 180 mg (92%); colorless solid.

^{1}H NMR (500 MHz, $CDCl_3$): δ = 9.21 (s, 1 H, HC2), 9.06 (s, 1 H, HC6), 8.47 (s, 1 H, HC8), 7.65 (t, ^3J = 7.4 Hz, 2 H, C_6H_5), 7.59–7.50 (m, 3 H, C_6H_5).

Conflict of Interest

The authors declare no conflict of interest.

Funding Information

This work is supported by the Latvia-Lithuania-Taiwan joint grant LV-LT-TW/2022/9 and Hubert Curien partnership program 'OSMOSE' Latvia-France mobility project LV-FR/2022/1 by the Latvian Council of Science.

Supporting Information

Supporting information for this article is available online at https://doi.org/10.1055/a-1898-9675.

References

(1) (a) Seley-Radtke, K. L.; Yates, M. K. *Antiviral Res.* **2018**, *154*, 66. (b) Zhou, D.; Xie, D.; He, F.; Song, B.; Hu, D. *Bioorg. Med. Chem. Lett.* **2018**, *28*, 2091. (c) *CLL Trialists' Collaborative Group* **2012**, *97*, 428. (d) Shelton, J.; Lu, X.; Hollenbaugh, J. A.; Cho, J. H.; Amblard, F.; Schinazi, R. F. *Chem. Rev.* **2016**, *116*, 14379. (e) Jordheim, L. P.; Durantel, D.; Zoulim, F.; Dumontet, C. *Nat. Rev. Drug Discov.* **2013**, *12*, 447.

(2) Yates, M. K.; Seley-Radtke, K. L. *Antiviral Res.* **2019**, *162*, 5.

(3) (a) Idris, M.; Kapper, S. C.; Tadle, A. C.; Batagoda, T.; Ravinson, D. S. M.; Abimbola, O.; Djurovich, P. I.; Kim, J.; Coburn, C.; Forrest, S. R.; Thompson, M. E. *Adv. Optical Mater.* **2021**, *9*, 2001994. (b) Yun, B.-S.; Kim, J.-H.; Kim, S.-Y.; Son, H.-J.; Cho, D. W.; Kang, S. O. *Phys. Chem. Chem. Phys.* **2019**, *21*, 7155. (c) Sebris, A.; Traskovskis, K.; Novosjolova, I.; Turks, M. *Chem. Heterocycl. Compd.* **2021**, *57*, 560. (d) Traskovskis, K.; Sebris, A.; Novosjolova, I.; Turks, M.; Guzauskas, M.; Volyniuk, D.; Bezvikonnyi, O.; Grazulevicius, J.; Mishnev, A.; Grzibovskis, R.; Vembris, A. *J. Mater. Chem. C* **2021**, *9*, 4532. (e) Sebris, A.; Novosjolova, I.; Traskovskis, K.; Kokars, V.; Tetervenoka, N.; Vembris, A.; Turks, M. *ACS Omega* **2022**, *7*, 5242.

(4) (a) Chen, S.; Graceffa, R. F.; Boezio, A. A. *Org. Lett.* **2015**, *18*, 16. (b) Stanovnik, B.; Tišler, M.; Hribar, A.; Barlin, G. B.; Brown, D. J. *Aust. J. Chem.* **1981**, *34*, 1729. (c) Lambertucci, C.; Cristalli, G.; Dal Ben, D.; Kachare, D. D.; Bolcato, C.; Klotz, K.-N.; Spalutto, G.; Volpini, R. *Purinergic Signal.* **2007**, *3*, 339. (d) Česnek, M.; Masojídková, M.; Holý, A.; Šolínová, V.; Koval, D.; Kašička, V. *Collect. Czech. Chem. Commun.* **2006**, *71*, 1303. (e) Toyota, A.; Katagiri, N.; Kaneko, C. *Synth. Commun.* **1993**, *23*, 1295.

(5) (a) Kotek, V.; Chudíková, N.; Tobrman, T.; Dvořák, D. *Org. Lett.* **2010**, *24*, 5724. (b) Aarhus, T. I.; Fritze, U. F.; Hennum, M.; Gundersen, L.-L. *Tetrahedron Lett.* **2014**, *55*, 5748. (c) Liu, J.; Dang, Q.; Wei, Z.; Shi, F.; Bai, X. *J. Comb. Chem.* **2006**, *8*, 410. (d) Fu, H.; Lam, Y. *J. Comb. Chem.* **2005**, *7*, 734.

(6) (a) Verkoyen, C.; Golovinsky, E.; Müller, G.; Kölbel, M.; Norpoth, K. *Liebigs Ann. Chem.* **1987**, 957. (b) Gruner, M.; Rehwald, M.; Eckert, K.; Gewald, K. *Heterocycles* **2000**, *53*, 2363.

(7) (a) Bredereck, H.; Effenberger, F.; Rainer, G. *Justus Liebigs Ann. Chem.* **1964**, *673*, 82. (b) Laufer, S. A.; Domeyer, D. M.; Scior, T. R. F.; Albrecht, W.; Hauser, D. R. J. *J. Med. Chem.* **2005**, *48*, 710. (c) Castillo, J.-C.; Orrego-Hernández, J.; Portilla, J. *Eur. J. Org. Chem.* **2016**, 3824.

(8) (a) McCoull, K. D.; Rindgen, D.; Blair, I. A.; Penning, T. M. *Chem. Res. Toxicol.* **1999**, *12*, 237. (b) Xue, W.; Siner, A.; Rance, M.; Jayasimhulu, K.; Talaska, G.; Warshawsky, D. *Chem. Res. Toxicol.* **2002**, *15*, 915. (c) Stack, D. E.; Li, G.; Hill, A.; Hoffman, N. *Chem. Res. Toxicol.* **2008**, *21*, 1415.

(9) Keder, R.; Dvořáková, H.; Dvořák, D. *Eur. J. Org. Chem.* **2009**, 1522.

(10) Sun, K.; Zhu, Z.; Sun, J.; Liu, L.; Wang, X. *J. Org. Chem.* **2016**, *81*, 1476; however, this paper provides disputable NMR data for the obtained N7 arylated product.

(11) Huang, H.; Strater, Z. M.; Rauch, M.; Shee, J.; Sisto, T. J.; Nuckolls, C.; Lambert, T. H. *Angew. Chem. Int. Ed.* **2019**, *58*, 13318.

(12) Fang, W.-P.; Cheng, Y.-T.; Cheng, Y.-R.; Cherng, Y.-J. *Tetrahedron* **2005**, *61*, 3107.

(13) (a) Li, S.; Yang, W.; Ji, M.; Cai, J.; Chen, J. *J. Chem. Res.* **2019**, *43*, 14. (b) Daluge, S. M.; Martin, M. T.; Sickles, B. R.; Livingston, D. A. *Nucleosides Nucleotides Nucleic Acids* **2000**, *19*, 297. (c) Showalter, H. D. H.; Bridges, A. J.; Zhou, H.; Sercel, A. D.; McMichael, A.; Fry, D. W. *J. Med. Chem.* **1999**, *42*, 5464. (d) Timoshenko, V. M.; Nikloin, Y. V.; Chernega, A. N.; Shermolovich, Y. G. *Eur. J. Org. Chem.* **2002**, 1619. (e) Wang, J.; Li, Y.-H.; Pan, S.-C.; Li, M.-F.; Du, W.; Yin, H.; Li, J. H. *Org. Process Res. Dev.* **2020**, *24*, 146.

(14) (a) Niu, H.-Y.; Xia, C.; Qu, G.-R.; Zhang, Q.; Jiang, Yi.; Mao, R.-Z.; Li, D.-Y.; Guo, H.-M. *Org. Biomol. Chem.* **2011**, *9*, 5039. (b) Jiang, J.; Li, J. *ChemistrySelect* **2020**, *5*, 542.

(15) Manna, S.; Serebrennikova, P. O.; Utepova, I. A.; Antonchik, A. P.; Chupakhin, O. N. *Org. Lett.* **2015**, *17*, 4588.

(16) Bielawski, M.; Zhu, M.; Olofsson, B. *Adv. Synth. Catal.* **2007**, *349*, 2610.

(17) Purkait, N.; Kervefors, G.; Linde, E.; Olofsson, B. *Angew. Chem. Int. Ed.* **2018**, *57*, 11427.

(18) Carroll, M. A.; Wood, R. A. *Tetrahedron* **2007**, *63*, 11349.

(19) Ma, C.; Zeng, Q.; Wu, X.; Zhou, L.; Huang, Y. *New J. Chem.* **2017**, *41*, 2873.

(20) Sharp, P. P.; Garnier, J.-M.; Hatfaludi, T.; Xu, Z.; Segal, D.; Jarman, K. E.; Jousset, H.; Garnham, A.; Feutrill, J. T.; Cuzzupe, A.; Hall, P.; Taylor, S.; Walkley, C. R.; Tyler, D.; Dawson, M. A.; Czabotar, P.; Wilks, A. F.; Glaser, S.; Huang, D. C. S.; Burns, C. J. *ACS Med. Chem. Lett.* **2017**, *8*, 1298.

(21) Matsuzaki, K.; Okuyama, K.; Tokunaga, E.; Saito, N.; Shiro, M.; Shibata, N. *Org. Lett.* **2015**, *17*, 3038.

(22) Zhu, M.; Jalalian, N.; Olofsson, B. *Synlett* **2008**, 592.

(23) Sokolovs, I.; Lubriks, D.; Sūna, E. *J. Am. Chem. Soc.* **2014**, *136*, 6920.

(24) Kasahara, T.; Jang, Y. J.; Racicot, L.; Panagopoulos, D.; Liang, S. H.; Ciufolini, M. A. *Angew. Chem. Int. Ed.* **2014**, *53*, 9637.

(25) Bielawski, M.; Malmgren, J.; Pardo, L. M.; Wikmark, Y.; Olofsson, B. *ChemistryOpen* **2014**, *3*, 19.

(26) Tibiletti, F.; Simonetti, M.; Nicholas, K. M.; Palmisano, G.; Parravicini, M.; Imbesi, F.; Tollari, S.; Penoni, A. *Tetrahedron* **2010**, *66*, 1280.

(27) Gordon, M. R.; Lindell, S. D.; Richards, D. *Synlett* **2018**, *29*, 473.

(28) Canela, M.-D.; Liekens, S.; Camarasa, M.-J.; Priego, E. M.; Pérez-Pérez, M.-J. *Eur. J. Med. Chem.* **2014**, *87*, 421.

(29) Easter, J. A.; Burrell, R. C.; Bonacorsi, S. J. Jr. *J. Labelled Compd. Radiopharm.* **2013**, *56*, 632.

(30) Šála, M.; Kögler, M.; Plačková, P.; Mejdrová, I.; Hřebabecký, H.; Procházková, E.; Strunin, D.; Lee, G.; Birkus, G.; Weber, J.; Mertlíková-Kaiserová, H.; Nencka, R. *Bioorg. Med. Chem. Lett.* **2016**, *26*, 2706.

(31) Mahajan, T. R.; Gundersen, L.-L. *Tetrahedron Lett.* **2015**, *56*, 5899.

(32) Šála, M.; De Palma, A. M.; Hřebabecký, H.; Dejmek, M.; Dračínský, M.; Leyssen, P.; Neyts, J.; Mertlíková-Kaiserová, H.; Nencka, R. *Bioorg. Med. Chem. Lett.* **2011**, *21*, 4271.

